THE UNIVERSITY *of* EDINBURGH

The Development of a Clinically Relevant Strategy to Promote Fracture Healing in an Atrophic Non-union Model Using Mesenchymal Stem Cells

Tulyapruek Tawonsawatruk

Doctor of Philosophy

The University of Edinburgh

2013

Declaration

I hereby declare that the work presented in this thesis was carried out by me, and where this is not the case, this is referred to in the text. This thesis has been composed by me. This thesis is submitted for the fulfilment of the degree of Doctor of Philosophy, and not for any other degree or qualification.

Tulyapruek Tawonsawatruk

December 2013

Abstract

Atrophic non-union is a major complication following fracture of a bone. It represents a biological failure of the fracture healing process and occurs in 5-10% of cases. A number of factors predispose to atrophic non-union including high energy injuries, open fractures, diabetes, and smoking. Atrophic non-unions cause immense patient morbidity and consume large amount of health care resources. Bone grafts taken from the iliac crest contain biologic components required for fracture healing and are considered as the gold standard treatment of aseptic atrophic non-union. However, harvesting bone grafts from the iliac crest is associated with significant patient morbidity which can reduce quality of life. Mesenchymal stem cells (MSCs) have the ability to proliferate and undergo multilineage differentiation. The emergence of MSC therapy provides an alternative strategy for treating impaired fracture healing. MSCs contribute to normal fracture healing both directly as bone progenitor cells and indirectly as mediator secreting cells. Although a number of studies have shown that MSCs can promote bone regeneration in small animal fresh critical size defects, this is not analogous to most clinical aseptic atrophic non-unions which do not have a significant bone gap. There remains therefore a clinical need for an appropriate strategy for using stem cells in atrophic non-unions. Thus, the aim of this study aim was to develop a clinically relevant strategy to promote fracture healing in an atrophic non-union model using the percutaneous injection of MSCs as a minimally invasive technique. An atrophic non-union model was established and validated. A small (1 mm) non-critical size defect was created at the mid shaft tibia and the fracture site was stabilised using an external fixator. Atrophic non-union was induced by stripping the periosteum for one bone diameter either side of the osteotomy site and curettage of the intramedullary canal over the same distance. The procedure reliably created an atrophic non-union. Fracture healing was evaluated using (1) serial radiography, (2) micro-computed tomography, (3) histomorphology and (5) biomechanical testing. Fracture scoring systems including the radiographic union scale in tibia (RUST) and the Lane & Sandhu score were validated in a pre-clinical model. A simple sample preparation technique for evaluating bone

mechanical properties was developed and used to assess the stiffness and strength of the fracture repair. Percutaneous injection of MSCs locally into the fracture site in the early 'post-injury' period at three weeks after induction of atrophic non-union was found to improve the fracture healing process significantly (83% of cases), while MSCs implantation in the late 'post-injury' period at eight weeks after induction of atrophic non-union showed no significant improvement of fracture healing (20% of cases). Percutaneous local implantation of MSCs rescued the fracture healing process in cases destined to progress to atrophic non-union. In clinical practice, there may be an advantage using MSCs from a universal donor as the processes of MSC isolation and preparation are expensive and time consuming. To investigate the feasibility of using non-autologous cells, the atrophic non-union was used to determine the bone regenerative potential of using xenogeneic donor hMSCs in an atrophic non-union. The results demonstrated that the therapeutic effect of using hMSCs in a xenogeneic manner to promote fracture healing in the rat atrophic non-union model was comparable with rMSCs (88% of cases in both hMSCs and rMSCs) and there were neither significant clinical adverse effects nor adverse immune responses with the xenogeneic transplantation. However, MSCs did not persist at the fracture following injection. Perivascular stem cells (PSCs) taken from adipose tissue, which is an expendable source, have advantages over conventional MSCs as they are a defined and homogenous population and can be used without culture expansion. The administration of PSC using percutaneous injection improved the fracture healing process in atrophic non-union (60% of cases). This suggested that PSCs may present an appropriate choice for use in cell therapies to promote fracture healing in atrophic non-union. The results from this thesis can be applied to the development of a clinically relevant strategy using MSCs as a minimally invasive technique to promote fracture healing in atrophic non-union, in particular (1) the effectiveness of a cell therapy is likely to be highly dependent of the timing of injection relative to the stage of fracture healing, (2) hMSCs were as effective as rMSCs in promoting fracture healing, suggesting that it may be feasible to use an allogeneic strategy in humans, (3) the injected MSCs were not detectable even in case of successful repair, suggesting that they may act through a paracrine effect and (4) PSCs isolated from adipose tissue contributed to fracture healing in the atrophic non-union model,

suggesting that adipose tissues can be used as an alternative cell sources for bone repair.

Acknowledgments

I was inspired by my patients to work on this thesis. There are a number of people who helped and supported me in the production of this thesis. First and foremost, I would like to extend my gratitude to my PhD supervisor Professor Hamish Simpson. He gave me not only the opportunity to study for a PhD but also an enjoyable and excellent PhD experience. He has taught me several aspects of orthopaedic research and especially how to be a good clinical scientist. This has given me confidence in myself and my ability as both a clinician & scientist in orthopaedics to continue my career in orthopaedic science.

I would also like to thank Professor Bruno Péault and Professor Sarah Howie for their contribution in this project. Professor Bruno Péault gave the opportunity to join his group and learn several techniques required in stem cells research, especially perivascular stem cells. Professor Sarah Howie has been a great support in the immunological aspect; she was always available when I needed advice.

Without the excellent support provided by all of my colleagues in orthopaedic engineering group, this project would not have been possible. Special thanks are extended to Robert Wallace who introduced the world of engineering, especially biomechanical and micro-CT. Thanks also to Antonio Spadaccino for his input to both cell and animal experiments, David Hamilton for statistical discussions and Deborah MacDonald for encouragement. My life was easier when working in the biological research facility for animal study with the assistance from William Mungall in an animal house unit. I have been extremely lucky to meet with these people who were not only labmates but also friends during my PhD life: Nataria, Tim, Chris, Zania, Jame who always shared and discussed many things in research and much more.

The writing of this thesis and timely submission has been aided by my best friend, Mr. Iain Murray, and the dedicated proof-readers who I thank profusely for taking the time to read parts of this thesis and providing pointers and advice.

I would like to thank Ramathibodi Hospital, Mahidol University, Bangkok,Thailand for providing the PhD scholarship and supporting me during the study period in UK.

Last but not least, thank you to Tarn, my wife, who wouldn't leave me alone and stayed with me even during the coldest time in the winter in Scotland.

Contents

Abstract ..... **ii**
Acknowledgments ..... **v**
Contents ..... **vii**
List of figures ..... **xiii**
List of tables ..... **xxv**
List of equations ..... **xxvii**
Abbreviations ..... **xxviii**
Part 1: The introduction and the literature review **1**
Introduction **2**
Hypothesis and objective of the thesis 4
Chapter 1: Literature review **5**
1.1 Bone biology 5
1.1.1 Gross morphology structure 6
1.1.2 The components of bone 7
1.1.3 Bone development 12
1.1.4 The physiology of bone remodelling 13
1.2 The fracture healing process 14
1.2.1 Primary bone healing 15
1.2.2 Secondary bone healing 16
1.3 Fracture Non-union 19
1.3.1 Definition of fracture non-union 20
1.3.2 Classification of fracture non-union 20
1.3.3 The pathophysiology of atrophic non-union fracture 21
1.3.4 Treatment of atrophic non-union 23
1.3.5 Augmentation in fracture non-unions 25
1.4 Animal models of non-union 28
1.4.1 Small animal models of fracture healing 29
1.4.2 Selecting the mode of fixation 30
1.4.3 Methods for creating atrophic non-union in animal models 31
1.5 Mesenchymal stem cells and their role for bone regeneration 32
1.5.1 Characteristics of bone marrow derived mesenchymal stromal/ Stem cells 33

1.5.2 The differentiation potential of MSCs 35
1.5.3 Mesenchymal stem cells as bone progenitor cells and trophic factor secreting cells for bone regeneration 36
1.5.4 Donor factors influencing MSC characteristics 39
1.6 Clinical issues relating to MSC transplantation for bone regeneration in atrophic non-union 43
1.6.1 The options for application of MSCs for bone regeneration 43
1.6.2 Immunological effect of MSCs 45
1.6.3 Considerations of MSC source and preparation 48
Part 2: General methods and experimental validation of methods **51**
Chapter 2: General materials and methods **52**
2.1 Primary cell isolation and culture 52
2.1.1 Media, reagents and materials used for cell culture 53
2.1.2 Preparation of media and reagents for cell culture 53
2.1.3 Cell Isolation 54
2.2 The Atrophic non-union procedure 65
2.2.1 Animals 65
2.2.2 Ethical considerations 65
2.2.3 Assembly of the External Fixator 66
2.2.4 Materials, surgical instruments and medicines 67
2.2.5 Operative procedure 69
2.2.6 Post-operative care 71
2.3 A minimally invasive technique for cell delivery 71
2.3.1 The optimisation of injection position in cadaveric study 71
2.3.2 Injection procedure 73
2.4 Radiographic evaluation of fracture healing 73
2.4.1 Radiographic settings 73
2.4.2 Radiological technique 75
2.5 Sample preparation for fracture healing evaluation 83
2.6 Micro-CT imaging 84
2.6.1 Calibration for micro-CT analysis using hydroxyapatite (HA) 85
2.6.2 Acquisition, processing and reconstruction of images 86
2.6.3 Micro-CT analysis 88
2.7 Biomechanical study 90

2.7.1 Sample preparation techniques 91
2.7.2 Machine and setting 91
2.7.3 Analysis of the biomechanical data 92
2.8 Histological evaluation 95
2.8.1 Histological assessment of fracture healing 96
2.8.2 Validation of tissue quantitation methods 99
2.9 Immunocytochemistry and immunohistochemistry 100
2.9.1 Antibodies 101
2.9.2 Specimen preparation 103
2.9.3 Antibody detection 104
2.9.4 Required Controls 104
2.10 Tracking implanted cells 105
2.11 Immunological reaction study 106
2.11.1 Evaluation of inflammatory cytokines 106
2.11.2 Popliteal lymph node evaluation 108
2.12 Statistical analysis 112
Chapter 3: Feasibility of producing mesenchymal stem cells from different sources 114
3.1 Introduction 114
3.2 Materials and methods 115
3.2.1 MSC preparation 115
3.2.2 MSC evaluation 115
3.2.3 Statistical analysis 116
3.3 Results 117
3.3.1 The characteristics of rMSC 117
3.3.2 Human mesenchymal stem cells derived from femoral head 124
3.4 Summary and discussion 129
Chapter 4: Validation of the Radiographic Union Scale in Tibia (RUST) and Lane & Sandhu scoring system in small animal study fracture model 131
4.1 Introduction 131
4.2 Materials and methods 132
4.2.1 Radiographs 132
4.2.2 General impression of the fracture healing and fracture scoring systems 132

4.2.3 Raters 132
4.2.4 Statistical analysis 133
4.3 Results 134
4.3.1 Validation of general impression 134
4.3.2 Validation of RUST score 135
4.3.3 Validation of the Lane & Sandhu score 137
4.3.4 The Bland-altman plot showing the limits of agreement between two scoring systems 139
4.4 Summary and discussion 140
Chapter 5: Comparison of the biomechanical testing using 4-point bending of the rat Tibia between specimens with and without the muscle attached 143
5.1 Introduction 143
5.2 Materials and Methods 144
5.3 Results 145
5.3.1 The characteristic of stress-strain curve 145
5.3.2 The comparison of biomechanical parameters between samples with and without muscle 146
5.3.3 The comparison of coefficient of variation 148
5.4 Summary and discussion 149
Part 3: The results **..... 151**
Chapter 6: The characteristics of the atrophic non-union Model: *in vitro* and *in vivo* experiments 152
6.1 Introduction 152
6.2 Materials and methods 152
6.2.1 Experiment design 153
6.2.2 Biomechanical testing in cadaveric model 153
6.2.3 The fracture assessment of atrophic non-union *in vivo* study 154
6.2.4 Progenitor isolation and colony forming assay 154
6.2.5 Statistical analysis 156
6.3 Results 156
6.3.1 The stiffness of the external fixator 156
6.3.2 The clinical behaviour and health status of the animals 157
6.3.3 Diagnosis of atrophic non –union fracture 158
6.4 Summary and discussion 166

Chapter 7: Determination of bone regeneration potential of mesenchymal stem cells implanted either at an early or at a late stage in the atrophic non-union model 169

7.1 Introduction 169

7.2 Materials and Methods 170

7.2.1 Experiment design 170

7.2.2 rMSCs preparation 170

7.2.3 Fracture assessments 171

7.2.4 Statistical Analysis 171

7.3 Results 172

7.3.1 Animal health status after the atrophic non-union procedure and cell implantation 172

7.3.2 The fracture healing assessment after injection at the early time point (3 weeks) 172

7.3.3 The fracture healing assessment after injection at late time point (8 weeks) 183

7.3.4 Comparison between early and late injection (groups 1and 3) 193

7.4 Summary and discussion 196

Chapter 8: Human bone marrow derived mesenchymal stem cells implantation in xenotransplantation model of an atrophic non-union 200

8.1 Introduction 200

8.2 Materials and Methods 201

8.2.1 Experiment design 201

8.2.2 Biomechanical evaluation 203

8.2.3 Cells tracking after injection 204

8.2.4 Evaluation of inflammatory cytokines from the serum 204

8.2.5 Histology of lymph node 204

8.2.6 Statistical analysis 205

8.3 Results 205

8.3.1 Health status of the animals after received MSC injection 205

8.3.2 Diagnosis of bone union in rat MSC, human MSC and PBS (controls) 206

8.3.3 Detailed radiographic assessment of the progression of fracture 207

8.3.4 Micro-CT evaluation 212

8.3.5 Biomechanical test for xenotransplantation 214

8.3.6 Histological evaluation 217

8.3.7 Tracking of injected cells 223
8.3.8 Evaluation of immune response after cells implantation 230
8.4 Summary and discussion 234
Chapter 9: Bone regeneration potential of adipose tissue derived perivascular stem cells or pericytes 237
9.1 Introduction 237
9.2 Materials and Methods 238
9.2.1 Experiment design 238
9.2.2 Statistical analysis 238
9.3 Results 239
9.3.1 Animal health status after PSCs implantation 239
9.3.2 Diagnosis of bone union in PSC group and control 239
9.3.3 The progression of the fracture healing process 240
9.3.4 Histology evaluation in hPSC treatment group compared to control group 244
9.3.5 Micro-CT analysis in the PSC and control groups 247
9.3.6 Biomechanical testing 249
9.4 Summary and discussion 249
***Part 4: General discussion, future direction and conclusion* 253**
Chapter 10: General discussion 254
10.1 Discussion of the main findings and their clinical implications 254
10.2 Limitations of the study 262
Future directions 265
Conclusion 268
Appendices 269
References 276

List of figures

Figure 1.1 Bone compartments in rat femur 6

Figure 1.2 Coronal sections of metaphysis of rat tibia: *Epiphysis, **growth plate and ***Metaphysis 6

Figure 1.3 Osteoblasts: Above image (arrow) shows (a) inactive osteoblasts (x400) and below section shows (b) active osteoblasts (x400) 8

Figure 1.4 Osteocytes at in ground bone cortex (x400) 9

Figure 1.5 Osteoclasts in a Howship's lacuna, arrow (x400) 10

Figure 1.6 The periosteal structure; (a) Periosteum (x100) and (b) periosteal layers (x200) 11

Figure 1.7 High magnification showing image of (a) a periosteal vessel, at arrow (x400) and (b) Immunostaining of periosteum containing alpha-SMA positive cells within periosteal vessels, at arrow (x200) 12

Figure 1.8 Types of bone healing: There are two mechanisms by which bones will heal: (a) primary bone healing occurs under conditions of absolute stability, such as when a compression plate is used and (b) secondary bone healing occurs under conditions of relative stability, such as using cast. Modified from AO foundation website (https://www2.aofoundation.org/wps/portal/surgery) 15

Figure 1.9 The phases of secondary bone fracture repair: There are three major phases of secondary bone healing: the inflammatory, reparative and remodelling phases. 17

Figure 1.10 Atrophic non-union of the tibia: Atrophic non-unions are characterised by an absence of callus and atrophic bone ends. (Images: courtesy of Professor Hamish Simpson) 19

Figure 1.11 Open tibial fracture: Open or compound fracture is a risk of fracture non-union. 22

Figure 1.12 Diamond concept of elements required for fracture healing: Modified from Giannoudis et al. (2007) 24

Figure 1.13 Atrophic non-union of the ulnar (a) and the bone graft from iliac crest (b) (yellow arrow) applied at the non-union site (green arrow) 25

Figure 1.14 Fixation devices in small animal models: (a) plate fixation from Histing et al. (2010), (b) intramedullary fixation from Histing et al. (2010) and (c) external fixator from Reed et al. (2002) 31

Figure 1.15 Mesenchymal stem cells: MSCs are capable of proliferation and differentiation into bone, fat and cartilage cells. Adapted from Pittenger (1999) 36

Figure 1.16 Preparation methods of MSCs 50

Figure 2.1 Harvesting of Inguinal adipose tissue from Wistar Rats: Following schedule 1 killing, (a) the skin overlying the lower limbs and inguinal region was shaved. (b) The skin overlying the groins and femora was incised and removed, revealing underlying inguinal adipose tissue. (c, d) This tissue was excised and placed in collection media for immediate processing. 55

Figure 2.2 Harvesting of Bone marrow tissue from femoral bone: Following schedule 1 killing, (a) excision of overlying skin and muscle incision was made (b) to reveal the underlying hip joint. (c) The femoral head was disarticulated and (d) the muscles and periosteum were stripped from the femora. (e) The femoral head was cut in order to expose the bone marrow, and (f) irrigation was performed of the distal femora. 56

Figure 2.3 Harvesting of periosteal tissue from Wistar Rats: (a) excision of overlying muscle and (b) the periosteum tissue was identified. 57

Figure 2.4 Extraction of bone marrow from a human femoral head. (a) Femoral heads were obtained from hip replacement procedures in which the proximal femur was divided through its surgical neck. (b) Cancellous bone and (c, d) marrow visible on inspection of the cut surface of the femoral neck was removed by curettage. 59

Figure 2.5 Gating strategy for the sorting of pericytes from adipose tissue. (a) Following double scatter cell and (b) singlet selection, (c) non-viable cells staining for 7-AAD (7-amino-actinomycin D) were excluded. (d) CD45+ haematopoetic cells and CD144+ endothelial cells were excluded, prior to (e, d) selection of the CD146high and CD34- pericytes. (with permission from Dr. Chris West) 60

Figure 2.6 Schematic of the markings on a haemocytometer: Each grid (highlighted here in red) holds 0.1 µl of volume following application of a cover slide 62

Figure 2.7 The External fixator devise used in the generation and fixation of non-unions in Rats: (a) layout prior to assembly (b) Coronal view and (c) lateral view of external fixator 67

Figure 2.8 The surgical technique for the atrophic non-union model 70

Figure 2.9 Locally percutaneous injection technique 72

Figure 2.10 Positioning of the Radiographic equipment 74

Figure 2.11 An aluminium step wedge consisting of multiple steps (from 2 to 20 mm in thickness) was used as the radiological reference for magnification and radiopacity..... 74

Figure 2.12 X-ray position of rat legs 75

Figure 2.13 The technique used to determine the radiopacity: (a) three regions from each step of the Aluminium wedge steps were chosen to generate the calibrated graph and equation . And then, (b) areas over callus (black) and soft tissue (yellow) were selected to calculate the radiopacity of the callus..... 77

Figure 2.14 Proximal and distal callus index measurement (a) demonstrating how to measure the proximal callus index (CD/AB, yellow) and the distal callus index (GH/EF, blue) (b) the correlation between the proximal callus index and the original callus index (P-value < 0.001, Pearson's r) (c) the correlation between the distal callus index and the original callus index (P-value = 0.001, Pearson's r) 79

Figure 2.15 The steps taken following retrieval of tibias from experimental animals including the healing assessments and sample preparation techniques 83

Figure 2.16 Micro-CT set up including (a) the micro-CT Scanner and (b) the hardware used to process and reconstruct images 85

Figure 2.17 The calibration regression curves using two different HA phantoms (250 mg/cm3 and 750 mg/cm3) and water..... 86

Figure 2.18 Defining volume of interest at a 1mm-gap (yellow line represents the middle of the fracture gap, and red lines represent the delineated areas at the top and the bottom of fracture gap)..... 87

Figure 2.19 Fixed global threshold applied to separate bone and non-bone tissues .. 87

Figure 2.20 The four point bending apparatus set up with the tibia (with overlying muscles in situ) prior to testing. 92

Figure 2.21 Cross sectional area; (a) normal bone (b_I and b_E = horizontal measurement of the internal and external width of bone, respectively, h_I and h_E = vertical measurement of the internal and external height of bone, respectively) (b) callus (b = horizontal measurement of callus and h = vertical measurement of callus 93

Figure 2.22 Diagram of four point bending; F = force, a = distance from outer to inner contact and L = span of outer contact 94

Figure 2.23 Tissue quantification method; 100 grids on the histological sections determining the percentage of tissue types (x100)..... 97

Figure 2.24 Bone area from histological section; (a) H&E staining, (b) Masson's trichrome staining 98

Figure 2.25 Cartilage tissue area from histological section; (a) H&E staining, (b) Safranin-O/Fast Green staining..... 98

Figure 2.26 Histological area demonstrating (a) Fibrous tissue and (b) bone marrow /empty space..... 99

Figure 2.27 Correlation of percentages of bone area using a counting grid method (estimated) and the actual bone area (delineated bone manually technique); Pearson r = 0.86, P-value = 0.0013, n = 10..... 100

Figure 2.28 Evaluation of rat inflammatory cytokines using multi-analyte ELISA array. Shown here are (a) the reagents used and (b) the ELISA array machine immediately prior to sample evaluation..... 106

Figure 2.29 Standard curve demonstrating high sensitivity and good linearity within the ELISA 108

Figure 2.30 Histomorphology of lymph node; (a) Lymph node histology (x40), (b) Size of lymph node (selected area in blue) (x40), (c) Secondary follicles (arrow) (x100), (d) an infiltrating cell at the subcapsular area (arrow) (x200) and (e) a macrophage at the medullary sinus area (arrow) (x400) 111

Figure 2.31 Immunohistofluorescence of CD 68 of lymph node (x100): (a) DAPI staining (blue) demonstrating cortex and medullary area of lymph node, (b) CD 68 staining (green) of macrophages and c) Merged image of DAPI/CD 68 (blue/green) demonstrating the presence of macrophages at the medullary area 112

Figure 2.32 The formulae for calculation of sample sizes and commonly used values for $c_{p,power}$..... 113

Figure 3.1 MSCs from 3 sources; bone marrow, adipose tissue and periosteum (x400)..... 117

Figure 3.2 Osteogenic (ALP staining), chondrogenic (Alcian blue staining), and adipogenic (Oil Red O staining) differentiation of MSCs from bone marrow (x400)..... 118

Figure 3.3 Osteogenic (ALP staining), chondrogenic (Alcian blue staining), and adipogenic (Oil Red O staining) differentiation of MSCs from periosteum (x400)..... 119

Figure 3.4 Osteogenic (ALP staining), chondrogenic (Alcian blue staining), and adipogenic (Oil Red O staining) differentiation of MSCs from adipose tissue (x400)..... 119

Figure 3.5 Fibroblast culture under the osteogenic (ALP staining), chodrongenic (Alcian blue staining), and adiposgenic (Oil red O staining) condition for control (x400)..... 120

Figure 3.6 The growth curves of MSCs from bone marrow, periosteum and adipose tissues under the 12-day period of culture; the growth of MSCs from bone marrow and periosteum were comparable and both of them were significantly faster than MSCs from adipose tissue (Bonferroni's test subsequent to ANOVA: * = P-value < 0.05, ** = P-value < 0.01 and *** = P-value < 0.001, data shown as mean and SEM, n = 4 per group and time)..... 121

Figure 3.7 The population doubling time (PDT) of MSCs from bone marrow, adipose tissue and periosteum; the PDT of bone marrow derived cells and the periosteum derived cells were more than the adipose derived cells 122

Figure 3.8 The percentage of colony forming units of MSCs from bone marrow, periosteum and adipose tissue; mean percentage of colony forming of bone marrow derived and periosteum derived MSCs were more than adipose derived MSCs (Bonferroni's test subsequent to ANOV A: * = P-value < 0.05 and *** = P-value < 0.001, data shown as mean and SEM, n = 6 per group) 123

Figure 3.9 The percentage of colony forming area of MSCs from bone marrow, periosteum and adipose tissue; mean area of colony forming of bone marrow derived and periosteum derived MSCs were larger than adipose derived MSCs (Bonferroni's test subsequent to ANOVA: * = P-value < 0.05, data shown as mean and SEM, n = 6 per group)..... 123

Figure 3.10 hMSCs from bone marrow at femoral heads (a) general morphology of hMSCs, (b) Colony forming of hMSCs under low density culture, (c) Alizaline red staining of hMSCs under osteogeneic induction (d) Alkaline phosphatase staining of hMSCs under osteogeneic induction (x400)..... 124

Figure 3.11 Immunolabelling of hMSCs at passage 3rd with FITC a) CD90 b) CD44 (x100)..... 125

Figure 3.12 Immunolabelling of hMSCs at passage 3rd with FITC a) CD146 b) NG2 (x200)..... 126

Figure 3.13 Immunolabelling at passage 3rd with FITC a) CD31 b) CD 34 and C) CD19 126

Figure 3.14 The growth curves of rMSCs and hMSCs from derived bone marrow under the 12-day period culture 128

Figure 3.15 Comparison of (a) the population doubling time (PDT) and (b) the percentage of colony forming units between rMSCs and hMSCs derived from bone marrow 128

Figure 4.1 Showing the normal distribution of average RUST scores from 6 raters136

Figure 4.2 Showing the normal distribution of average Lane & Sandhu scores from 6 raters 138

Figure 4.3 The limits of agreement between RUST and Lane and Sandhu scoring system 140

Figure 5.1 Bone samples after muscle cleaning; (a) and (b) The micro-CT images from two specimens; arrows show small defects after cleaning, (c) gross morphology of sample 144

Figure 5.2 Comparison between the mechanical testing of samples with and without muscle; (a) sample without muscle (b) sample with muscle 145

Figure 5.3 The stress-strain curve from the mechanical testing; (a) from sample with muscle and (b) from sample without muscle 146

Figure 5.4 The comparisons of biomechanical parameters between bones with and without muscle detached 148

Figure 5.5 The coefficient of variation of biomechanical results obtained from bone with and without muscle (* p-value <0.029) 149

Figure 6.1 Graph showing load-displacement of one of cadaveric test 157

Figure 6.2 Health status of the animal following surgical procedure: (a) The ability to weight bearing immediately after surgery, (b) The appearance of skin at the pin tract b) and (c) Mean weight change of animal after operation 158

Figure 6.3 Gross morphology at fracture site: (a) The fracture gap is clearly visible and (b) the tibia shows gross motion; when grasped at one end and held horizontally, movement occurs at the non-union site so it cannot even support its own weight. 159

Figure 6.4 The radiographic assessment: serial radiographs; AP (above) and Oblique views (below) every 2 weeks from immediately post-operative to 8 week post-surgery. 160

Figure 6.5 Histology assessments of atrophic non-union model: a) H&E stain (x100): At the end of the experiment, the gap was filled with fibrous tissue, loosed areolar tissue and also infiltration of muscle fibres and adipose tissue into the gap b) H&E stain (x400): There were osteoclasts resorbing bone at the end of fracture site. c) Masson's Trichrome stain (x100) There were no bone formation at the fracture at 8 weeks; d) Masson's Trichrome stain (x100) The periosteum area around the pin tract, there were new bone formation. e) Safranin-O/Fast Green stain (x100) There was no cartilage formation or endochondral ossification at the fracture gap at 8 weeks f) Safranin-O/Fast Green stain (x100) The new cartilage formation was show at the proximal tibia epiphysis 161

Figure 6.6 Three dimensional images of atrophic non-union: Three different views of three dimensional images from MCT show clearly rounded ends both proximal and distal. 162

Figure 6.7 The plotted bone fraction area from proximal to distal part of the volume selection between normal bone and atrophic non-union 163

Figure 6.8 The colony forming assay for remote bone marrow from the atrophic non-union model: (a) The mean number of colony forming unit from the bone marrow from the contralateral femur of the atrophic non-unions and also from normal control animals. The appearance of the colony formed from the femoral bone marrow of (b) a normal rat and with (c) atrophic non-union 165

Figure 6.9 The cultured cells obtained from non-union tissues: a)-b)The culture of mononuclear cells from atrophic non-union tissues after culture for 2 weeks, x100 (a) and x200 (b), c)-d) The culture of mononuclear cells of from periosteal tissues after culture for 2 weeks, x100 (c) and x200 (d) 166

Figure 7.1 Gross appearance and radiographic at 8 weeks following the early intervention (3 weeks): from (a) PBS treatment group and (b) rat MSCs injection group 173

Figure 7.2 Radiographs at 8 weeks post injected of the animals treated with rMSC that was graded as a non-union 174

Figure 7.3 Serial radiographic assessment: The serial radiographs of the fractures in the rat MSCs treatment group showed progression of healing (above), whereas the radiographs from the PBS treatment group showed no sign of fracture healing (below) 175

Figure 7.4 The comparison of opacity between treatment (rMSC) and control (PBS) over the 8 week period post injection (Bonferroni's test subsequent to ANOVA: ** = P-value < 0.01, and *** = P-value < 0.001, data shown as mean and SEM, n= 3-6 per group and time) 176

Figure 7.5 The comparison of callus index; (a) proximal and (b) Distal between treatment (rMSC) and control (PBS) over the 8 week period post injection (Bonferroni's test subsequent to ANOVA: ** = P-value < 0.01, and *** = P-value < 0.001, data shown as mean and SEM, n= 3-6 per group and time) 177

Figure 7.6 The comparison of the percentage callus increase between treatment (rMSC) and control (PBS) over the 8 weeks period post injection (Bonferroni's test subsequent to ANOVA: * P-value <0.05, ** = P-value < 0.01, and *** = P-value < 0.001, data shown as me an and SEM, n= 3-6 per group and time) ... 178

Figure 7.7 The fracture scoring systems: (a) The RUST score evaluation and (b) Lane and Sandhu score evaluation (Bonferroni's test subsequent to ANOVA: * P-value <0.05, and ** = P-value < 0.01, data shown as mean and SEM, n= 3-6 per group and time) 179

Figure 7.8 H&E staining of the fracture site of a MSC injected rat: a)-d) Cortical remodelling can be found at the fracture gap (x100, a), (x200, b) and both bone formation (x200, c) and cartilage formation (x200, d) were found at the fracture gap 180

Figure 7.9 Safranin-O/Fast Green and Masson's trichrome staining at the fracture site of a rat MSc injected rat: Safranin-O/Fast Green staining shows the area of cartilage formation (x100, a) and Masson's Trichrome staining shows the bone trabeculae at the fracture (x100, b) 180

Figure 7.10 H&E staining at fracture site of PBS injected rat: (a) The fracture end (arrow) has become rounded and (b) fibrous tissue is present at fracture gap (x100) 181

Figure 7.11 Quantitative evaluation of the tissue component in the fracture gap (* =P-value <0.01, unpaired t-test) 181

Figure 7.12 The results from Micro computed tomography of the early treatment groups: Three dimension image of (a) control group and (b) rat MSCs injected group 182

Figure 7.13 Radiographs of one of the animals in the rMSC injection at late time point that healed 184

Figure 7.14 Radiographs of one of the animals in the rMSC injection at the late time point that progressed to non-union 185

Figure 7.15 Radiographs of one of the control animals in the PBS injection at late time point demonstrated an established atrophic non-union 185

Figure 7.16 Radiographs of the single animal in the PBS injection at late time point that processed to union; (a) after 2 week post injection and (b) after 8 weeks post injection 186

Figure 7.17 The comparison of radiopacity between treatment (rMSC) and control (PBS) over the 8 week period post injection at the 8 week time point 187

Figure 7.18 The comparison of callus index; (a) proximal and (b) Distal between treatment (rMSC) and control (PBS) over the 8 week period post injection ... 188

Figure 7.19 The comparison of the percentage callus increase between treatment (rMSC) and control (PBS) over 8 weeks period post injection in the 'late' treatment group 189

Figure 7.20 Fracture healing assessed by Fracture scoring system (a) the RUST score evaluation and (b) the Lane and Sandhu score evaluation 190

Figure 7.21 H&E staining from the fracture site in (a) the rat MSC injected group, and (b) the control PBS injected group; Fibrous component was dominant in the fracture gap (x100) 190

Figure 7.22 H&E staining from the fracture site of one of the animals in MSC injected group; a cartilage component could be found in the middle of the fracture gap (x100) 191

Figure 7.23 Quantitative evaluation of the tissue components in the fracture gap .. 191

Figure 7.24 The results from Micro computed tomography of the late treatment groups: Three dimension image of (a) control group and (b) rat MSCs injected group 192

Figure 7.25 The comparison of radiographic parameters between early and late time injection groups 194

Figure 7.26 The tissue components at the fracture gap at early and late injection time points 195

Figure 7.27 The comparison of bone structural parameters and bone mineral density between early treatment and late treatment groups (* statistically significant difference, P-value < 0.05, unpaired t-test) 196

Figure 8.1 Flow diagram of experimental plan in this study 203

Figure 8.2 The Kaplan-Meier curves showing the number of animals that had achieved radiographic bone union over the 8 week-period (P-value = 0.02, Log-rank test) 207

Figure 8.3 Radiographic progressions after injection over the 8 week period after injection 208

Figure 8.4 The comparison of radiopacity between treatment groups over the 8 week period after injection; the radiopecity at the fracture site in the rMSC and hMSC group were comparable and both of them were significantly higher than in the PBS treatment (Bonferroni's test subsequent to ANOVA: * = P-value < 0.05, ** = P-value < 0.01 and *** = P-value < 0.001, data shown as mean and SEM, n = 4 or 8 per group and time) 209

Figure 8.5 The comparison of callus index; (a) proximal and (b) distal between the treatment groups (rMSC and hMSC) and control (PBS) over the 8 week period post injection which were significantly differences compared to the control group (Bonferroni's test subsequent to ANOVA: * = P-value < 0.05, ** = P-value < 0.01 and *** = P-value < 0.001, data shown as mean and SEM, n = 4 or 8 per group and time) 210

Figure 8.6 The comparison of the percentage callus increase between treatment groups (rMSC and hMSC) and control (PBS) over the 8 weeks period post

injection; there were significant increases in the area of radiopaque bone tissue in the MSC treatment groups compared to the control group. (Bonferroni's test subsequent to ANOVA: * = P-value < 0.05, and *** = P-value < 0.001, data shown as mean and SEM, n = 4 or 8 per group and time) 211

Figure 8.7 The evaluation of fracture healing using the fracture scoring systems; (a) the RUST score evaluation, and the (b) Lane and Sandhu score evaluation (Bonferroni's test subsequent to ANOVA: * = P-value < 0.05, ** = P-value < 0.01 and *** = P-value < 0.001, data shown as mean and SEM, n = 4 or 8 per group and time) 212

Figure 8.8 Three dimensional images from Micro computed tomography; (a) animal with rMSC treatment, (b) animal with hMSC treatment and (c) animal with PBS injection (control) 213

Figure 8.9 Representative load-displacement curves from (a) the rMSC injection group, (b) the hMSC injection group and (c) the PBS injection group 216

Figure 8.10 At week 4 post rMSC injection histological sections. (a) H&E stain demonstrating an area of bone formation, arrow and the osteotomy site, asterisk (x100), (b) Masson's trichrome stain (x100), (c) Safranin-O/Fast Green demonstrating an area of cartilage template, box (x100) and (d) higher magnification image (x400) 218

Figure 8.11 At week 4 post hMSC injection histological sections.: (a) H&E stain demonstrating an area of bone formation, arrow and the osteotomy site, asterisk (x100), (b) Masson's trichrome stain (x100), (c) Safranin-O/Fast Green demonstrating an area of cartilage template, box (x100) and (d) higher magnification image (x200) 219

Figure 8.12 At week 4 post PBS injection (control) histological sections: (a) H&E stain demonstrating the presence of a fracture gap containing fibrous tissue, arrow and the osteotomy site, asterisk (x100), (b) fracture gap at higher magnification (x200), (c) Masson's Trichrome stain (x100), (d) Safranin-O/Fast Green (x100) 220

Figure 8.13 At week 8 post rMSC injection histological sections: (a) H&E stain demonstrating bone bridges, arrows (x40), (b) Masson's Trichrome stain demonstrating an area of new bone formation, asterisk (x40) 221

Figure 8.14 At week 8 post rMSC injection histological sections: (a) H&E stain demonstrating bone bridges, arrows (x40), (b) Masson's Trichrome stain demonstrating an area of new bone formation, asterisk (x40) 221

Figure 8.15 At week 8 post PBS injection (control) histological sections. (a) H&E stain demonstrating full characteristics of atrophic non-union (x40), (b) Masson's Trichrome stain (x40) 222

Figure 8.16 Quantitative evaluation of the tissue component in the fracture gap of the rMSC, hMSC and PBS (control) treatment groups; (a) Bone tissue component, (b) Cartilage tissue component, (c) Fibrous tissue component and (d) Bone marrow component 223

Figure 8.17 rMSCs labelling with CM-Dil in an in vitro culture: (a) rMSC under phase contrast microscope (x200) and (b) rMSC under fluorescence microscope (x200) 224

Figure 8.18 hMSCs labelling with CM-Dil in an in vitro culture: (a) hMSC under phase contrast microscope (x200) and (b) hMSC under fluorescence microscope (x200) 224

Figure 8.19 CM-Dil staining rMSC (Red) at the fracture gap at 0 weeks, 4 weeks and 8 weeks after cell injection with corresponding nuclear (DAPI, Blue) counter stain (x400) 226

Figure 8.20 CM-Dil staining hMSC (Red) at the fracture gap at 0 weeks, 4 weeks and 8 weeks after cell injection with corresponding nuclear (DAPI, Blue) counter stain (x400) 227

Figure 8.21 Anti-nucleic positive staining for hMSC in the in vitro culture (Green) with corresponding nuclear (DAPI, Blue) counter-stain (x400) 228

Figure 8.22 Anti-nucleic positive staining for hMSC (Green) at the fracture gap at 4 weeks and 8 weeks after cell injection with corresponding nuclear (DAPI, Blue) counter stain (x400) and (a,b,c) foetal human tissue from upper limb was used as the positive control 229

Figure 8.23 Inflammatory cytokines from multiple ELISA assay from (a) the rMSC injection group (b) the hMSC injection group and (c) the PBS (control) group 231

Figure 8.24 Histomorphology of popliteal lymph nodes from both operated and unoperated (control) side 4 and 8 weeks after injection with rMSC, hMSC and PBS control; (a) Size of Lymph nodes , (b) Number of secondary follicles, (c) Number of infiltrating cells at capsular sinus, and (d) Number of macrophages at the medullary sinus 233

Figure 9.1 Radiographic at 8 weeks of injected PSCs animal who developed atrophic non-union (Arrows show bone callus at the fracture gap) 240

Figure 9.2 The comparison of radiopacity between treatment (hPSC) and control (PBS) over 8 weeks period post injection (*P-value < 0.05, Post-tests using bonferroni) 241

Figure 9.3 The comparison of callus index; a) proximal and b) Distal between treatment (hPSCs) and control (PBS) over the 8 week period post injection .. 242

Figure 9.4 The comparison of the percentage callus area increase between treatment (hPSC) and control (PBS) over 8 weeks period post injection (*p<0.05, Post-tests using bonferroni)..... 243

Figure 9.5 Fracture scoring systems: (a) The RUST score evaluation and (b) Lane and Sandhu score evaluation..... 243

Figure 9.6 H&E staining from the fracture site of (a) hPSC injected animal, x100 and of (b) control animal, x100..... 244

Figure 9.7 Histological sections: (a) H&E staining, x100 and (b) Masson's Trichrome, x100 at fracture site of hPSC injected animals demonstrating the area of new bone formation (Arrow) 245

Figure 9.8 Non-union gap of one of the animals in the hPSC injection at 8 weeks after cell injection demonstrating soft (Black arrow) and hard callus (White arrow); there was no bony bridge present. (a) H&E, x100 , (b) Masson's Trichrome, x10 and (c) Safronin O/Fast Green, x100 246

Figure 9.9 Quantitative evaluation of the tissue components in the fracture gap (a) bone tissue component, (b) cartilage tissue component, (c) fibrous tissue component and (d) bone marrow/empty space component (*P-value < 0.05, unpaired t-test) 247

Figure 9.10 The results from 3D Micro computed tomography of five animals in the PSC injected group..... 248

List of tables

Table 2.1 List of equipment and medicine required in the animal studies 68

Table 2.2 RUST scoring system: based on points to a given set of AP and oblique radiograhs based on assessments of healing at each of the four cortices 81

Table 2.3 Lane & Sandhu scoring system; based on three dimensions present in radiographs 82

Table 2.4 Antibodies used in this study 102

Table 3.1 Summary of human mesenchymal stem cell markers 127

Table 4.1 Inter-observer agreements of general impression 134

Table 4.2 Intra-observer agreements of general impression from individual rater .. 135

Table 4.3 Inter-observer agreements of the RUST score 136

Table 4.4 Intra-observer agreements of the RUST score from individual rater 137

Table 4.5 Inter-observer agreements of the Lane & Sandhu score 138

Table 4.6 Intra-observer agreements of the Lane & Sandhu score from individual rater 139

Table 5.1 Summary of biomechanical parameters between sample with and without muscle 147

Table 6.1 Sumary of load used to close 1mm gap and predicted displacement of 5 animals 157

Table 7.1 The number of the animals used in the early time point and results of bone union between group 1 and group 2 174

Table 7.2 Micro CT analysis between control and rMSC at early time point 183

Table 7.3 The number of the animals used at the late time point and numbers that achieved bone union rates 184

Table 7.4 Micro-CT analysis between control and rMSC from animals injected at the late time point 193

Table 8.1 Outcome of fracture union (inclusive of four and eight week results) according to group. The number of the animals used and results of bone union between three groups 206

Table 8.2 The summary of micro CT analysis from the animals from different groups at 4 weeks and 8 week after injection 214

Table 8.3 The summary of biomechanical properties of healing bone in the animals with rMSC injections and the animals with hMSC injections 216

Table 9.1 The number of the animals used in the early time point and results of bone union between the PSC injection group and the PBS (control) injection group 239

Table 9.2 Micro CT analysis between PSC and PBS control 248

Table 9.3 Biomechanical properties of bone for bone samples from limbs injected with hPSC and from normal bone from the contralateral unoperated side 249

List of equations

Equation 2.1 Total cells/ml = Average grid cell count x 10^4 x Dilution factor 61

Equation 2.2 PDN =log (N/N_0) x3.31 63

Equation 2.3 PDT=CT/PDN 63

Equation 2.4 BMD = (HU object − 110.80)/ 3852.36 g/cm3 89

Equation 2.5 I = 1/36[bEhE3 − bIhI3..... 93

Equation 2.6 I = 1/4πbh3 94

Equation 2.7 σb = (F × a × c)/2I 94

Equation 2.8 ε = (6 × c × displacment)/a(3L − 4a) 95

Equation 2.9 E = (F/displacement) × (a2/12I) × (3L − 4a) 95

Abbreviations

BMD	Bone mineral density
BS	Bone surface
BV	Bone volume
CM-Dil	Chloromethyl-benzamidodialkylcarbocyanine
DMEM	Dulbecco's Modified Eagle Medium
CFU-F	Colony forming unit fibroblasts
2D	two dimensional
3D	three dimensional
ELISA	Enzyme-Linked ImmunoSorbent Assay
FBS	Fetal Bovine Serum
H&E	Hematoxylin and Eosin staining
Micro-CT	Micro computed tomography
MSC	Mesenchymal stem cell
rMSC	rat Mesenchymal stem cell
hMSC	human Mesenchymal stem cell
mg	milligram
mL	microliter
µL	microliter

mm	millimetre
M	Molar
Mpa	Megapascal
N	Newton
PSC	Perivascular stem cell
PBS	Phosphate buffered saline
PDT	Population doubling time
PFA	Paraformaldehyde
P/S	penicillin/streptomycin
g	gram
rpm	Round per minute
RT	Room temperature
TV	Total volume
Tb.N	Trabecular number
Tb.Th	Trabecular thickness
Tb.Sp	Trabecular separation
THR	Total Hip Replacement

Part 1: The introduction and the literature review

Introduction

"Prevention is better than cure"

Desiderius Erasmus, 1523

An epidemiological study at the Royal Infirmary of Edinburgh, Scotland in the year 2000 reported the incidence of fracture to be 11.3 per 1,000 people (5,953 fractures in a population of 534,715 (Court-Brown and Caesar, 2006). In general, bone has a physiologically reparative response to injury consisting of three basic steps: inflammation, proliferation and remodelling, allowing the spontaneous healing of fractures (Simmons, 1985). Failure of these physiological processes may results in fracture non-union, a complication that occurs in 5-10% of cases (Littenberg et al., 1998, Tzioupis and Giannoudis, 2007). Recently, the overall incidence of non-union in Scotland over the period 2005-2010 was reported as 18.94 per 100,000 (979 non-unions per year in a population of 5,169,140) (Mills and Simpson, 2013). Non-unions cause considerable morbidity and consume large amounts of health care resources. Bone grafts taken from the iliac crest contain biologic components required for fracture healing and transplantation to the non-union site is currently considered the gold standard treatment. In this procedure the non-union site is decorticated to encourage local bleeding and the bone graft, harvested from an alternative site (commonly the iliac crest), is applied (Sen and Miclau, 2007). Harvesting bone graft from the iliac crest can result in infection, painful scaring and numbness around the harvest site affecting quality of life (Schwartz et al., 2009).

Good surgical technique and appropriate implant selection can prevent non-union. Surgeons should use techniques that are mindful of the contribution of surrounding soft tissues to the fracture healing process. Procedures that minimise tissue trauma can preserve vital biological components around the fracture site (Perren, 2002) and prevent atrophic non-union. High energy or open fractures inherently result in severe

soft tissue damage thus impairing the biological capacity for fracture healing (Megas, 2005) and increasing the risk of atrophic non-union. It has therefore been suggested that augmentation of biologic components at the fracture site may enhance the fracture healing process in patients at high risk of atrophic non-union. The biological components that support bone healing consist of cellular components, including mesenchymal stem cells (MSCs) or bone progenitors, and soluble mediators, such as growth factors or cytokines: both parts are required in the process of fracture healing (Giannoudis et al., 2007).

The transplantation of MSCs holds great promise as a strategy to improve bone healing in atrophic non-union. Most studies have used bone defect models to evaluate the effects of MSCs in bone repair (Bruder et al., 1998, Peterson et al., 2005, Nair et al., 2009). Pre-clinical models should closely represent clinical scenarios to best evaluate new therapeutic interventions in atrophic non-union. However, a discrete bone defect or bone loss is not a common cause of atrophic non-union in the clinical setting. Thus, a non-critical size defect atrophic non-union model is a more appropriate setting in which to study a role for MSCs in fracture repair. A minimally invasive strategy for delivery of MSCs is desirable in modern clinical practice. Therefore, the aim of this study is to develop a clinically relevant strategy to improve fracture healing in atrophic non-union using an injectable MSC-based approach. This minimally invasive intervention can be applied for prevention in patients at high risk of atrophic non-union.

Hypothesis and objective of the thesis

The hypothesis of this study was:

"**Percutaneous injection of MSCs promotes the process of fracture repair in a small animal model of atrophic non-union**"

To evaluate this hypothesis, the following objectives were set:

1. To establish and validate a clinically relevant atrophic non-union model, and to evaluate the characteristics of local progenitors at the site of atrophic non-union and systemic progenitors from a remote site (contralateral femoral bone).

2. To determine an optimal time for rat Mesenchymal Stem Cells (rMSCs) injection in atrophic non-union model.

3. To investigate the therapeutic effects of human Mesenchymal Stem Cells (hMSCs) injection on fracture healing in an atrophic non-union model, determine cell fate and immune reactions after hMSC injection.

4. To evaluate the feasibility of using purified human perivascular stem cells (PSCs) from adipose tissue as an alternative to bone marrow derived MSCs for fracture repair in a small animal model of atrophic non-union.

Chapter 1: Literature review

The aim of this thesis is to develop a clinically relevant strategy for using Mesenchymal stem cells (MSCs) to improve fracture healing in atrophic non-union. In the first part of this chapter, the background knowledge relevant to the study is reviewed, including basic bone biology, the fracture healing process and the pathological mechanisms involved in the development of atrophic non-union. In addition recent treatments for atrophic non-union are reviewed. The rationales as well as the prerequisites for stem cell treatment are defined. Pre-clinical non-union fracture models relevant to the project are summarised. The second part of this chapter considers a role for MSCs in bone regeneration. The biology of MSCs and their potential in bone regeneration are reviewed. Issues and challenges relating to the use of MSCs in clinical settings including appropriate modes of cell delivery, immune responses after treatment and suitable cell types for implantation are discussed. This literature review provides a basis for understanding clinical strategies utilising MSCs in bone repair. It also refines and defines the key questions that are addressed in this study.

1.1 Bone biology

Bone is a unique tissue, as it has the potential to regenerate after injury without scar formation. A central function of bone is to provide structural support to the body, protecting vital internal organs such as the brain, heart and lungs. In addition, it facilitates movement of the body and extremities through tendinous attachments to muscle. It also plays a crucial role in calcium homeostasis, as it contains 99% of total body calcium. Knowledge of bone biology and structures is fundamental to the understanding of the fracture healing process and the developing therapeutic interventions to facilitate fracture repair.

1.1.1 **Gross morphology structure**

There are two types of bone tissue at the macroscopic level. Cortical (compact) bone and trabecular (cancellous) bone (**Figure 1.1**). Distribution of these two major bone types varies throughout different regions of bones. Trabecular bone is mainly found in short bone and at the metaphyses of long bones, whereas cortical bone is dominant in diaphyseal areas (**Figure 1.2**).

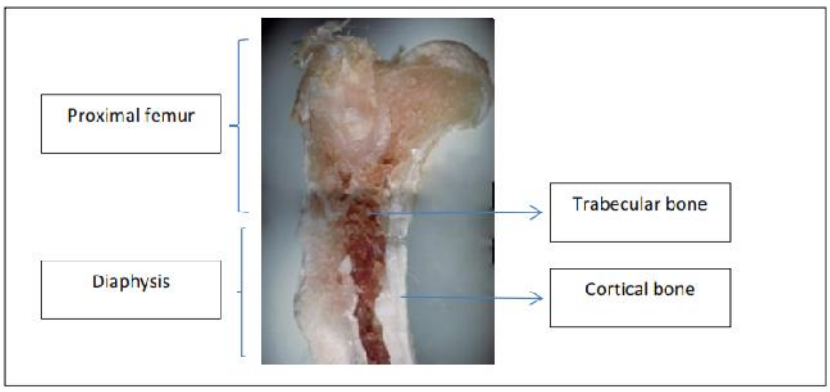

Figure 1.1 Bone compartments in rat femur

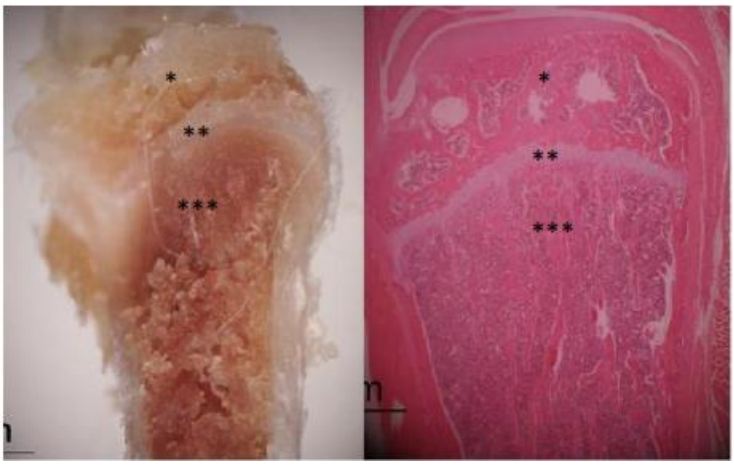

Figure 1.2 Coronal sections of metaphysis of rat tibia: *Epiphysis, **growth plate and ***Metaphysis

1.1.2 **The components of bone**

Bone is a connective tissue, which consists of cells and mineralized extracellular matrix. The mineral content is predominantly calcium phosphate, in the form of hydroxyapatite [$Ca_{10}(PO_4)_6(OH)_2$]. Besides the calcified components of bone matrix, the extracellular matrix contains several proteins which can be classified as either collagenous or non-collagenous protein. Type I collagen is the major collagenous protein, but there also significant amounts of type V collagen present, which are structural backbone of bone (Niyibizi and Eyre, 1989). Non-collagenous proteins are present in the bone matrix as 'ground substances'. These include glycosaminoglycans, glycoproteins (osteocalcin, osteonectin and osteopontin) and sialoprotein. Glycoprotein and sialoprotein play a role as calcium binding proteins in the mineralization process (Zurick et al., 2013). These proteins are secreted by osteoblasts, which are one of the cellular components of bone tissue.

1.1.2.1 Cellular components

There are three main types of cells in bone: osteoblasts, osteocytes and osteoclasts. Osteoblasts and osteocytes are differentiated from basic cell types known as bone progenitor cells (MSCs or osteoprogenitor cells), whereas osteoclasts originate from haematoprogenitor cells.

Osteoblasts are bone-forming cells that secrete several proteins present in the bone matrix. This includes osteoid which is first laid down in unmineralised bone. Inactive osteoblasts are flat, covering the bone surface. When active, these cells are characteristically cuboidal or polygonal in shape (**Figure 1.3**). During the differentiation process from osteoprogenitors, important cell-cell and cell-matrix interactions occur. It has been reported that extracellular matrix-intergrin (ECM-integrin) interactions are important in osteoblast gene expression (Gronthos et al., 1997). β1 intergrins on the osteoblast membrane adhere to the RGD-containing

protein (the peptide sequence Arg-Gly-Asp) at the bone matrix and this interaction stimulates intracellular kinase pathway via a spectrum of transcription factors including Runx2 (Xiao et al., 2002). Mutations in this gene have been associated with cleidocranial dysplasia, which presents with delayed or absent intramembranous ossification (Mundlos, 1999).

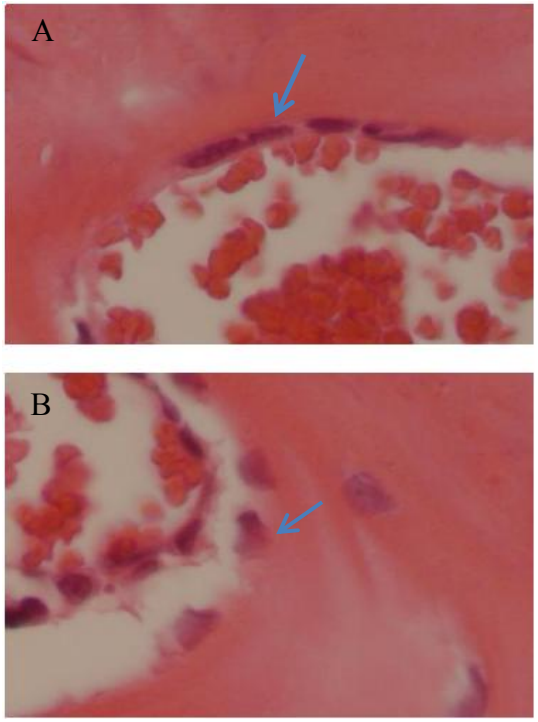

Figure 1.3 Osteoblasts: Above image (arrow) shows (a) inactive osteoblasts (x400) and below section shows (b) active osteoblasts (x400)

As osteoid deposition appears, the osteoblast is surrounded by an osteoid matrix and then becomes an osteocyte. Osteocytes are typically smaller than the osteoblast cells from which they derive (**Figure 1.4**) and are responsible for maintaining the bone matrix. Osteocytes reside in spaces called lacunae, interacting with adjacent cells via canaliculi. These cells respond to mechanical stimuli (mechanical strain and fluid flow) though GAP junctions (Cherian et al., 2003). Recently, it has been shown that mechanical loading can suppress the secretion of sclerostin which is a small

molecule secreted by osteocytes (Robling et al., 2008). The inhibition of sclerostin secretion can increase the osteogenic effect of the Wnt pathway (van Bezooijen et al., 2007). Studies using genetically modified animals deficient in sclerostin have demonstrated an association with increased bone formation and bone mass (Li et al., 2008).

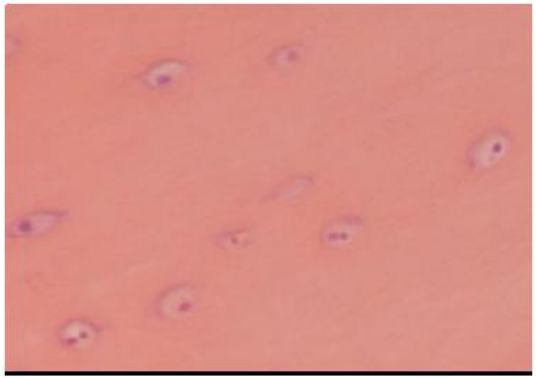

Figure 1.4 Osteocytes at in ground bone cortex (x400)

Osteoclasts are large, multinucleated cells that can be found at areas where bone is being removed or remodelled (**Figure 1.5**). Osteoclasts contain numerous lysosomes for bone matrix resorption. Howship's lacunae, which are present at sites of bone resorption contain osteoclasts. These cells play an important role in calcium metabolism in a process mediated by parathyroid hormone (PTH) and calcitirol (Faucheux et al., 2002). Unlike osteoblasts and osteocytes, the progenitor from which osteoclasts derive is of haematopoietic stem cell origin. Monocytes fuse and become multinucleated cells. Osteoclasts play a key role in bone resorption and remodelling. Microfracture can stimulate and recruit osteoclasts into functional sites (Klein-Nulend et al., 1995). The process of osteoclast formation or osteoclastogenesis is dependent on monocyte stimulation factor (M-CSF) and receptor activator of nuclear factor kappa B ligand (RANKL), which are produced by osteoblasts (Takahashi et al., 2011). Osteoclast formation is inhibited by osteoprotegrin (OPG), which is also

secreted by osteoblasts. These substances are involved in the physiology of osteoclast formation.

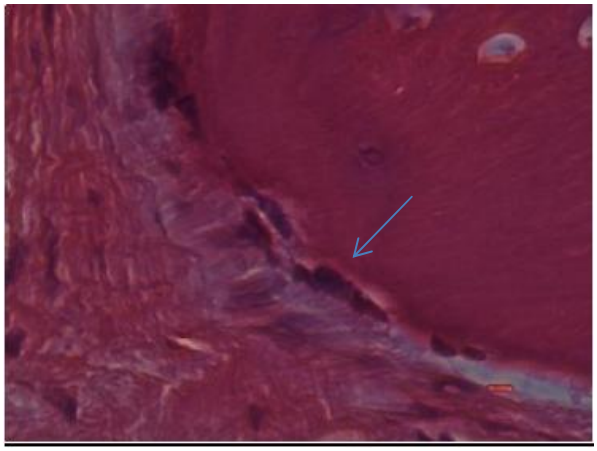

Figure 1.5 Osteoclasts in a Howship's lacuna, arrow (x400)

1.1.2.2 Periosteum and blood vessel of bone

The periosteum is a sheath of dense fibrous connective tissue covering the bone surface that contains osteoprogenitor cells and the blood vessels that nourish the underlying bone. Histologically, there are two layers of the periosteum (**Figure 1.6**): an outer fibrous layer and an inner layer known as the cambium layer, where the ostoprogenitor cells can be found. However, a report on the ultrastructure of the periosteum using electron microscope suggested that there were three different zones at the periosteum: Zone I consisted of predominately osteoprogenitor cells that located adjacent to the bone surface, Zone II was a relatively translucent zone where fibroblasts and collagen fibrils were found equally with numerous capillaries, and Zone III consisted of predominately collagen fibrils and fibroblasts (Squier et al., 1990). The inner layer or zone of periosteum plays an important role for bone regeneration as it contains progenitor cells that are able to proliferate and become osteoblasts under appropriate stimuli, such as, fracture or injury.

The main blood vessel supplying the shaft of long bones is the nutrient artery. It gives branches within the Harversian and Volkmann's canals. Periosteal arteries provide the blood supply for the periosteum (**Figure 1.7**). These structures are important in the fracture healing process. In high energy fractures, the periosteum and surrounding soft tissues can be significantly disrupted (Govender et al., 2002). A number of both clinical and experimental studies have demonstrated that periosteal disruption at the fracture site is associated with impaired fracture healing (Landry et al., 2000, Kokubu et al., 2003, McKibbin, 1978)

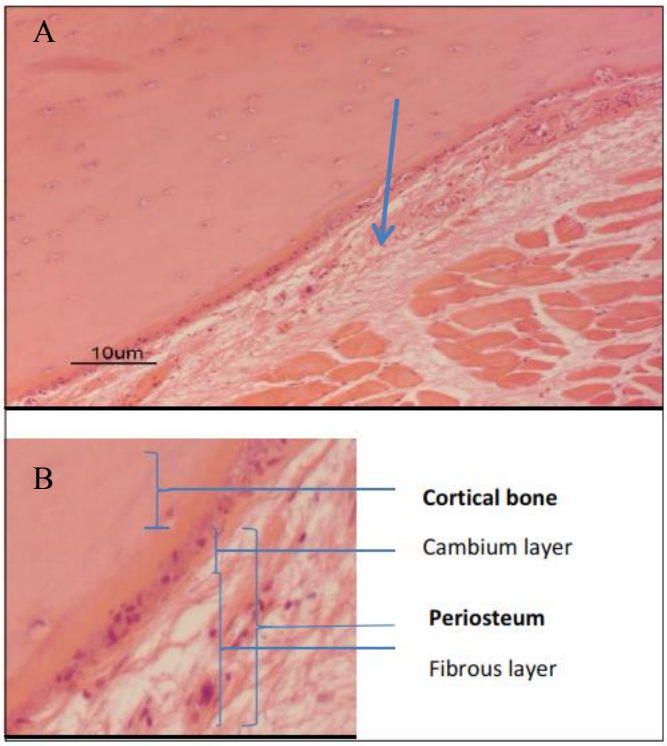

Figure 1.6 The periosteal structure; (a) Periosteum (x100) and (b) periosteal layers (x200)

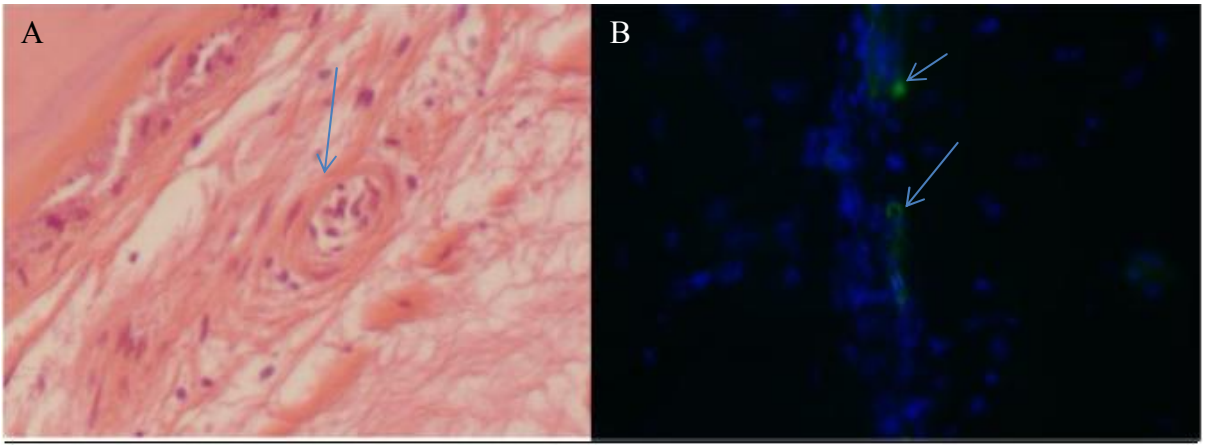

Figure 1.7 High magnification showing image of (a) a periosteal vessel, at arrow (x400) and (b) Immunostaining of periosteum containing alpha-SMA positive cells within periosteal vessels, at arrow (x200)

1.1.3 **Bone development**

There are two processes by which bone may form; (1) Intramembranous bone formation and (2) Endochondral bone formation

1.1.3.1 Intramembranous bone formation

This type of bone formation is the developmental pathway of flat bones including the cranial bones, and pelvic bones. The progenitors of bone cells, namely MSCs, differentiate directly into bone cells during their development without a cartilage template. This process starts with the condensation of mesenchymal progenitors. After aggregating, these cells start differentiating into pre-osteoblasts and produce initial osteoid which contains a number of cell-binding proteins such as sialoprotein and osteopontin. Type 1 collagen and small proteoglycans are laid down and they form cross-links as the bone matures. Osteocalcin is the most abundant of non-collagenous matrix proteins. It is a Calcium-binding protein that appears at the

mineralization stage of bone formation. Collagen fibres are less organized in the early stages of bone mineralisation in immature woven bone. Woven bone is subsequently replaced by lamellar bone in which the collagen fibers are more oriented in layers.

1.1.3.2 Endochondral bone formation

This is the process by which long bones and the vertebrae develop. It involves the initial formation of cartilage tissue as the template. This structure is surrounded by periosteum and perichondrium, which serve as a reservoir of progenitor cells. The progenitor cells differentiate into chondrocytes, which become enlarged and produce a calcified cartilage matrix. These cells provide and secrete vascular endothelial growth factor (VEGF), which stimulates blood vessel formation. Vascular buds are formed which invade the central zone of the cartilage matrix. A cavity forms in the centre of the calcified cartilage matrix; this subsequently forms the primary spongiosa, which is the immature trabeculae and bone marrow cavity. This is surrounded with lamellar bone. As the bone develops, the secondary spongiosa, which is the secondary centre of ossification is found in the epiphyseal regions.

1.1.4 The physiology of bone remodelling

As a viable tissue, bone has a regular turnover and remodels during the period of its lifetime. This physiological process requires a diverse group of cells which take part in the process and are known as the bone remodelling unit. The rate of bone turnover is dependent on the bone type. In cancellous bone, the turnover is higher than in compact bone (Burr, 2002, Parfitt, 2002). Dysregulation of this process can result in osteoporotic fractures particularly of sites such as the vertebrae, the proximal femur

and the distal end of the radius, which have greater proportion of cancellous bone than in the diaphysis (Sandhu and Hampson, 2011).

There are four phases in the bone remodelling cycle: activation, resorption, reversal and formation (Clarke, 2008) . Osteoclasts are activated and recruited into the bone in response to local cytokines (M-CSF and RANKL) (Boyle et al., 2003). Subsequently, fully differentiated osteoclasts secrete proteolytic enzymes including capthesin K and matrix metalloproteinases (MMPs) (Delaisse et al., 2003). This is a part of the resorption phase and results in the formation of Howship's lacunae. Due to the resorption of bone matrix, several growth factors including transforming growth factor (TGF)-β, bone morphogenetic proteins (BMPs), platelet-derived growth factor (PDGF), insulin-like growth factor (IGF)-I and II and fibroblasts growth factor (FGF) are released (Mohan and Baylink, 1991). These growth factors promote and stimulate the differentiation of MSCs and other tissue resident bone progenitors. The differentiated osteoblasts then start to synthesise a new bone matrix in the formation phase, which is subsequently mineralised.

1.2 The fracture healing process

Fracture healing is a complex process which involves many biological events. There are two categories of bone healing which depend on the size of the fracture gap and the stability at the fracture site during the healing process (McKibbin, 1978, Ito and Perren, 2007) (**Figure 1.8**).

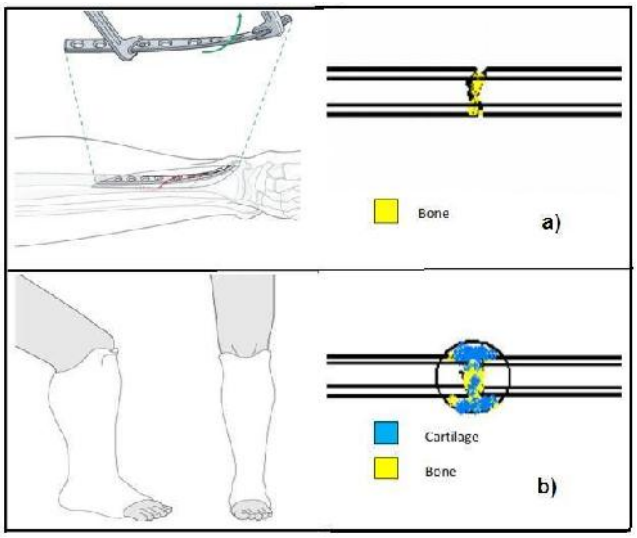

Figure 1.8 Types of bone healing: There are two mechanisms by which bones will heal: (a) primary bone healing occurs under conditions of absolute stability, such as when a compression plate is used and (b) secondary bone healing occurs under conditions of relative stability, such as using cast. Modified from AO foundation website (https://www2.aofoundation.org/wps/portal/surgery)

1.2.1 **Primary bone healing**

Primary healing, sometimes known as direct healing, requires absolute stability of fracture fixation (Jagodzinski and Krettek, 2007). Fractures treated with compression plating heal by the primary healing process. Here, bone regenerates without external callus, and cartilage and fibrous tissue formation at the fracture gap does not occur. Progenitor cells differentiate directly into bone cells and form the bone matrix essential for healing at the fracture site (McKibbin, 1978). Intra-articular fractures, such as those of the tibial plateau or femoral neck fractures require absolute stability and these fractures should heal by primary healing. Primary healing can be sub-classified into contact healing and gap healing according to the size of the gap between the healing bone ends.

1.2.1.1 Contact healing

When the fracture sites are in direct apposition with no separating gap, healing can occur without intramembranous bone formation. Osteoclasts make cutting cones or bone resorption cavities crossing the fracture site. New osteons, which are the basic fundamental functional unit of compact bone, form and establish a harversian system with the original orientation.

1.2.1.2 Gap healing

Gap healing requires intramembranous bone formation as new osteons cannot cross the fracture line directly. The process begins with differentiating bone progenitor cells forming woven bone at the gap. The woven bone is then remodelled and re-orientated into lamellar bone that has parallel fibres similar to the orientation of an uninjured bone.

1.2.2 Secondary bone healing

Another type of fracture healing is secondary or indirect healing. This is the most common way by which fracture healing occurs. Most of fractures are managed without rigid fixation (relative stability) such as cast immobilisation, external fixation or intramedullary fixation, in a process that involves the formation of callus. Secondary fracture healing can be divided into three phases: the inflammatory, reparative and remodelling phases (McKibbin, 1978). These phases may overlap and affect one another during the fracture healing process (**Figure 1.9**).

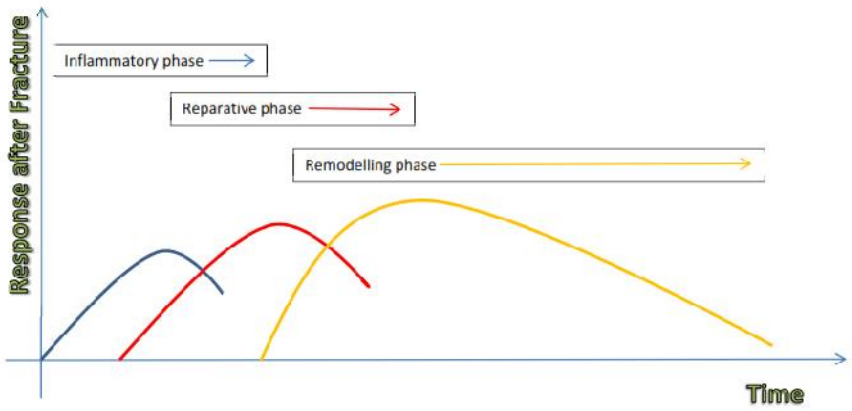

Figure 1.9 The phases of secondary bone fracture repair: There are three major phases of secondary bone healing: the inflammatory, reparative and remodelling phases.

1.2.2.1 The inflammatory phase

In addition to the bone itself, surrounding soft tissues are also injured with trauma. After injury, a haematoma forms at the fracture gap and in the surrounding area. Inflammatory cells such as macrophages that release interleukin-1 and 6 (IL-1 and IL-6), and tumour necrosis factor-alpha (TNF-α) are recruited, while degranulating platelets also release platelet-derived growth factor (PDGF) and transforming growth factor-beta (TGF-β) (Bolander, 1992). These pro-inflammatory cytokines and growth factors can induce a cascading inflammatory response, which stimulates the healing process (Warren, 1990). MSCs and progenitors originating from bone marrow, periosteum and the soft tissues around the fracture sites are triggered to proliferate and differentiate for fracture healing (Yoo and Johnstone, 1998).

1.2.2.2 The reparative phase

This phase follows the inflammatory phase, although it may begin before the inflammatory phase has fully subsided. Bone formation or ossification occurs in this

phase through intramembranous ossification or endochondral ossification. With intramembranous ossification, the precursor cells differentiate into bone progenitors and osteoblasts directly and form woven bone (Yoo and Johnstone, 1998), whereas with endochondral ossification, cartilage is formed in an intermediate step before the woven bone appears (McKibbin, 1978). The formation of tissues at the fracture sites depends on numerous factors including strain and oxygen tension (Zuscik et al., 2008). The enchondral ossification process is driven by relative hypoxic conditions and some degree of motion. The progenitors differentiate into chondrocytes, which proliferate rapidly and become hypertrophic. They create extracellular matrix and provide a template for bone formation. This process is called chondrogenesis. When the chondrocytes die, new vascular structures invade, which transport bone progenitors that can form osteoid and eventually woven bone. Internal callus formation (or endosteal healing) occurs through intramembranous ossification, which requires high oxygen tension and low strain conditions (Claes and Heigele, 1999, Carter et al., 1998, Lacroix and Prendergast, 2002).

1.2.2.3 The remodelling phase

The bone remodelling process may take up to two years. The callus which contains the woven bone is gradually replaced by lamellar bone. The lamellar bone has an isotrophic property, which is characterised by parallel organisation of collagen fibres contributing to the greater mechanical strength of lamellar bone over woven bone. It is thought that mechanical factors are important in the process of bone remodelling. According to Wolff‘s Law as cited by Goldstein (1987), the remodelling of bone trabeculae depends on external loading. Recently, a biological mechanism responding to a mechanical stimulus has been reported, which can be explained through a function of sclerostin or the SOST gene expressed on osteocytes (Bonewald and Johnson, 2008). Fluid shift in the canaliculi network from mechanical loading can reduce SOST protein production, which antagonizes the WNT pathway.

Mechanical factors play a major role in this final stage of fracture healing, as bone remodels into its original form and structure (Robling et al., 2008, Tu et al., 2012).

1.3 Fracture Non-union

Impairment of the normal fracture healing can result in fracture non-union (**Figure 1.10**). Non-union occurs in about 5-10% of fractures (Littenberg et al., 1998, Tzioupis and Giannoudis, 2007). The treatment of fractures that develop non-union requires numerous operations with associated morbidity and financial costs (Schwartz et al., 2009, Heckman and Sarasohn-Kahn, 1997)

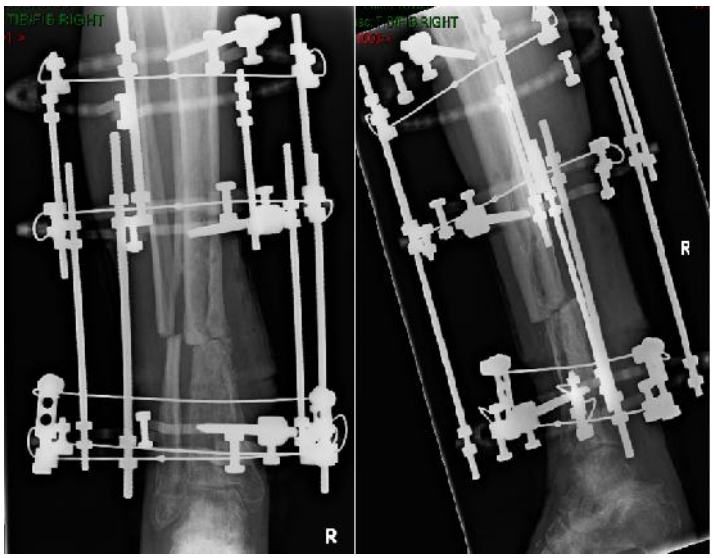

Figure 1.10 Atrophic non-union of the tibia: Atrophic non-unions are characterised by an absence of callus and atrophic bone ends. (Images: courtesy of Professor Hamish Simpson)

1.3.1 **Definition of fracture non-union**

Fracture non-union is a pathological condition in which the fractured bone ends cannot unite without additional intervention, either surgical or non-surgical. There are no true consensus criteria for the diagnosis of non-union (Bhandari et al., 2002). Recently, a systematic review revealed that 62% (n=123) of clinical studies, based the diagnosis of union/non-union of long bones on both clinical and radiographic features. Clinical criteria for union included the ability to weight bear and the capacity to perform activities of daily living. Radiographic criteria included an evaluation of bridging callus at the fracture site and obliteration of the fracture line (Corrales et al., 2008).

Several definitions of fracture non-union have been proposed (Marsh, 1998, Green et al., 1988, Bassett et al., 1981). According to the United States Food and Drug Administration (FDA), a fracture non-union is defined as a fracture that is at least nine months old that has not shown any signs of progression of healing for three consecutive months.

1.3.2 **Classification of fracture non-union**

The classic classification of fracture non-union was proposed by Weber and Cech (1976). Two broad groups (Hypertrophic and Atrophic) of non-union are described, according to the radiographic appearance, which correlates with aetiology. With respect to treatment, however, non-unions should be investigated for evidence of infection. In the presence of infection, non-unions are described as septic non-unions (Simpson et al., 2002).

Hypertrophic non-union has good biological activity with an abundance of callus formation. The fracture cannot heal properly due to mechanical insufficiency. Hypertrophic non-unions can be further divided by the amount of callus on

radiographs as either; elephant's foot, horse's foot or oligotrophic. Conversely, atrophic non-union is a pathological condition that occurs from biological impairment resulting in an absence of the callus at the ends of the bone at the fracture site. These bone ends may be rounded and sclerotic.

Atrophic non-union can be divided into types of atrophic non-union based on mechanical and histological features; 1) stiff atrophic non-union 2) mobile atrophic non-union. Although, there are no signs of radiographic bone healing in stiff atrophic non-unions, fibrous tissue can be found across the non-union site, which provides some mechanical stiffness. In contrast, the non-union gap in mobile atrophic non-unions has a cystic cavity and is devoid of mechanical stability. This type of atrophic non-union should be termed as typical pseudarthrosis (Mills and Simpson, 2012).

1.3.3 **The pathophysiology of atrophic non-union fracture**

Atrophic non-union is associated with biological failure. The severity of fracture has a considerable impact on the risk of atrophic non-union (Karladani et al., 2001). Open fractures are associated with significant soft tissue injury (**Figure 1.11**). The periosteum, which is a rich source of the mesenchymal progenitor cells, may be destroyed with high energy injuries and open fractures (Ozaki et al., 2000, Ball et al., 2011). A prospective observational study performed in 41 trauma centres reported that the risk of delayed or non-union in open fractures with a wound either less than 5 cm or, greater than 5 cm was increased by 3.6 and 5.7 times respectively, when compared to fractures with no skin injuries (Audige et al., 2005). Other factors predisposing to atrophic non-union have been described. It has been reported from clinical studies that smoking (Schmitz et al., 1999) and vitamin D deficiency (Brinker et al., 2007) predispose to fracture non-unions. In addition, reports from animal studies suggest that nonsteroidal anti-inflammatory drugs (NSAIDs) can also inhibit the fracture healing process (Allen et al., 1980, Gerstenfeld et al., 2003). The retrospective study, comparing 32 patients with non-union and 67 matched patient

with united fracture (Giannoudis et al., 2000), identified an increase in the risk of non-union of femoral diaphysis in patients who had NSAIDs with odds ratio of 10.73. It has been reported in patients who received indomethacin for heterotopic ossification prophylaxis of the acetabulum; the risk of non-union of concurrent fractures was a significant difference between patient with (26%) and without indomethacin treatment (7%) (Burd et al., 2003).

It has been thought that atrophic non-unions occur in the setting of impaired biological activity, especially blood supply. Recent evidence does not, however, support this hypothesis. Reed et al. (2002) demonstrated no difference in the number of blood vessels in human atrophic non-union tissue when compare to hypertrophic non-union tissue. Animal studies have shown the pattern of change in vascularity at different time points in normal fracture healing and in atrophic non-union. The vascularity of atrophic non-unions was less in the first three weeks following injury but reached the same level as that in normal healing bone at later time-points (Reed et al., 2003). Bajada et al (2009) successfully isolated MSCs from atrophic non-union tissues; however, the growth kinetic and the osteogenic ability of these cells were diminished. These findings suggest that risk of atrophic non-union might be related to the number and functionality of progenitor cells at the site of atrophic non-union. An understanding of the biological components contributing to atrophic non-union might help to develop appropriate treatment strategies to restore the fracture healing process.

Figure 1.11 Open tibial fracture: Open or compound fracture is a risk of fracture non-union.

1.3.4 **Treatment of atrophic non-union**

Patient history, examination and investigation are all important in the management of atrophic non-union. Fracture severity and associated soft tissue injury should be reviewed. High injury trauma and open fractures are frequently associated with destruction of soft tissues, which may contribute to abnormal fracture healing. Poor general health status and co-morbidities such as diabetes or malnutrition may further impair the healing process, so these factors should be explored. The initial treatment of fractures influences the management of established non-unions. Fixation techniques that are used in fracture fixation have differing effects on the residual soft tissues as well as the remaining blood supply to the fracture site (Wagner, 2003). Infection of primary fixation increases the risk of septic non-union. Routine full blood count (FBC), erythrocyte sedimentation rate (ESR) and C- reactive protein (CRP) are useful for septic investigation. The CRP is the most sensitive biochemical test for infection, but is non-specific (Wright and Khan, 2010). In most cases, radiography is important in confirming the diagnosis, and in addition demonstrates if there is any deformity. CT and MRI may be useful for investigation in some circumstances where the diagnosis is unclear.

For any non-union, the cause should be identified and any deficient elements should be corrected. For example, hypertrophic non-union results from excessive movement especially in the later stages, and the treatment consists of increasing the stability of the fracture. In atrophic non-union, which can occur as a result of deficient biological support, cells and growth factors may be required. Non-unions with an associated bone defect may need the defect to be filled by distraction osteogenesis, a tissue engineered construct with an osteoconductive/inductive/genic scaffold or by bone graft. The diamond concept describes four main elements required for tissue engineering of bone: Osteogenic cells, Osteoconductive scaffolds, Mechanical environment and Growth factors (**Figure 1.12**) (Giannoudis et al., 2007).

Conventional bone graft from the iliac crest (also known as iliac crest bone graft (ICBG)) still remains the standard treatment for non-union as it contains osteogenic

(osteogenic cells, bone progenitor cells), osteoinductive (growth factors) and osteoconductive (bone matrix) properties. **Figure 1.13** shows an atrophic non-union that developed following fracture of the ulnar shaft that was subsequently treated with ICBG. Chip bone grafts that are harvested from the iliac crest are applied into the non-union site. However, the harvest of ICBG is associated with donor site morbidities, including post-operative pain, immobility and prolonged hospital stay (Schwartz et al., 2009).

Therefore, alternative methods to improve bone healing such as cellular therapy, synthetic bone substitutes and other growth factors or adjuvant therapies e.g. ultrasound, and electromagnetic radiation have been investigated in fracture non-union. These interventions may promote and prevent atrophic non-unions in fractures at greatest risk. However, further investigation of their effectiveness and mechanisms by which they influence bone healing is still required.

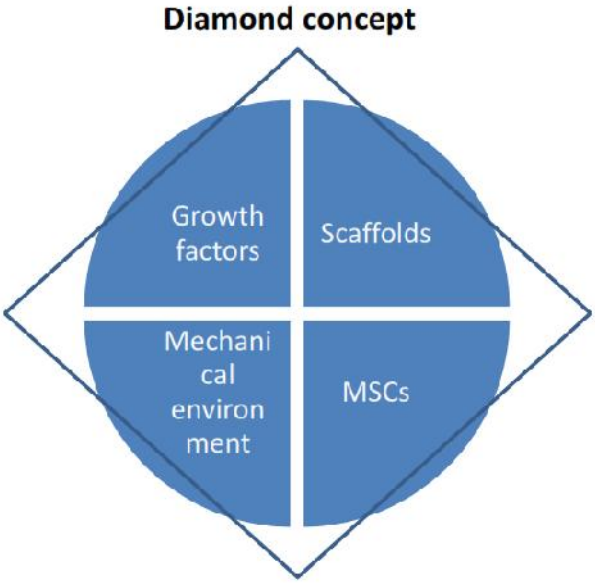

Figure 1.12 Diamond concept of elements required for fracture healing: Modified from Giannoudis et al. (2007)

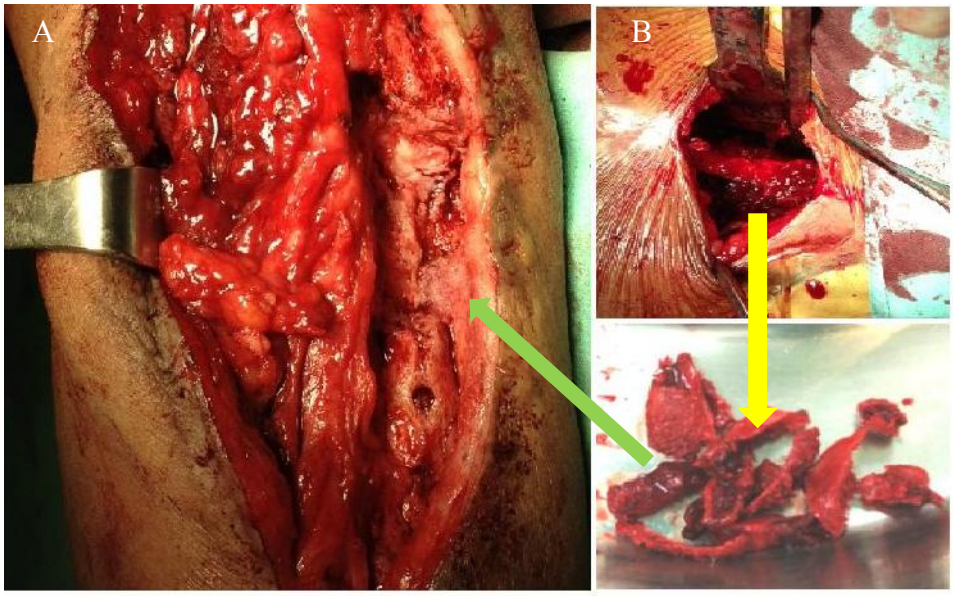

Figure 1.13 Atrophic non-union of the ulnar (a) and the bone graft from iliac crest (b) (yellow arrow) applied at the non-union site (green arrow)

1.3.5 **Augmentation in fracture non-unions**

There are a number of reports in the literature of biophysical stimulation devices such as ultrasound and electromagnetic units as well as orthobiologics such as BMP proteins used in the management of fracture non-unions. Recently, cell therapies such as stem cells have attracted great interest in the treatment of non-union of fractures. These modalities should, however, be used at only appropriate time points and only in selected patients.

Low intensity pulsatile ultrasound (LIPUS) is a biophysical technique that utilizes mechanical energy (high acoustic pressure wave) transmitted from the skin into bone. It has been suggested that LIPUS influences cellular activity via micromechanical stimulation of matrix or protein synthesis from osteoblasts and progenitor cells (Li et al., 2003, Yang et al., 1996). Although the mechanisms by which biophysical treatments exert their effect remain unclear, several clinical trials have shown that these treatments can improve fracture healing process (Gebauer et al., 2005, Bashardoust Tajali et al., 2011). A meta-analysis of LIPUS treatment in

early stage of fracture healing (fresh fractures) has reported that time to healing in the LIPUS treatment arm was less than in the placebo group (Bashardoust Tajali et al., 2011). According to a study from Japan, in which 72 cases of long bone fracture were analysed, the overall union rate from LIPUS treatment was 75%, whereas the cases which were treated within six months had 89.7% of union rate. The study group recommended that LIPUS treatment should be started within six months of the most recent treatment (Jingushi et al., 2007). These studies confirm that it is important to consider the most appropriate timing of interventions when considering the treatment of non-union.

Extracorporeal shock wave therapy (ESWT) has been introduced in the treatment of non-unions. This technique was originally described in urology, where it was utilized to breakdown ureteric stones. There are several proposed mechanisms by which ESWT may promote bone regeneration. The finding from a study using a rabbit model showed that ESWT induced micro-fractures which resulted in subperiosteal haemorrhages, foci of fractures and displaced bony trabeculae. A radiolucent area was observed in the bone marrow, but no gross fracture. In addition, intense bone formation at cortical bone was demonstrated (Delius et al., 1995). It was considered that micro-fractures created by ESWT may trigger neovascularization, proliferation and activation of bone progenitors and stimulation of bone matrix synthesis. It has been reported from clinical studies demonstrating the success of using ESWT in management of cases with abnormal fracture healing without adverse effects (Elster et al., 2010, Wang et al., 2001). Bara and Synder (2007) reported that there was an unsatisfactory outcome in patients with atrophic non-unions who had a large fracture gap. The authors considered that it was important to use ESWT for specific indications in well-selected patients.

The effects of electromagnetic field on non-union have been widely investigated. This technique was originally developed by Bassett et al in 1981. In a case series of 127 ununited fractures of the tibial diaphysis, they reported that 87% of cases were successfully treated by electromagnetic stimulation (Bassett et al., 1981). Electromagnetic coils were connected to a portable generator, which delivered the current to the area around the fracture site (Aaron et al., 2004). It has been reported

that electromagnetic field upregulates gene expression in osteoblasts to produce growth and stimulate factors that contribute to fracture healing, as well as stimulating the synthesis of extracellular matrix (Fitzsimmons et al., 1995, Chalidis et al., 2011). Randomised, double-blind studies showed that the combination of either surgical (Simonis et al., 2003) or non-surgical treatment (Sharrard, 1990) with electromagnetic approach resulted in a better outcome. These studies conclude that electromagnetic therapy may be best used as an adjunct to other treatment options.

A number cytokines, growth factors and hormones play important roles in the fracture healing process. Bone Morphogenetic protein-7 (BMP-7) has already been adopted in the management of fracture non-unions. BMP-7 plays a key role in osteoblast differentiation via induction of Smad1 (Yavropoulou and Yovos, 2007). A prospective randomised clinical study was conducted in 122 patients diagnosed with tibial pseudoarthrosis of at least nine months duration. An intramedullary nail was used for all cases with the authors comparing the influence of adjunctive autologous bone graft and BMP-7. The success rate of both treatments was comparable. However, in smokers, BMP-7 showed better healing outcomes than autologous bone graft (Friedlaender et al., 2001). Regarding cost-effectiveness, the use of BMP-7 has been recommended selected cases such as for severe open fractures or in high risk patients (Garrison et al., 2007, Garrison et al., 2010)

Bone marrow aspirate contains cellular components, which may be beneficial in the treatment of fracture non-union. Bone Marrow Aspirate contains a heterogeneous population of mononuclear cells, including MSCs. MSCs are capable of osteogenic differentiation and are involved in the normal fracture repair process. The first use of bone marrow aspirate was reported in a case of an infected non-union of the tibia(Connolly and Shindell, 1986). These authors subsequently reported a case series of 100 tibial non-unions with an 80% success rate with bone marrow aspirate injection (Connolly, 1998). In a study reported by Goel et al (2005), the treatment was performed under local anaesthesia; 3 to 5 millilitres of bone marrow aspirate was harvested each time from the iliac crest. Up to a maximum of 15 millilitres was injected into the non-union site under fluoroscopy guidance. The procedure was repeated at four to six weeks in the absence of clinical and radiological union. The

union rate was 75 % (n=15), with average time following first injection of 14 weeks (Goel et al., 2005). This study suggested that cellular injection might be used as a minimally invasive technique. However, the technique was limited by the volume of bone marrow aspirate that could be injected at the fracture site. Hence, concentrated bone marrow aspirate has been introduced to increase the yield of MSC with less overall volume. Hernigou et al. (2005) studied 60 atrophic non-union patients treated with concentrated autologous bone marrow aspiration. The concentrated autologous bone marrow aspirate was introduced using a percutaneous technique. This study reported a success rate approximately 90% (n=53) with average time to union of 12 weeks. The number of colony forming unit fibroblasts from concentrated autologous bone marrow aspirate in those cases, which failed to unite, was significantly lower than the number of cells in successful cases. It was concluded that the success rate of treatment was dependent on the number of MSCs. This supports the expansion of MSCs isolated from bone marrow in cultures to increase the yield of cells available to inject into the non-union. Until now, only case reports have reported the use of MSCs in non-union (Bajada et al., 2007, Funk et al., 2007). Further investigations are still required before the widespread clinical use of MSCs in the management of non-union.

There are several emerging technologies that aim to improve and promote fracture healing. They are of intent interests to orthopaedic surgeons and scientists. However, the mechanisms by which these treatments bring about effects require further investigation. Patient selection and the time point for delivering any intervention are critical. It would be preferable to have an effective treatment to prevent non-union rather than purely for treating well established non-union.

1.4 Animal models of non-union

Since the 1990s, major progress has been made in the field of regenerative medicine. Developments in adult and embryonic stem cell research as well as the

improvements of material sciences hold great promise for the regeneration of bone. Pre-clinical research using appropriate animal models are needed before this work can be translated into benefits for patients. Animal models should be selected for appropriateness in order to gain the most accurate answer to the research question (Einhorn, 1999). In this thesis, the primary question was to investigate the therapeutic effects of adult stem cells in the prevention of atrophic non-union. Thus, it was important to have a disease model of atrophic non-union that accurately reflected the abnormal physiological process of fracture healing. Important considerations included choosing an appropriate animal species, types of fixation and mode of generation of the atrophic non-union.

1.4.1 **Small animal models of fracture healing**

Small animals are widely used in studies of fracture healing. Experimental models in small animals present advantages over using larger animals. For example the cost of maintenance is lower, the experimental time points are shorter, and a larger number of animals can be used. Rats are the most commonly used animals in fracture healing studies (O'Loughlin et al., 2008). In considering an appropriate animal model the following factors should be taken into account: 1) appropriateness as an analog, 2) transferability of information, 3) genetic uniformity of organisms, where applicable, 4) background knowledge of biological properties, 5) cost and availability, 6) generalisability of the results, 7) ease of, and adaptability to experimental manipulation, 8) ecological consequences, and 9) ethical implications (Davidson et al., 1987). The process of fracture healing has been investigated in small animals such as mice and rats in order to understand the process of fracture healing in human (Urist and Mc, 1950, Nunamaker, 1998). Although large animals may be more appropriate for bone healing studies, the bone remodelling process in rats and mice involves the generation of a resorption cavity that is similar to the large animals. Moreover, the costs for maintenance of animals and biological agents given to the animal are less in small animals than in large animals. There are also more molecular

tools available for the investigation and assessment of fracture healing in the rodent model. The rat model is more commonly used than the mouse model in fracture healing studies, because the stabilization procedure is more reproducible. Rat bones also are larger than mouse bones so the biomechanical aspects of fixation are more easily controlled.

The animal model of fracture healing should reflect the clinical scenario. Therefore, the fracture models have been classified into nine categories depended on the clinical scenario; 1) normal fracture repair, 2) established delayed non-union, 4) established hypertrophic nonunion, 5) atrophic non-union, 6) segmental or critical size defect, 7) high-energy, comminuted and open injury models, 8) bone repair with infection 9) fracture repair in compromised host models (Mills and Simpson, 2012). Understanding these models is important and the best model should be selected based on the central question being asked in the study.

1.4.2 **Selecting the mode of fixation**

Because of the small size of the rodent model, development of a fixation device is challenging. Fixation devices contribute to the mechanical environment at the fracture site with implications for the healing process. Many fracture fixations have been reported in small animals. They can be simply divided into three categories (**Figure 1.14**); intramedullary fixation device, plate fixation device and external fixation device. Intramedullary fixation devices, for instance intramedullary pins (Bhandari and Shaughnessy, 2001), locking nails (Holstein et al., 2007) or interlocking nails (Garcia et al., 2011) and intramedullary compression screws (Holstein et al., 2009) can be applied using less invasive surgical techniques for surgical exposure. These fixations, however, introduce damage to the medullary canal making histological assessment of the fracture gap difficult. Plate fixation is the most reliable technique for anatomical reduction and stable fixation (Histing et al., 2010). The drawback of plate fixation is that it requires an invasive surgical

approach that disrupts soft tissues around the fracture site. External fixators have a high axial and rotational stability (Claes et al., 2009). The fracture site is totally unaffected by the presence of the fixators allowing histological assessment of the fracture site.

Figure 1.14 Fixation devices in small animal models: (a) plate fixation from Histing et al. (2010), (b) intramedullary fixation from Histing et al. (2010) and (c) external fixator from Reed et al. (2002)

1.4.3 **Methods for creating atrophic non-union in animal models**

Models used in bone healing research can be applied to evaluate normal fracture healing, healing of segmental bone defects, critical size defects and fracture non-union without a critical size defects. The critical-size defect model describes a model in which the fracture gap is sufficiently large to prevent bone healing or bone bridging. Conversely, in an atrophic non-union model or non-union model without a critical size defect, mechanical manipulation at the fracture that destroys soft tissues or biological components around the fracture site is required. Pre-clinical studies evaluating stem cell augmentation in bone repair have largely utilised critical-defect models (Wolff et al., 1994, Tsuruga et al., 1997). However, in clinical practice, atrophic non-union usually occurs in association with high energy mechanisms of injury that causes severe soft tissue injury or loss, regardless of bone defect size. Non-union models without critical size defects may be more appropriate in the study

of stem cell therapy for established atrophic non-union or fractures at risk of atrophic non-union. Procedures used to produce soft tissue injury or periosteal disruption from high injury trauma have included cauterization (Kokubu et al., 2003, Kaspar et al., 2008) or stripping of the periosteum with intramedullary curettage (Brownlow and Simpson, 2000, Reed et al., 2003). The method using periosteum stripping and intramedullary curettage is relatively simple and does not require specialised equipment. Reed et al. (2003) reported that atrophic non-union can be induced at the tibial mid shaft by stripping the periosteum and endosteum as well as creating a small (1.0 mm) non-critical size gap. Here, the tibia was stabilised with an external fixator. They also found that in the early stages of atrophic non-union the gap between the bone ends was deficient of biological components such as vessels, growth factors or cells that might cause an atrophic non-union. This technique is thought to be appropriate and closely reflect atrophic non-union seen in clinical scenario.

1.5 Mesenchymal stem cells and their role for bone regeneration

There are two types of natural stem cells based on their origin; embryonic stem (ES) cells and adult stem cells. ES cells are derived from the inner cell mass of the blastocyst. They are pluripotential stem cells with the capacity to differentiate into cells of all primary germ layers: ectoderm, mesoderm and endoderm (Thomson et al., 1998). However, they are limited by a number of factors including a technical limitation such as isolation and culture techniques, concern regarding tumour formation and major ethical controversy (Baschetti, 2005, Vats et al., 2005). Recently, it has been reported that somatic cells can be genetically induced to pluripotent stem cells by introducing four factors including Oct3/4, Sox2, c-Myc, and Klf4 (Takahashi and Yamanaka, 2006, Takahashi et al., 2007). These cells are known as induce pluripotent stem (iPS) cells. Although these cell have high proliferative potential and pluripotency, the induction of this cells is an artificial

process which may also increase risk of forming teratoma (Gutierrez-Aranda et al., 2010). For these reasons, it is unlikely that ES and iPS cells will be used for orthopaedic clinical applications in the near future. Adult stem cells are found in adult tissue. These cells can be used autologously, negating much of the ethical controversy. They have been isolated from several tissue types (Zuk et al., 2002, Noth et al., 2002, Tuli et al., 2003, Miura et al., 2003, Young et al., 2001, De Bari et al., 2001, De Bari et al., 2006). Mesenchymal Stromal /Stem Cells (MSCs) derived from the bone marrow are the most commonly described source of MSCs and have been widely used to promote tissue regeneration in orthopaedic conditions.

1.5.1 Characteristics of bone marrow derived mesenchymal stromal/ Stem cells

In orthopedic surgery, iliac bone graft is commonly used to treat fracture non-unions and also used in other procedures such as spinal fusion. Bone marrow from iliac bone contains MSCs that constitute approximately 1 in 10,000 of all nucleated cells (Chamberlain et al., 2007). Friedenstein et al. (1970) reported that this rare population of cells could be isolated on the basis of their ability to adhere to culture plastic. These cells were capable of proliferation and differentiation into multiple mesodermal lineages (Pittenger et al., 1999, Caplan, 1991). There is controversy concerning which antigens identify MSCs and immunological techniques are therefore not widely used to isolate MSCs. Currently, most of MSCs used in studies are isolated by plastic adherence in a process similar to that described by Friedenstein et al. (1970). A direct bone marrow plating method is commonly used for cells from small animals (Lennon and Caplan, 2006, Nadri et al., 2007). With human bone marrow, density gradient centrifugation is the most commonly used method for isolating MSCs.

MSCs are identified by their ability to proliferate and undergo mutilineage differentiation. The colony-forming unit–fibroblast (CFU-F) is defined as a highly adherent colony of fibroblastic-like cells formed from a single mother cell. Thus, the

CFU-F assay has been used to assess bone marrow progenitors. The number of colonies formed from the total number of seeded marrow cells indicates colony-forming efficiency (CFE). This assay indicates the percentage of cells in the marrow that are capable of clonogenic expansion. It has been demonstrated that CFU-F populations are not homogeneous but rather contain a hierarchy of progenitors including multipotential MSCs and committed progenitors (Friedenstein et al., 1992, Latsinik et al., 1986).

MSCs express a number of surface markers. These markers include a mixture of cell surface receptors, adhesion molecules, extracellular matrix proteins, cytokines and other molecules whose function is to communicate with other cells. These markers are used to characterise MSCs. However, controversy remains regarding the set of surface markers that are expressed by bone marrow-derived stem cells. MSCs do not express: CD45 which is expressed in Hematopoietic stem cell (HSC) (McKinney-Freeman et al., 2009), CD14 which is expressed in innate immune cells (Cros et al., 2010) and CD34 which is expressed in HSCs, satellite cells and endothelial progenitors (Nielsen and McNagny, 2008, Parant et al., 2009).

Mesenchymal stem cells have been reported to express: STRO-1, CD105, CD90, CD73, CD166, CD44, CD29 and CD54. These markers are expressed on all isolated MSCs from bone marrow (Pittenger et al., 1999, Jiang et al., 2002). STRO-1 is an early marker for stromal precursors and the subpopulation of cells from bone marrow which are STRO-1 positive are able to generate CFU-F as well as differentiate into multiple mesenchymal lineages (Simmons and Torok-Storb, 1991).

Up until now, no unique marker for MSCs has been described. Thus, a combination of markers is used to identify and sort MSCs. The combination of CD10+, CD13+, CD56+, and MHC Class-I + markers has been reported to identify a population of lineage-committed progenitor cells and lineage-uncommitted pluripotent cells(Young et al., 1999). The combination of VCAM+, STRO-1+, CD73+, CD105+ markers has been reported to isolate MSCs from human trabecular bone (Tuli et al., 2003). D7-FIB+, CD13+; CD45-, GPA-, LNGFR+ has been reported to select adherent cell

monolayers that undergo chondrogenesis, osteogenesis, and adipogenesis (Jones et al., 2002).

MSCs constitute a heterogeneous population of cells, in terms of their morphology, physiology and expression of surface antigens. The Mesenchymal and Tissue Stem Cell Committee of the International Society for Cellular Therapy has proposed criteria necessary to define human MSCs. First, MSCs must be plastic-adherent when maintained in standard culture conditions. Second, MSCs must express CD105, CD73 and CD90, and lack expression of CD45, CD34, CD14 or CD11b, CD79a or CD19 and HLA-DR surface molecules. Third, MSCs must differentiate to osteoblasts, adipocytes and chondroblasts in vitro (Dominici et al., 2006)

1.5.2 **The differentiation potential of MSCs**

MSCs have an ability to differentiate in *vitro* in specific culture media (**Figure1.15**). For osteogenic differentiation, dexamethasone, ascorbate and β-glycerophosphate are required (Stenderup et al., 2001). 1, 25-vitamin D3 has been reported to increase mineralization in human bone marrow-derived stem cells culture (Jorgensen et al., 2004). Their morphology and cytoskeletal components are changed when they differentiate into osteoblasts. Furthermore, they express several different markers with osteogenesis such as Runx-2/Cbfa-1, Osterix, alkaline phosphatase, Bone sialoprotein, Osteopontin, Osteocalcin, Osteonectin and Osteocrin (Heng et al., 2004).

For chrondrogenesis, transforming growth factor beta, ascorbate, and dexamethasone are required. MSCs are capable of chrondrogenesis and the expression of biochemical markers including transcription factors (sox-9, scleraxis) and extracellular matrix (ECM) genes (collagen types II and IX, aggrecan, biglycan, decorin, and cartilage oligomeric matrix protein) are associated with chrondrogenesis which can be found during their development (Yoo and Johnstone, 1998, Herlofsen et al., 2011, Pittenger et al., 1999).

To induce adipogenesis, adipogenic media consisting of dexamethasone, insulin, isobutylmethylxanthine, and indomethacin is required (Pittenger, 2008). In these conditions, cells will differentiate increasing PPAR-γ (Peroxisome proliferator-activated receptor gamma) and other adipose specific factors such as lipoprotein lipase. PPAR-γ has been found to be important in the development of adipocytes (Rosen and Spiegelman, 2000). It can also be used as a marker for adipogenic differentiation.

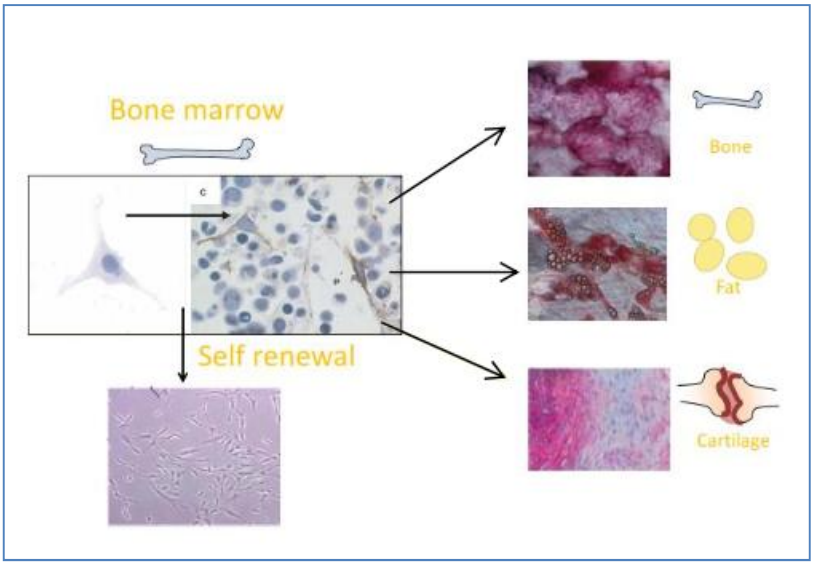

Figure 1.15 Mesenchymal stem cells: MSCs are capable of proliferation and differentiation into bone, fat and cartilage cells. Adapted from Pittenger (1999)

1.5.3 **Mesenchymal stem cells as bone progenitor cells and trophic factor secreting cells for bone regeneration**

Osteogeneic differentiation of MSCs in bone repair or regeneration is desirable because MSCs are believed to represent *in vivo* bone precursors. In *in vitro* culture, it has long been accepted that MSCs can differentiate into osteoblasts (Pittenger et al., 1999, Muraglia et al., 2000). MSCs contribute not only in a physiological process but also in a reparative process. As bone is a dynamic tissue, which degrades and

regenerates throughout life, it has an inherent capacity for remodelling. In this process, osteoclasts make a tunnel into the bone (i.e. a cutting cone) and then MSCs, osteoprogenitor cells and osteoblasts fill up the cone with new bone with living cells (Buckwalter et al., 1996). Bone is unique in that it can regenerate itself without scar formation after injury. MSCs play an important role in bone regeneration after injury or trauma. They originate from the periosteum, endosteum, bone marrow, and possibly the vasculature of the muscle tissue and are recruited to differentiate into osteoblasts. Although bone can be generated through intramembranous or endochondral formation, both processes result in mature osteoblasts which make a mineralised tissue or bone nodule recognisable as bone. This process has three developmental stages: proliferation, extracellular matrix development/maturation and mineralization (Aubin, 1998).

Each stage involves several mediators. Bone morphogenetic proteins (BMPs) have been widely reported to be integral to the bone formation process. BMP-mediated osteoblast differentiation is dependent on the Smad signaling pathway. BMP inducible transcription factors, Runx2 (Cbfa1) and Osx, play an essential role in osteoblast differentiation and osteogenesis (Harada and Rodan, 2003). Runx2 is expressed in mesenchymal cell condensations of the embryonic endochondral skeleton and induces an osteoblast-specific pattern of gene expression (Ducy et al., 1997). Osx is a novel zinc finger-containing transcription factor that is specifically expressed in developing bones. Ectopic expression of Osx in non-osteoblastic lineages induced expression of osteocalcin and collagen I which are osteoblast producing proteins (Nakashima et al., 2002). Abnormality of these genes may lead to congenital bone disease. Runx2 gene defects cause Cleidocranial dysostosis syndrome which is characterized by abnormal intramembranous ossification. This phenotype has been demonstrated in a mouse model in which animals die at birth and lack bone and tooth development (Aberg et al., 2004).

There are also several markers expressed during the developmental stage where MSCs differentiate into osteoblasts. Osteocalcin which is a bone-specific glycoprotein may promote bone matrix calcification. Osteopontin which is a phosphoprotein that plays role in cell attachment and proliferation as well as

mineralization of bone matrix. Osteonectin is one of the important non-collagenous proteins associated with bone mineralization stages (Aubin, 1998). Expression of all these factors could be used to indicate late osteogenesis in *in vitro* culture of MSCs (Donzelli et al., 2007).

However, the role of MSCs in bone repair is not only to act as progenitors but also to secrete trophic factors. Several studies have demonstrated that MSCs produce many cytokines and mediators including interleukin-1, -6, -7, -8, -11, -14 and-15, leukaemia inhibitory factor (LIF), stromal cell-derived factor (SDF-1), stem cell factor (SCF-1), Flt-3 ligand, macrophage-, granulocyte- and granulocytemacrophage-colony stimulating factors (M-, G-, and GM-CSF) and vascular endothelial growth factor (VEGF) (Haynesworth et al., 1996, Majumdar et al., 1998, Hung et al., 2007)

Trophic mediators from MSCs are thought to contribute to regulation of the fracture healing process. Pro-inflammatory cytokines which play a role in the inflammatory phase of fracture healing include IL-1,-6 and TNF-α (Kon et al., 2001). These pro-inflammatory cytokines recruit inflammatory cells and remote MSCs to the site of injury as well as stimulating the synthesis of extracellular matrix (Einhorn et al., 1995). Bone morphogenetic proteins (BMPs) are important in the process by which MSCs differentiate into more committed osteoprogenitor cells and osteoblasts (Chen et al., 2012). The FGFs and VEGFs are angiogenic factors involved in neovascularization during the proliferative phase (Ferrara and Davis-Smyth, 1997). Moreover, a number of other cytokines including platelet-derived growth factor (PDGF), transforming growth factor-beta (TGF-b), growth differentiation factors (GDFs) stimulate and enhance MSCs during fracture repair (Lieberman et al., 2002).

In addition to their contribution to bone healing, the paracrine effects of MSCs have been shown to be chrondroprotective in OA models (Murphy et al., 2003). Furthermore, evidence from cardiovascular regeneration studies confirms that the therapeutic improvement seen following the application of MSCs in a heart injury models occurs not only through engraftment, but also through enhancement of angiogenesis and prevention of cardiomyocyte apoptosis (Xiang et al., 2009, Tang et

al., 2005). It has been therefore suggested that secretion of growth factors and cytokines is a major way by which MSCs may promote tissue regeneration.

1.5.4 **Donor factors influencing MSC characteristics**

There are several conditions such as aging, excessive alcohol ingestion, smoking, and osteogenesis imperfecta that affect the behaviour and quantity of MSCs within tissues. MSCs from patients with these conditions may be impaired and have perturbed function in bone regeneration and fracture healing. In high energy trauma or open fractures, the periosteum at the fracture site, which serves as a major source of bone progenitors is damaged. This can negatively affect the fracture healing capacity and increase an individual's risk of non-union. Thus, in these impaired hosts, an exogenous source of MSCs should be considered as a therapeutic option to augment fracture healing.

It has been reported that ageing influences the behavior MSCs. (Stolzing et al., 2008, Nishida et al., 1999, Muschler et al., 2001, Majors et al., 1997). There is a decrease in the yield of MSCs isolated from the bone marrow of older patients. The CFU-F assay is a classic method to determine the number of MSCs with in any given tissue. The number of colony forming of bone marrow cells was found to fall with increasing age of donors. Aging affects the differentiation potential of MSCs. MSCs from older donors cultured under osteogenic and chondrogenic *in vitro* condition had significant less ALP activity and GAG content compared to younger or donors (Sethe et al., 2006). The finding from studies into osteoporosis have shown that the aging process accelerates adipogenic differentiation capacity of MSCs and favours adipogenic over osteogenic differentiation (Rodriguez et al., 2008). The fall in osteogenic potential is a result of imbalance of two main transcription factors, namely RUNX-2 and PPAR-γ (Kim et al., 2012). A report from animal study evaluating the effects of transplantation of BMMSC in mice, animals underwent whole body X-irradiation (500 cGy) to eradicate host bone marrow stem cells.

Animals who subsequently received MSCs isolated from young mice had significant improvement in bone mineral density over the period of six months after transplantation compare to those who received cells isolated from aged mice (Shen et al., 2011). The use of autologous MSCs in elderly patients may be limited by reduced potency of the cell's ability to promote bone repair and regeneration, so alternative cell sources or interventions should be considered to promote the fracture healing in this particular group.

A reduction in bone progenitors is associated with heavy alcohol consumption. It has been reported from *in vitro* and *in vivo* studies (Giuliani et al., 1999) that the ability of MSCs to form the colonies was reduced when cells were exposed to ethanol and acetaldehyde and this effect was dosed dependent. The same study also reported that CFU-F formation in bone marrow cultures from alcoholic patients was significantly less than healthy controls. Alcohol also affects the gene expression of type I collagen and significantly reduced its synthesis during the *in vitro* osteogeneic induction of human bone marrow derived MSCs. It alters osteogenic differentiation (Gong and Wezeman, 2004) and may distrup in the reparative process. It has been reported that alcohol suppresses osteogenic differentiation and matrix synthesis by MSCs, while adipogenesis is promoted (Chakkalakal, 2005). In this animal study, rats that were given alcohol daily for 3 months (7.6 g of 95 % ethanol/ kg body weight per day) had lower bone mineral density than controls (Broulik et al., 2010, Hogan et al., 1999). Bone morphology and mechanical properties also deteriorated in animals treated with alcohol (Broulik et al., 2010). The number of MSCs from patients, who have chronic heavy alcohol consumption and their ability to differentiate is impaired, suggesting that excessive alcohol intake may impair the fracture healing process and inhibit bone regeneration.

Nicotine is an organic substance found in all types of cigarettes and is responsible for smoking addiction (Sofuoglu and LeSage, 2012). A number of studies have shown that nicotine has negative effects on bone quality including bone mass, bone turnover and bone strength in small animals (Akhter et al., 2003, Iwaniec et al., 2001, Broulik et al., 2007). Smoking is a risk factor for delayed healing of fractures and non-union. In prospective cohort studies, smoking has been shown to increase the mean time to

union and to be associated with other fracture complications such as osteomyelitis (Adams et al., 2001, Castillo et al., 2005). It has been reported that smoking is significantly associated with failure of operative treatment of established non-unions of the scaphoid bone. In this study, the operative fixation consisted of internal fixation with autologous bone grafting. There was a significant difference in the rate of union between non-smokers (the success rate was 82.4%) and smokers (the success rate was 40.0%). Smoking not only reduces the blood supply to the fracture site but also impairs progenitor cells (Gullihorn et al., 2005). MSCs in autologous bone grafts of smokers may be impaired because of the effects of smoking. The yield of MSCs in bone marrow from smokers has been found to be significantly lower than from non-smokers (Beyth et al., 2008). In addition there is a reduced yield of VEGF-A and IL-6 from MSCs isolated and cultured from fracture heamatoma (Sloan et al., 2009). Thus, the contribution of autologous MSCs to fracture healing in smokers may be reduced. Therefore an alternative exogenous source of MSCs should be considered if MSCs are used to treat non-unions in smokers.

High blood glucose alters the function of vascular progenitors (Khan and Chakrabarti, 2006). Similarly, high glucose affects the growth and differentiation potential of bone marrow MSCs (Keats and Khan, 2012, Li et al., 2007). Results from *in vitro* studies (Keats and Khan, 2012) demonstrate that high blood glucose decreases the expression of Runx-2 and SP7 (osteogenic transcription factors) by MSCs in osteogenic media but increases the expression of Sox9 and Nkx3.2 (chondrogenic transcription factors) in chondrogenic conditions. The ability for MSCs to resist glucose toxicity is dependent on MSC stemness (Li et al., 2007). Results from pre-clinical studies indicate that MSCs from type 2 diabetic db/db mice do not improve neovascularization in an ischemic limb model, while adipogenesis is promoted. This study also showed that Nox4-acitvity generated oxidative stress and decreased the multipotency of MSCs (Yan et al., 2012). Overall, these studies suggest that the blood glucose levels should be well controlled, especially during the fracture healing period. However, the evidence that high blood glucose levels impair MSCs in fracture healing remains limited.

Some congenital bone diseases increase the risk of fracture. Osteogenesis imperfecta (OI) is a genetic disorder in which the collagen type 1 gene is mutated. OI patients present with multiple fractures and the severity of disease depends on the type of OI (van Dijk et al., 2011). There is abnormal collagen type 1 structure, which is the main collagenous component of bone matrix. Autologous cell based therapy may be problematic because of the effects of disease causing the alteration of MSCs or bone progenitors (Gioia et al., 2012), unless the cells are genetically manipulated to correct the mutation (Chamberlain et al., 2008). The cells for transplantations for OI treatment can be donated from healthy bone marrow and preliminary results from clinical studies show promising results with MSC treatment (Horwitz et al., 2002). This suggests that allogeneic transplantation of MSC for bone regeneration is possible.

Local progenitors that contribute to bone healing are found at the peristeoum and also within the fracture haematoma (Oe et al., 2007, Malizos and Papatheodorou, 2005). In more severe injuries and especially with open fractures, the risk of fracture non-union is increased, which may be as a consequence of damage to the source of progenitor cells. It has been demonstrated in animal models that removal of the periosteum and fracture haematoma at the initial phase of fracture healing impairs the process of fracture repair and there was a decrease in periosteal cell proliferation compared to the control group (Ozaki et al., 2000, Grundnes and Reikeras, 1993). Local anaesthetics such as levobupivacaine, lidocaine or bupivacaine that are used to control pain locally, for example as a part of a haematoma block of distal end radius fracture, may influence healing by having a negative effect on bone marrow MSC proliferation and osteogenesis (Tayton et al., 2012). The local biological components contributing to fracture healing are impaired in high energy fractures, so augmentation of biological factors such as by providing additional bone marrow cells during healing may improve fracture healing and prevent progression to non-union.

Bone fracture has a systemic effect on bone marrow MSCs. It has been reported that the yield of MSC from bone marrow from patients with multiple fractures was significantly increased whereas the yield and proliferation ability of MSC from bone marrow decreased in an established atrophic non-union (Seebach et al., 2007). It has

been reported that cells isolated from human non-union tissues demonstrate increased levels of cell senescence and reduced capacity to form osteoblasts which is associated with significantly elevated secretion of Dickkopf-1 (Dkk-1) (Bajada et al., 2009). In addition, there is significant down-regulation of factors including canonical Wnt-, IGF-, TGF-beta-, and FGF-signaling pathways in non-union osteoblasts. These factors are involved in the proliferation and differentiation of bone progenitors (Hofmann et al., 2008). These results suggest that progenitors at the site of atrophic non-union have impaired function. Thus, exogenous MSCs or growth factors may be required to support fracture healing.

1.6 Clinical issues relating to MSC transplantation for bone regeneration in atrophic non-union

1.6.1 The options for application of MSCs for bone regeneration

MSCs can be delivered systemically via intravenous injection. It has been reported that MSCs can migrate to an injured site (Li and Jiang, 2011, Van Linthout et al., 2011). Recently, the mechanism by which homing occurs has been investigated. The matrix metalloproteinase (MMP)-dependent pathway may be associated with cell trafficking. Hypoxia-inducible factor-1 (HIF-1) promotes stromal –derive factor-1 (SDF-1) which is a ligand of CXC chemokine receptor-4 (CXCR-4) on the progenitor cells (Ceradini et al., 2004). The injury site is hypoxic and thus this pathway may contribute to recruitment of MSCs to sites of injury. Furthermore, it has been reported that a systemic intravenous injection of CXCR4-expressing MSCs can reduce bone resorption, increase bone matrix formation and improve bone stiffness and strength in osteoporotic mice induced by dexamethasone (Lien et al., 2009). Horwitz et al. (2002) demonstrated the beneficial effects of intravenous administration of MSCs in patients with osteogenesis imperfecta. Although, it was a small cohort study, the results showed significant more acceleration of growth

velocity in the MSC treatment group than in the control. The growth velocity was improved from 60% to 94% (median, 70%) of the predicted median values for age- and sex-matched unaffected children. In a fracture healing study, it was reported that intravenous MSC transplantation had a positive effect on fracture healing in mouse models and transplanted MSCs could migrate and engraft at the callus endosteal niche (Granero-Molto et al., 2009). However, the exact mechanism by which this occurs remains controversial and the migration efficacy is extremely low for systemic transplantation of MSCs. MSCs may distribute not only to the fracture site but also to other tissues (Gao et al., 2001, Devine et al., 2003). Previous reports demonstrated that most of the MSCs delivered by intravenous infusion were trapped in the lungs (Gao et al., 2001, Schrepfer et al., 2007). Therefore, an alternative method of delivery such as local injection may be more practical for orthopaedic applications, particularly in the case of fracture non-union, which usually results from local biological failure.

To overcome issues of migration and homing, local implantation at the fracture site can be used. As mentioned in section 1.4, it has been demonstrated that percutaneous injection of either bone marrow aspirate or bone marrow concentration technique are reliable methods of delivery. Connolly (1998) reported that bone marrow aspirate injection in fracture non-unions could improve the healing rate. Hernigou et al. (2005) demonstrated that percutaneous injection of bone marrow concentrate could treat fracture non-union. This mode of delivery is simple, and minimally invasive. Thus, the delivery of expanded MSCs, isolated from bone marrow, might be also applied by this technique. This technique overcomes problems with MSC migration and other adverse systematic effects.

In non-union cases associated with extensive bone loss or bone defects, iliac bone grafting remains the gold standard treatment. It provides bone and progenitor cells, growth factors as well as the construct for bone regeneration. However, the amount of autologous bone graft is limited and harvesting bone graft from iliac crest can result in a painful scar and numbness around the harvested site, both of which affect quality of life (Littenberg et al., 1998). To address this, bioengineered materials have been developed and have already applied in clinical practice. Many artificial

materials are available for clinical use. So far, calcium phosphate based ceramics such as hydroxyapatite (HA), β-tricalcium phosphate (β-TCP), bioactive glass and ceramic based graft artificial materials have been most used in the fields of orthopaedic trauma and arthroplasty. Calcium phosphate ceramics are synthetic scaffolds that have been used as bone substitute in orthopaedics since 1980s (Hak, 2007, Bohner, 2000). Autologous MSC transplantation with ceramic cylinders has been successfully used to treat segmental femoral defects in rats (Ohgushi et al., 1989) and also in murine craniotomy defects (Krebsbach et al., 1998). In large animal studies using dogs and sheeps, autologous bone marrow derived MSC were delivered together with bioceramic scaffolds. They were reported to have good outcomes for healing segmental defects (Arinzeh et al., 2003, Bruder et al., 1998). Injectable biomaterial is desirable particular for a minimally invasive surgery and can be used as a carrier for stem cell based-therapy for bone repair. Injectable silicate-substituted calcium phosphate bone substitute material has been reported to be an appropriate bone graft material with a particle size of 250–500 μm (Coathup et al., 2013a).

1.6.2 **Immunological effect of MSCs**

Sufficient numbers of MSCs and their functional potential of differentiation are important contributory factors to treatment outcomes (Zhang et al., 2008, Hernigou et al., 2005). However, as mentioned in section 1.3.5, in the clinical setting, the autologous source may be often limited as 1) the yield and differentiation capacity of these cells in bone marrow is decreased in older patients, smokers and those with medical co-morbidities, 2) isolation and expansion of autologous MSCs is time consuming and such delays may detrimental, particularly where the timing of implantation is crucial. Due to the limitation of autologous BMSCs in clinical application, allogeneic sources of BMSCs may be a viable alternative option in atrophic non-union repair. Allogeneic BMSCs can be isolated from young healthy donors. In principle, it should be possible to use MSCs from a universal donor

because of their immune-privileged properties. Thus, harvested MSCs would have the potential to be expanded and cryopreserved for future use, so these cells can be used immediately as required.

Previous studies have demonstrated that BMSCs are immune-privileged. These cells can avoid or actively suppress immunological responses (Aggarwal and Pittenger, 2005, Jones and McTaggart, 2008). MSCs do not induce significant alloreactivity (Barry et al., 2005). These cells are immune-privileged because they lack a major histocompatibility complex (MHC). It has been reported that MSCs express low-intermediate levels of MHC class I and they do not express MHC class II on their surface membrane (Le Blanc et al., 2003). They also lack co-simulation molecules such as CD80, CD86 or CD40 (Tse et al., 2003). Although it has been reported that MCH class II can be induce for expression on the surface of MSCs by interferon gamma (IFN-γ), induced MSCs failed to stimulate proliferation in allogeneic lymphocytes (Le Blanc et al., 2003) because of the absence of co-stimulation molecules.

Several studies have shown that the immunomodulatory properties of MSCs can be beneficial. MSCs have been used in the treatment of graft-versus-host disease (GvHD) in combination with allogeneic HSC transplantation. Here they reduce the host immune response and improve engraftment of HSCs (Cohen and Sudres, 2009, Sato et al., 2010). Systemic delivery of allogeneic MSCs in bone disease has also been reported (Le Blanc et al., 2005). A female fetus with multiple intrauterine fractures, diagnosed as having severe osteogenesis imperfecta was transplanted with allogeneic HLA-mismatched male fetal MSCs at the 32nd week of gestation in the absence of immunosuppressive therapy. There was no evidence of immune rejection of the transplanted cells and donor MSCs could be detected using centromeric XY-specific probe at the age of nine months. This study demonstrated the possibility of allogeneic transplantation in bone systemic bone disease, however, well-controlled clinical trials are yet to be performed.

Xenotransplantation can be used to model extreme immune response conditions (Samstein and Platt, 2001). Due to the unique immunologic tolerance of MSC, it may

be feasible to use MSCs from a universal donor cells. Xenogeneic models have been evaluated in *in vivo* cross-species administration of MSC in a variety of experimental models (Li et al., 2012). The benefit of MSCs being immune privileged has been shown in xenotransplantation for bone defect. Regeneration of the bone tissue after unilateral xenogeneic transplantation of human MSCs was studied in rats with injury to both femurs. The animals did not have local pathological reactions or complications after implantation. Implantation of MSCs was reported to significantly stimulate the reparative osteogenesis. The bone tissue formed after transplantation of MSCs was integrated into bone and underwent complete remodeling (Fatkhudinov et al., 2005). The authors suggested that xenotransplantation of prenatal MSCs without immunosuppression was not followed by the development of early or delayed complications or local reactions of graft rejection. The potential of human MSCs and human osteoblasts for bone regeneration was also compared in rat calvarial defects (Zong et al., 2010). Either human MSCs or human osteoblast in poly-lactic-co-glycolic acid (PLGA) were transplanted into 5 mm in diameter full thickness defect of nonimmunosupressed rat calvarium. Histological analysis showed that the human MSC construct had effective bone regeneration and it was superior to the osteoblast construct. These results suggest that immunogenic characteristics of the cell construct affect functions of the implanted cells.

However, the results of xenotransplantation are inconsistent. Niemeyer et al (2010c), investigated the bone regeneration potential of hMSC after xenogeneic transplantation compared with autogenous rabbit MSC in a critical-size bone defect. Xenogeneic transplantation showed inferior clinical outcomes for bone regeneration. The same group reported results from a large animal study (Niemeyer et al., 2010b). They investigated the effect of xenogeneic transplantation using a 3.0-cm-long sheep tibia bone defect. Autologous bone marrow MSCs resulted in improved bone regeneration potential as demonstrated using radiology and histology when compared to xenogeneic hMSC. However, there were no significant local or systemic adverse effects in both xenotransplantation and autotransplantation.

Using MSCs from a universal donor still remains controversial with recent studies producing conflicting results of the bone regeneration potential of xenogeneic MSCs.

There would be several advantages if allogeneic bone marrow derived MSCs could be used in atrophic non-union without using immunosuppressive therapy. Before adopting MSCs for augmentation therapy in non-union, it is important to understand mechanisms how MSCs enhance the fracture healing process and to evaluate any adverse effects that may result from an immune response.

1.6.3 **Considerations of MSC source and preparation**

In most of the studies that have been conducted to evaluate the therapeutic potential of cell based therapy for bone regeneration utilise bone marrow stromal cells, concentrated bone marrow cells, cultured MSCs or sorted MSCs. Bone marrow derived MSCs represent a heterogeneous population (Huang et al., 2011). It has been demonstrated that MSCs from primary culture of bone marrow contained at least three types of cells based on morphology; spindle shape cells, star shaped cells and large flat cells (Xiao et al., 2010). Bone marrow stromal cells are able to form colonies under low density culture (Pochampally, 2008). This capacity indicates the yield of MSC enrichment and differentiation potential, which can be determined using the colony forming assay (CFU-F). Colonies varies in morphologies including the number of cells, size and shape. It has been reported that circularity of colony can be used as a parameter to select the highly potency MSC clone (Gothard et al., 2013).

MSCs from their native tissues can be isolated and expanded in specific culture conditions. However, culture conditions can alter their phenotype and the expanded cells may be heterogeneous. Recently, as mentioned in section 1.5.1, the several markers of MSCs have been identified. These makers can be used for purification of the MSCs immediately after extraction from tissues. Because of the absence of a unique *in vivo* maker for MSC as well as possibility of changing phenotype after expansion in culture condition, the identification of markers of MSCs in their *in vivo* niche is important. With this information, MSCs can be isolated, sorted and utilised for clinical application without expansion in culture.

Recently, perivascular stem cells (PSCs) or pericytes have been comprehensively characterised in terms of their MSC potential's. Crisan et al. (2008) have been demonstrated a perivascular origin of MSCs in multiple human organs including fat tissues and bone marrow. These cells are known as multipotent pericytes or pericyte precursor cells which express CD146, NG2 and PDGF-Rβ. These cells can be found in perivascular areas with the blood vessel walls representing niche of these cells. It was demonstrated that these cells express all known MSC markers and had the ability to proliferate and differentiate into multiple mesodermal lineages including bone. As these cells share MSCs characteristics, they could potentially contribute to the fracture healing process and may have positive effects when used to treat atrophic non-unions. It has been reported that the bone regeneration potential of PSCs after intramuscular implantation in SCID mice (James et al., 2012b). PSCs were isolated from lipoaspiration and purified using CD146+, CD34- and CD45- as the immunophenotype markers. These cells were implanted with tricalcium phosphate into the muscular pocket of biceps femoris muscles of mice. Ectopic bone formation significantly increased in the presence of hPSCs in comparison with patient-matched hSVF cells (human stromal vascular fraction). It should be possible and more advantageous to use PSCs for bone regeneration as these cells represent a well-defined population (CD146+, CD34-, CD45-) with potent bone regeneration potential. Pericytes can be isolated in sufficient number to be in the non-union fracture without the requirement for culture expansion.

Strategies for preparing MSCs are summarised in **Figure 1.16.** It is not clear which technique is most appropriate for bone regeneration. However, *in vitro* studies suggest that early passage MSCs have better osteogenic potential (Sugiura et al., 2004) and so the use of non-cultured cells may represent the optimal strategy.

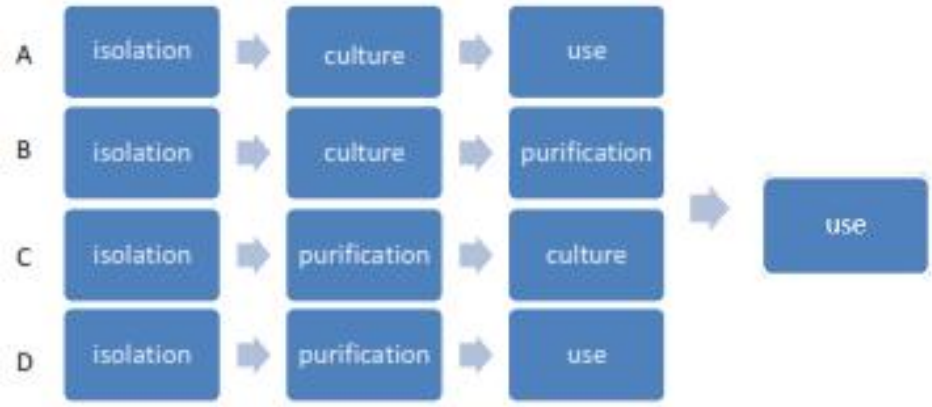

Figure 1.16 Preparation methods of MSCs

Part 2: General methods and experimental validation of methods

Chapter 2: General materials and methods

This chapter details the general materials and methods used in this thesis. The methods of primary MSC isolation from both rat and human, culture techniques, common cell assays and the method of MSC characterisation are described. Common methods, techniques and materials required to establish an atrophic non-union model are presented. A minimally invasive delivery technique using percutaneous injections is described. Imaging techniques to facilitate evaluation of fracture healing are provided including radiological assessments to determine of the progression of fracture healing and detailed micro-CT evaluation. The Radiographic Union in Tibia (RUST) scale and Lane & Sandhu fracture scoring systems were validated and used in this study. The details of sample preparation and histological assessment are given. Immunohistochemistry and Immunocytochemistry for cell tracking and characterisation are detailed. Immunological responses following cell injection were evaluated using the enzyme-linked immunosorbent assay (ELISA) from serum and lymph node histomorphometric assessment. However, the experimental design and methods specific to each chapter are listed separately in the relevant chapters.

2.1 Primary cell isolation and culture

In this study, the cell culture system was based on a mammalian cell culture. Primary cells were derived from both rat and human tissues. A number of cell types were isolated: (1) rat MSCs (rMSCs) derived from three sources, including bone marrow, periosteum and fat tissue; (2) human MSCs (hMSCs) derived from bone marrow (femoral head) and; (3) human perivascular stem cells (PSCs or "pericytes") derived from adipose tissue. All cell culture procedures were conducted in a class two, High-Efficiency Particulate Air (HEPA) filtered laminar flow hood using sterile equipment. Cell growth kinetics, morphology and characterisation studies were performed *in vitro*. The functional or therapeutic potential for bone regeneration of

these cells were determined in *in vivo* studies using rat model, simulating the clinical scenario of atrophic non-union. This section details the general materials & reagents used and describes the techniques & methods used in cell cultures.

2.1.1 **Media, reagents and materials used for cell culture**

The general chemicals and their manufacturer are listed below:

- Dulbecco's Modified Eagle's Medium (DMEM) - Low glucose (Gibco, UK)
- Dulbecco's Modified Eagle's Medium (DMEM) - High glucose (Gibco, UK)
- Fetal bovine serum (FBS) (Gibco, UK)
- Penicillin (10,000 units/ml) and streptomycin (10,000 µg/mL) (Gibco, UK)
- Phosphate-Buffered Saline (PBS) (Gibco, UK)
- 0.05% Trypsin-EDTA (Gibco, UK)
- Dimethyl sulfoxide (DMSO) (Sigma-Aldrich)
- 0.4% Trypan Blue Solution (Gibco, UK)
- Plasticware for cell culture (Corning, UK)
- Collagenase type II (Sigma-Aldrich, UK)
- Bovine serum albumin (BSA) (Sigma-Aldrich, UK)

2.1.2 **Preparation of media and reagents for cell culture**

These following solutions were prepared for use in the experiments.

- **Basal medium for rMSC and hMSC cultures**

This medium was used for rMSC, rat fibroblast (isolated from tail tips) and hMSC cultures. It consists of DMEM-Low glucose, 10% heat-inactivated FBS and 1% penicillin/streptomycin.

- **Basal medial for human pericyte cells**

This medium was used for pericyte culture. It consists of DMEM-high glucose, 10% heat-inactivated FBS and 1% penicillin/streptomycin.

- **Freezing medium**

Freezing medium consists of 90% FBS and 10% DMSO.

- **Collagenase solution**

Collagenase solution for the digestion of tissues was composed of 1 mg/mL collagenase type II and 3.5% BSA in DMEM

- **Red blood cell lysis buffer**

Red cell lysis buffer consisted of 9 parts of 0.83% (w/v) ammonium chloride and 1 part of 2.059% (w/v) Tri base. The pH of this solution was adjusted using 1M hydrochloric acid to 7.65.

2.1.3 Cell Isolation

2.1.3.1 Preparation of rat tissue and rMSC isolation

The rMSCs used in this study were isolated from adult (3-4-month-old) male Wistar rats obtained from a recognised biological service. The animals were humanely sacrificed using a carbon dioxide overdose (schedule 1, as per UK Home Office Procedural Guidelines). Following confirmation of death, the skin around the groin and both hind limbs was shaved and cleaned using 70% alcohol. Adipose tissue from the inguinal areas was harvested for subsequent isolation of cells (**Figure 2.1**). For

the isolation of rMSCs from bone marrow, femora were removed and cleared of overlying skin and muscle (**Figure 2.2**). Periosteal tissues were carefully dissected from the femur (**Figure 2.3**). All samples were then placed in sterile containers with basal media and immediately transported from the animal facility to the laboratory on ice (with 30 minutes). Each sample was then rinsed three times in sterile PBS.

Figure 2.1 Harvesting of Inguinal adipose tissue from Wistar Rats: Following schedule 1 killing, (a) the skin overlying the lower limbs and inguinal region was shaved. (b) The skin overlying the groins and femora was incised and removed, revealing underlying inguinal adipose tissue. (c, d) This tissue was excised and placed in collection media for immediate processing.

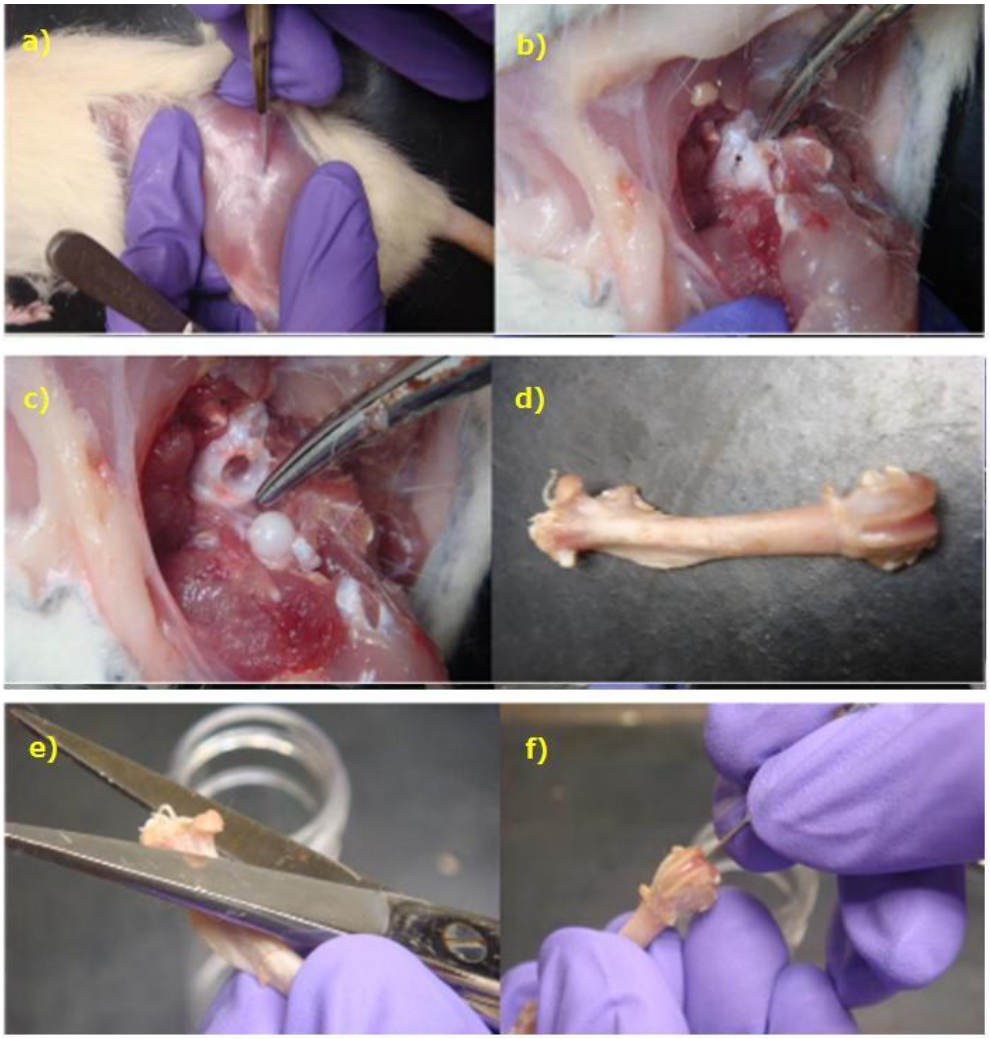

Figure 2.2 Harvesting of Bone marrow tissue from femoral bone: Following schedule 1 killing, (a) excision of overlying skin and muscle incision was made (b) to reveal the underlying hip joint. (c) The femoral head was disarticulated and (d) the muscles and periosteum were stripped from the femora. (e) The femoral head was cut in order to expose the bone marrow, and (f) irrigation was performed of the distal femora.

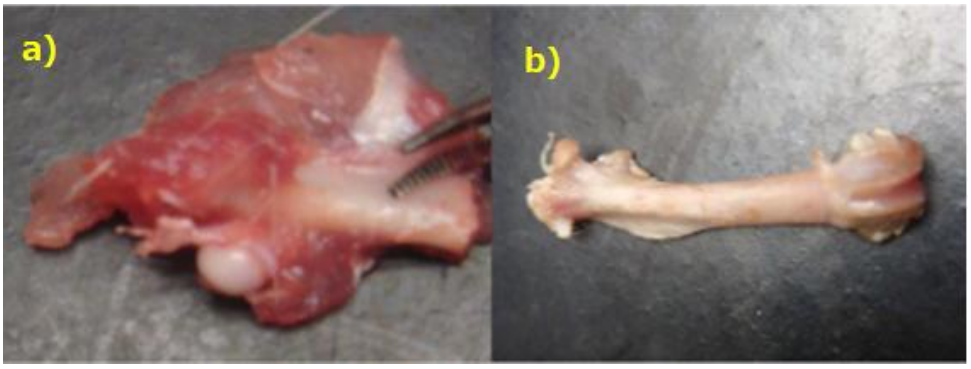

Figure 2.3 Harvesting of periosteal tissue from Wistar Rats: (a) excision of overlying muscle and (b) the periosteum tissue was identified.

The isolation of rMSCs was performed under sterile conditions. The tibia and femur were separated before soft tissues were removed and the bone ends were cut using scissors to expose the marrow. Bone marrow was obtained by flushing the femora with DMEM using a 21-G needle and a 1-mL syringe using a published protocol (Lennon and Caplan, 2006). Cells were liberated from adipose tissue and periosteum by digestion in collagenase containing medium as described in a previously reported technique (Zuk et al., 2002) for 45 minutes in a shaking water bath (180 rpm) at 37^{o}C. An equal volume of basal medium was added to halt the digestion and the total suspension was passed through a sterilised nylon mesh to remove large clumps. The suspension was then passed through a 100µm followed by a 70µm strainer and centrifuged (1,200 rpm, RT, 5 mins). The supernatant was discarded and the pellet was resuspended in 10 mL red cell lysis buffer and incubated at RT for 10 minutes. An equal volume of basal medium was added and the suspension centrifuged (1,200 rpm, RT, 5 mins). The supernatant was again discarded and the pellet was resuspended. The cell suspension was then passed through a 40µm strainer. Cell solution was centrifuged at 1,200 rpm for 5 min and resuspended in 3 mL basal medium and counted using a haemocytometer using tryphan blue to distinguish non-viable cells. Isolated cells were then placed into 75 cm^2 flasks containing basal medium and incubated at 37 °C and 5% CO_2. Cells from passage 2-4 from the primary cultures were used in experiments to establish growth curves, population

doubling time (PDT) and colony forming ability or were preserved in freezing medium (10% DMSO in FBS) in liquid nitrogen for further experiments.

2.1.3.2 Preparation of human tissue and hMSC isolation

hMSCs were isolated from the femoral heads of patients taken during a hip replacement operation. These tissues were obtained under informed consent with the approval of the local ethical committee (LREC 2002/1/22). The established protocol for isolating hMSC in this study was previously reported. Isolated cells from this technique expressed CD105 (one of MSC surface markers) in about 90% of the isolated cells (Tremoleda et al., 2012). Samples were kept in basal medium at 4°C until processing and cell extraction (maximum of 24 hours). Samples were prepared under sterile conditions (**Figure 2.4**). Bone marrow and cancellous bone from the femoral head were removed and transferred into 25 mL of basal medium in a 50 mL-falcon tube. The tissue was digested using a collagenase solution for 45 minutes in a shaking water bath (180 rpm) at 37^{o}C. An equal volume of basal medium was added to halt the digestion and the total suspension was passed through a sterilised nylon mesh to remove large clumps. The suspension was then passed through a 100 µm followed by a 70 µm strainer and centrifuged (1,200 rmp, RT, 5mins). The supernatant was discarded and the pellet was re-suspended in 10 mL red cell lysis buffer and incubated at RT for 10 minutes. An equal volume of basal medium was added and the suspension centrifuged (1,200 rpm, RT, 5mins). The supernatant was again discarded and the pellet was resuspended in 5 mL basal medium and counted using a haemocytometer using tryphan blue to distinguish non-viable cells. Nucleated cells were seeded in a 75 cm^2 flask and maintained at 37 °C in 5% CO_2 incubator for 48 hours. After incubation, the culture medium containing non-adherent cells was removed and the remaining adherent cells were washed with 1xPBS three times before addition of fresh basal medium. Primary isolated adherent cells were maintained with addition of fresh culture medium every three days until the cells reached 80% confluence. Isolated cells were preserved in freezing medium (10%DMSO in FBS) in liquid nitrogen after passages 2-3.

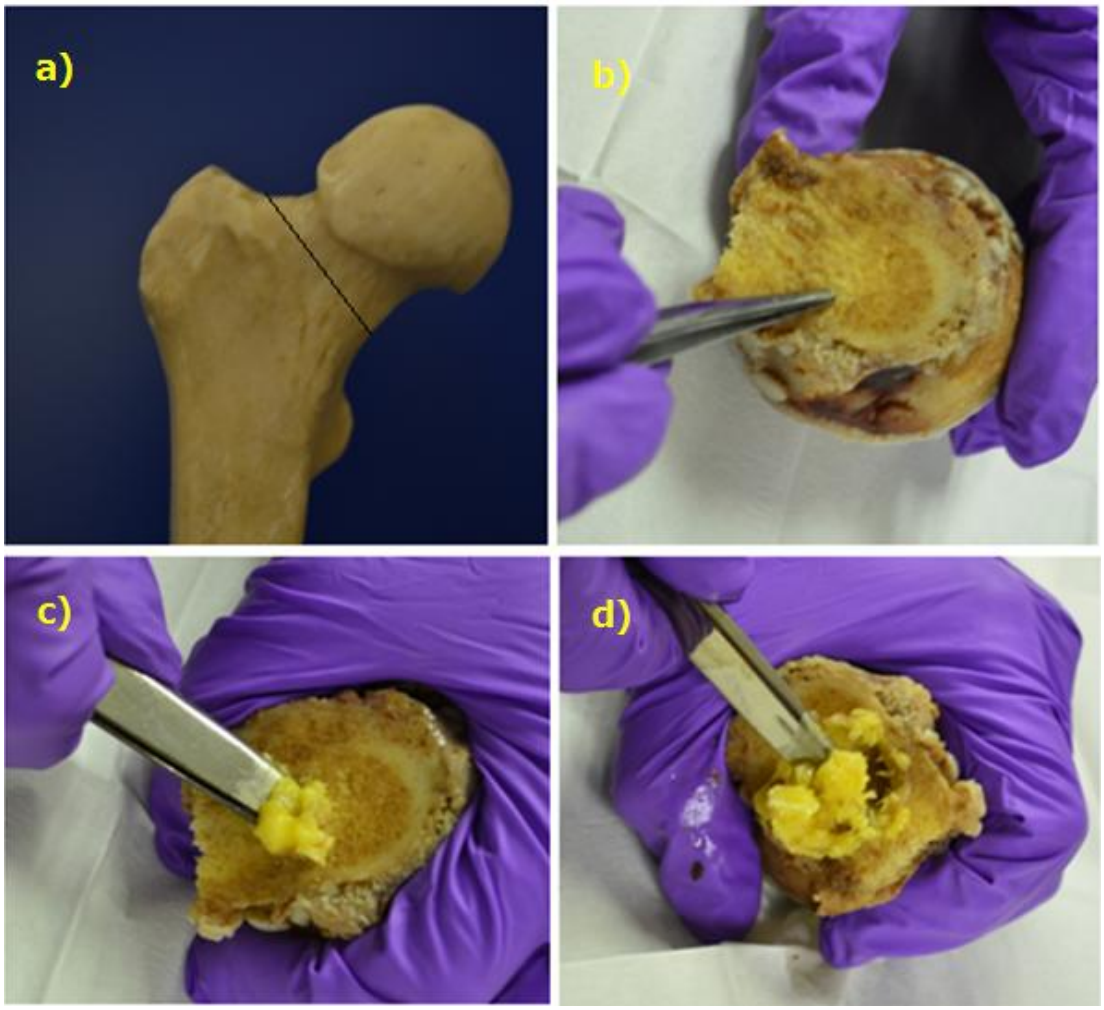

Figure 2.4 Extraction of bone marrow from a human femoral head. (a) Femoral heads were obtained from hip replacement procedures in which the proximal femur was divided through its surgical neck. (b) Cancellous bone and (c, d) marrow visible on inspection of the cut surface of the femoral neck was removed by curettage.

2.1.3.3 Isolation of human perivascular stem cells (PSCs) or Pericytes

PSCs at passage 3-4 were supplied by Dr. Christopher West. These cells were extracted and isolated from whole fat or lipoaspirate which had been obtained from patients during cosmetic surgery (Lothian Research Ethics Committee reference;

10/S1103/45). After digestion with collagenase solution, cells from the stromal vascular fraction (SVF) of adipose tissue were sorted using CD45, CD144, CD34 as negative markers and CD 146 as the specific marker for PSCs from the subvascular fraction (SVF) after collagenase digestion (**Figure 2.5**), according to a previous report. (Crisan et al., 2008).

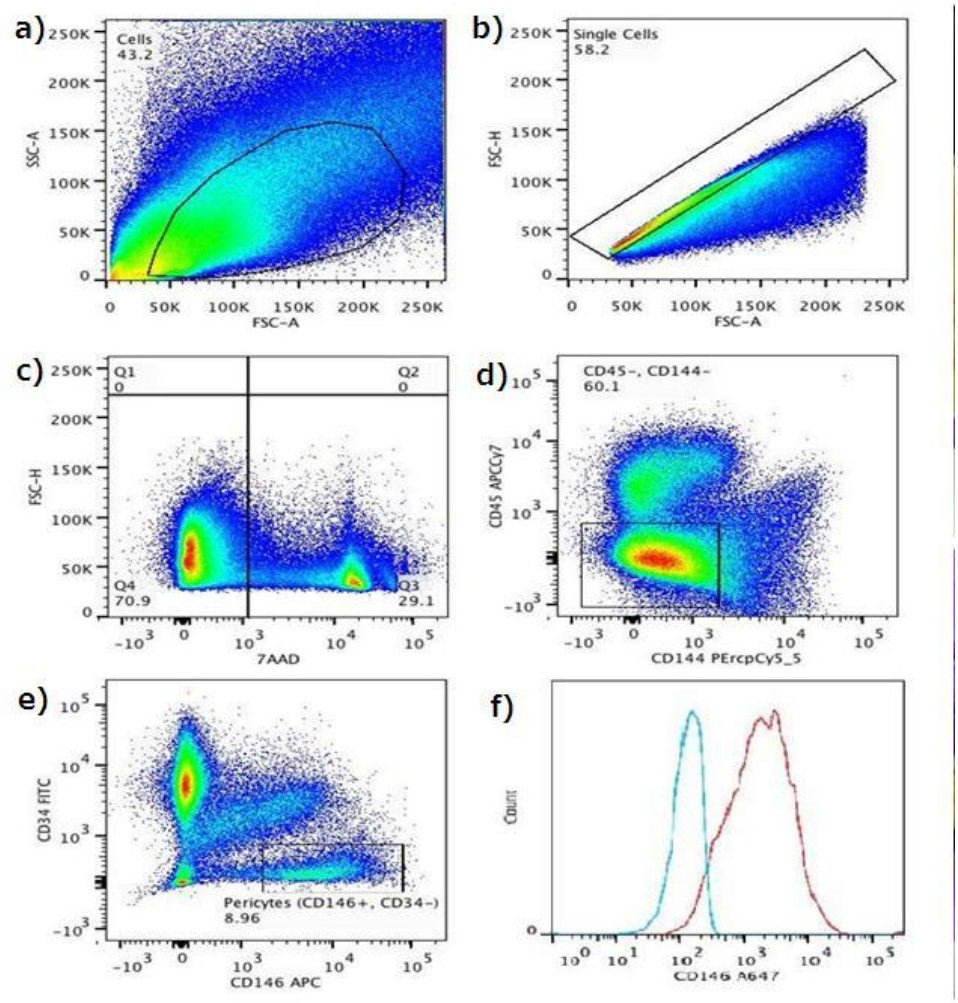

Figure 2.5 Gating strategy for the sorting of pericytes from adipose tissue. (a) Following double scatter cell and (b) singlet selection, (c) non-viable cells staining for 7-AAD (7-amino-actinomycin D) were excluded. (d) CD45+ haematopoetic cells and CD144+ endothelial cells were excluded, prior to (e, d) selection of the CD146high and CD34- pericytes. (with permission from Dr. Chris West)

2.1.3.4 Cell cultures and expansions

Prior to experimentation, the cells, which had been stored in cryo-vials in liquid nitrogen were thawed rapidly in a water bath at 35.5 °C, prior to resuspension in 10 mL of basal media. This cell suspension was then centrifuged at 1,200 rpm for 5 minutes. The supernatant was removed and the cells were resuspended in 15 mL of basal media and seeded onto new tissue culture flasks. Cell cultures were maintained at 37 °C in 5% CO_2 with basal media replaced every three days. When the cells had reached confluence, they were detached using 0.25% trypsin with 0.1 mM EDTA for 5 min at 37°C. The cells were counted and split into fresh flasks (ratio 1:3) for expansion.

2.1.3.5 Cell counting

Cell counting is an important technique used to study cell growth, proliferation and colony forming *in vitro* and to prepare the cells for implantation experiments (*in vivo*). The haemocytometer cell counting method was used to count cells in this study. This technique is simple, convenient and readily available. It is considered to be the gold standard method for counting cells. Cell viability was determined using the dye-exclusion method. Dead cells and debris taken in trypan blue can be distinguished and excluded from live cells. The haemocytometer consists of two chambers divided into nine 1-mm squares (grid) (**Figure 2.6**). After applying a cover slide, each grid occupies 0.1 µL of volume. Cells were counted from four outer quarter grids of both chambers to determine average cell counts in 0.1 µL. The average cell counts within grids together with the dilution factor used in the preparation of cells are used to calculate the number of cell/mL as per the following equation **(**2.1):

$$\text{Total cells/ml} = \text{Average grid cell count} \times 10^4 \times \text{Dilution factor} \qquad \textbf{Equation 2.1}$$

The Dilution factor is the ratio of the total volume of cell suspension and trypan blue to the volume of the original working cell suspension

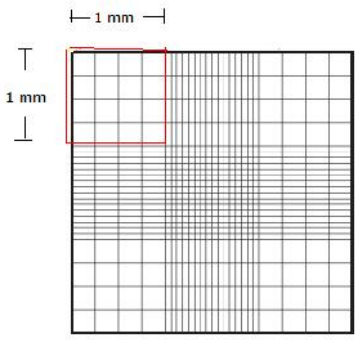

Figure 2.6 Schematic of the markings on a haemocytometer: Each grid (highlighted here in red) holds 0.1 µl of volume following application of a cover slide

2.1.3.6 Growth curves

To investigate the growth pattern of rMSCs from the 3 sources (bone marrow, periosteum and adipose tissue) and hMSC from bone marrow tissue, 3rd-4th passaged cells from each source were seeded at 5×10^4 cells/well in 6-well culture plates. The culture medium was changed every three days until the end of experiment. Cells were trypsinised and counted using a haemocytometer every second day. Growth curves were plotted from these data (in replicate).

2.1.3.7 Determination of Population doubling time

To determine the population doubling time (PDT), rMSCs (from rat bone marrow, periosteum and adipose tissue) and hMSC (from human bone marrow tissue) at passage two from each source were seeded in 25 cm^2 flasks at a density of 1.5×10^5 cells. When the cells reached 80% confluence (average 1 week after seeding), the

cells were counted and reseeded at 1.5×10^5 cells. Cell counting was performed from the third to the fifth passage. Population doubling number (PDN) and population doubling time (PDT) were calculated according to the following equations (2.2 and 2.3):

$$PDN = \log (N/N_0) \times 3.31 \qquad \textbf{Equation 2.2}$$

PDN the population doubling number,
N= the number at the end of the period (which was 7 days),
N_0= the initial number of cell which was 1.5× 105 cells

$$PDT = CT/PDN \qquad \textbf{Equation 2.3}$$

PDT= population doubling time
CT= the duration of culture which was 7 days

2.1.3.8 Colony forming assay

2nd -4th passaged MSCs were evaluated for their clonogenic ability by using colony forming assays. Cells were seeded at low density (20 cells per cm^2) and cultured in 10% FBS DMEM with 1% penicillin/streptomycin for 2 weeks without a change of the medium. After two weeks, colonies were stained with Giemsa stain. Colonies consisting of over 50 cells were counted manually under a light microscope. The colony forming ability was compared by calculating the percentage of cells that formed colonies [(Number of colonies/Number of cells seeded) x100]. To determine the area covered by MSC colonies, six regions of each well were randomly captured under 20x microscope and the images were analysed on image J (National Institutes of Health, Bethesda, Maryland, USA, http://imagej.nih.gov/ij/) to establish the percentage of the surface area of the well covered by colonies.

2.1.3.9 Differentiation assays

To demonstrate the differentiation potential of MSCs, passage 3-4 MSCs were cultured *in vitro* under (a) osteogenic, (b) chondrogenic and (c) adipogenic conditions. (a) Osteogenic potential: to induce osteogenesis, cells were cultured in basal medium until 60-70% confluent before being changed to osteogenic differentiation medium (basal medium supplemented of 100 nM dexamethasone, 10mM β-glycerophosphate and 50 μg/ml L-ascorbic acid). Osteogenic medium was refreshed every 3 days for 2 weeks. The cells were stained with Alkaline Phosphatase (ALP) assay kit (Sigma-Aldrich®, UK) using the manufacturer's protocol. (b) Chondrogenic potential: to induce chondrogenesis using the micromass culture technique, 4×10^5 cells were resuspended in polypropylene tubes, centrifuged gently to form a micromass, then cultured in serum-free medium containing high-glucose DMEM supplemented with 100 nM dexamethasone, 1x Insulin-transferrin-selenium plus premix (ITS Premix, from BD®); final concentration: 6.25 μg/mL bovine insulin, 6.25 μg/mL transferrin, 6.25 μg/mL selenous acid, 5.33 μg/mL linoleic acid and 1.25 μg/mL bovine serum albumin), 50 μg/mL L-ascorbic acid, 100 μg/mL sodium pyruvate, 50 μg/mL proline, and 20 ng/mL transforming growth factor-β3 (TGF-β3). The medium was changed every 3 days. After 3 weeks, cultured pellets were frozen, sectioned (6 μm thick), and stained with Alcian blue. (c) Adipogenic potential: to induce adipogenesis, cells were cultured in basal medium until 60-70% confluence and then changed to adipogenic differentiation medium (basal medium supplemented with 1 μM dexamethasone, 10 μg/mL insulin, 0.5 mM isobutyl-methylxanthine (IBMX) and 0.5 mM indomethacin). Adipogenic medium was changed every three days for two weeks. Oil Red O staining was used to assess lipid accumulation in the cells.

2.2 The Atrophic non-union procedure

2.2.1 Animals

The animals used in this thesis were Wistar rats, which are an outbred strain of albino rats belonging to the species *Rattus norvegicus*. They were bred in house at the biological research facility (BRF), the University of Edinburgh. Rats were housed individually for at least seven days before starting experiments. Rats are commonly used in fracture healing studies: approximately 38% of fracture healing experiments published in the orthopaedic literature have been conducted using rats (O'Loughlin et al., 2008). Rats are easy to operate on because their anatomy is larger than mice. In addition, fixation is more predictable in terms of mechanical control. In this study, the fracture site was created at the tibial mid shaft because it is an easily accessible subcutaneous bone and easy to operate on. Importantly, the tibia is a common site of fracture non-union (Antonova et al., 2013, Mills and Simpson, 2013), and therefore animal studies evaluating healing in this bone have considerable clinical relevance.

2.2.2 Ethical considerations

All procedures were conducted following approval by the Local Research Ethics Committee and the UK Home Office, and in accordance with the animal (Scientific Procedure) Act 1986. It is known that a number of orthopaedic procedures such as fracture models, osteotomies and fracture fixation studies have the potential to cause discomfort and painful distress to animals. Therefore, great care was taken to minimise and control discomfort through consultation with the local veterinarian and Named Animal Care Welfare Officer (NACWO) before embarking on any animal works. Each animal s' health status was closely monitored by a qualified veterinary surgeon. The surgical skills required to perform each procedure were first gained on

cadaveric rats. More than 20 cadaveric procedures were performed to ensure competency before embarking on procedures with live animals. The design of external fixator was modified during the experiment to ensure that it did not interfere with animal movement and it was stable enough for bone immobilisation. All experiments were designed with consideration of published guidelines (Kilkenny et al., 2010, Festing and Altman, 2002, Auer et al., 2007). The "3R" approach to animal studies (Replacement, Reduction and Refinement) of Russell and Burch (1959) was applied where possible. The number of animals used in each experiment is detailed within the relevant chapter.

2.2.3 **Assembly of the External Fixator**

All the components of the external fixator were manufactured by the Physics workshop at the University of Edinburgh, UK. The external fixator construct consisted of aluminium rings, brass screws and nylon and brass nuts (**Figure 2.7**). The construct was evaluated using an axial compression test in five cadaveric rats prior to *in vivo* experiments (results detailed in Chapter 6). In the cadaveric setting, the fixator was found to be strong and stiff enough to stabilise fracture fragments.

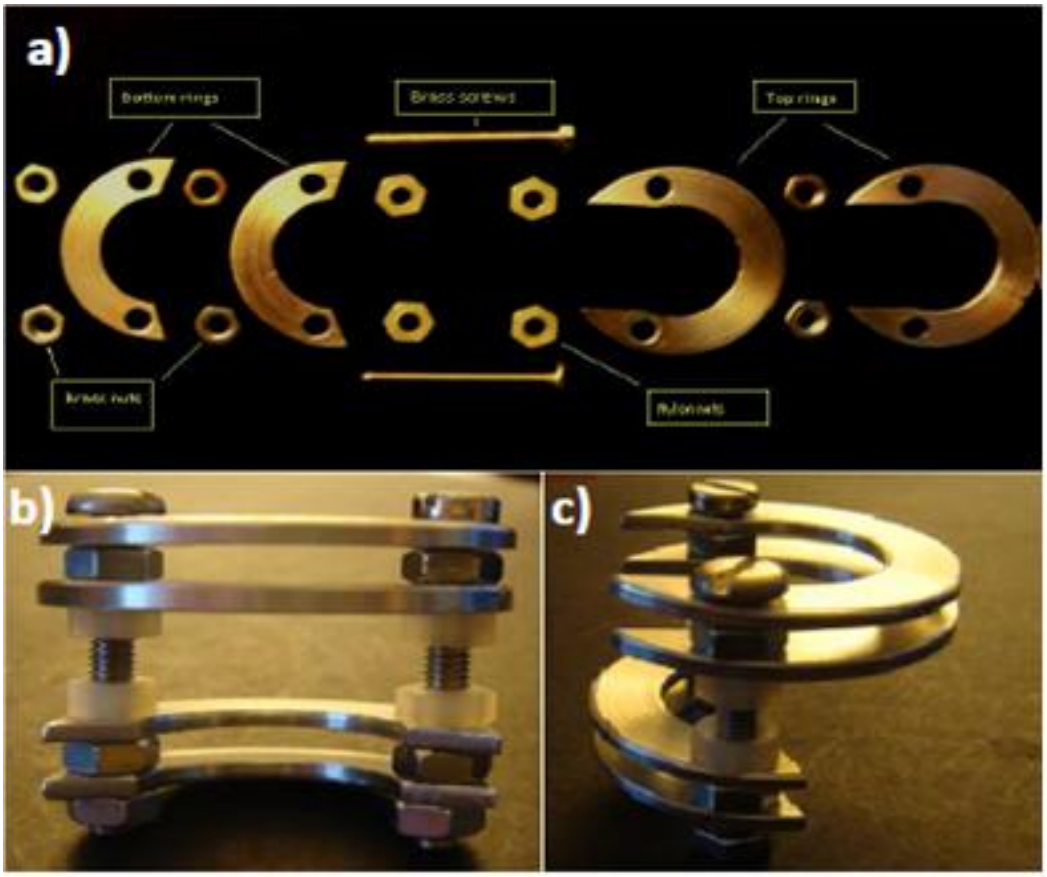

Figure 2.7 The External fixator devise used in the generation and fixation of non-unions in Rats: (a) layout prior to assembly (b) Coronal view and (c) lateral view of external fixator

2.2.4 **Materials, surgical instruments and medicines**

A list of materials, surgical instruments and medicines that were used as part of the surgical procedure to create atrophic non-unions are detailed in **Table 2.1**. The external fixator and surgical instruments were sterilised using a steam autoclave before use.

Table 2.1 List of equipment and medicine required in the animal studies

Materials	Surgical instruments	Medicines
Complete set of External fixator	Needle holders	1 ml/kg of Synulox
Electric blanket	Scissors	0.05mg/kg of buprenorphine
Surgical board	Blunt forceps	10ml/kg of 0.9% saline
Sterile wound package	Toothed forceps	PBS
Marker pen	Scalpel blades	Xylocaine® spray (10mg each dose)
Gloves	Periosteal dissector	Fucidin® ointment
Safety glasses	Small soft tissue protector	
Sutures (Vicryl rapide, 4/0)	Scalpel blades	
27G needle (Sterican, Braun, Melsungen) X 6 needles	Mini Drill (RS Components Ltd, Northamptonshire)	
Syringes (Sterican, Braun, Melsungen)	Burrs (1mm) and circular saws (1cm)	
	Pliers	

2.2.5 **Operative procedure**

All procedures were performed under sterile conditions. The surgical steps are outlined in **Figure 2.8.** Animals were placed on a heat pad and anaesthetised with inhalation anaesthesia (Isoflurane; 5% for induction and 2% for maintenance). Pre-medications (Synulox, buprenorphine and 0.9% saline) were introduced subcutaneously. The right hind leg was placed centrally through the fixator. The position of the fixation was in the middle of Tibia; the line of knee and ankle acted as the reference position (**Figure 2.8 A and B**). Six 27G- needles were drilled through the tibia using a Dremmel® Multitool and secured using compressive force between ring and nut devices (**Figure 2.8 C**). An antero-medial skin incision was made, exploiting the interval between tibialis anterior and tibialis posterior (**Figure 2.8 D**). Following satisfactory exposure of the tibia, an osteotomy was created at its mid shaft using a circular saw (RS Components, UK) ensuring that the surrounding soft tissues were protected and regularly irrigated with 0.9% saline. The 1 mm gap was created according to the thickness of the surgical saw blade (**Figure 2.8 E**). To induce atrophic non-union, the periosteum was stripped one-diameter length of the tibia bone both proximal and distal to the osteotomy site (**Figure 2.8 F**). The endosteum and intramedullary canal were also curetted using a 23G needle (**Figure 2.8 G**). Finally, the wound was washed with saline and closed in layers using 3-0 vicryl (**Figure 2.8 H**). Post-operative analgesia with buprenorphine (0.3mg/kg) was administered through jelly cubes for all animals in the initial 24 hours postoperatively.

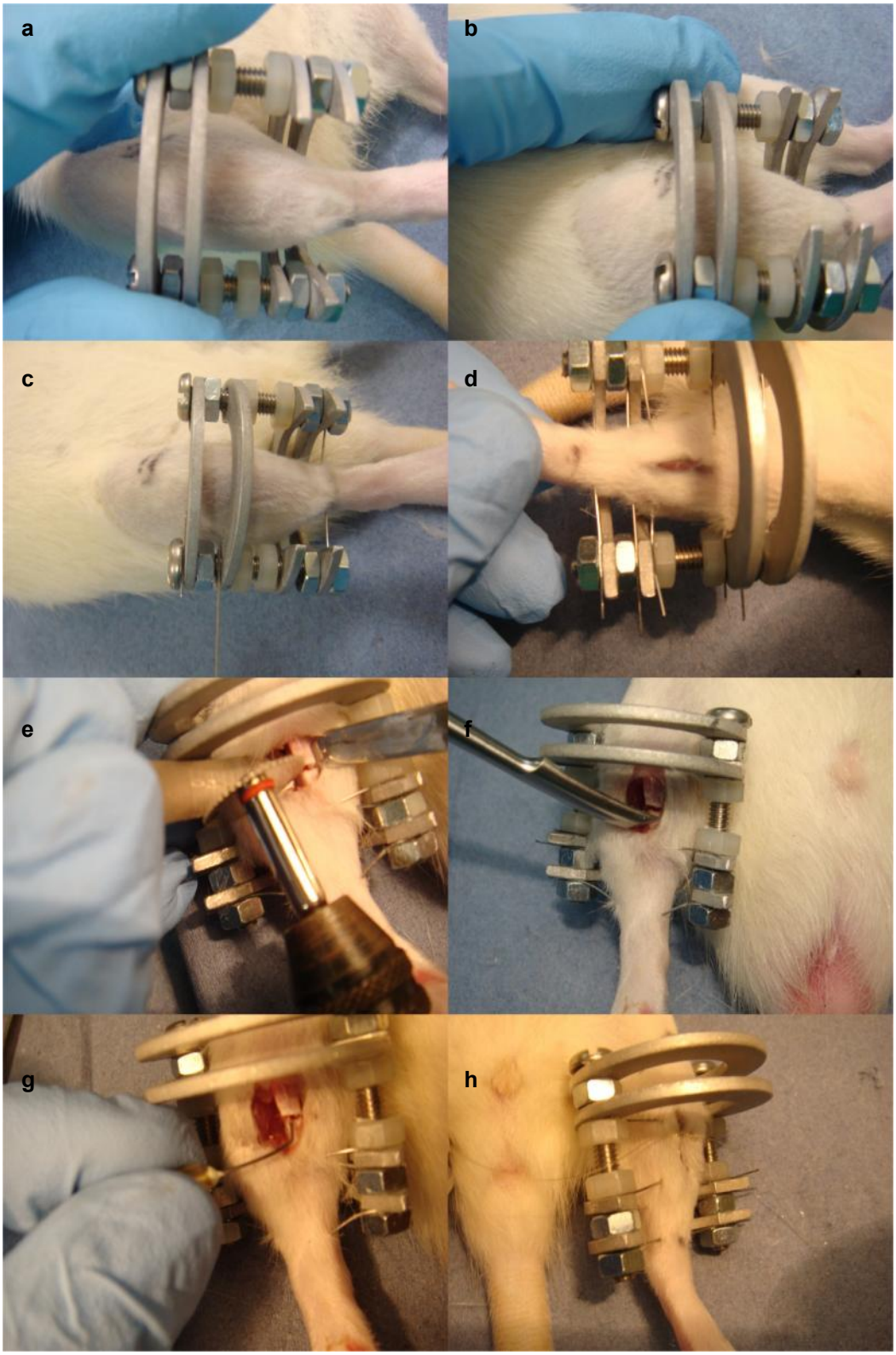

Figure 2.8 The surgical technique for the atrophic non-union model

2.2.6 **Post-operative care**

Monitoring and clinical assessments of animals were carried out for 15 minutes post-operation, at six hours after operation and daily until the completion of experiments. Buprenorphine was given postoperatively for pain control at six hours after each procedure. If there was evidence of discharge or swelling at the surgical site, local wound care with 0.9%NSS and fucidin® ointment was used. On the rare occasion that a wound became infected wound, Synulox® was prescribed under the direction of the veterinarian physician for a short period of time (3-5 days). If a leg was entrapped by the ring in the post-operative period, the external fixator was adjusted.

2.3 A minimally invasive technique for cell delivery

MSCs may be administered operatively within scaffolds, through local injection without scaffolds, or intravenously, depending on the clinical situation. Percutaneous injection is a minimally invasive method of delivering MSCs to the fracture site.

2.3.1 **The optimisation of injection position in cadaveric study**

The injection procedure was performed using cadavers to determine an optimal distance and position of the needle for cell injection. Use of an appropriately size of needle is essential in this procedure. A standard 26G needle BD with 0.45 mm diameter was used for injection as MSCs average 11-19 μm in diameters (Majore et al., 2009), allowing easy passage of the cells through the needle. The most appropriate position for needle placement was optimised using 5 cadavers. An x-ray was taken to assess the optimal depth of the needle from the medial side of the tibia. The fracture gap was directly palpable. The optimum depth of needle was found to

be 2.5 mm (**Figure 2.9**). A potential limitation of this technique was leakage of the injected solution, which would result in a reduction of the final number of cells reaching the desired location. Appropriate needle size and slow injection of the cell suspension can minimise leakage. Importantly, cells should be injected only when the surgical wound has completely healed as the cell suspension may leak through unhealed surgical wounds.

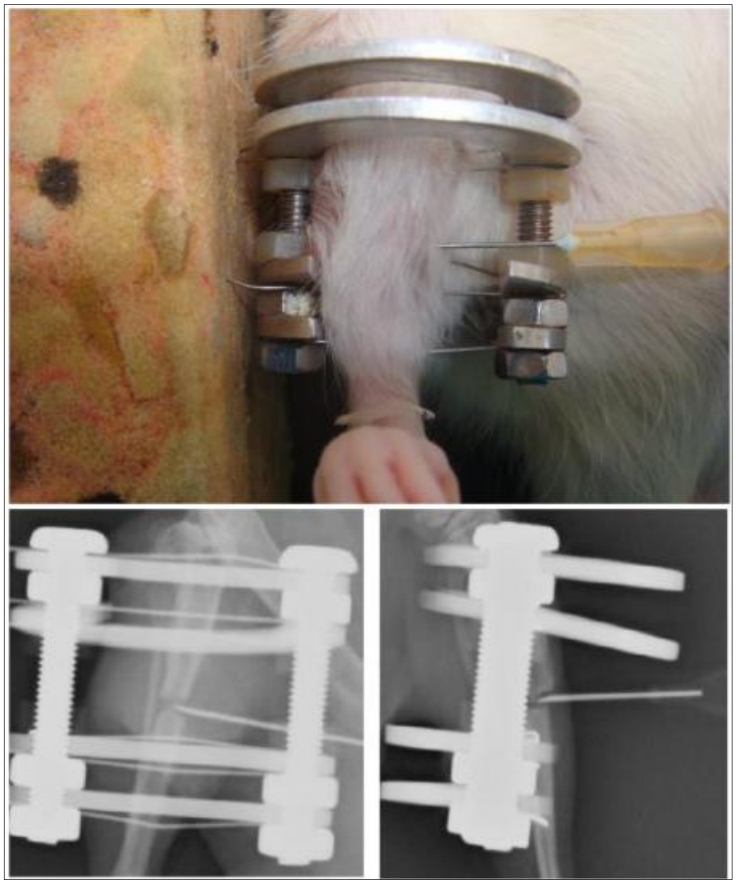

Figure 2.9 Locally percutaneous injection technique

2.3.2 Injection procedure

The animals were anaesthetised with inhalation anaesthesia (2.5% Isoflurane). The fracture gap was identified between proximal and distal pins and confirmed using palpation. The skin was cleansed with 70% alcohol. The cell suspension was then injected slowly in order to avoid leakage. After injection, animals were routinely monitored to ensure ongoing health of animal and welfare with particular attention paid to animal weight, behaviour, and condition of the injected site.

2.4 Radiographic evaluation of fracture healing

Fracture alignment and fixation after operation was monitored radiographically. Radiographs are a common and non-invasive method of evaluating the progression of fracture healing and can be used to determine bone union. This section outlines the radiographic settings used in this study, detailing the radiographic parameters applied to compare the fracture healing process. In all animal experiments, X-rays were taken immediately following operations (while still under anaesthesia) to confirm fracture position, at the cell injection time, and every two weeks following injection to evaluate the fracture healing process until completion of the study.

2.4.1 Radiographic settings

Fracture healing was monitored and evaluated using serial radiographs with digital imaging every 2 weeks. A portable X-ray unit (Acu-Ray JR, Stern Manufacturing Toronto, Canada) with an output of 60 kV, 2mAs and exposure time of 0.1 ms was used. The focus-to-film distance was 90 cm (**Figure 2.10**). Images were captured on digital X-ray plates (Fuji CR Cassette, Fuji Photo Film Co Ltd, Japan). An

aluminium wedge was used to allow density standardisation of radiographic images (**Figure 2.11**). Image J was used for analysis of the radiographic parameters of fracture healing.

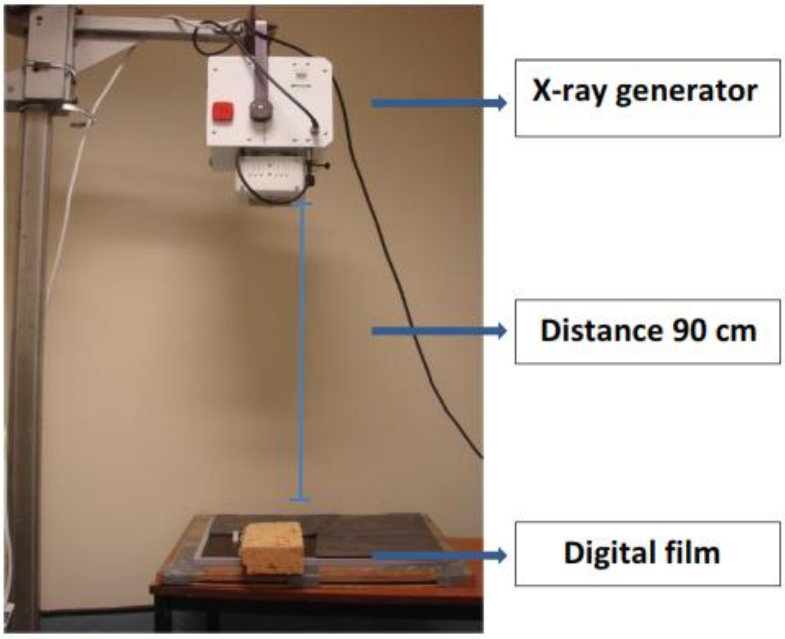

Figure 2.10 Positioning of the Radiographic equipment

Figure 2.11 An aluminium step wedge consisting of multiple steps (from 2 to 20 mm in thickness) was used as the radiological reference for magnification and radiopacity

2.4.2 **Radiological technique**

2.4.2.1 Position of rat legs for x-ray

Radiographs were taken immediately following the procedure to generate atrophic non-union and cell injections under the same anaesthesia. For subsequent radiographs, rats were induced with inhalation anaesthesia (2.5% Isoflurance) and placed centrally alongside the aluminium wedge using laser crosshairs as guidance. Radiographs were taken in antero-posterior and oblique views. The position of the rat's leg was controlled using the bar of the external fixator and the position of sponge as the references (**Figure 2.12**).

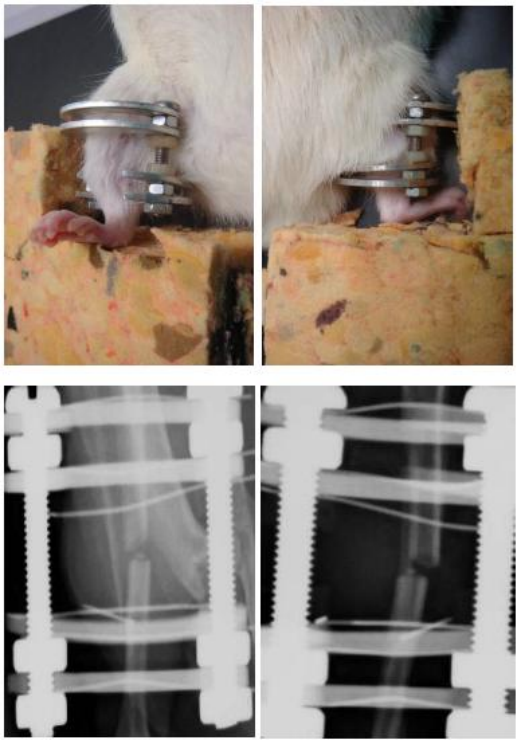

Figure 2.12 X-ray position of rat legs

2.4.2.2 The diagnosis of bone union

Following careful removal of the external fixator, bone samples were examined by manual clinical assessment of non-union. Non-union was indicated by the presence of motion at the facture site at the end of the study. Bone union was diagnosed in all animals using serial digital radiographs every two weeks by two blinded orthopaedic surgeons according to the criteria outlined in the AO-ASIF manual (Muller et al. 1991). The diagnosis of bone unions was also confirmed using the 3D images from micro-CT evaluation.

2.4.2.3 Radiographic parameters

The progression to fracture healing was determined from serial radiographs. The fracture healing process was evaluated using techniques including callus density, callus index, callus area and fracture scoring systems. These parameters were determined using image J (Image J 1.37v, Wayne Rasband, National Institutes of Health, Bethesda, MD, USA). The size of the aluminium wedge was used to calibrate the radiograph and to obtain the actual size of the fracture callus.

2.4.2.3.1 Callus radiopacity

The radiopacity of the callus at the fracture gap in the AP view was determined as an equivalent thickness of the aluminium step wedge (Furtos et al., 2012, Cook and Cunningham, 1995). The aluminium equivalent thickness (in mm) for the fracture callus was calculated using a calibration curve generated from the correlation between gray scale values and aluminium thickness from each image. Three equal regions from each step were selected and the gray scale value was measured. A linear regression model was used to generate an equation using gray scale values and the

aluminium thickness from each step (**Figure 2.13a**). To determine the radiopacity of callus, three equal regions at the fracture gap (one in the central area and two in the periphery) and three equal regions at the soft tissue adjacent to the fracture gap were selected for measurement (**Figure 2.13b**). The average gray value from both areas was converted into equivalent aluminium thickness using the equation from the linear regression model. Finally, the value of aluminium thickness at the soft tissue was subtracted from the value at the callus area to obtain the radiopacity of callus.

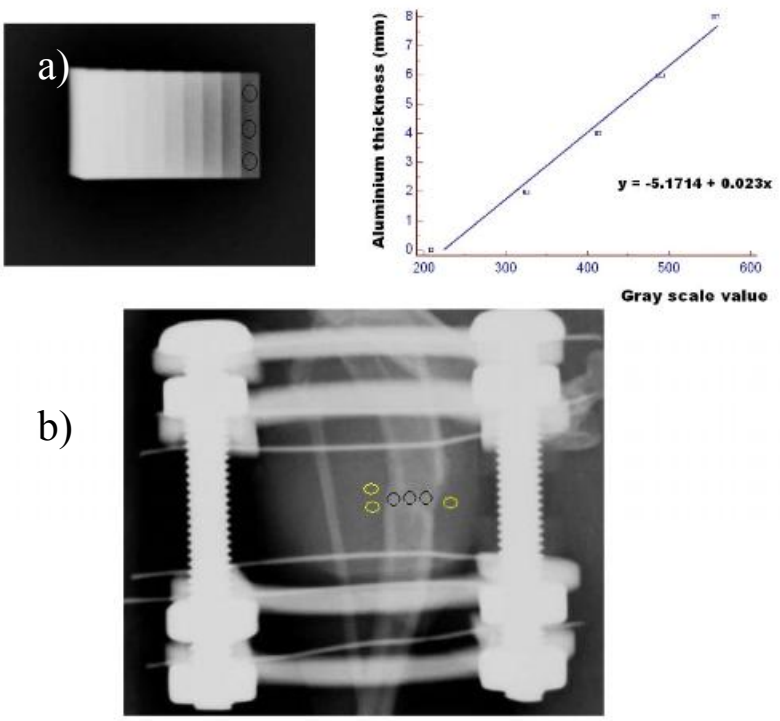

Figure 2.13 The technique used to determine the radiopacity: (a) three regions from each step of the Aluminium wedge steps were chosen to generate the calibrated graph and equation . And then, (b) areas over callus (black) and soft tissue (yellow) were selected to calculate the radiopacity of the callus

2.4.2.3.2 Callus index (proximal and distal)

These callus indexes were determined using the AP view on radiographs. The original callus index is the maximal transverse width of callus divided by the width of the bone at the fracture site (Eastaugh-Waring et al., 2009). However, it was found that it was not possible to use the original callus index to compare non-unions gap during bone healing. Thus, the modified proximal and distal callus indexes were used in order to compare the callus index from the different treatment groups during fracture healing. The initial differences in bone size were corrected by callus index. The proximal callus index was the transverse width of callus at the proximal end of the fracture divided by the width of bone at the proximal end and the distal callus index was the transverse width of callus at the distal end of the fracture divided by the width of bone at the distal end (**Figure 2.14a**). These modified callus indexes were validated using original callus index and they showed the strong agreements (**Figure2.14 b, c**).

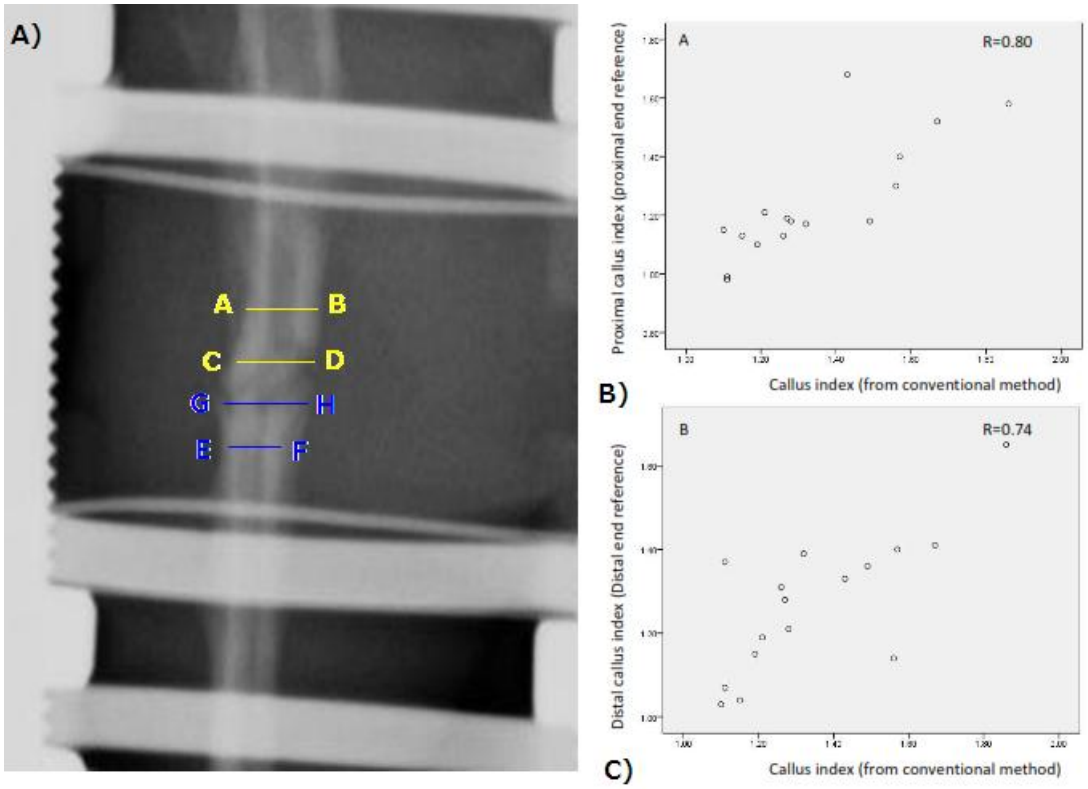

Figure 2.14 Proximal and distal callus index measurement (a) demonstrating how to measure the proximal callus index (CD/AB, yellow) and the distal callus index (GH/EF, blue) (b) the correlation between the proximal callus index and the original callus index (P-value < 0.001, Pearson's r) (c) the correlation between the distal callus index and the original callus index (P-value = 0.001, Pearson's r)

2.4.2.3.3 The percentage increase in callus area

The method used to determine the callus area in this study has been described in a previous report (Brownlow and Simpson, 2000). The marquee tool was used to delineate the area of bone from AP initial (injection time) radiographs using the pins of external fixator as the reference point. This area was measured and used as the original bone area. The callus area from radiographs at each time point was then delineated circumferentially and subtracted by the original bone area to obtain from the area in area callus. The percentage increase in the callus area was reported in

order to control for the initial size of bone when comparing between the different treatment groups.

2.4.2.3.4 Fracture scoring systems

Fracture scoring systems are commonly used by both orthopaedic surgeons and researchers to evaluate fracture healing in experimental and clinical fracture healing studies. The Radiographic Union Score for Tibial fractures (RUST) was introduced in clinical tibial study in 2010 (Whelan et al., 2010, Kooistra et al., 2010). It was reported that its agreement was substantial among assessors. In this study, this scoring system was used as a clinically relevant semi-quantitative fracture assessment tool. The Lane & Sandhu scoring system has been used for fracture evaluation in several pre-clinical animal studies (Bigham et al., 2008, Yang and Park, 2001, Kerimoglu et al., 2013, Kurklu et al., 2011). It was originally described in 1987 (Lane and Sandhu, 1987). As this scoring system describes bone healing at the fracture site differently from RUST, it was also used in this study to determine the progression of fracture healing.

The RUST scoring system shown in **Table 2.2** assigns points to a given set of AP and oblique radiographs based on assessments of healing at each of the four cortices visible on these projections (i.e., medial and lateral cortices on an anteroposterior radiographic image, anterior and posterior cortices on an oblique radiographic image). Each cortex receives a score of 1 point if it appears to have a fracture line with no callus; 2 points if there is callus present but a fracture line is still visible; and 3 points if there is bridging callus with no evidence of a fracture line. The summation of the individual cortical scores is used to give a total for the set of films (range between 4 and 12). The minimum score (4) indicating that the fracture has definitely not healed and the maximum score (12) indicating that the fracture has definitely healed. This score was not used for diagnostic purposes but for evaluating the fracture progress.

Table 2.2 RUST scoring system: based on points to a given set of AP and oblique radiograhs based on assessments of healing at each of the four cortices

Point	Bone bridge/bone callus	Fracture line
1	Absent	Visible
2	Present	Visible
3	Present	Invisible

The Lane & Sandhu scoring system is based on three factors present in the radiographic image including 1) bone formation at the fracture gap, 2) presence of a fracture line, and 3) bone remodelling. **Table 2.3** outlines how scoring in each category should be performed. The minimum score in this system is 0 and the maximum is 12. The total scores were summarised from each category (range between 0 and 4). This score was also used for evaluation of fracture healing over the period of the experiment.

Table 2.3 Lane & Sandhu scoring system; based on three dimensions present in radiographs

Categories	*Points*
Bone formation at fracture gap (the maximum score is 4)	
No evidence of bone formation	0
Bone formation occupying 25% of the defect	1
Bone formation occupying 50% of the defect	2
Bone formation occupying 75% of the defect	3
Full gap bone formation	4
Presence of fracture line (the maximum score is 4)	
Full fracture line	0
Partial fracture line	2
Absent fracture line	4
Remodelling (the maximum score is 4)	
No remodelling	0
Remodelling of the intramedullary channel	2
Full remodelling of cortex	4
Sum of radiographic scores	12

Before using the RUST and Lane & Sandhu scoring systems for fracture evaluation in fracture healing studies, both scoring systems were fully validated demonstrating strong agreements both inter and intra observer (Chapter 4) with the same setting of fixator, anatomic location and animal model. Radiographic evaluation in this study was performed by a blinded orthopaedic surgeon.

2.5 Sample preparation for fracture healing evaluation

At the end of each experiment, the animals were humanely sacrificed using carbon dioxide overdose (schedule 1, in accordance with UK Home Office procedures). The external fixator was removed carefully minimising callus disruption. Tibias were stored in PBS before examination using Micro-CT and biomechanical testing. The sample were then bisected and subjected to fixing with 4% Paraformaldehyde (PFA) or freezing with OCT compound (Optimum Cutting Temperature compound) for further histological evaluation. These steps were performed subsequently in order to minimise the number of animals used for fracture healing evaluation (**Figure 2.15**).

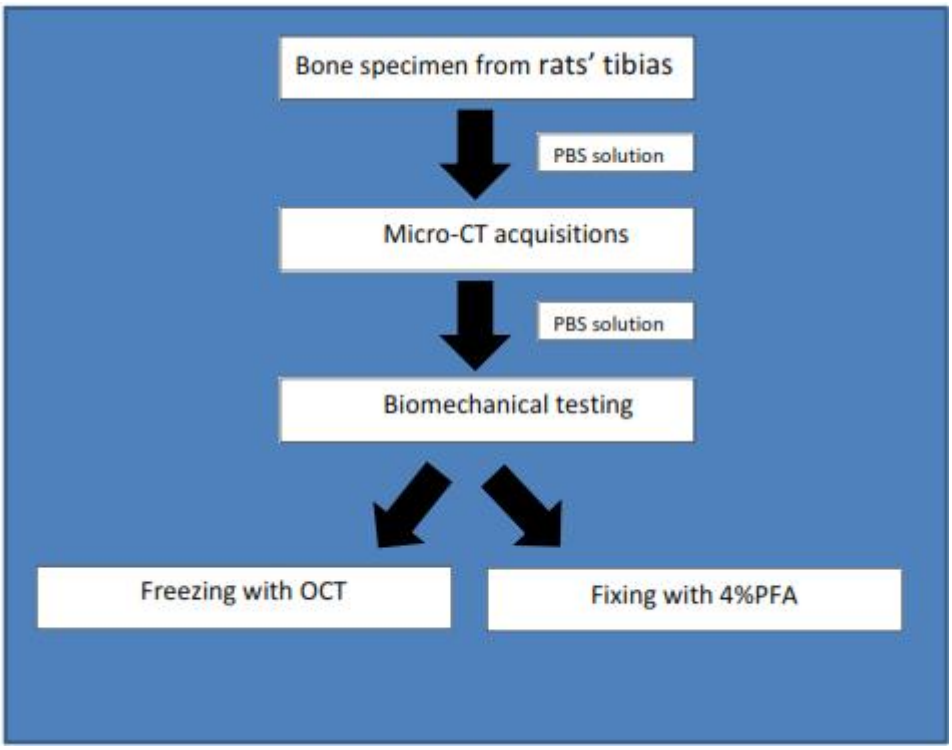

Figure 2.15 The steps taken following retrieval of tibias from experimental animals including the healing assessments and sample preparation techniques

2.6 Micro-CT imaging

Micro-computed tomography (micro-CT) is x-ray imaging in 3D. It is a similar technique to conventional CT commonly used in hospitals. In micro-CT imaging, a high intensity of x-ray are required and projected to objects or samples. The projection of x-ray beam attenuation (the reduction in the x-ray beam intensity as it passes through objects) is acquired at multiple views using a 360°-rotation platform to reconstruct a 3D-image which provides very fine scale internal structure of objects without destruction of samples. This technique has been widely used in bone research for evaluation of small bone samples from pre-clinical studies. This is a non-invasive technique that can be used to assess the component of fracture healing and also to evaluate fracture healing qualitatively and quantitatively. In this study, bone samples using micro-CT were assessed according to published guidelines (Bouxsein et al., 2010).

Tibial samples were scanned using micro-CT at the end of the experiments. Fracture sites were evaluated using a Skyscan® 1172 X-ray micro-CT scanner (SkyScan, Belgium) (**Figure 2.16**) with the beam set at 54 kVp, 185 μA and a 16-μm isometric voxel size with 0.5-mm aluminium filter. Image reconstructions were created using Skyscan® NRecon software and the analysis of fracture healing was performed using Skyscan® CTan software.

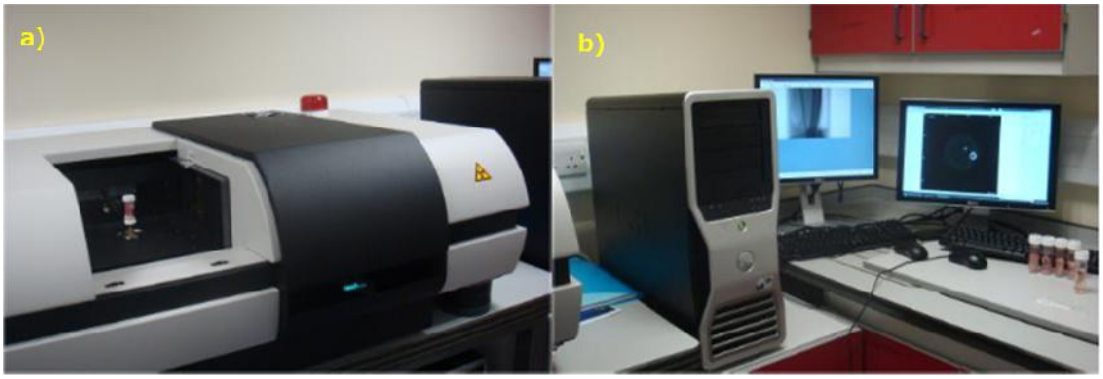

Figure 2.16 Micro-CT set up including (a) the micro-CT Scanner and (b) the hardware used to process and reconstruct images

2.6.1 **Calibration for micro-CT analysis using hydroxyapatite (HA)**

The Hounsfield unit (HU) is a universally available accepted reference for describing radiodensity in computed tomography. It is a quantitative scale which is a linear transformation of the linear attenuation coefficient measurement based on the linear attenuation coefficients of water (Goldman, 2007). It has been reported that HU of bone tissue was greater than 700 depending on the types (woven or cortical) of bone tissues (Norton and Gamble, 2001).

In this study, HUs were used to describe the radiodensity of scanned samples. Prior sample acquisition using 250 and 750 mg/cm^3 Hydroxyapatite (HA) phantoms were used for calibration of bone mineral density (BMD) (**Figure 2.17**) according to the equation from the regression model. This allowed the BMD of the fracture callus to be determined.

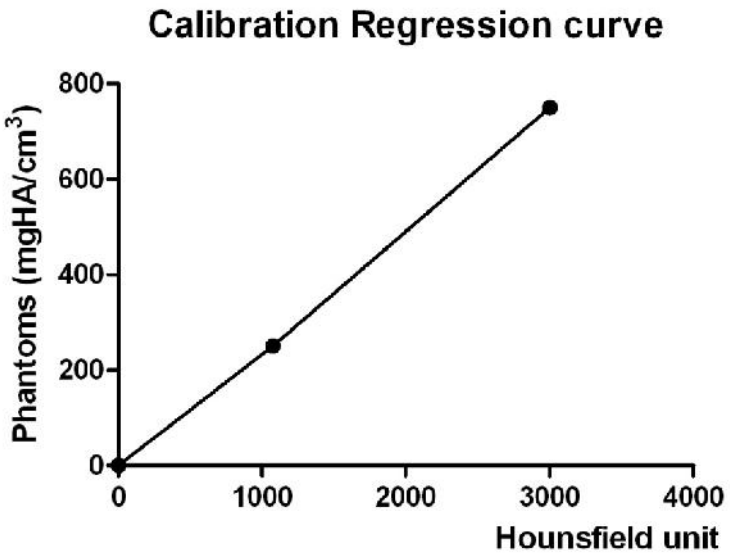

Figure 2.17 The calibration regression curves using two different HA phantoms (250 mg/cm3 and 750 mg/cm3) and water

2.6.2 **Acquisition, processing and reconstruction of images**

In preparation for scanning, each rat tibia was placed in a plastic tube filled with PBS. The bone (in the vertical axis) was then scanned in a plane perdendicular to the x-ray beam. The image files were reconstructed using Skyscan® NRecon software. For evaluation, the volume of interest (VOI) was selected by the following steps. The central plane of fracture callus was selected based on the proximal and distal ends of the osteotomy site. The regions of interest (ROI) were manually delineated around the callus at the top plane (0.5 mm. upper from mid-plane) and the bottom plane (0.5 mm. lower from mid-plane) (**Figure 2.18**). The VOI was defined using automated interpolarization in Skyscan® CTan software and the VOI was then evaluated for accuracy. Then, the VOI was obtained over 1 mm. at the fracture site. The next step was to segment the contents of the VOI to separate the mineralised tissues from soft tissues. HU was used as the reference, the threshold of bone tissue was defined according to universal HU for bone (above 750 Hounsfield units) and was applied as

a fixed global threshold (**Figure 2.19**) (Goldstein, 1987); it was found that this selected threshold gave the least change in the BV/TV from normal bone samples.

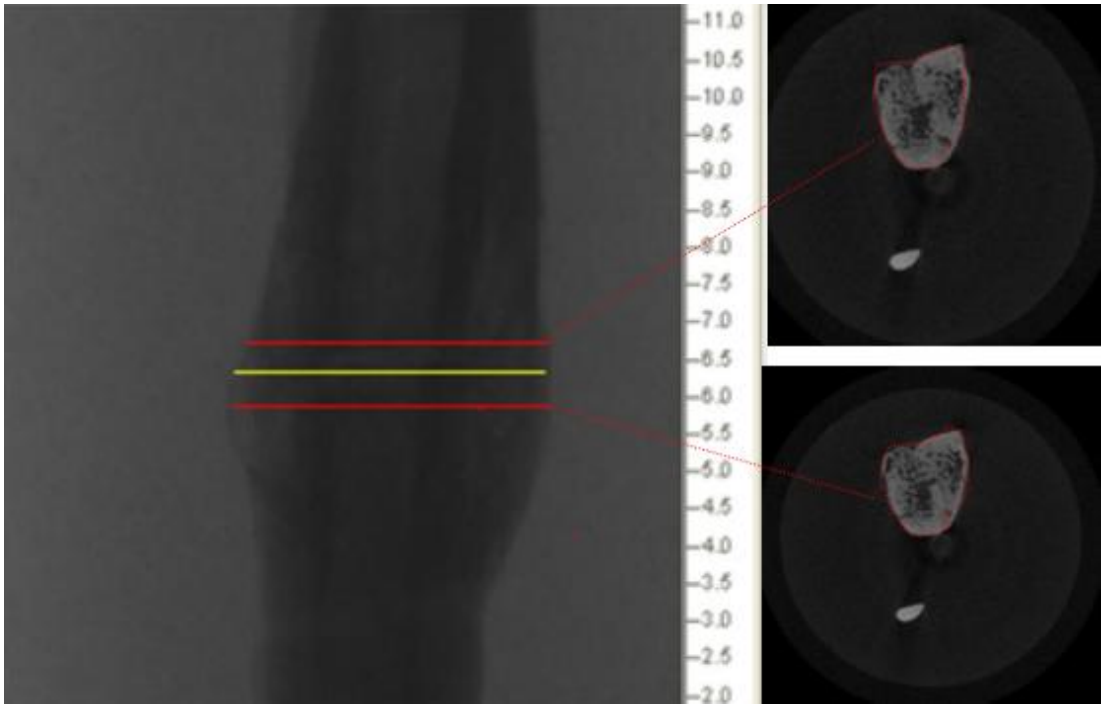

Figure 2.18 Defining volume of interest at a 1mm-gap (yellow line represents the middle of the fracture gap, and red lines represent the delineated areas at the top and the bottom of fracture gap)

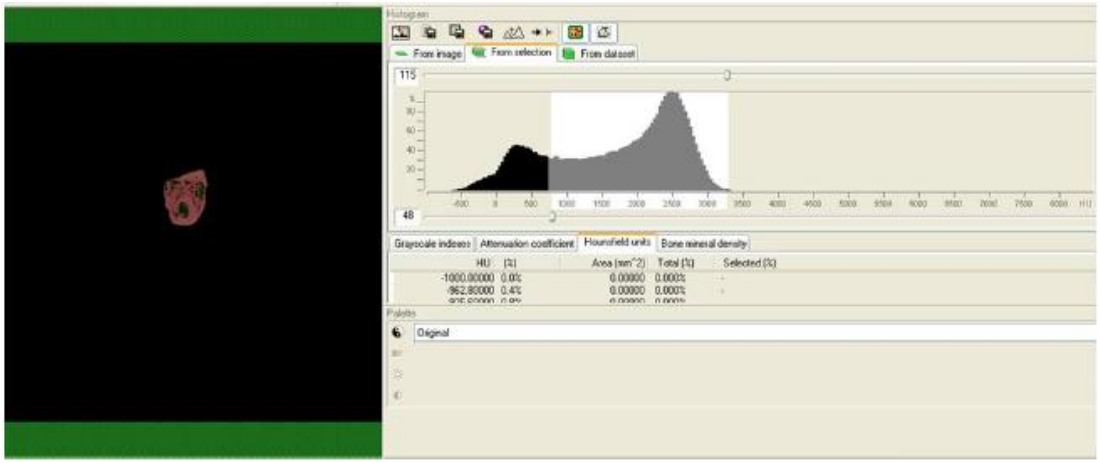

Figure 2.19 Fixed global threshold applied to separate bone and non-bone tissues

2.6.3 **Micro-CT analysis**

Four main aspects of the micro-CT analysis are present in this study.

2.6.3.1 Fracture callus morphometric parameters

After acquisition of samples and segmentation of images, 3D reconstructed images from VOI were analysed using Skyscan® CTan software to determine properties of the fracture callus in the osteotomy gap including: Bone volume/Total volume (BV/TV), Bone surface area/Total volume (BS/TV), Trabecular number (Tb.N) Trabecular thickness (Tb.Th) and Trabecular separation (Tb.Sp) in order to facilitate comparison between different treatments. Each parameter from this analysis was described in different aspect of bone morphology.

BV/TV: The fraction of the total bone volume as defined by the threshold values to the total volume of interested (VOI) (Parfitt et al., 1987). This parameter was presented a percentage value as a normalised parameter in order to compare samples of different size.

BS/TV: The bone surface density, given by the ratio of the segmented BS to the VOI, where BS was computed using the Marching Cube algorithm (Muller and Ruegsegger, 1995).

Tb.N: The inverse of the mean distance between the mid-axes of bone structures from the VOI (Hildebrand et al., 1999).

Tb.Th: This represented the average of thickness of bone structures in the VOI. It was determined using the mean diameters of fitting maximal spheres fitted into the bone structure (Hildebrand and Ruegsegger 1997).

Tb.Sp: This represented the average space between bone structures in the VOI. It was determined using the mean diameters of fitting maximal spheres fitted into the non-bone structure (Hildebrand and Ruegsegger 1997).

2.6.3.2 Bone mineral density of callus

Bone mineral density (BMD) is a parameter that determines the degree of mineralization in fracture callus and is an important determinant of bone quality (Miller et al., 1999). In this study, bone-equivalent phantoms were used to calibrate and calculate the BMD of scanned object based on HU scale according to the following equation (2.4).

$$BML = \frac{HUobject - 110.80}{3852.36} g/cm3 \qquad \textbf{Equation 2.4}$$

(HU object: an HU value of scanned bone samples)

2.6.3.3 Describing bone continuity using minimal bone area fraction across the fracture site

This technique was previously reported (Schmidhammer et al., 2006) to evaluate and quantify the connectivity of the bridging cortices of the callus. The original cortical area was delineated circumferentially at proximal and distal parts across the fracture site over 10 mm as the references and ROI each section across the fracture were defined using automated interpolarization in the Skyscan® CTan software. The bone fractions (the bone area/ the total area) from each plane were assessed using 2D analysis and these values were plotted across 10 mm-section over the fracture site. The minimal value of bone area fraction of each sample was determined.

2.6.3.4 Presentation of 3D images

3D images of bone samples or callus at the fracture that were presented in this study were created and modified using Skyscan® CTvol software.

2.7 Biomechanical study

Biomechanical testing is used to determine the effects of force on biological materials. In this study, bone samples with callus were assessed for their mechanical properties. Bone healing was compared using biomechanical parameters in response to given interventions.

The loading mode of testing is dependent on the direction of the force applied to the samples. Loading modes include axial loading (compressive or tensile) bending, torsional loading and multi-axial loading. Loading due to bending was selected to use for evaluation of the bone samples. It has been reported that the bending test is appropriate for determining the mechanical properties of a small animal bones such as from rodents. This is because compression, tension and torsion tests require that the object being tested is uniform in shape: this is not applicable for whole bone samples particularly with long bone specimens (Turner and Burr, 1993). Bending results in a build-up of tensile and compressive stress in the sample. Tensile bone strength is weaker than compressive bone strength, thus the fracture propagates from the tensile side of the sample which is the opposite side of the load cell to the compressive side (Reilly and Burstein, 1975).

Bending can be applied using 3 or 4 point-bending. 4 point-bending is considered to be more appropriate to test bone with callus samples. The loading point will not touch the callus. There is no shear force in load section so it is only loaded by “pure bending”. The bending moment is constant over the load section (Wilson and Carlsson 1991). In this study, four-point bending test was performed to measure the

maximum load, ultimate stress, stiffness, and toughness of fracture callus at the mid-diaphysis of the tibia.

2.7.1 **Sample preparation techniques**

Tibias were harvested from experimental animals. In this study, all samples were tested without debriding overlying muscle, unless otherwise stated. It was found, from examining micro-CT images during a preliminary study that removal of overlying muscle may disrupt callus. Moreover, the muscle was found to hold the sample in the stable position during testing. This preparation technique was validated and compared with the standard technique in chapter 5.

2.7.2 **Machine and setting**

Samples were tested using a Zwick/Roell Z005 material testing machine (series 4500, Instron Corp. Canton, Mass, USA) using the four-point bending. The bone was placed on four point loading jig shown in **Figure 2.20**. This jig was designed and provided by the University of Edinburgh Engineering Workshop (King Building, Edinburgh). The upper loading had a span of 8 mm. and was manufactured to incorporate a pivot to allow both load application points to contact the specimen during testing. The lower loading had two supporting bars with a span of 20 mm. The upper and lower loading bar were rounded to eliminate notching when testing. All samples were tested in the same direction from the medial aspect of tibiae. It was found that the samples with muscle were stable during loading. The two loading points contacted the sample at the same time, thus, these should produce an accurate result. The loading rate was 5mm/min. Samples were preloaded with 5 N forces. The biomechanical testing was performed at room temperature.

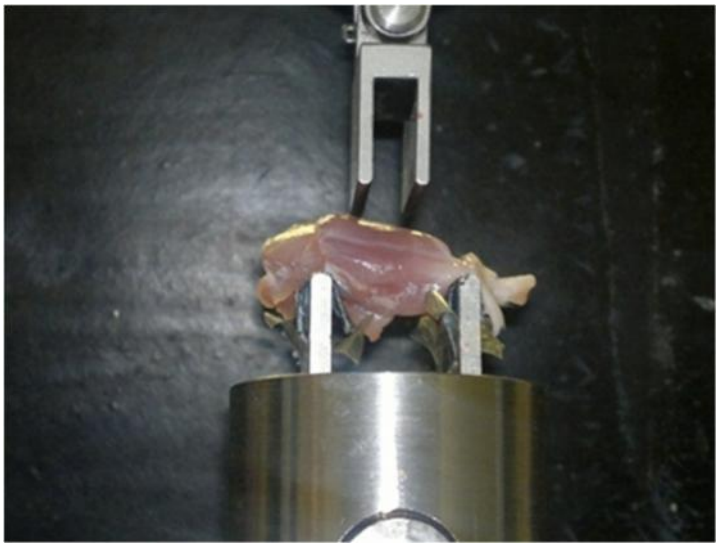

Figure 2.20 The four point bending apparatus set up with the tibia (with overlying muscles in situ) prior to testing.

2.7.3 **Analysis of the biomechanical data**

The testing machine was interfaced with the laboratory data acquisition program, "TestXpert™", providing simultaneous measurements of deflection and load. The program displayed the data sets as load (N) to displacement (mm). It also showed the load-displacement graph enabling real-time monitoring during the test. Ultimate load was taken from load-deformation curve. Ultimate load is the maximal load that a sample can sustain before failure (N). The recorded load-deformation curves were normalized by cross-sectional area and this curve could be converted to stress–strain curves. Ultimate stress, young's modulus and toughness were determined from this curve. The cross sectional area of normal bone appeared to be a hollow triangular shape. The observation was done in cadaver.

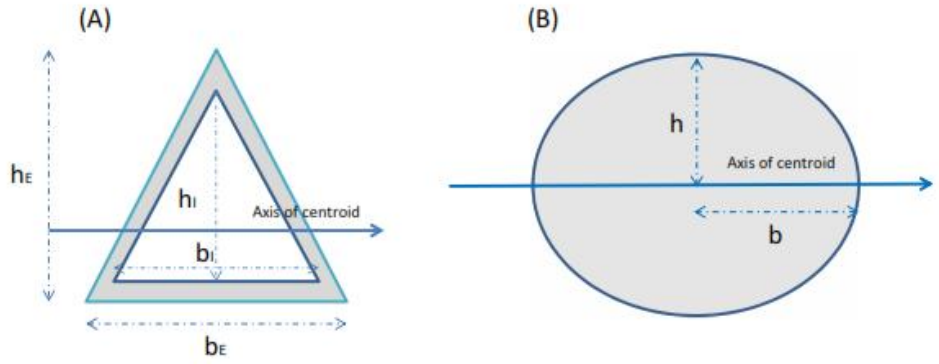

Figure 2.21 Cross sectional area; (a) normal bone (b_I and b_E = horizontal measurement of the internal and external width of bone, respectively, h_I and h_E = vertical measurement of the internal and external height of bone, respectively) (b) callus (b = horizontal measurement of callus and h = vertical measurement of callus

The cross section moment of inertial of the tibia was calculated based on a triangular shape with a base width of b and height h with respect to an axis through the centroid, which was one third of the height from the base of triangle. The cross section moment of inertia of the internal triangle was deducted from the cross section moment of inertia of external triangle (**Figure 2.21a**). Cross sectional motion of inertia of bone was calculated from the following equation (2.5):

$$\boldsymbol{I = \frac{1}{36}\left[\left(b_E h_E^3\right) - \left(b_I h_I^3\right)\right]} \quad \textbf{Equation 2.5}$$

The fracture callus was considered to be a solid ellipse (**Figure 2.21b**), thus cross sectional motion of inertia of callus was calculated from the following equation (2.6):

$$I = \frac{1}{4}\pi b h^3$$ **Equation 2.6**

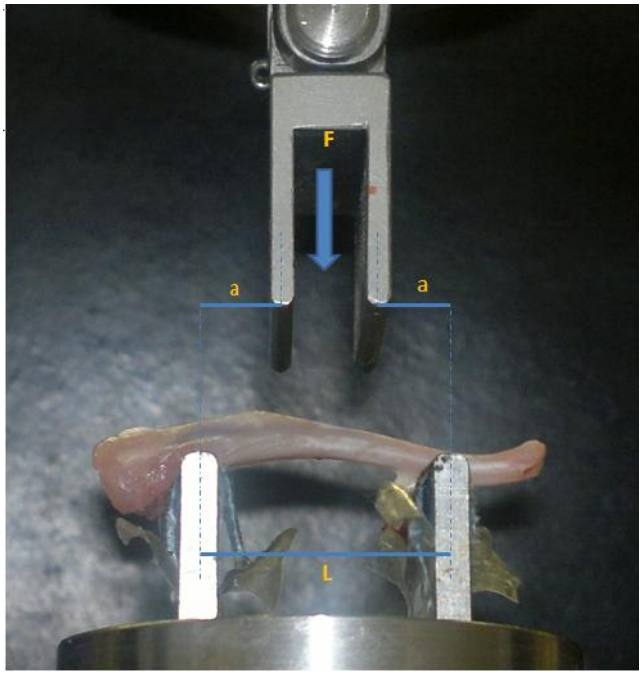

Figure 2.22 Diagram of four point bending; F = force, a = distance from outer to inner contact and L = span of outer contact

Then, the cross sectional moment of inertia and diagram of four point bending (**Figure 2.22**) were used to calculate bending stress using the following equation (2.7):

$$\sigma_b = \frac{(F \times a \times c)}{2I}$$ **Equation 2.7**

(where c = distance from the centre of the mass)

Strain from this study was calculated from the following equation (2.8):

$$\varepsilon = \frac{(6 \times c \times displacment)}{a(3L - 4a)}$$ **Equation 2.8**

Young's modulus (E) was calculated from a ratio between Stress (σ_b) and strain (ε). It was defined by the slope of the linear portion of the stress-strain curve (N/mm).

$$E = \left(\frac{F}{displacement}\right) \times \left(\frac{a^2}{12I}\right) \times (3L - 4a)$$ **Equation 2.9**

The area under the stress–strain curve is the toughness, which represents the energy absorbed when the sample was loaded. The toughness was the energy required per unit volume of sample to produce fracture. It was computed using GraphPad programme using the calculation area under curve option.

2.8 Histological evaluation

According to the fracture assessment protocol (**Figure 2.15**), samples were processed for histological evaluation following micro-CT and biomechanical testing. To prepare samples for histological evaluation of fracture healing, 4% PFA was used for fixation over a period of 48 hours. It has been reported that this period provides optimal fixation (Helander, 1994). Samples were then decalcified in Ethlyenediaminetetraacetic acid, disodium (EDTA), a gentle decalcifying agent which perseveres most of the protein during decalcification at PH 7 for 3 weeks. This

solution was changed every 3-4 days (McKee et al., 1991). Decalcified samples were embedded in paraffin. 6 μm sections were cut using microtome (Shandon, Thermo Fisher Scientific ™, Waltham, MA) and mounted onto "Superfrost plus" slides (BDH biosciences ™, Poole, UK). These processes and the preparation of histological sections from samples were performed at the Queen's Medical Research Institute Shared University Research Facilities (SuRF @ QMRI) with the assistance from staff in the unit.

2.8.1 **Histological assessment of fracture healing**

Prepared sections of harvested samples obtained from animal studies were stained with Haematoxylin and Eosin (H&E). The H&E sections were observed using a light microscope (Eclipse E800, Nikon). General morphology and bone bridging were evaluated. The presentation of either intramedullary or cortical bone bridges confirmed a bone union. To quantify the different tissue types present within the fracture gap, images of the inter-fragmentary gaps were captured at x10 magnification using the microscope camera (Digital Sight DS-Fi2, Nikon). The images were processed in NIS-Elements Br Microscope Imaging Software (Nikon) and analysed using image J software. 10x10 grids were created and placed over the images. The area of the grid taken up by the area of interest was divided by the total area to calculate the percentage. (**Figure 2.23**) Three sections at the middle of each sample were examined systematically from triplicate samples.

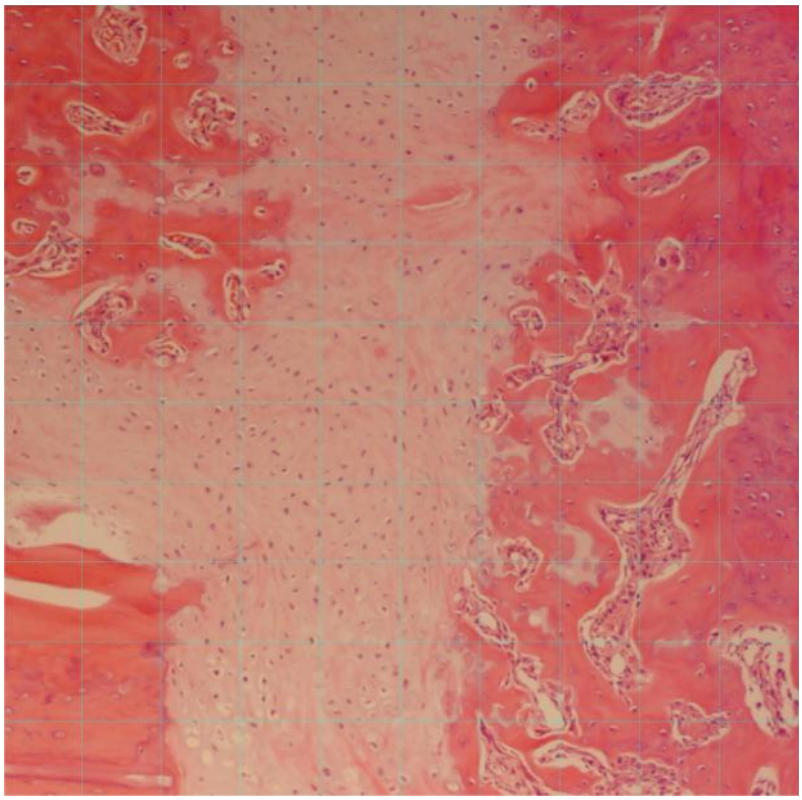

Figure 2.23 Tissue quantification method; 100 grids on the histological sections determining the percentage of tissue types (x100)

The tissue at the fracture gap was defined as bone, cartilage, fibrous tissue and bone marrow/empty space and tissue types were expressed as a percentage. The histological appearance of each tissue was determined from H&E staining. Bone tissue was defined from mineralised osteoid tissue (**Figure 2.24a**). Masson's Trichrome staining was used to demonstrate and observe the area of new bone formation (**Figure2.24b**). Chondrocytes were observed in defined cartilage tissue and they can be seen to be clustered in groups (**Figure2.25a**). Safranin-O/Fast green staining was used to stain the area of cartilage tissue (**Figure 2.25b**). Fibrous tissue was observed (**Figure 2.26a**) and bone marrow or empty space was demonstrated in **Figure 2.26b**.

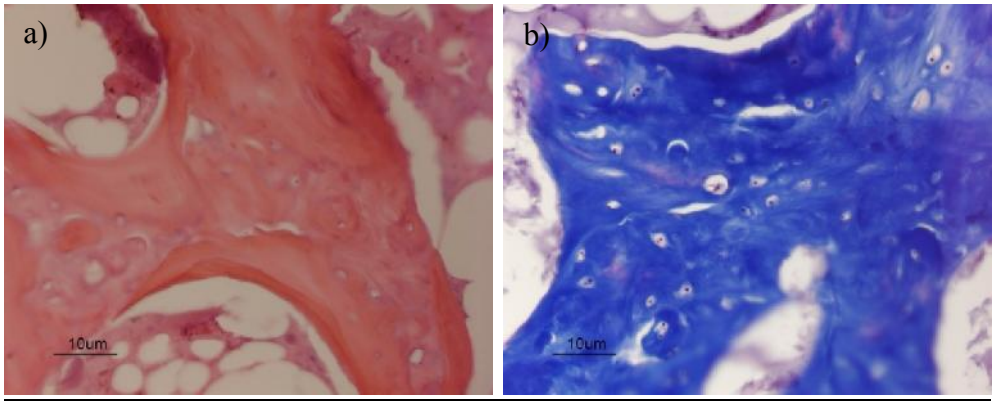

Figure 2.24 Bone area from histological section; (a) H&E staining, (b) Masson's trichrome staining

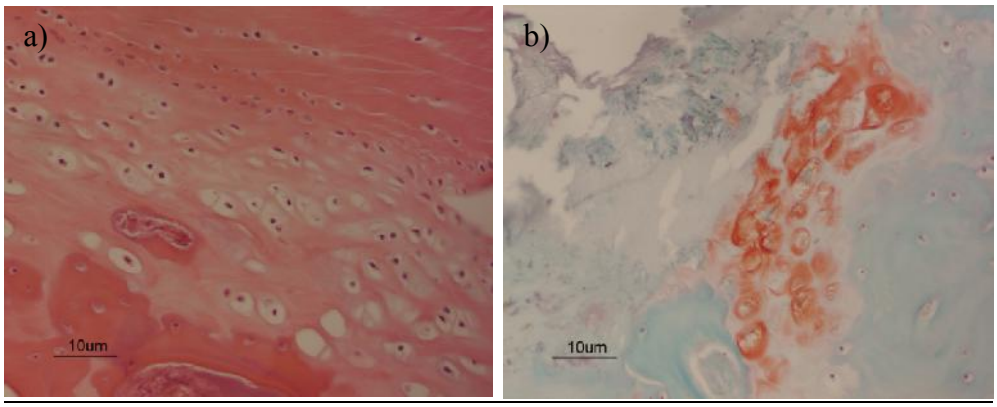

Figure 2.25 Cartilage tissue area from histological section; (a) H&E staining, (b) Safranin-O/Fast Green staining

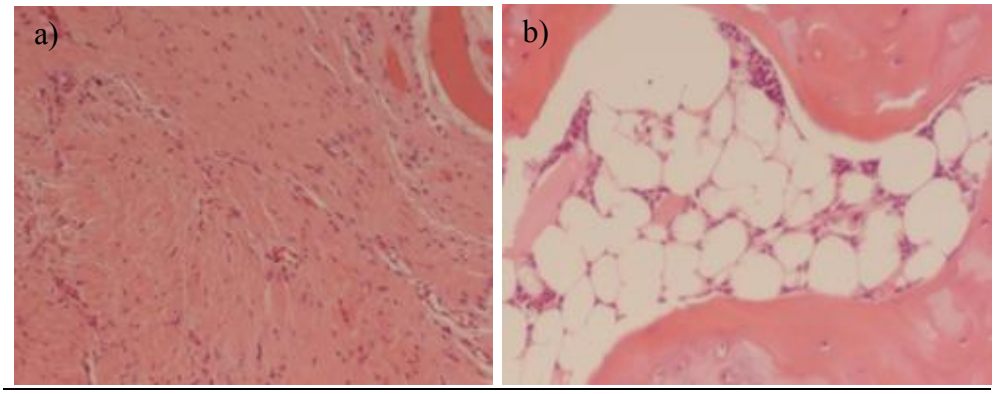

Figure 2.26 Histological area demonstrating (a) Fibrous tissue and (b) bone marrow /empty space

2.8.2 **Validation of tissue quantitation methods**

The counting grid method to assess the tissue components was classified as a semi-quantitative technique. The results represent the estimated percentage determined from the dominant tissue from each grid. Thus, a percentage of bone area using a counting grid method (estimate) and a percentage of actual bone area, calculated from delineated bone using ImageJ software were assessed for their correlation. Bone area was used for validation as it was a key parameter for fracture healing evaluation. There was a strong agreement between the semi-quantitative technique and direct selection of delineated bone area (**Figure 2.27**).

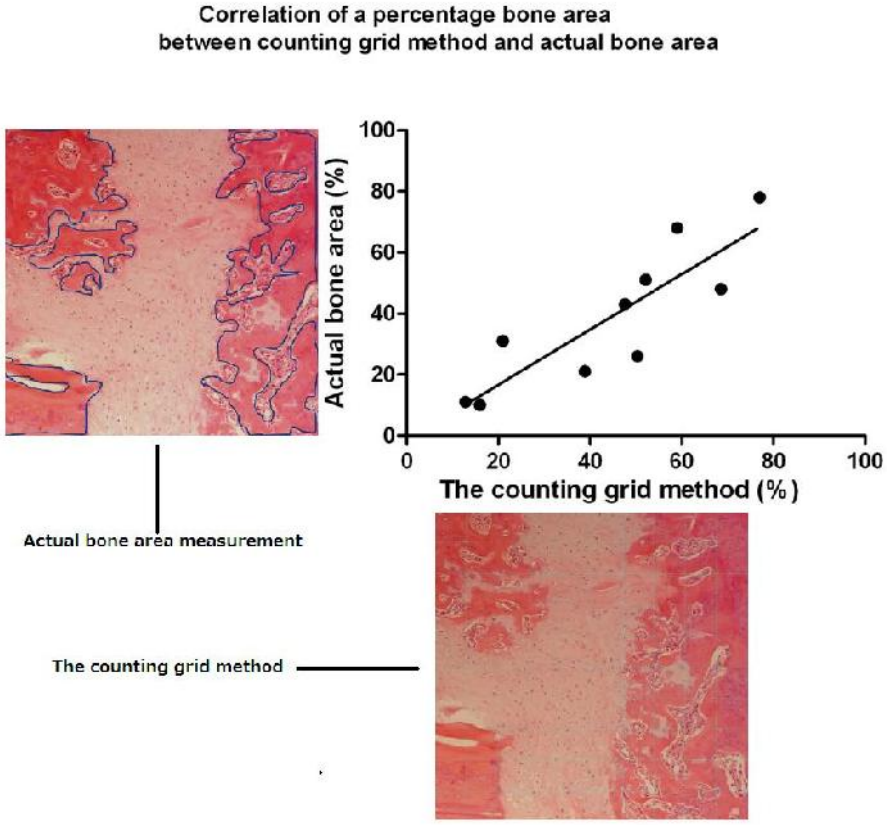

Figure 2.27 Correlation of percentages of bone area using a counting grid method (estimated) and the actual bone area (delineated bone manually technique); Pearson r = 0.86, P-value = 0.0013, n = 10

2.9 Immunocytochemistry and immunohistochemistry

Both immunocytochemistry (ICC) and immunohistochemistry (IHC) were applied to label specified antigens such as proteins, synthetic polypeptides, nucleic acids, lipids, carbohydrates and small chemical groups using an antibody from cell culture or histological sections. These methods rely on the specificity, affinity and sensitivity of antibody-antigen interactions. The localisation of the antibody can be visualised microscopically using either enzyme mediated reactions visualised in brightfield or fluorescent labelling. In this study, ICC has been used for characterising human MSC

and human PSC with specific cell membrane markers. In addition, IHC has been used to demonstrate the injected human cells at the fracture site from the histological section using a human specific nuclei antibody.

2.9.1 **Antibodies**

Antibodies, which are also known as immunoglobulin (Ig) have a specific interaction with targeted antigens, which forms the basis of immunochemical methods. This principle can be applied to discriminate between related compounds. The region of the antigen that blinds with an antibody is defined as the epitope. This forms molecule of epitope of one molecule can be found similar to the others, this is known as cross-reaction. The number of antibodies that are required depends on the methods of immunocytochemistry. There are two common techniques: direct and indirect. With the direct method, a labelled primary antibody is used to detect the targeted antigen, where the interaction of antibody-antigen can be visualised directly. This method is simple and requires only a single antibody, but it provides limited signal visualisation. In this study, the direct technique was mainly applied for ICC in cell cultures. With the indirect methods, an unlabelled primary antibody is used and a labelled secondary antibody is added to provide signal amplification (Manning et al., 2012). The secondary antibody interacts with the immunoglobulin of the animal in which the primary antibody was raised. This method is more sensitive than the direct method because the secondary antibody can react with different antigenic sites on the primary antibody. In this study, this method was applied to paraffin sections in order to stain antigens specific to human nuclei. This following table lists the various antibodies used in this study.

Table 2.4 Antibodies used in this study

Antibody	Host	Clone	Company	Dilution
Purified Anti-Human CD90	Mouse	5E10	BD Pharmingen™	1:100 for ICC
Purified Anti-Human CD44	Mouse	G44-26	BD Pharmingen™	1:100 for ICC
Purified Anti-Human CD146	Mouse	P1H12	BD Pharmingen™	1:100 for ICC
Anti- Human CD34-FITC	Mouse	581/CD34	BD Pharmingen™	1:50 for ICC
Anti-Human CD31	Mouse	JC70A	Dako™	1:50 for ICC
Anti-Human CD19-FITC	Mouse	HIB19	BD Pharmingen™	1:50 for ICC
Purified Anti-Human NG2	Mouse	9.2.27	BD Pharmingen™	1:100 for ICC
Anti-Actin,α-Smooth Muscle-FITC	Mouse	1A4	Sigma-Aldrich™	1:200 for IF
Anti-Rat CD68	Mouse	ED1	Abcam™	1:800 for IHP
Anti-Human Nuclei Antibody	Mouse	235-1	Chemicon™	1:50 for ICC, 1:20 for IHP
Alexa Fluor® 488 Anti-Mouse IgG (H+L) Antibody	Goat	N/A	Life Technology™	1:500

2.9.2 **Specimen preparation**

Before antibody staining, a fixative step, antigen retrieval, permeabilization of cells membrane and blocking non-specific background labelling were required. Samples from either cultured cell or histological sections were fixed to preserved morphology. A mixture of Methanol and Acetone (50:50) was used for the cell culture sample or the frozen tissue section and 4% paraformaldehyde was used with the paraffin embedded samples. This step protected the samples from the rigours of subsequent processing and staining. However, use of fixative can damage antibodies, so they have to be removed or neutralized with PBS before immunolabelling. The process of fixation or paraffin embedding may lead to the formation of cross-linkages or protein denaturation which causes epitope masking. This may result in false negative staining.

Paraffin sections require unmasking of the antigen in a process called "antigen retrieval". There are several techniques that can retrieve the antigens and maximise the presence of antigens for interaction with a specific antibodies. In this study, heat-induced epitope retrieval through microwave irradiation was selected.

It is important to permeablilize cell membranes to allow an antibody to penetrate into intracellular components. To stain the human specific nuclei, histological sections or human cell cultures were treated with 0.1% triton X-100 in PBS.

False-positive staining may occur with "background staining" and "non-specific labelling", in which the antibodies interact with sites not specific to the target epitope. Blocking agents, such as serum which contains a high concentration of proteins, can be used to saturate these non-specific binding sites to minimise this phenomenon. The host from which the blocking serum is derived is usually equivalent to the host of the secondary antibody. For example if the secondary antibody is goat anti mouse, the most appropriate blocking serum would be goat serum. However, because of the availability of commercial serum-free protein block, protein Block Serum-Free (DAKO, UK) was used in this study as it can be used with

any primary or secondary antibody and eliminates cross reactivities. Blocking solution was applied to the tissue before the primary antibody.

2.9.3 **Antibody detection**

There are three common detection methods; 1) colorimetric or enzyme mediated, 2) fluorescence and 3) colloid gold. The fluorescent detection method was used in this study. This method was used to label intact cells in culture, which was required for cell characterisation. The enzymatic method is limited by diffusibility of the enzyme product and unable to label intact cells in culture. A fluorescent detection method technique requires basic fluorescent microscopy, whereas the immunogold method requires more complex electron microscopy. In this study, fluorescent detection was found to be a suitable method in our laboratory setting.

2.9.4 **Required Controls**

Controls are essential for the accurate interpretation of immunochemical results and the avoidance either false positive or false negative results. Positive controls used in this study confirmed the reactivity of the antigens, antibodies and substrate markers used. In this study, human bone marrow cells were used as the positive controls for hMSC characterisation using hMSC marker specific antibodies. Human foetal tissues were used as positive controls for the implanted hMSC tracing study using anti human nuclei antibody. Negative controls assess the non-specificity of the immunolabelling technique. There are several methods by which this can be carried out. A tissue can be used where it is known that the target antigen is absent. A section from non-union tissue without cell injection was used as negative control for the implanted hMSC tracing study using anti human nuclei antibody. Either omitting primary antibodies or using an isotype control antibody as per company's

recommendation was applied to act as negative controls for hMSC characterisation using hMSC marker specific antibodies.

2.10 Tracking implanted cells

In order to trace implanted cells from both animal and human source, cells were labelled using CM-Dil (Invitrogen, USA) prior to injection. The labelling protocol was performed as per manufacturer's guidelines. To determine the effects of CM-Dil at different dilution on cell viability and proliferation, a dye exclusion method (Trypan blue) and a functional assay of colony forming-unit were used (Appendix A). Cultured cells that were prepared for transplantation by labelling with 2.5 µg/ml CM-Dil for about 1 hour at 37 °C followed by three PBS washes to remove the excess dye. Thus, the labelled cells were clearly visible in *in vitro* condition and therefore this method could be used to trace the implanted cells delivered to the fracture area using fluorescence microscopy. CM-Dil labelling has been used for tracking the distribution of MSCs *in vivo* and differentiation following transplantation over long term periods (Weir et al., 2008).

Besides the CM-labelling method, a IHC technique using anti-human Nuclei Antibody (Chemicon, UK) was also applied to identify the human cells. The sample preparation and staining protocol was performed according to the company's recommendation, using a dilution of 1:50. Goat Anti-Mouse IgG (H+L) – Alexa Fluor® 488 (Life technology, UK) was used as a secondary antibody at 1:500 dilution. Sections of paraffin embedded human foetal upper limb tissue (kindly provided by Miss Angela Briski, Péault Bruno's group) were used as positive controls. The details of the IHC technique are described in section 2.9. This antibody is specific to the human-specific nuclei, so it can be used to visualise and localise the donor material in the host environment to identify human cells in xenograft models under fluorescence microscope.

2.11 Immunological reaction study

2.11.1 Evaluation of inflammatory cytokines

2.11.1.1 Assay kit for evaluation of inflammatory cytokines

A panel of inflammatory cytokines from rat serum were assessed using the commercial kit; Rat Inflammatory Cytokines Multi-Analyte ELISArray Kit: MER-004A (SABiosciences^{TM}, USA) (**Figure 2.28**). This kit was used to determine 12 pro-inflammatory cytokines simultaneously (IL1A, IL1B, IL2, IL4, IL6, IL10, IL12, IL13, IFNγ, TNFα, GM-CSF, and RANTES). A conventional ELISA (Enzyme-Linked ImmunoSorbent Assay) protocol all at once under uniform conditions has been designed accurate and easy use. The protocol for this assay is provided in appendix B. An optical density (OD) from each well was interpreted within ranges recommended by the company.

Figure 2.28 Evaluation of rat inflammatory cytokines using multi-analyte ELISA array. Shown here are (a) the reagents used and (b) the ELISA array machine immediately prior to sample evaluation

2.11.1.2 Serum collection

Blood samples were obtained from animals at the time of cell injection, 2, 4, 6, and 8 weeks post injection. Approximately 1.0 ml of blood was taken from the tail vein (Parasuraman et al., 2010). The harvested blood was collected in a sterile tube (without EDTA) and incubated at room temperature allowing samples to clot for 30 minutes before centrifugation for 15 minutes at 1,200 rpm. Then, serum (the top part of column) was collected and stored at -20°C. The samples were always aliquoted to avoid repeated freeze / thaw cycles. Rat serum samples required a 2-fold dilution with sample dilution buffer before proceeding with the assay (following kit's recommendation).

2.11.1.3 Rationale for using Multi-Analyte ELISArray

Cytokines or antigens present in rat serum were detected using the principle of ELISA. Firstly, the antibodies targeting a specific antigen attach to the well of plate in which it can bind specifically to the antigen and then another antibody linked to enzyme for detection and amplification. Originally, this method was used to measure only one cytokine or antigen at a time in a given sample. However, this may be a problem if the amount of sample is limited and there are several target antigens required in the study. In this study, the volume of serum that was harvested at each time point was limited because the excess blood loss can affect the animals' health. Therefore the multiplex array was selected allowing the determination of several inflammatory cytokines in the same sample simultaneously. The optimisation of ELISA for multiple analytes kit requires two processes during assay development. Firstly, screening for capture and detection antibody pairs with the best performance, the criteria included are the high sensitivity and good linearity (**Figure 2.29**). Secondly, in order to optimise for the ELISA experimental conditions to allow simultaneous development of the read out, multiple cytokines have been evaluated

simultaneously at the same time and condition, so their concentrations have to be optimised under the same experimental ELISA conditions to achieve the same development or incubation time.

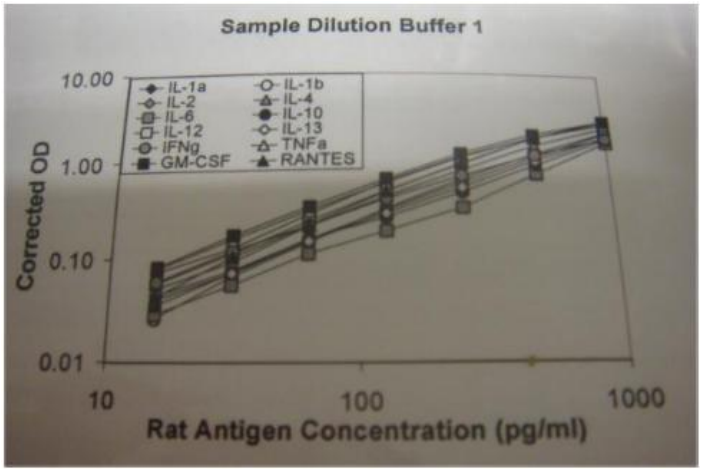

Figure 2.29 Standard curve demonstrating high sensitivity and good linearity within the ELISA

2.11.4 Data interpretation

As per the manufacturing company's recommendations, the corrected Optical Density (OD) value was subtracted from the negative controls for each cytokine. The data were present as the fold change using the corrected OD from the serum that was collected at the 0 time point as the reference.

2.11.2 **Popliteal lymph node evaluation**

Lymph node reactions are part of the host defensive responses associated with inflammatory stimuli (Elmore, 2006). Popliteal lymph nodes receive the lymphatic drainage from the lower limb. They are sited around tibial blood vessels (Sainte-Marie et al., 1982), so any inflammation or stimuli at the tibia may result in morphological changes in this regional lymph node. They have been the object of

histological evaluation for immune response in previous reports (Willard-Mack, 2006, Bondarenko et al., 2011).

2.11.2.1 Sample preparation

One popliteal lymph node was harvested from each animal receiving different treatments, fixed in 4%PFA, and embedded in paraffin. Lymph nodes from the contralateral side (non-operated site) were used as controls. Histological sections from the middle portion of the lymph node were cut at 6 μm thickness using a microtome (Shandon, Thermo Fisher Scientific TM, Waltham, MA). Sections were stained with H&E and three selected sections, consisting of the cortex area, the medullary are and the hilum were used for the morphological assessment (**Figure 2.30**).

2.11.2.2 Lymph node response

All Sections were visualised under a light microscope (Eclipse E800, Nikon). The images were captured using a microscopic camera (Digital Sight DS-Fi2, Nikon) and they were processed in NIS-Elements Br Microscope Imaging Software (Nikon) and analysed using image J software. The morphological changes in the popliteal lymph node, which may reflect the condition of local immune response after exogenous cell transplantation, were assessed using (1) the size of lymph node, (2) the number of secondary follicles, (3) the number of infiltrated cells in the sub-capsular sinus area, and (4) the number of macrophages in the medullary cord area.

The size of lymph node

Lymph node enlargement or lymphadenopathy is associated with immune responses against foreign antigens (Kumar et al 2004). The size of lymph nodes reflects the

degree of the inflammatory response. To compare the size of lymph nodes in the different groups and the normal control, sections of prepared popliteal lymph node were captured under x4 magnification and the area of lymph node was selected (**Figure 2.30b**) and measured using Image J. The area was expressed in mm^2.

The number of secondary follicles

The lymphoid follicles are located in the cortex area of lymph nodes. In the absence of immune stimulation, there are only primary follicles which consist of small B cells (memory B cells). In the presence of immune reaction, the primary follicles are activated and display secondary follicles or germinal centres which consist of antigen recognizing B cells. The increase in the number of secondary follicles or presence of follicular hyperplasia is an indication of an ongoing immunological reaction. In this study, the number of secondary follicles (the enlarged follicle with a light germinal centre) were counted manually at 10x magnifications (**Figure 2.30c**).

The number of infiltrating cells in the subcapsular sinus area

The subcapsular sinus which surrounds the lymph node is a gateway for afferent lymphatic drainage. The antigens and immune complexes from the inflammatory site will initially be drained into this area (Kamperdijk et al., 1987). In this study, the number of infiltrating cells (lymphocytes and macrophages) in the subcapsular sinus area were counted under 20x magnification (**Figure 2.30d**).

The number of macrophages in the medullary sinus area.

The medullary sinus is located at the medulla area of lymph nodes (deep to the cortex area). It is irregularly shaped and has fluid-containing spaces which predominantly contain macrophages. Macrophages play a role in the innate immune response as phagocytic cells that internalize and degrade foreign antigens and release mediators to activate an adaptive immune system (Gordon, 2007).An increase in the numbers of macrophages in the medullary sinus area is associated with the inflammatory response (Steer and Foot, 1987, Gray and Cyster, 2012). In this study, macrophages which were observed as large and round cells with rich cytoplasm were counted at

40x magnifications (**figure 2.30e**) on H&E sections. The presence of macrophages was demonstrated using IHC for CD68 (**Figure 2.31**).

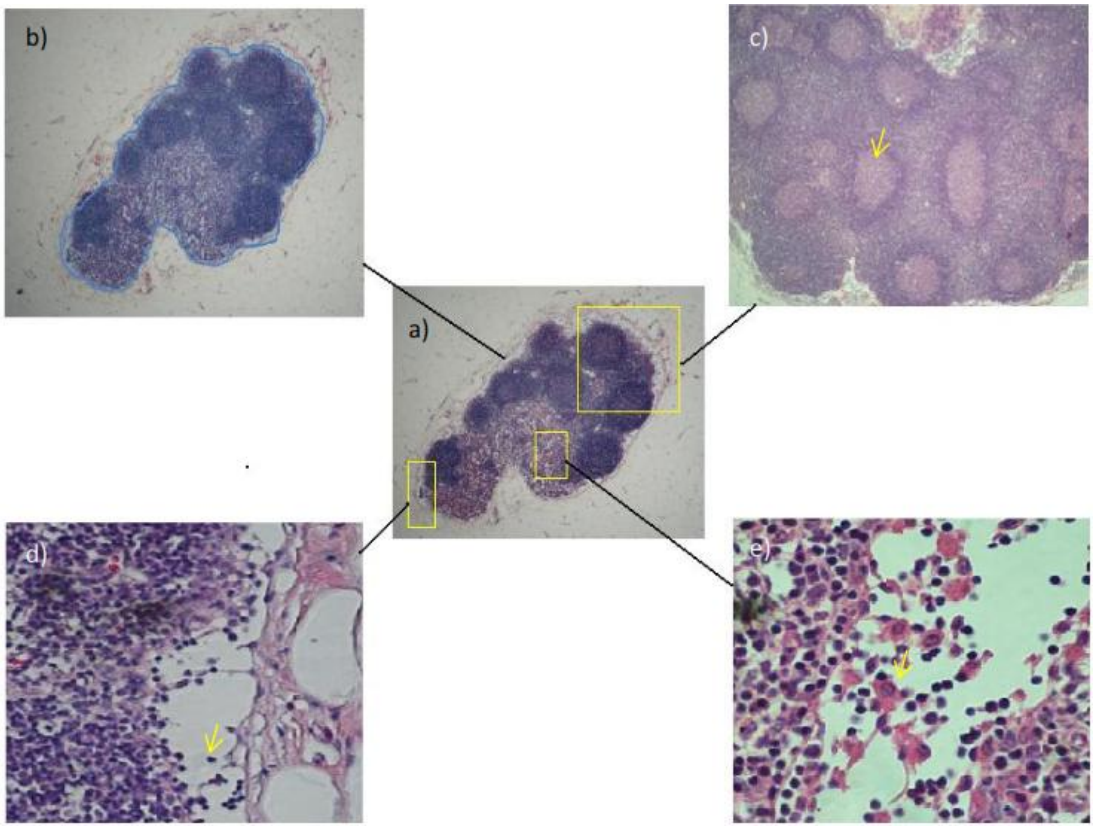

Figure 2.30 Histomorphology of lymph node; (a) Lymph node histology (x40), (b) Size of lymph node (selected area in blue) (x40), (c) Secondary follicles (arrow) (x100), (d) an infiltrating cell at the subcapsular area (arrow) (x200) and (e) a macrophage at the medullary sinus area (arrow) (x400)

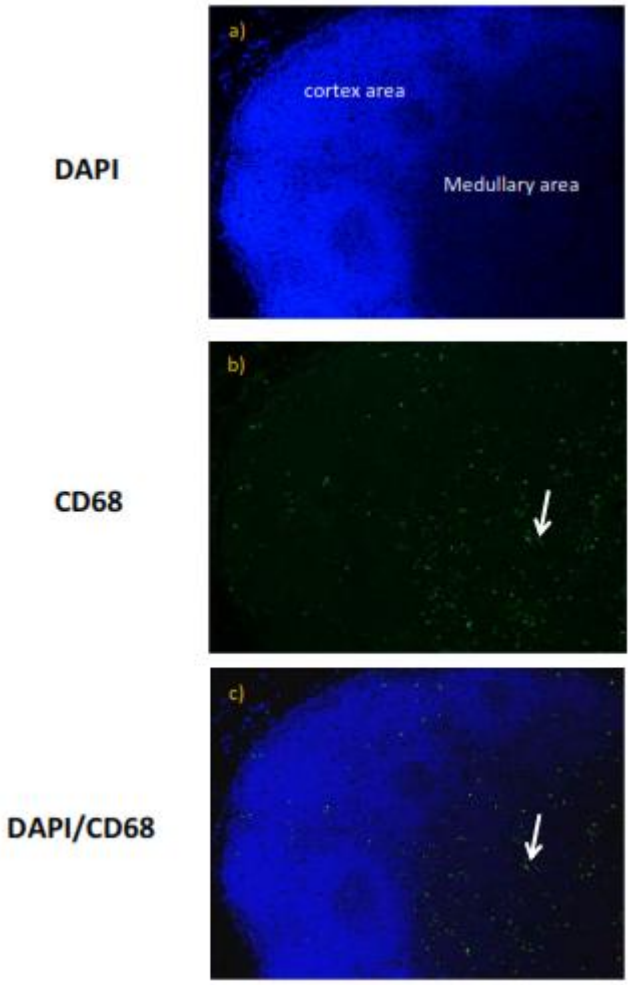

Figure 2.31 Immunohistofluorescence of CD 68 of lymph node (x100): (a) DAPI staining (blue) demonstrating cortex and medullary area of lymph node, (b) CD 68 staining (green) of macrophages and c) Merged image of DAPI/CD 68 (blue/green) demonstrating the presence of macrophages at the medullary area

2.12 Statistical analysis

Data that were obtained from experiments in this thesis were recorded in Microsoft Excel (2007). Each data set was then imported into statistical analysis programmes. Graphpad Prism for windows (GraphPad Software, LA Jolla California, USA). and SPSS version 19.0 (SPSS Inc., Chicago, IL, USA) were used for statistical analysis

and graph plotting. The normal distribution of each data set was initially tested using the Kolmogorov-Smirnov test in order to select an appropriate statistical test (parametric or non-parametric test). When data sets were too small to determine normality, parametric tests were chosen to evaluate statistical significance as this was recommended by (Bland and Altman, 2009).

Sample size calculation was based on a previously published study (Geris et al., 2010). It is recommended by UK Home Office governing the experimental use of animals that a minimum number of animals consistent with a statistically significant result should be used. The following equation was used to calculate the sample size required to compare proportions in two equally sized groups (Whitley and Ball, 2002).

$$n = \frac{\left[p_1(1-p_1)+p_2(1-p_2)\right]}{(p_1-p_2)^2} \times c_{p,power}$$

Commonly used values for $c_{p,power}$

	Power (%)			
P	50	80	90	95
0.05	3.8	7.9	10.5	13.0
0.01	6.6	11.7	14.9	17.8

Figure 2.32 The formulae for calculation of sample sizes and commonly used values for $c_{p,power}$

According to a previous study (Geris et al., 2010) the ratio of bone union in the MSC injection group was 0.75 (p_1), while in control was 0 (p_2). A probability limit of P-value < 0.05 ($\alpha = 0.05$) and a power goal of 0.9 were stipulated, gives the sample size in each group of 3.5 (at least 4 samples in each group).

Types of data and specific tests used for statistical analysis are described individually in each chapter.

Chapter 3: Feasibility of producing mesenchymal stem cells from different sources

Aim: *To demonstrate the growth characteristics and differentiation abilities of rMSCs from bone marrow, periosteal and adipose tissues and to determine the characteristics of hMSCs from bone marrow from the femoral head*

3.1 Introduction

Because of their bone regeneration potential, MSCs have been investigated for a therapeutic potential in fracture repair. It has been reported in both pre-clinical studies and clinical studies that MSCs can improve the bone regeneration process (Bielby et al., 2007, Granero-Molto et al., 2008). To investigate the therapeutic potential of MSCs, it is important to know that the sources of MSCs will produce MSCs in sufficient number of good quality. It has been reported that MSCs can be isolated from a variety of adult tissues (Barry and Murphy, 2004). Three sources that are relevant for orthopaedic applications are bone marrow, periosteum and adipose tissue.

In this thesis, rat MSCs (rMSCs) and human MSCs (hMSCs) from primary cells cultures were utilised in transplantation experiments (Chapter 7 and Chapter 8). It was considered important to define the optimal sources for MSC preparation. For the preparations of rMSC, the selected source of the rMSCs was based on the growth kinetics and colony forming ability of cultured MSCs from rat tissue from 3 different sources. For hMSC preparation, cells were isolated from femoral heads, according to a protocol routinely used in our group (Tremoleda et al., 2012).This technique of MSC isolation was modified from a previous protocol (Haynesworth et al., 1996). In the present study, Immunophenotypes of hMSC were demonstrated using Immunocytofluorescence.

Thus, the objectives of this chapter were (1) to compare and determine the *in vitro* growth kinetics using growth curve, population doubling time (PDT) and clonogenic ability of rMSCs from 3 different sources: namely bone marrow, periosteum and adipose tissue. The secondary aim was (2) to demonstrate the immunophenotypes of the hMSCs derived from the human femoral heads and to assess their *in vitro* potential for osteogenesis.

3.2 Materials and methods

The full lists of materials that were used in this study are detailed in Chapter 2. The techniques for MSC isolation and culture are provided in Chapter 2. This section briefly summarises the techniques specifically used in this chapter.

3.2.1 MSC preparation

Bone marrow from the femur, periosteum from the femoral diaphysis and adipose tissue from the inguinal area of Wistar rats were harvested for rMSC isolation. Femoral head samples that were obtained from THR patients with osteoarthritis undergoing primary total hip replacement were used for hMSC isolation

3.2.2 MSC evaluation

rMSCs and hMSCs of primary culture were evaluated for their growth curves, PDT and colony forming ability. To induce cell differentiation, the cells were cultured under osteogenic, chondrongenic and adipogenic conditions. These conditions have been described in Chapter 2. Rat fibroblasts which had been isolated from rat tails were used for negative controls. To isolate fibroblasts from the tips of the rat tails,

the tails were digested with 0.1% trypsin and plated on plastic dishes. Attached fibroblasts were cultured for 7 days and then the osteogenic, chondrongenic and adipogenic supplement, similar to the conditions that had been used, for rMSCs cultures was added.

Immunophenotyping of surface markers in hMSCs was determined using immunocytofluorescence staining. 50% confluent MSC cultures were fixed with 4% PFA, blocked for 1 hour with universal blocking solution (Dako^{TM}, UK) and incubated with an antibody against human CD90, CD44, CD31, CD34, CD19, NG2, CD146 (further details in chapter 2). The levels of staining were observed and classified as strong, weak and negative depending on the magnification used for visualization. The staining with could be clearly observed at 20x magnification was classified as strong and if the staining was visible at 40x magnification, it was classified as weak. If it could not be seen at any magnification, it was classified as negative.

3.2.3 **Statistical analysis**

The growth curves rMSCs from three sources and hMSCs were compared using repeated measures ANOVA and mean values of population doubling time study and clonogenic study were reported as mean $\pm$ SEM. These data were analysed using parametric tests. The data from the three sources were compared using one-way ANOVA followed by the bonferroni's multiple comparison tests. A P-value < 0.05 was considered to be statistically significant.

3.3 Results

3.3.1 The characteristics of rMSC

3.3.1.1 The morphology of rMSC from 3 sources

The cells derived from these three sources showed no obvious differences in their morphology (**Figure 3.1**). They attached to plastic flasks and showed similar heterogeneous morphology at initial plating and then became a homogenous monolayer of fibroblast-like cells with passaging. Cells from each source could be passaged at least 12 times; however, they exhibited slightly large and flatted shape in later passages.

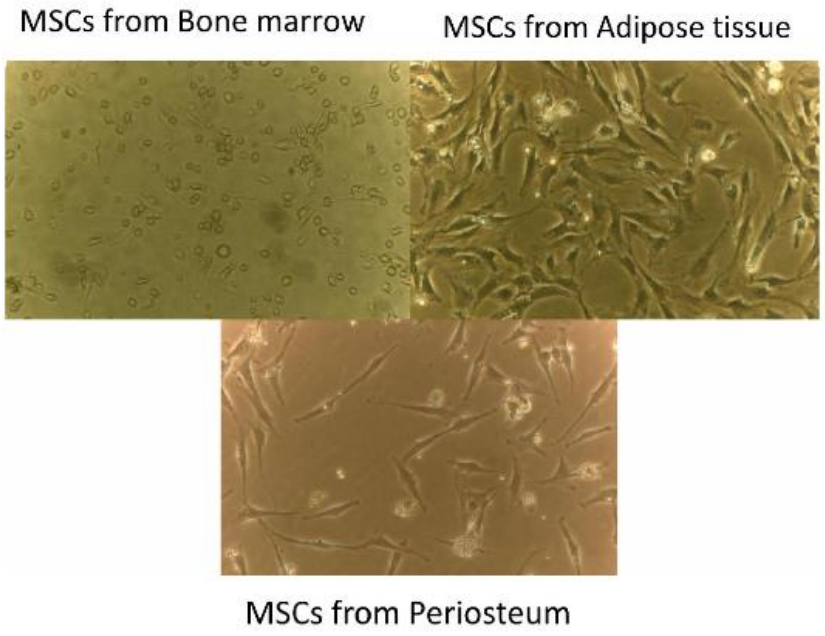

Figure 3.1 MSCs from 3 sources; bone marrow, adipose tissue and periosteum (x400)

3.3.1.2 Differentiation ability

Due to the lack of a single specific marker of rMSCs, the isolated cells from the three were validated using physical, phenotypic and functional properties. The tri-linage differentiation potential including (a) osteogenesis, (b) chondrogenesis and (c) adipogenesis was demonstrated. Cells from the three sources were able to differentiate into the direction of bone, cartilage and adipose tissue (**Figure 3.2-3.4**). The cells under the osteogenic condition showed the presence of ALP activity, the cells within the micromass culture under the chondrogeneic condition demonstrated positive staining with Alcian blue and the cells under the adipogenic condition formed intracellular lipid droplets which were revealed using Oil Red O staining. Fibroblasts cells which were used as controls were not able to differentiate under osteogenic, chondrogeneic or adipogenic conditions (**Figure 3.5**).

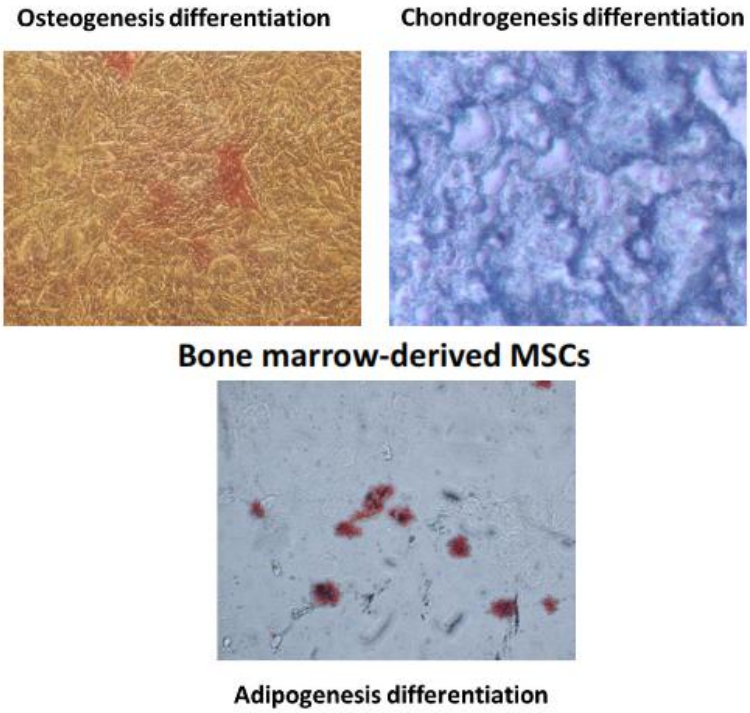

Figure 3.2 Osteogenic (ALP staining), chondrogenic (Alcian blue staining), and adipogenic (Oil Red O staining) differentiation of MSCs from bone marrow (x400)

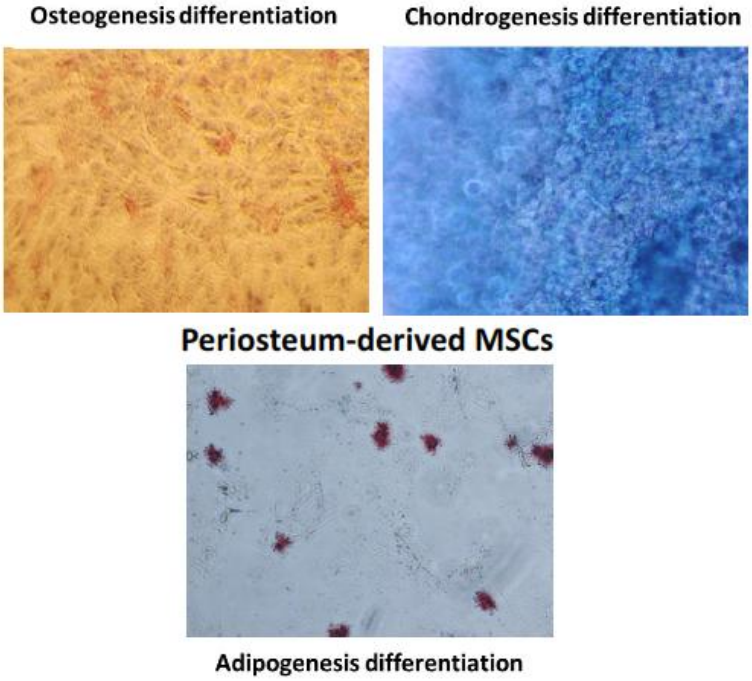

Figure 3.3 Osteogenic (ALP staining), chondrogenic (Alcian blue staining), and adipogenic (Oil Red O staining) differentiation of MSCs from periosteum (x400)

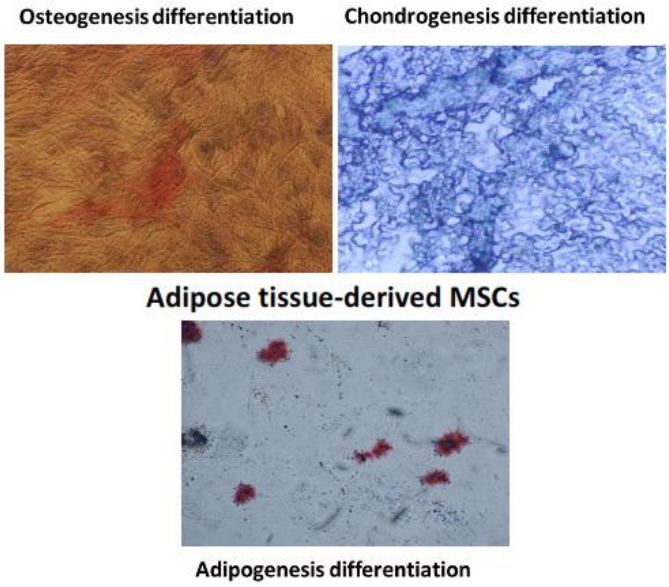

Figure 3.4 Osteogenic (ALP staining), chondrogenic (Alcian blue staining), and adipogenic (Oil Red O staining) differentiation of MSCs from adipose tissue (x400)

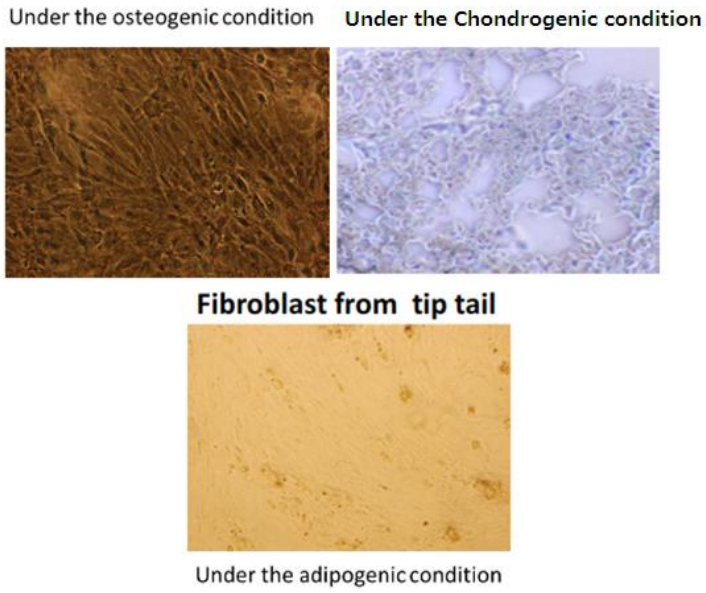

Figure 3.5 Fibroblast culture under the osteogenic (ALP staining), chodrongenic (Alcian blue staining), and adiposgenic (Oil red O staining) condition for control (x400)

3.3.1.3 Growth kinetics of MSCs from three sources

3.3.1.3.1 Growth curves

The growth curves from rMSCs from the three sources (bone marrow, periosteal and adipose tissues) revealed the same 'exponential' growth pattern which had three phases. Initially there was a lag phase of 0-2 days' duration following which there was a log phase of rapid cell proliferation from day 4 to day 6. Finally, there was a plateau phase after the 8^{th} day. The growth curves from the different sources demonstrated significant differences during the 12 -day period in cultures (P value < 0.001 for cell source and time, and P value < 0.001 for interaction effects, two-way repeated ANOVA) (**Figure 3.6**). The growth of MSCs from bone marrow and

periosteum were comparable and both of them were significantly faster than MSCs from adipose tissue.

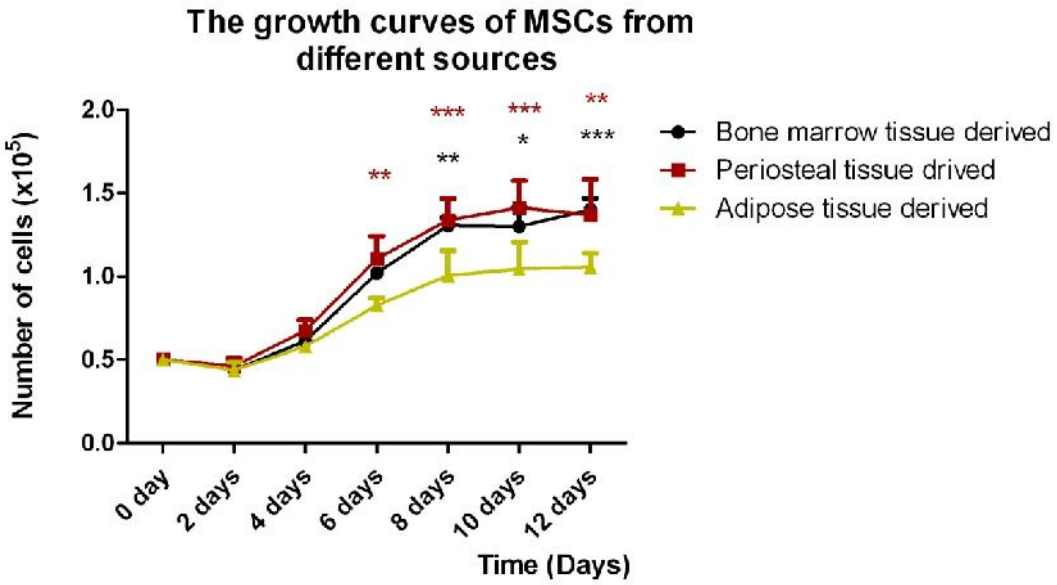

Figure 3.6 The growth curves of MSCs from bone marrow, periosteum and adipose tissues under the 12-day period of culture; the growth of MSCs from bone marrow and periosteum were comparable and both of them were significantly faster than MSCs from adipose tissue (Bonferroni's test subsequent to ANOVA: * = P-value < 0.05, ** = P-value < 0.01 and *** = P-value < 0.001, data shown as mean and SEM, n = 4 per group and time)

3.3.1.3.2 Population doubling time

The growth kinetics of cells from the 3 sources were compared using the population doubling time (**Figure 3.7**).The mean PDT of MSCs from bone marrow from was 4.00 days (SEM = 0.49, n = 6), from periosteum was 3.6 days (SEM = 0.49, n= 6) and from adipose tissue was 4.6 days (SEM = 0.62, n= 6).The bone marrow derived cells and the periosteum derived cells had faster growth kinetics than the adipose derived cells, but this difference did not reach statistical significance (P-value = 0.37, one-way ANOVA)

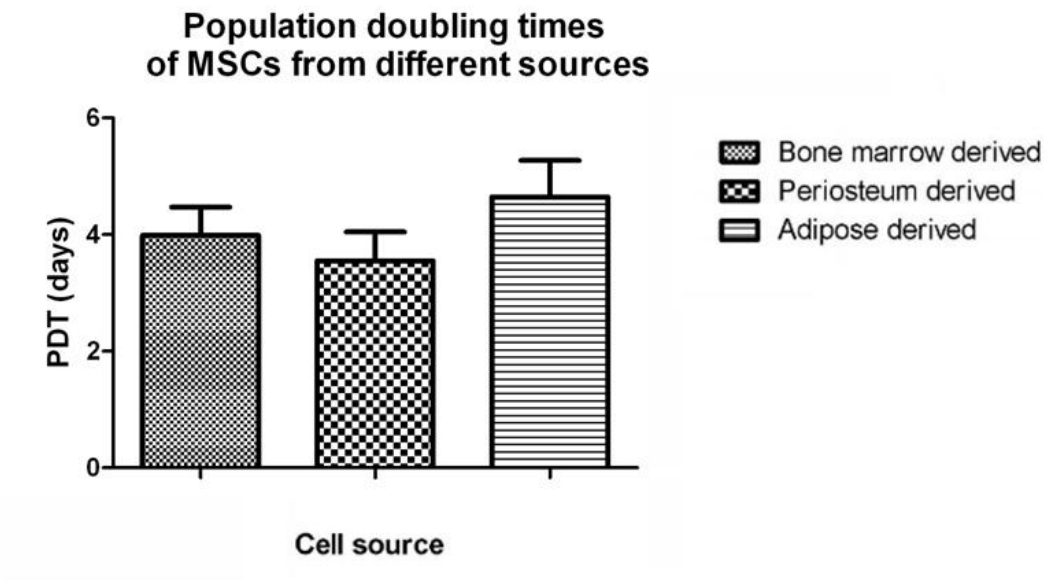

Figure 3.7 The population doubling time (PDT) of MSCs from bone marrow, adipose tissue and periosteum; the PDT of bone marrow derived cells and the periosteum derived cells were more than the adipose derived cells

3.3.1.3.3 Percentages of colony forming units and area

The percentages of colony forming units from bone marrow, periosteum and adipose tissue derived cells were 8.58 (SEM = 0.55, n = 6), 9.92 (SEM = 0.84, n = 6) and 5.91 (SEM = 0.32, n = 6), respectively. There were statistical differences in the percentages of colony forming units from different three sources (P-value = 0.001, one-way ANOVA) (**Figure 3.8**). The percentages of the area covered with colonies from bone marrow, periosteum and adipose tissue derived cells were 25.12 (SEM = 2.98, n = 6), 32.45 (SEM = 4.39, n = 6) and 15.80 (SEM = 3.69, n = 6), respectively. There were statistical differences in the percentages of the area covered with colonies from different three sources (P-value = 0.02, 1-way ANOVA) (**Figure 3.9**). These results indicated that the clonogenic abilty of MSCs from bone marrow and periosteum were significantly higher than for adipose derived cells.

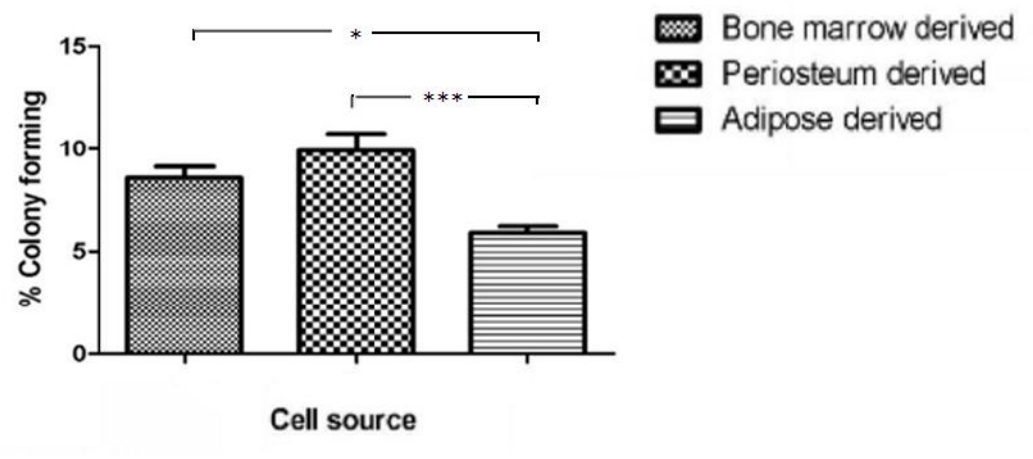

Figure 3.8 The percentage of colony forming units of MSCs from bone marrow, periosteum and adipose tissue; mean percentage of colony forming of bone marrow derived and periosteum derived MSCs were more than adipose derived MSCs (Bonferroni's test subsequent to ANOV A: * = P-value < 0.05 and *** = P-value < 0.001, data shown as mean and SEM, n = 6 per group)

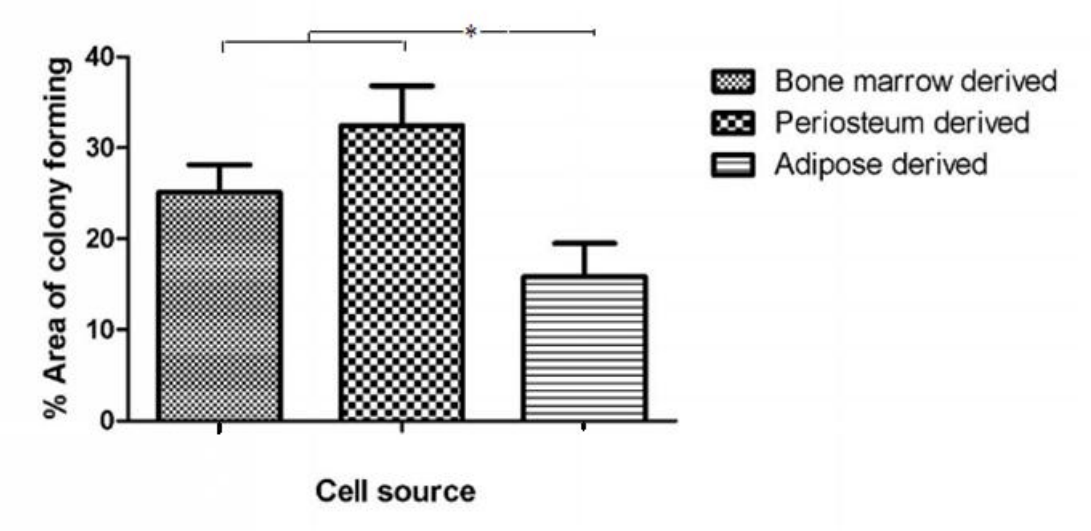

Figure 3.9 The percentage of colony forming area of MSCs from bone marrow, periosteum and adipose tissue; mean area of colony forming of bone marrow derived and periosteum derived MSCs were larger than adipose derived MSCs (Bonferroni's test subsequent to ANOVA: * = P-value < 0.05, data shown as mean and SEM, n = 6 per group)

3.3.2 Human mesenchymal stem cells derived from femoral head

3.3.2.1 The physical morphology and osteogenesic capacity of human mesenchymal stem cells obtained from the femoral head

Cultured hMSCs from bone marrow tissue at femoral heads had a typical shape for MSCs, i.e. they were spindle shape and had a fibroblast-like morphology (**Figure 3.10 a**). They could be cultured to at least the 12th passage and were able to form the colonies under low density seeding (**Figure 3.10 b**). These cells were able to differentiate into bone forming cells in osteogenic medium (**Figure 3.10 c and 3.10 d**).

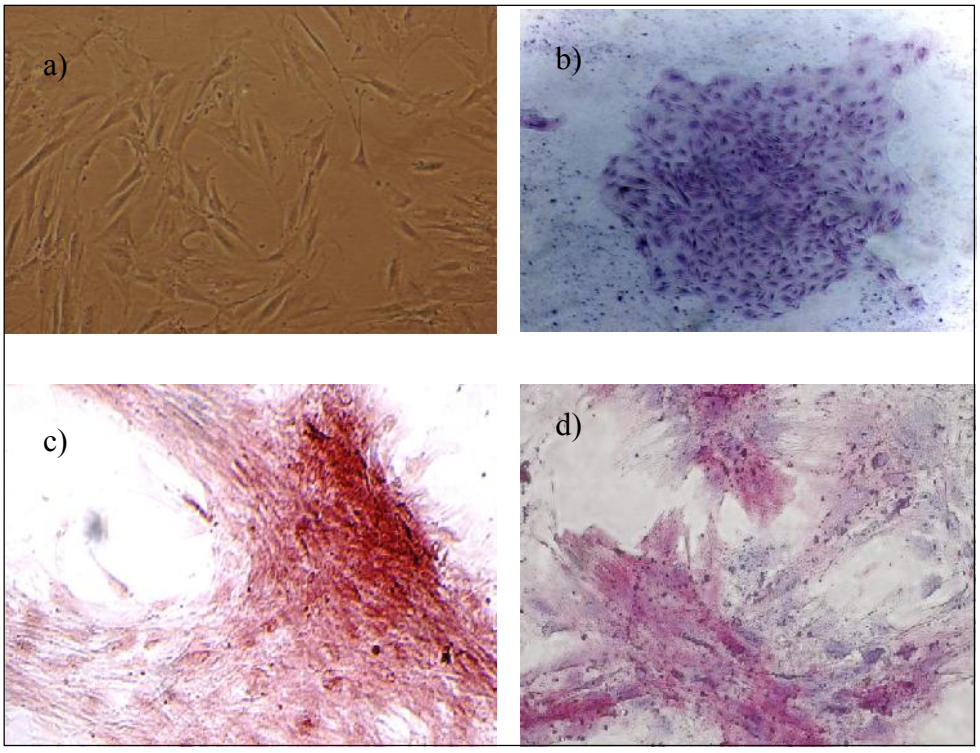

Figure 3.10 hMSCs from bone marrow at femoral heads (a) general morphology of hMSCs, (b) Colony forming of hMSCs under low density culture, (c) Alizaline red staining of hMSCs under osteogeneic induction (d) Alkaline phosphatase staining of hMSCs under osteogeneic induction (x400)

3.3.2.2 Immunophenotypes of human MSCs

Isolated hMSCs were examined for some markers of MSC using Immunolabelling. The results showed that cultured hMSCs exhibited the markers CD90 and CD44 and did not exhibit the haematopoetic cell markers (CD19), CD34 and CD31. Cultured hMSC also weakly expressed CD146 and NG2 markers.

A) Strong positive staining makers

CD90 and CD44 markers were observed clearly under low magnification (x100) indicating strong staining.

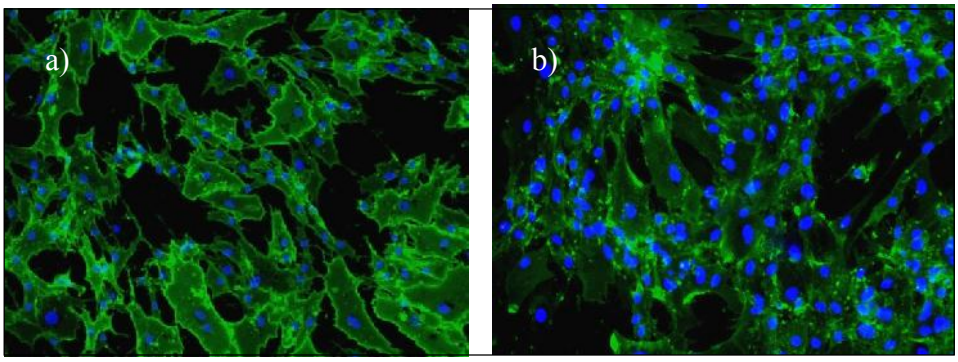

Figure 3.11 Immunolabelling of hMSCs at passage 3rd with FITC a) CD90 b) CD44 (x100)

B) Weak positive staining makers

CD146 and NG2 markers were weakly positive. Staining was observed under higher magnification (x200).

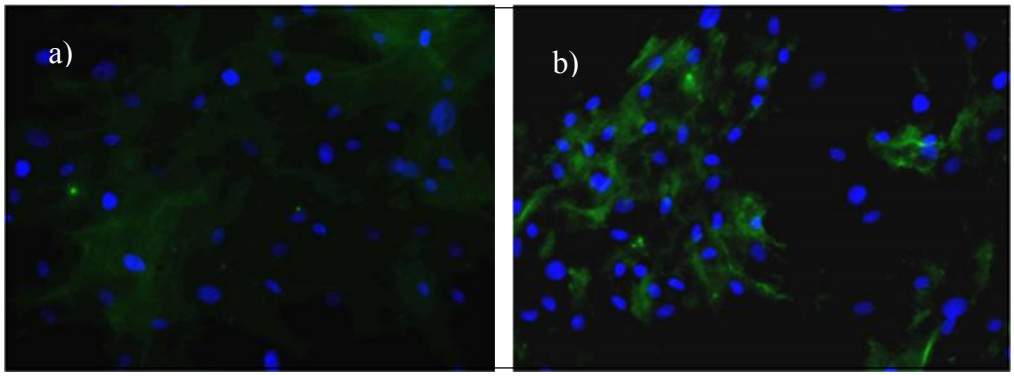

Figure 3.12 Immunolabelling of hMSCs at passage 3rd with FITC a) CD146 b) NG2 (x200)

C) Negative staining markers

CD31, CD34 and CD19 markers were all negative.

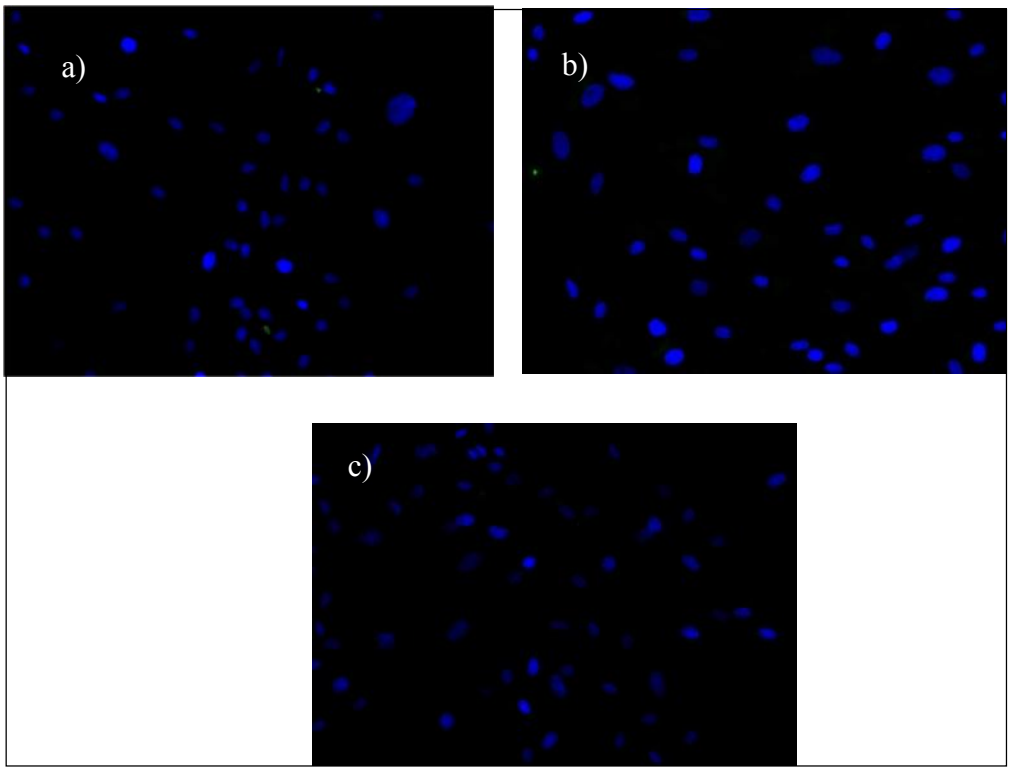

Figure 3.13 Immunolabelling at passage 3rd with FITC a) CD31 b) CD 34 and C) CD19

3.3.2.3 Summary of immunophenotypes of hMSC from femoral heads

The table 3.1 shows hMSC characteristics using immunolabelling from culture hMSCs from bone marrow at femoral head samples.

Table 3.1 Summary of human mesenchymal stem cell markers

Human MSC markers	Staining level*
CD 90	++
CD 44	++
CD 146	+
NG2	+
CD 34	–
CD 31	–
CD 19	–

***++ strong positive staining, + weak positive staining and – negative staining**

3.3.2.4 Comparison of growth kinetic between rMSC and hMSC

This section demonstrated the comparison of the growth curves, population doubling times and the percentages of colony forming between rMSCs derived from bone marrow tissue and hMSCs derived from bone marrow tissue. There was no significant difference in the growth curve over the 12 day-period in cultures between

rMSCs and hMSCs (P-value = 0.82 for group, two-way repeated ANOVA) (**Figure 3.14**). The mean PDT of rMSCs was 4.00 days (SEM = 0.49, n = 6) and hMSC was 4.7 days (SEM = 0.24, n = 9). There was no difference in PDT between rMSCs and hMSCs (P- value = 0.37, unpaired t-test). The percentages of colony forming units of rMSCs and hMSCs were 8.6 (SEM = 0.54, n = 6), 7.2 (SEM = 1.17, n = 9), respectively. There was no difference in the percentages of colony forming units between rMSCs and hMSCs (P-value = 0.37, unpaired t-test). The growth kinetic characteristics of rMSCs were similar to hMSCs.

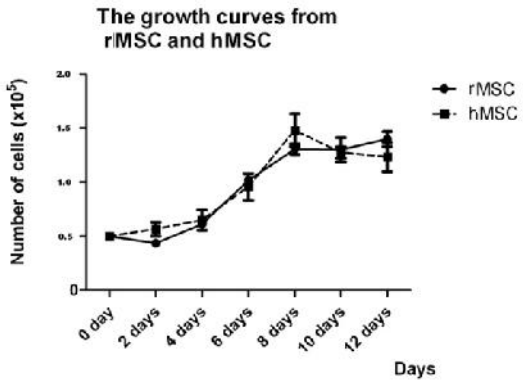

Figure 3.14 The growth curves of rMSCs and hMSCs from derived bone marrow under the 12-day period culture

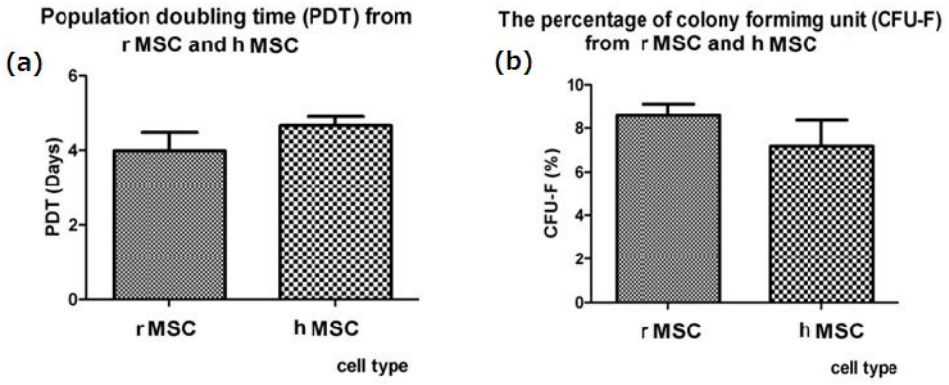

Figure 3.15 Comparison of (a) the population doubling time (PDT) and (b) the percentage of colony forming units between rMSCs and hMSCs derived from bone marrow

3.4 Summary and discussion

Mesenchymal stem cell research is an extremely active field both in regenerative medicine and in orthopaedics. MSCs are able to differentiate into bone, cartilage and fat tissue in *in vitro* conditions and retain the ability for self-renewal capacity or "stemness" (Pittenger et al., 1999). Therefore, MSCs have the potential to be expanded and to regenerate bone and cartilage for use in bone defects, fracture non-unions, or cartilage injuries. MSCs have been identified in a variety of adult human tissues including bone trabeculae, teeth, skin, muscle, synovium, and umbilical cord blood (Barry and Murphy, 2004). However, three potential sources which are relevant to orthopaedic surgeons are bone marrow, periosteum and adipose tissue.

In this study, it has been confirmed that MSCs can be isolated from bone marrow, periosteum and adipose tissue. Cells attached to plastic flasks and demonstrated heterogeneous morphology on the initial plating and then became a homogenous monolayer of fibroblast-like cells with passaging. Cells from each source could be passaged at least 12 times and they formed colonies under low-cell density. The isolated cells from these three sources were capable of osteogenesis, chondrogenesis and adipogenesis. Thus, these results demonstrated that isolated cells in this study have the characteristics of MSCs.

The yield of MSCs has been reported to be an important factor in determining a successful outcome (Hernigou et al., 2005). It has been suggested that MSCs should be efficiently expanded in culture to obtain sufficient cells. Thus, it is important to consider the growth kinetics of the cells from different sources. The results of this study have shown that the bone marrow derived cells and the periosteum derived cells had faster growth kinetics than the adipose derived cells. The percentage of colony forming units and the colony forming area from the bone marrow derived cells and the periosteum derived cells were significantly greater than for adipose derived cells. The in vitro growth kinetics and the clonogenic ability of MSCs may also reflect their power of tissue regeneration in vivo. This conjecture is supported by Niemeyer et al (2010a) who reported the osteogenic potential of bone marrow

derived MSCs and adipose-tissue derived stem cells (ASCs) in a sheep using a bone defect model. They found that the bone regeneration potential of bone marrow derived MSCs was superior to ASCs. MCSs from periosteum have also been shown both *in vitro* and *in vivo* to have superior osteogenic differentiation potential in comparison with adipose tissue (Hayashi et al., 2008). However, the periosteum is a limited source and is more difficult to harvest. Furthermore, its removal will interfere with the blood supply of the bone. Thus, in clinical practice, the bone marrow should be still considered as an appropriate source. In this study, MSCs derived from animal tissues have been shown to demonstrate the rMSC characteristics using several physical, phenotypic and functional properties (Dominici et al., 2006). Classical assays have been used to identify MSCs; i.e. the ability of adherent spindle-shaped cells to proliferate to form colonies that can be induced to differentiate into adipocytes, osteocytes, and chondrocytes.

Regarding the isolation of hMSC, human femoral heads were used as they were readily available source and could be used in *in vivo* experiment for bone regeneration potential. Because of the heterogeneity of hMSCs, in 2006, the mesenchymal and tissue stem cell committee of the International Society for Cellular Therapy (ISCT) has proposed the criteria necessary to define human MSCs. Firstly, MSCs must be plastic-adherent when maintained in standard culture conditions. Secondly, MSCs must express CD105, CD73 and CD90, and lack expression of CD45, CD34, CD14 or CD11b, CD79a or CD19 and HLA-DR surface molecules. Thirdly, MSCs must differentiate into osteoblasts, adipocytes and chondroblasts *in vitro*. In this study, isolated hMSCs were characterised using their immunophenotype, plastic adherence ability, and ability to differentiate into bone.

In conclusion, the results reported in this chapter have shown the growth kinetics of rMSCs from three potential sources namely bone marrow, periosteum and adipose tissue. rMSCs and hMSCs derived from bone marrow were used in chapter 7 and 8 to develop strategies for promoting fracture healing in an atrophic non-union model.

Chapter 4: Validation of the Radiographic Union Scale in Tibia (RUST) and Lane & Sandhu scoring system in small animal study fracture model

Aim: *To validate the inter- and intra-observer agreement of the RUST score and Lane & Sandhu in the assessment of animal fracture healing*

4.1 Introduction

Fracture models are used to investigate the mechanism of bone repair and the therapeutic potential of a wide range of novel interventions such as ultrasound (Bashardoust Tajali et al., 2011), growth factors (Friedlaender et al., 2001) and cell therapy (Bajada et al., 2007). Valid and reliable outcome measurements are essential for assessing fracture healing. X-ray assessment of fracture healing is a simple and inexpensive technique, which is commonly used in orthopaedic practice (Corrales et al., 2008). Clinical scoring systems have been developed to standardise the interpretation of the radiographs. The Radiographic Union scale in Tibia (RUST) is a recent fracture assessment tool that assesses the presence of (a) bridging callus (b) the fracture line on each cortex on the antero-posterior and lateral radiographs. It has been reported that this scoring system has an excellent inter-rater reliability in clinical practice for tibial fractures treated with intramedullary nails (Kooistra et al., 2010, Whelan et al., 2010). However to date, the RUST score has not been evaluated in a preclinical model. The Lane & Sandhu score has been used in animal studies (Yang and Park, 2001, Bigham et al., 2008, Kurklu et al., 2011, Kerimoglu et al., 2013) but has not been validated fully for fracture healing research.

Therefore, the objectives of this study were (1) to determine the intra- and inter-observer reliability of the RUST and Lane & Sandhu scoring systems, when used by orthopaedic surgeons and researchers in the orthopaedic field and (2) to demonstrate the limits of agreement of both scoring systems using the Bland-Altman Plot.

4.2 Materials and methods

4.2.1 Radiographs

Thirty sets of antero-posterior and oblique radiographs of tibial shaft fractures treated with external fixation in pre-clinical model were selected so that the full spectrum of the various stages of normal fracture healing, delayed union and non-union were represented.

4.2.2 General impression of the fracture healing and fracture scoring systems

The general impression of fracture healing was determined according to the AO-ASIF manual (Muller et al. 1991). The details of the RUST and the Lane & Sandhu scoring systems are provided in the general method section (Chapter 2).

4.2.3 Raters

The criteria of scoring RUST and Lane and Sandhu were explained to six raters, including three orthopaedic surgeons and three orthopaedic researchers (one laboratory researcher, one bioengineer and one physiotherapist. They evaluated the

radiographs of the fractures using the RUST and Lane and Sandhu scoring system independently. The examiners were blinded to time since fracture/osteotomy and to additional treatment the fracture might have had. Inter-observer reliability was determined from the scores of six observers at the initial viewing of the radiographs. To determine intra-observer consistency, each reviewer was asked to score the same set radiographs but in a different order 2-3 weeks after the initial assessment.

4.2.4 **Statistical analysis**

The agreement of general impression of bone union was determined using Fleiss's Kappa which is similar to Cohen's unweighted Kappa. This method can be used to evaluate concordance or agreements of categorical variable between multiple raters. The agreement of the summary of RUST score and Lane & sandhu score were evaluated using the intra-class correlation coefficient (ICC). The scores were considered as continuous variables. Komogorov-Smirnov test was used to determine the normal distribution of the scores obtained from data sets from either RUST or Lane & Sandhu. Kappa agreement can be interpreted as following; kappa of 0 to 0.2 represents “slight agreement,” 0.21 to 0.40 “fair agreement,” 0.41 to 0.60 “moderate agreement,” and 0.61 to 0.80 “substantial agreement.” A value above 0.80 to 0.99 is considered almost “perfect agreement.” (Viera and Garrett, 2005).The value of the ICC ranges from +1, in which case there is “perfect agreement,” to -1, which corresponds to “absolute disagreement.” (Shrout and Fleiss, 1979) The online statistic programme was used for Fleiss's Kappa (Geertzen 2012). The statistical package SPSS, version 19.0 (SPSS Inc., Chicago, IL, USA) was used for ICC calculation. The Bland-altman plot graph was generated from GraphPad Prism for windows (GraphPad Software, LA Jolla, California, USA).

4.3 Results

All raters found both scoring systems were practical and they were able to score all the radiographs given to them. However, they found it difficult to decide on the definitive diagnosis of bone union (uncertain category) about 6-16 %. Non-surgeons used the category of "uncertain" for general impression more than surgeons.

4.3.1 Validation of general impression

The inter-observer agreement for general impression is summarised in **Table 4.1**. It had moderate agreement. The inter-observer for surgeons was slightly better than for non-surgeons. The intra-observer agreement for general impression is summarised in **Table 4.2**. Similarly, the intra-observer agreement for surgeons was better than for non-surgeons. Two raters in the surgeon group had almost perfect agreement, whereas all of the raters in non-surgeon group had moderate agreement.

Table 4.1 Inter-observer agreements of general impression

Reviewers	Kappa	95%CI
Orthopaedic surgeons	0.6400	0.4334 - 0.8466
Researchers	0.5508	0.3895 - 0.7122
Overall	0.5754	0.4956 - 0.6553

Table 4.2 Intra-observer agreements of general impression from individual rater

Reviewers	Kappa	95%CI
Non-surgeon 1	0.5706	0.2920 - 0.8491
Non-surgeon 2	0.4854	0.2250 - 0.7458
Non-surgeon 3	0.5969	0.3355 - 0.8584
Surgeon 1	0.5833	0.3131 - 0.8536
Surgeon 2	0.9268	0.7858 - 1.0678
Surgeon 3	0.8093	0.6046 - 1.0140

4.3.2 **Validation of RUST score**

The normal distribution of average RUST scores from raters scoring the data (**Figure 4.1**) was determined by Komogorov-Smirnov Test; they were distributed normally (P-value = 0.31).

The inter-observer agreements of the RUST score are shown in **Table 5.3.** The overall inter-observer agreement of the RUST scores was almost perfect. There were strong agreement with non-surgeon raters and almost perfect with surgeon raters. The intra-observer agreements of the RUST scores are shown in **Table 5.4.** Five out of six raters had almost perfect intra-observer agreements.

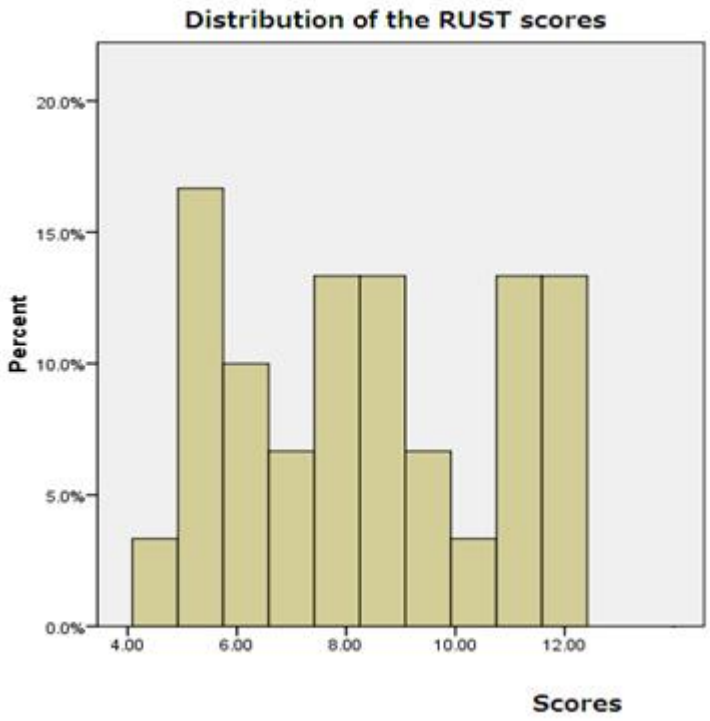

Figure 4.1 Showing the normal distribution of average RUST scores from 6 raters

Table 4.3 Inter-observer agreements of the RUST score

Reviewers	**ICC**	**95%CI**
Orthopaedic surgeons	0.896	0.820 - 0.945
Researchers	0.768	0.623 - 0.872
Overall	0.814	0.718 - 0.893

Table 4.4 Intra-observer agreements of the RUST score from individual rater

Reviewers	ICC	95%CI
Non-surgeon 1	0.613	0.330 - 0.795
Non-surgeon 2	0.873	0.751 - 0.938
Non-surgeon 3	0.876	0.756 - 0.939
Surgeon 1	0.906	0.812 - 0.954
Surgeon 2	0.944	0.886 - 0.973
Surgeon 3	0.971	0.940 - 0.986

4.3.3 **Validation of the Lane & Sandhu score**

The normal distribution of average Lane and Sandhu scores from raters scoring the data (**Figure 4.2**) were determined by Komogorov-Smirnov Test; they were distributed normally (P-value = 0.21).

The overall inter-observer agreement of the lane & Sandhu score was almost perfect (**Table 4.5**). There were almost perfect agreements in both non-surgeon and surgeon raters. The intra-observer agreements of the lane & Sandhu score are demonstrated in **Table 4.6**. All of the raters had almost perfect agreement using the lane & Sandhu score.

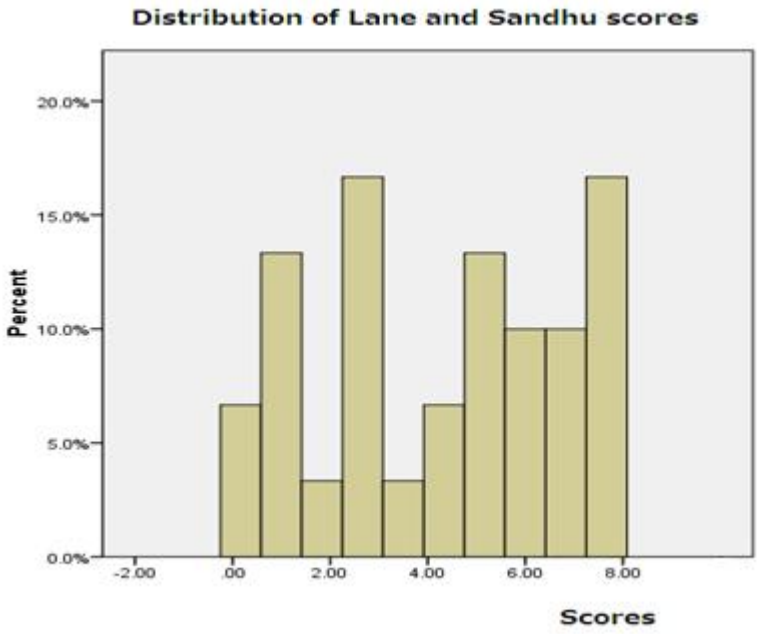

Figure 4.2 Showing the normal distribution of average Lane & Sandhu scores from 6 raters

Table 4.5 Inter-observer agreements of the Lane & Sandhu score

Reviewers	ICC	95%CI
Orthopaedists	0.883	0.798 - 0.938
Researchers	0.898	0.823 - 0.946
Overall	0.880	0.811 - 0.933

Table 4.6 Intra-observer agreements of the Lane & Sandhu score from individual rater

Reviewers	ICC	95%CI
Non-surgeon 1	0.944	0.877 - 0.973
Non-surgeon 2	0.879	0.762 - 0.941
Non-surgeon 3	0.915	0.829 - 0.958
Surgeon 1	0.852	0.712 - 0.927
Surgeon 2	0.874	0.753 - 0.938
Surgeon 3	0.947	0.891 - 0.974

4.3.4 The Bland-altman plot showing the limits of agreement between two scoring systems

The difference between the two scoring systems was assessed using a bland-Altman plot (**Figure 5.3**). The difference between the two scoring systems (Y axis) was plotted against the average of the score from both scoring systems (X axis). The two scoring systems had very similar results on average, and the difference between the means was 4.01. The 95% limits of agreement were between 2.84 and 5.18. The minimal score of the RUST system was 4, whereas the Lane & Sandhu, it was 0. Thus, the RUST scores would be expected to be 4 points higher than the Land & Sandu scores, as the baseline is 4 points higher. The dot plot of the difference and average scores between two scoring systems was close to 4, thus, both scoring systems had a very good agreement.

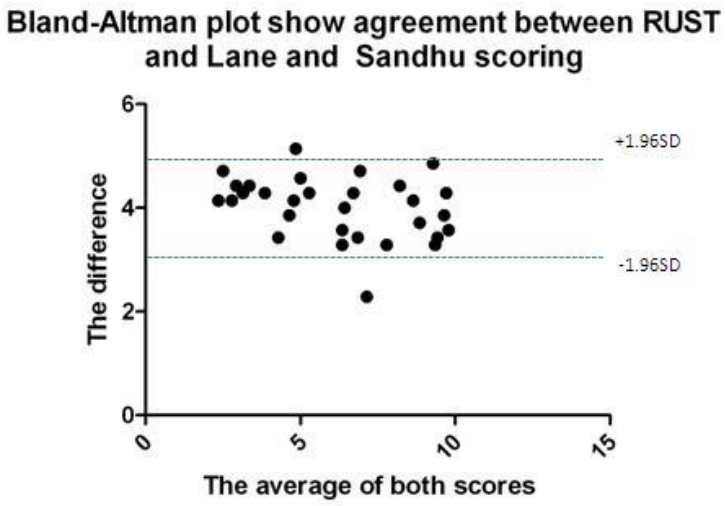

Figure 4.3 The limits of agreement between RUST and Lane and Sandhu scoring system

4.4 Summary and discussion

This study validated the inter- and intra- observer variability of fracture healing using (a) general impression and (b) two fracture scoring systems namely the RUST score and the Lane and Sandhu score in a pre-clinical fracture model. The results showed that the fracture scoring systems allowed researchers to evaluate fracture healing with better inter- and intra- observer agreement. In contrast, the general impression of bone union or non-union was found to be more difficult to use, particularly for non-surgeons.

For the general impression rating the inter-observer agreement was considered as substantial for the orthopaedic surgeon group, but only moderate for the non-surgeon group. Interestingly, the intra-observer agreements for the orthopaedic surgeons were graded as perfect. These results suggested that the "general impression" rating for whether a bone was healed or not should be graded by an orthopaedic surgeon. In a

clinical study, it has been reported that the inter-observer agreement using "general impression" in the assessment of the healing of tibial fractures after intramedullary fixation between orthopaedic surgeons was substantial (kappa = 0.60; 95% confidence interval (95%CI) 0.52 to 0.68) (Whelan et al., 2002). However, the limitation of "general impression" is that it is assessor dependent. It is also difficult to give a diagnosis of bone union in the early stage of the fracture healing process. As a result, it cannot be used for evaluation and comparison of the fracture progression in different time points which is normally required in preclinical studies. Thus, appropriate scoring systems should be of great use for assessing multiple aspects of the fracture healing process.

The radiographic Union Scale of Tibia Fracture (RUST) was developed to assess tibial fracture healing. This scoring system is based on the presence or absence of callus and a visible fracture line at each of the 4 cortices from the antero-posterior and lateral radiographs. It is scored from 4 points (minimum) to 12 points (maximum). The results presented here showed that the inter-observer agreement increased was 0.81 (perfect agreement). Both inter-and intra-observer rating for non-surgeons were better than using general impression. The findings concerning inter-observer agreement were similar to the previous report using the RUST score in clinical study. The findings showed a strong inter-observer reliability of using RUST score to determine 549 sets of tibial shaft fracture (ICC = 0.84) (Bhandari et al 2011) The results presented here showed that the RUST score was a reliable outcome assessment tool for preclinical studies of fracture healing.

The Lane & Sandhu scoring system has been used in pre-clinical studies. The scores are based on the extent of bone healing, the state of the bone cortex and remodelling. The inter-and intra-observers agreements for non-surgeons were about 0.8-0.9. This compared favourably with the reliability found for the RUST score. The bland-altman plot showed the agreement of the two scoring systems. Most of the results were scattered within +/-1.96 SD. The results demonstrated that the RUST score as well as the Lane and Sandhu score were reliable and repeatable in the pre-clinical setting.

Both the RUST and the Lane & Sandhu score were demonstrated to be superior to "general impression" in the pre-clinical setting. These scores were especially useful if non-surgeons were assessing the healing process on x-ray. Both scores were comparable with excellent reliability. However, although the RUST score was not better than the Lane & Sandhu score in term of reliability, it was easier to assess and more objective than the Lane & Sandhu score. As the scoring systems examined different aspects of healing, it was decided that they both would be applied in the further chapters (Chapter 6, 7, 8) for assessing the fracture healing process.

Chapter 5: Comparison of the biomechanical testing using 4-point bending of the rat Tibia between specimens with and without the muscle attached

Aim: *To compare the biomechanical parameters due to different sample preparation techniques using sample with and without muscle from 4-point bending mechanical testing*

5.1 Introduction

The biomechanical properties of bone are important when evaluating the functional outcomes of the fracture healing process. Bending tests are common methods used to evaluate the mechanical behaviour of small animal bones such as mice or rats (Turner and Burr, 1993). Proper preparation of the specimen is necessary for accurate biomechanical testing. When testing whole bones, it is recommended that the soft tissue should be removed before testing (Aspden, 2003). In practice, it was noticed that it was difficult and time-consuming to clean the bone specimen, particularly when there was a callus on the harvested sample, as this is a relatively soft structure which can be easily damaged. The use of a scalpel to remove the soft tissue and clean the specimens can disturb the callus structure and create stress raisers (**Figure 5.1**) which may interfere with the mechanical properties of the callus.

It could be more appropriate to test bone samples without the muscle removal. Thus, this study aimed to compare the mechanical properties of the rat tibia specimens with and without muscle removal.

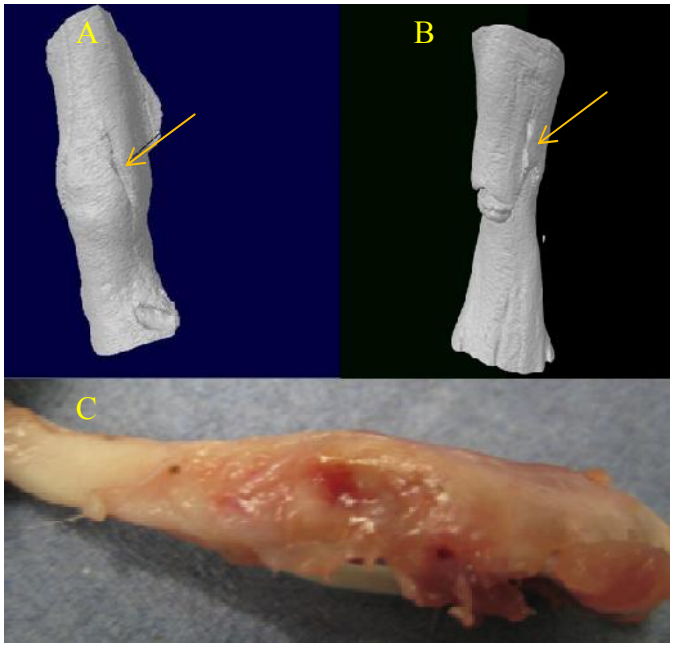

Figure 5.1 Bone samples after muscle cleaning; (a) and (b) The micro-CT images from two specimens; arrows show small defects after cleaning, (c) gross morphology of sample

5.2 Materials and Methods

Twelve Wistar rat cadavers (mean weight = 355.33, SEM=19.34) were used for this study. One rat tibia from each of 12 pairs was harvested for biomechanical testing. All soft tissues including skin and muscle were dissected from the right tibias, whereas muscles on the left tibias were left intact. The mechanical properties of specimen with and without muscles were tested using 4-point bending conducted on a custom designed test rig mounted on a Zwick/Roell 2005 mechanical test machine (Zwick, Ulm, Germany). (**Figure 5.2**) Ultimate load, ultimate stress, Young‘s modulus and toughness from each group were compared. The details of the mechanical testing protocols and the parameters for calculation are described in the general methods (chapter 2). A paired t-test was used to determine the statistical significance of the biomechanical parameters with normally distributed data and the Wilcoxon signed-rank test was used for non-normally distributed data. Levene’s test

was used to determine the significant difference of data variation between two techniques of specimen preparation.

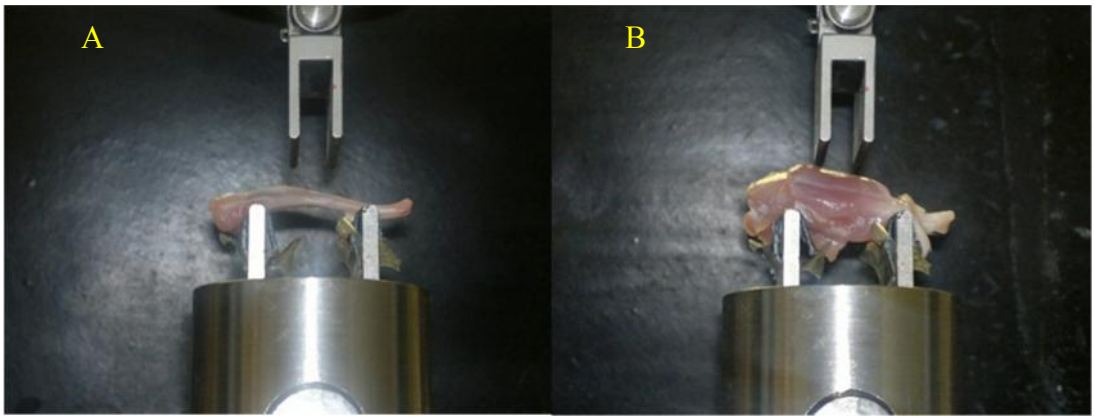

Figure 5.2 Comparison between the mechanical testing of samples with and without muscle; (a) sample without muscle (b) sample with muscle

5.3 Results

5.3.1 The characteristic of stress-strain curve

Examples of the stress-strain curves from samples with and without and muscle are shown in **Figure 5.3**. This curve was derived from the recorded results from the biomechanical testing. The toe region of the stress-strain curve from the specimen with muscle was larger than in the specimen without muscle (**the arrow in Figure 5.3**). This indicated that there was an initial increase in displacement for a small increase in load. This was because the load was transmitted through soft tissue and muscle before reaching the bone sample. As the stiffness of bone is considerably higher than muscle (hard vs soft tissue), it allowed simple differentiation between the low load deformation of the muscle in compression and the onset of load carried by the bone in bending. As shown in, **Figure 5.3.**, red lines define the slope of the linear

portion of the curve, representing the Young's modulus and green lines which indicate the maximum stress required (ultimate stress). The area under the curve is defined as the toughness. The toe regions of specimens with muscle were not included when calculating the area under the curve, as this area represented the energy absorption from muscle associated with the deformation of muscle prior to loading the bone.

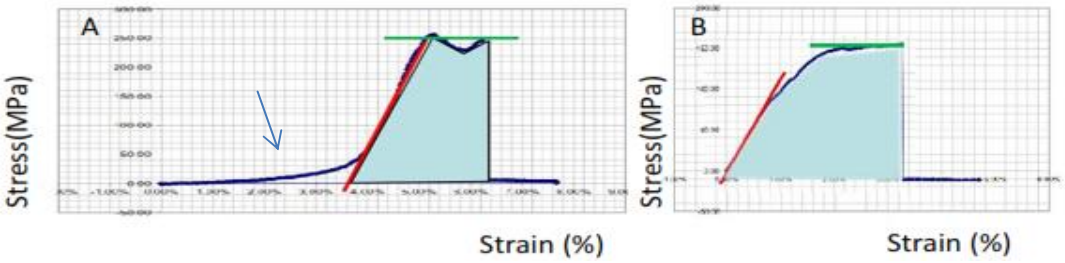

Figure 5.3 The stress-strain curve from the mechanical testing; (a) from sample with muscle and (b) from sample without muscle

5.3.2 The comparison of biomechanical parameters between samples with and without muscle

The **table 5.1** shows the summary of biomechanical parameters from sample with and without muscle. The average of the ultimate load, ultimate stress, Young's modulus and modulus of toughness from the specimen with muscle and without muscle are shown. Each parameter between specimen with muscle and without muscle is shown in the **Figure 5.4**. No statically significant differences were found for any parameters using either the paired t-test (for normally distributed data) or the Wilcoxon signed-rank test (for non-normally distributed data).

Table 5.1 Summary of biomechanical parameters between sample with and without muscle

Mechanical property	**Units**	**Mean**	**Standard deviation**	**Coefficient of variation**
Tibia without muscle sample*(n=12)*				
Ultimate load	N	105.18	26.34	0.25
Ultimate stress	MPa	281.47	121.18	0.43
Young's modulus	GPa	9.89	5.00	0.50
Modulus of toughness	MPa	4.72	1.83	0.35
Tibia with muscle sample *(n=12)*				
Ultimate load	N	101.62	25.38	0.25
Ultimate stress	MPa	288.45	72.16	0.25
Young's modulus	GPa	10.45	2.38	0.24
Modulus of toughness	MPa	4.33	1.50	0.39

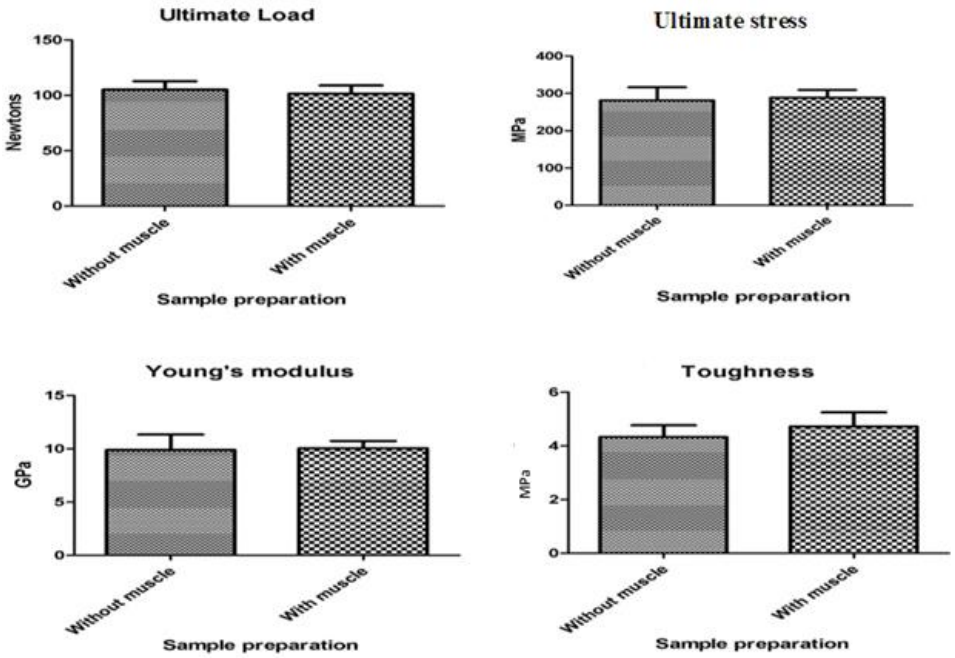

Figure 5.4 The comparisons of biomechanical parameters between bones with and without muscle detached

5.3.3 **The comparison of coefficient of variation**

The Coefficient of Variation (CV) is defined as the ratio of the standard deviation to the mean. It expresses the variation of the data in this case obtained from sample with and without muscle. The CV of stress and young's modulus from the sample with muscle was less than the sample without muscle, whereas the CV of the load and toughness was comparable (**Figure 5.5**). Although there were no statistically significant differences in the biomechanical parameters from between sample preparation techniques, testing samples without cleaning muscle was shown to be a technique which produced less variation.

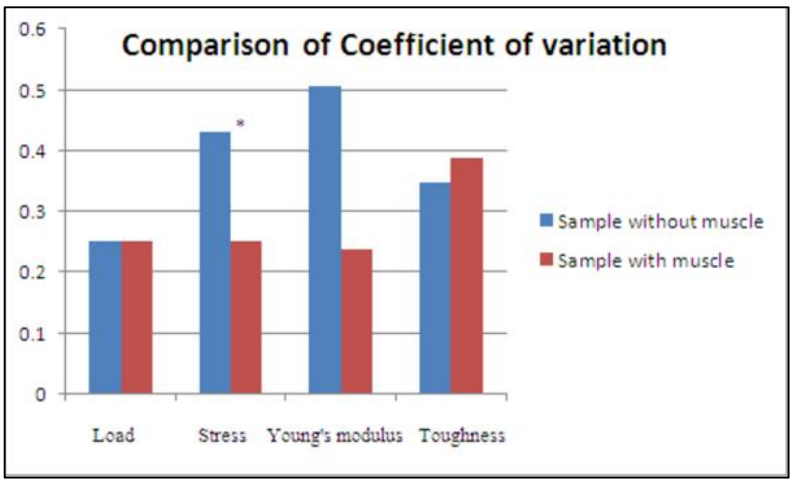

Figure 5.5 The coefficient of variation of biomechanical results obtained from bone with and without muscle (* p-value <0.029)

5.4 Summary and discussion

It has been suggested that soft tissue including muscle and subcutaneous tissue around bone samples should be removed prior to testing. However, during this experiment, despite careful dissection, notching caused by the scalpel in the callus region of bone sample was revealed by the three-dimensional images produced by micro-CT. This notching might affect the biomechanical properties and increase variation. Additionally, removal of the soft tissue and muscle around the bone specimen increased the sample preparation time. Thus, testing a sample without removal of the soft tissue minimised the risk of disrupting the fracture callus and decreased the sample preparation time. However, it was important to determine whether the mechanical properties of sample with and without muscle were different or not before using this preparation technique to assess the biomechanical properties of whole specimens.

The results from this study demonstrated that soft tissues and muscle did not have any effects on the mean of the mechanical properties; ultimate load, ultimate stress, Young's modulus and toughness. These parameters were comparable between the

groups, i.e. bone with and without muscle. In addition, that the coefficients of variation which were calculated from the ratio of the standard deviations to the mean of each parameter were found to be less for the biomechanical parameters from samples with muscle compared to those without muscle.

One area of evaluation that required special consideration was the toughness, as this property was derived from the area under the stress/strain curve. In this study, the toe region of the specimens with muscle was subtracted in order to derive the toughness that reflected the energy absorption from just the bone. When the areas under the curve representing the deformation of the bone were analysed, the results showed that the toughness of bone from the two sample preparation techniques investigated was comparable.

In conclusion, the advantages of testing the bone without prior removal of soft tissue and muscle were (a) a reduction in specimen preparation time, b) a reduced risk of creating a stress raiser at the callus and, c) a reduction in variability. This modified sample preparation technique for mechanical testing was used for sample preparation for biomechanical testing in chapter 8 and 9 in this thesis.

Part 3: The results

Chapter 6: The characteristics of the atrophic non-union Model: *in vitro* and *in vivo* experiments

Aim: *The aim of this chapter was to characterise an established atrophic non-union model both biomechanically and biologically*.

6.1 Introduction

This model is analogous to the clinical scenario of a patient with a stiff atrophic non-union. An osteotomy was created with a small gap (1 mm) which was a "non-critical size defect". The periosteal stripping and intramedullary curettage were performed in order to induce an atrophic non-union. There were three objectives of this study; (1) to demonstrate the mechanical stability of the external fixator; the fixation should maintain the osteotomy site under the physiological weight-bearing of the rat (2) to determine the reproducibility of this technique in creating an atrophic non-union in *vivo* (3) to evaluate the number of MSCs in the atrophic non-union model from both the local site and from a remote site using a colony forming assay.

6.2 Materials and methods

The surgical technique and fracture evaluation have been described in full in chapter 2. This section provides only specific details that related to this chapter.

6.2.1 **Experiment design**

Twenty one male Wistar rats (4-5 months of age) were used for this study. Five rat cadavers were used to determine the stability of the fixator devices. Twelve rats were used to validate the atrophic non-union model for the *in vivo* study. Another four rats were used as normal controls for comparing the number of MSCs. The operated rats and controls were kept in the same conditions.

6.2.2 **Biomechanical testing in cadaveric model**

An osteotomy was created in the mid shaft of the tibia and an external fixator was placed to stabilise the bone in 5 rat cadavers (as described in chapter 2). Then, the lower leg was disarticulated from the knee. Proximally, for approximately 5 mm. the soft tissue was removed from the proximal Tibia to expose the bone. The foot was then removed by disarticulation at the ankle. Distally, for approximately 5 mm. the surrounding soft tissue was removed to expose the distal tibia. The sample was then custom mounted using poly methyl methacrylate (PMMA) and put between load cells. Biomechanical testing was performed using a standard mechanical test machine (Zwick/Roell) and its software (as described in chapter 2). However, in this study the axial compression mode was employed. The load required to close the 1 mm gap was noted and used to calculate the expected displacement from physiological forces. For the hind leg, the magnitudes of physiological forces have been estimated to be approximately 50% of body weight (Clarke, 1995). The axial stiffness of the external fixator was determined from the slope of the load-displacement graph.

6.2.3 The fracture assessment of atrophic non-union *in vivo* study

To determine the reproducibility of the model, twelve rats were used to create atrophic non-union. Atrophic non-union was diagnosed in all animals using serial radiographs with digital imaging every two weeks (as described in chapter 2). The diagnoses were judged by two independent orthopaedic surgeons. At eight weeks, the external fixator was carefully removed, and the animals were examined by manual clinical assessment, which confirmed the presence of motion at the fracture site at eight weeks. The fracture site was also scanned with a micro-CT (Skyscan®) (n = 7) in order to assess of the bone bridge at the fracture site in detail (see details in chapter 2). Four randomly selected samples were processed for histological examination. Haematoxylin and Eosin staining was used for general histology, Modified Masson's Trichrome for new bone formation and Safranin O/Fast Green for new cartilage formation. Stained sections at the fracture gap were observed using light microscopy under 10x and 20x magnification.

6.2.4 Progenitor isolation and colony forming assay

6.2.4.1 Colony forming fibroblast assay from bone marrow at contralateral femur

Bone marrow derived MSCs from the contralateral femurs of nine atrophic non-union rats and four age-matched normal rats (control) were isolated using a previously reported technique (Lennon and Caplan, 2006). In brief, using sterile technique, the soft tissues were cleaned from the femurs and then the bones were flushed using a 21-gauge needle and the cell suspension produced was filtrated with 100 and then 70 μL. filters. The filtrated cell suspension was added to 10 mL. of low glucose (LG) DMEM containing 10% FBS and 1% penicillin/streptomycin (P/S)

and centrifuged at 1,200 rpm for 5 minutes. The mononuclear cells were counted and processed for colony forming assessment. The mononuclear cells obtained from bone marrow isolation were seeded in 6-well plates at varying densities ($1x10^5$, $0.5x10^6$ and $1x10^6$ per cm^2) in duplicate in the LG DMEM containing 10% FBS and 1% P/S for two weeks without change of the medium.

6.2.4.2 Colony forming fibroblast assay from tissues at the fracture site

To isolate the mononuclear cells from the non-union gap (n=3), the tissues from the atrophic non-union gap were collected and digested using 1% collagenase type 1 solution (Sigma) at 37^oC for 45 minutes. Periosteal tissues from the mid shaft of femur from the same animal were also isolated by the same method as the tissues from the non-union gap. The suspension obtained from this digestion was centrifuged at 1,200 rpm for five minutes. The pellet was suspended in 10 ml. of 10% FBS DMEM with 1% penicillin/streptomycin and filtrated with 100 and then 70 μL filters. The mononuclear cells were counted and processed for colony forming assessment. An equal number of mononuclear cells from the non-union gap and from the periosteum were seeded directly at a concentration of $0.5x10^6$ per cm^2 in 6 well-plates in duplicate in the LG DMEM containing 10% FBS and 1% P/S for three weeks without the medium be changed. The cultures were left for a longer period than the bone marrow cell culture to ensure plastic adhered cells with colony forming ability were able to develop.

6.2.4.3 Giemsa staining for colony counting

Following culture of the cells for two weeks (bone marrow) or three weeks (tissues from fracture gap) without the medium being changed, the cultures were fixed in

100% methanol for 5 min and stained with Giemsa. The number of colonies which contained more than 50 cells was counted using light microscopy.

6.2.5 **Statistical analysis**

GraphPad Prism for windows (GraphPad Software, LA Jolla, California, USA) was used for statistical analysis of data. Paired and unpaired t-test were used to compare the mean minimal bone fraction obtained with micro-CT and the mean number of colony forming units from mononuclear cells of bone marrow, respectively. A p-value of <0.05 was considered statistically significant.

6.3 Results

6.3.1 **The stiffness of the external fixator**

The axial stiffness of the external fixator was derived from the gradient of the load-displacement graph shown in **Figure 6.1**. The mean axial stiffness was 6.90×10^3 N/m ($\pm$ 0.20 SEM, n=5). The load (N) required to close the 1 mm-gap and predicted displacement (mm) of the fracture gap with 50% of animal weight were shown in **Table 6.1**. The mean weight required to close 1 mm.-gap was 0.70 kg ($\pm$ 0.02 SEM, n=5), whereas the mean predicted physiological weight bearing of animals was 0.23 kg ($\pm$ 0.003 SEM, n=5). The weight required to close 1 mm-gap was significantly more than the physiological weight bearing ($p < 0.01$), so this result demonstrated that the gap would be maintained by the external fixator.

Table 6.1 Sumary of load used to close 1mm gap and predicted displacement of 5 animals

Sample	Load (N) for 1mm displacement	Load (kg-force) for 1 mm displacement	Animal weight (kg-mass)	Predicted displacement (mm)
1	6.75	0.67	0.45	0.34
2	6.25	0.63	0.46	0.37
3	7.5	0.76	0.47	0.31
4	7	0.71	0.49	0.35
5	7	0.71	0.47	0.35

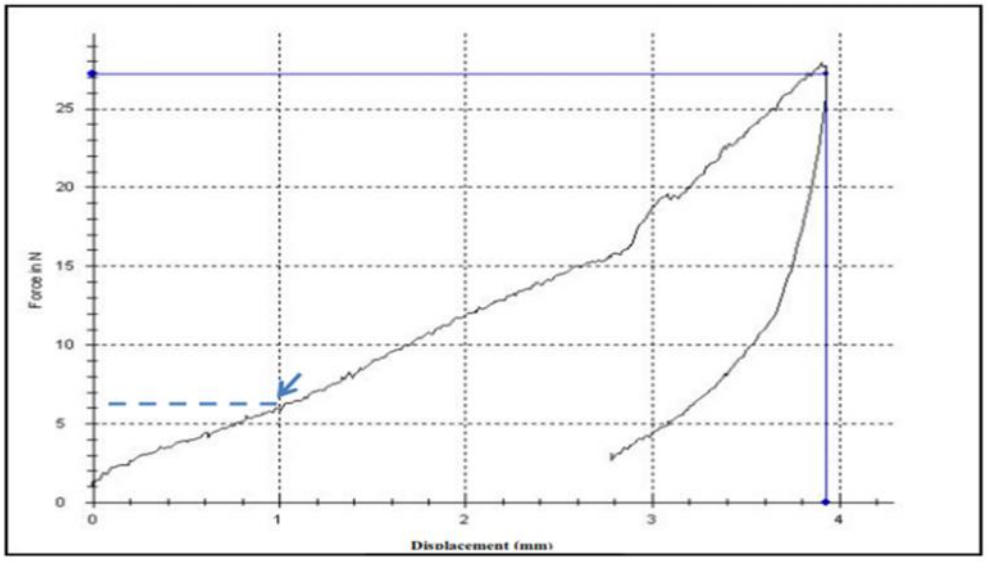

Figure 6.1 Graph showing load-displacement of one of cadaveric test

6.3.2 **The clinical behaviour and health status of the animals**

Twelve rats were fully recovery after the procedure. There were wound complications three days following surgery in two rats during development of the procedure, necessitating euthanasia before completion of the experiment. All of the remaining animals (10 rats) were able to eat and drink normally and had no significant weight loss. The animals had no abnormal posture (piloerection) and no abnormal behaviour. The animals were able to weight-bear fully immediately

following surgery. Their surgical wounds healed by one week and no pin tract infections were noted for the duration of the experiment (**Figure 6.2**).

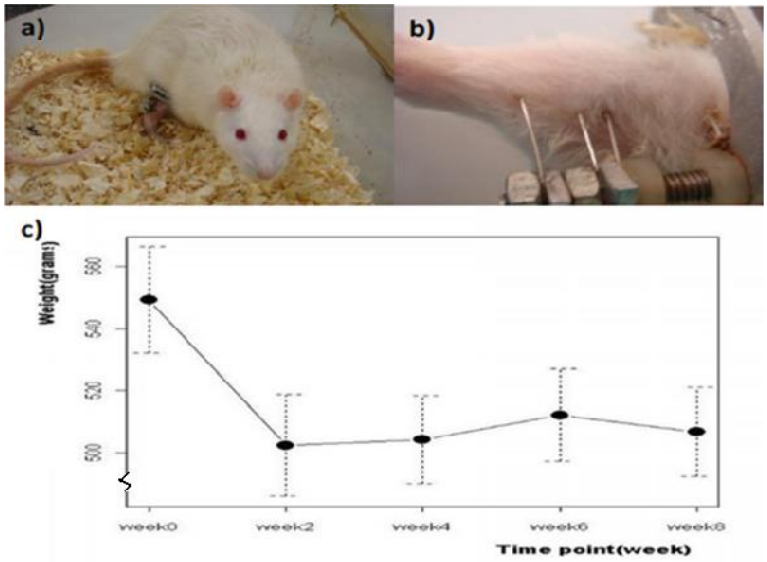

Figure 6.2 Health status of the animal following surgical procedure: (a) The ability to weight bearing immediately after surgery, (b) The appearance of skin at the pin tract b) and (c) Mean weight change of animal after operation

6.3.3 **Diagnosis of atrophic non –union fracture**

6.3.3.1 Clinical diagnosis

At eight weeks after the operation, all animals (n=10) had developed atrophic non-unions. The fracture gaps were grossly palpable at the osteomy site. After removal of the external fixators, the tibias showed gross motion on clinical examination. **Figure 6.3** shows the gross morphology of atrophic non-union.

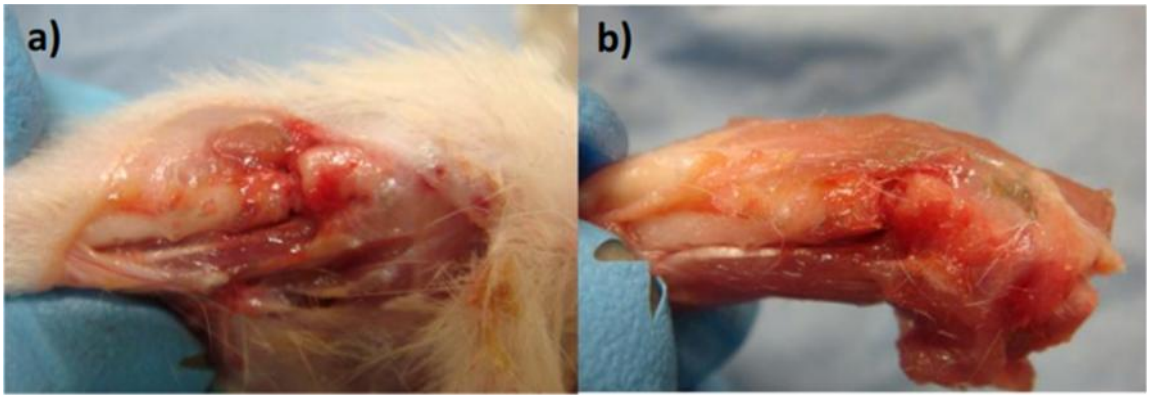

Figure 6.3 Gross morphology at fracture site: (a) The fracture gap is clearly visible and (b) the tibia shows gross motion; when grasped at one end and held horizontally, movement occurs at the non-union site so it cannot even support its own weight.

6.3.3.2 Serial radiographs

In all of the animals (n=10), serial radiographs revealed a persistent gap. There was an absence of callus formation from both the proximal and the distal fragments (**Figure 6.4**). The immediate post-operative radiographic images showed the good bone alignment and the required position of the pins and the external fixator needed to maintain the 1 mm-gap without significant movement of the bone fragments. Two weeks after the operation, radiographic images showed no significant difference from immediate post-operative images. The 1 mm-gap was maintained and there was still no callus formation and no change in the size of the fracture gap. Four weeks after the operation, there continued to be no change in the radiographic appearance in all animals. Six weeks after operation, radiographic images showed an increase in gap size in some animals. Both the proximal and the distal bone ends developed blunt edges. Eight weeks after operation, the bone ends remained rounded and the gap appeared to increase. These results demonstrated the pattern of development of an atrophic non-union.

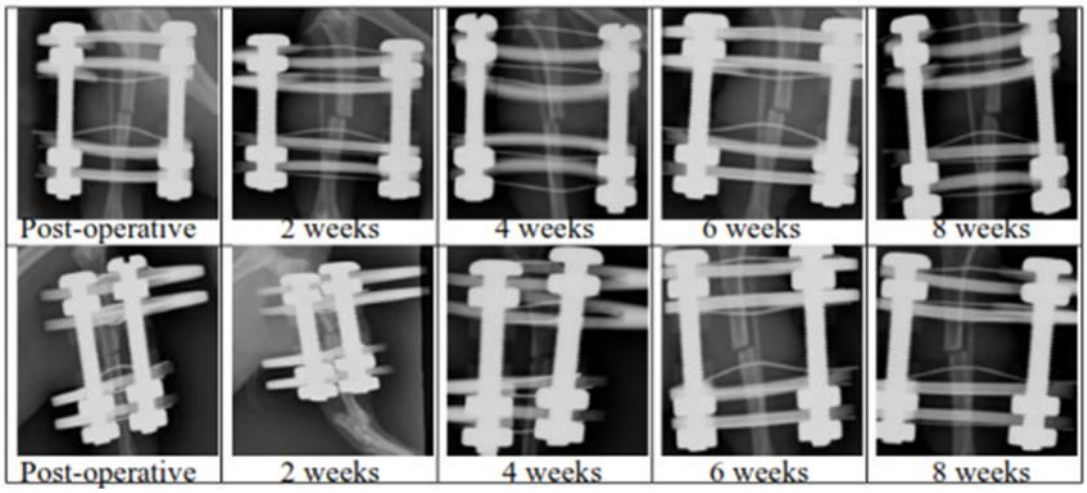

Figure 6.4 The radiographic assessment: serial radiographs; AP (above) and Oblique views (below) every 2 weeks from immediately post-operative to 8 week post-surgery.

6.3.3.3 Histological appearance of fracture gap

Four of the ten tibiae were randomly selected for histological assessment. In all of the selected samples, the fracture site had formed a clear atrophic non-union with rounded bone ends and fibrous tissue present in the inter-fragmentary gap. There was no woven bone or cartilaginous callus at the fracture gap. (**Figure 6.5 (a)**) There were active osteoclasts creating rounded bone ends (**Figure 6.5 (b)**) producing the typical appearance of an atrophic non-union. Neither intramembranous nor endochondral ossification could be detected (Masson's Trichrome stain and Safranin-O/Fast Green, respectively). (**Figure 6.5 (c-f)**)

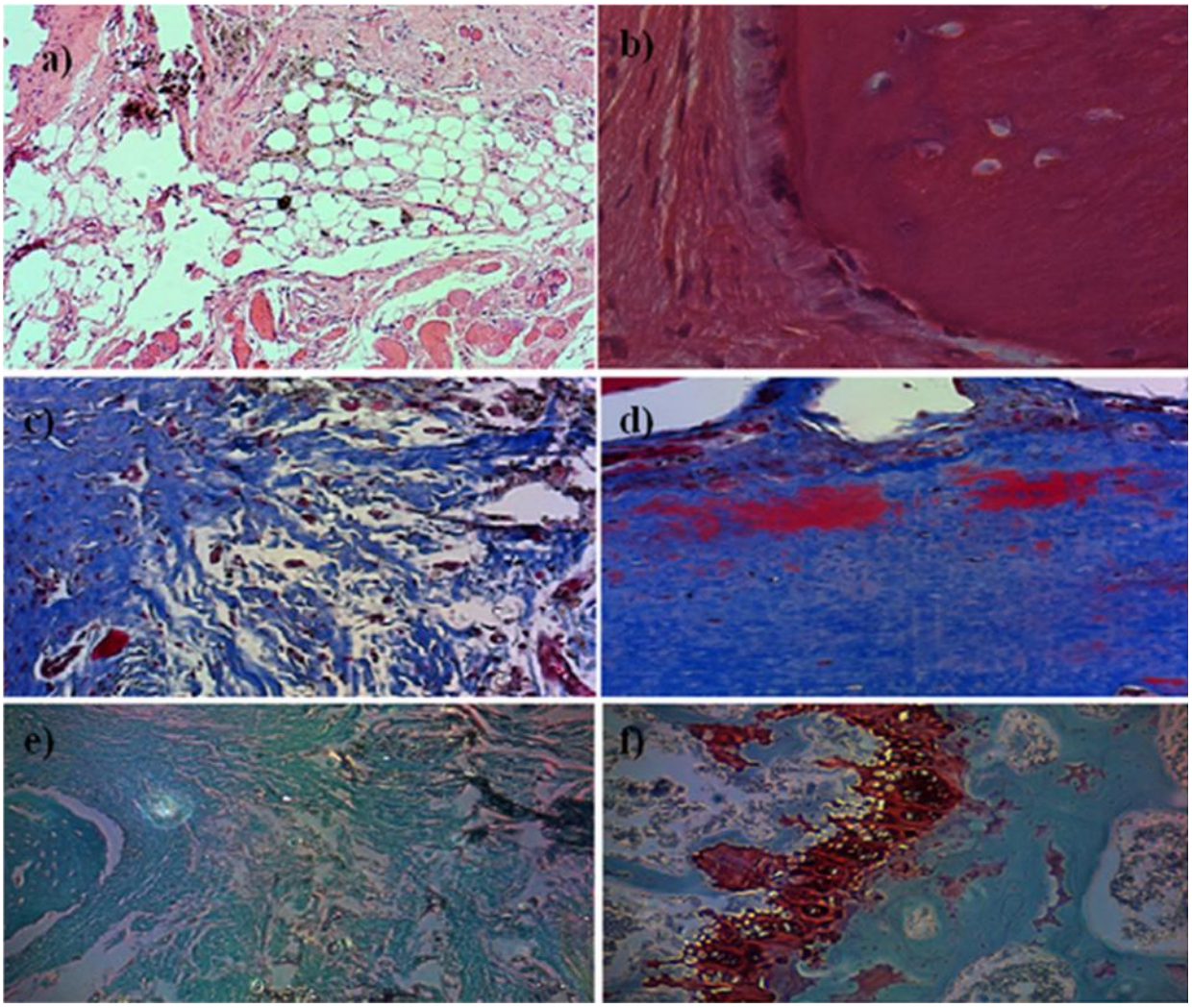

Figure 6.5 Histology assessments of atrophic non-union model: a) H&E stain (x100): At the end of the experiment, the gap was filled with fibrous tissue, loosed areolar tissue and also infiltration of muscle fibres and adipose tissue into the gap b) H&E stain (x400): There were osteoclasts resorbing bone at the end of fracture site. c) Masson's Trichrome stain (x100) There were no bone formation at the fracture at 8 weeks; d) Masson's Trichrome stain (x100) The periosteum area around the pin tract, there were new bone formation. e) Safranin-O/Fast Green stain (x100) There was no cartilage formation or endochondral ossification at the fracture gap at 8 weeks f) Safranin-O/Fast Green stain (x100) The new cartilage formation was show at the proximal tibia epiphysis.

6.3.3.4 Three-dimension micro-computed tomography

Three dimensional images from Micro-CT showed the fracture gap clearly. Neither external callus formation nor bone bridges could be detected. The fracture ends became round, reflecting atrophic non-union (**Figure 6.6**). The shape of the non-union was also demonstrated by the bone area fracture, that is, the fraction of area formed by the external borders of the diaphysis and the continuation of these borders across the fracture site that was filled with bone (see details in chapter 2). This was plotted across the fracture site from proximally to distally along the region of interest. Proximal and distal to the atrophic non-union was approximately 0.9. The bone area fraction dropped to a minimum at the middle of fracture gap. The bone area fraction then rose back to nearly 0.9 in the distal fragment (**Figure 6.7**). The bone area from the region of interest in the atrophic non-union was significantly less than from the equivalent position of the unoperated side (0.84 vs 0.12, $p < 0.01$)

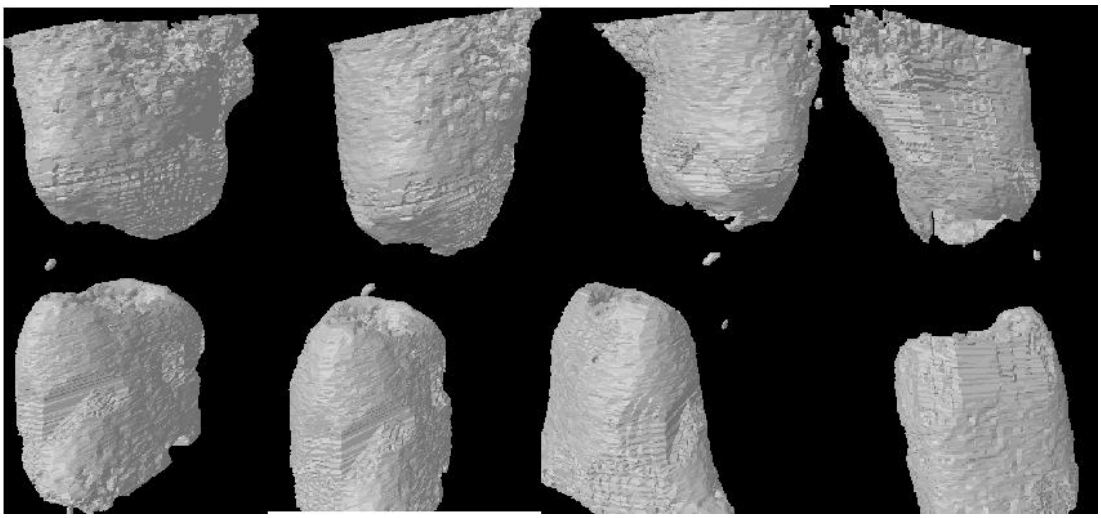

Figure 6.6 Three dimensional images of atrophic non-union: Three different views of three dimensional images from MCT show clearly rounded ends both proximal and distal.

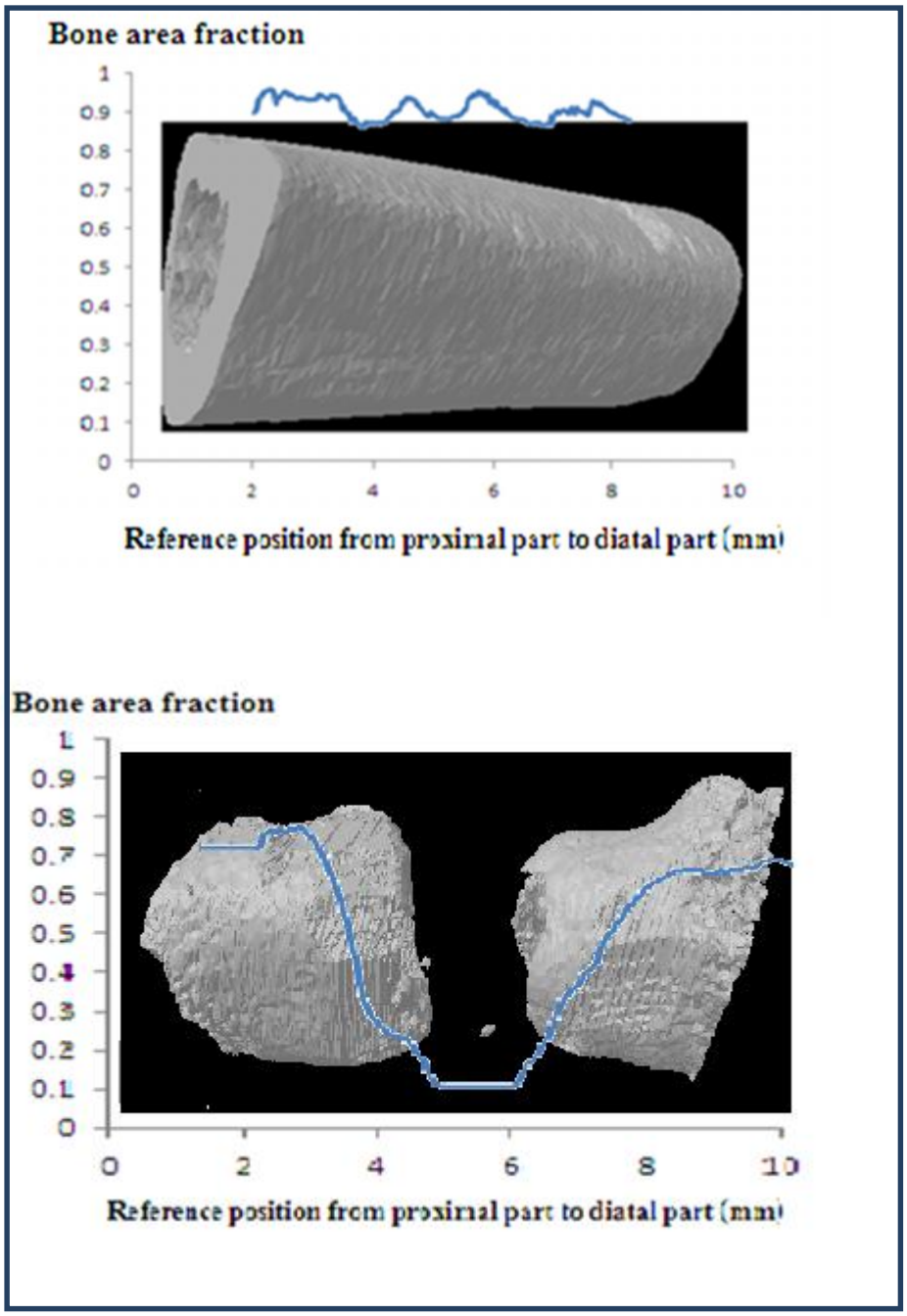

Figure 6.7 The plotted bone fraction area from proximal to distal part of the volume selection between normal bone and atrophic non-union

6.3.3.5 Colony forming units of mesenchymal stem cells in atrophic non-union

6.3.3.5.1 Assessment of the increase in the number of the colony forming units from bone marrow from a remote site in the atrophic non-union model

The number of mononuclear cells from atrophic non-union rats and control rats was 55.9 ± 4.8 x 10^6 (mean ± SEM, n=9) and 47.1 ± 4.1 x 10^6 (mean ± SEM, n=4) cells, respectively. There was no statistically significant difference in the mean cell count between atrophic non-union and control (P-value=0.19). The densities of colonies of the well plates seeded at 5x10^5 cells (0.5x10^5 cells per cm^2) were found to be appropriate for counting. The colony forming units from both atrophic non-union and normal controls had a similar morphology and the fibroblast-like cells in the colonies were also similar. The number of colony forming unit counts from atrophic non-union was significantly higher compared with control. The mean number of colony forming from atrophic non-union group was 10.4 ± 1.1 (mean ± SEM, n=9), whereas from control group was 5.8 ± 0.7 (mean ± SEM, n=4); (P-value=0.0041). (**Figure 6.8**)

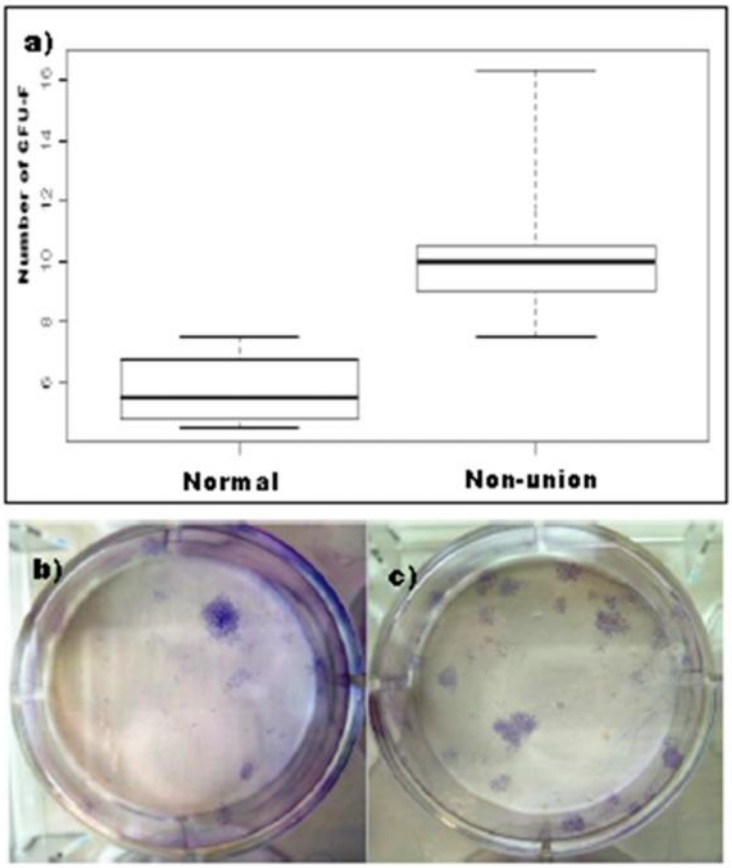

Figure 6.8 The colony forming assay for remote bone marrow from the atrophic non-union model: (a) The mean number of colony forming unit from the bone marrow from the contralateral femur of the atrophic non-unions and also from normal control animals. The appearance of the colony formed from the femoral bone marrow of (b) a normal rat and with (c) atrophic non-union

6.3.3.5.2 Assessment of atrophic non-union tissue for colony forming units of mononuclear cells

Tissues from the non-union gap (n=3) were digested with collagenase type one solution in order to isolate stromal cells. Periosteal tissues from the mid shaft of femur from the same rats were used as the control. Following digestion of the tissues with collagenase, $5x10^5$ mononuclear cells from each source were seeded onto six well plates ($0.5x10^5$ cells per cm^2) and the media was left unchanged for three weeks. No colony forming units were obtained from the atrophic non-union tissue from any

of the three samples, whereas colony forming units of mononuclear cells were obtained from the periosteal tissues. The morphology of the cells in the colonies formed from the periosteum was similar to MSCs derived from bone marrow (**Figure 6.9**).

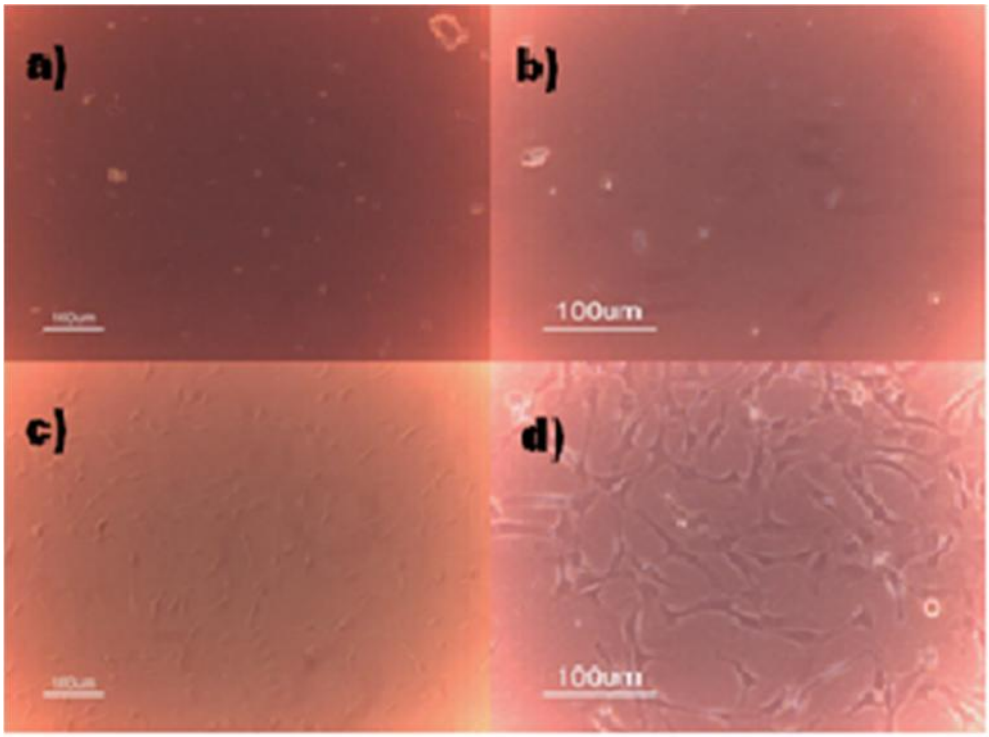

Figure 6.9 The cultured cells obtained from non-union tissues: a)-b)The culture of mononuclear cells from atrophic non-union tissues after culture for 2 weeks, x100 (a) and x200 (b), c)-d) The culture of mononuclear cells of from periosteal tissues after culture for 2 weeks, x100 (c) and x200 (d)

6.4 Summary and discussion

In order to investigate the therapeutic effect of new interventions for fracture healing, clinically relevant atrophic non-union models are essential. This study was conducted to characterise an atrophic non-union animal model for studying the therapeutic potential of adult stem cells. The model involved stripping of the periosteum for one

bone diameter either side of and osteotomy and removal of the local bone marrow over the same distance. A small (1 mm.) non-critical size defect was created and the tibia was stabilised with an external fixator. The atrophic non-union model presented in this study was originally reported by Reed et al (2003). However, the components of the external fixator have been modified in that aluminium rings were used instead of plastic because the plastic rings were chewed by rats (Mills and Simpson, 2012). The stability of the fixation was tested using the axial compression in a cadaveric study and found to be sufficiently strong and stiff.

In this study, the procedures used for creating atrophic non-unions were found to be simple and reproducible. A 23G needle was used to remove the bone marrow and endosteal components. Periosteal tissues were destroyed both proximal and distal to the osteotomy site using a periosteal elevator. It has been reported that the periosteal elevator can remove both the cambial and fibrous layers of the periosteum (Brownlow et al., 2000).

In this study the atrophic non-union was confirmed by (1) by direct inspecting, (2) serial radiographs, (3) histology and (4) three-dimensional imaging using micro-CT was used to demonstrate connectivity across the fracture site. From the CT images the bone fraction area was derived using 2D analysis of the region of interest at the cortical area across the fracture site. The bone cortex of proximal and distal bone was used as the reference, providing a quantitative measurement of the shape of the fracture repair.

Eight weeks after the non-union operation, all of the animals that had undergone this procedure had developed a non-union. There were only 2 animals, who suffered from wound complications and needed euthanasia before the completion of the experiment. This complication occurred at the initial period of study; before the operation technique had been refined.

In addition, the progenitor cells in the atrophic non-union model were characterised both systemically and locally. Colony forming assays were used to determine the number of MSCs in the atrophic non-union both at a remote site and at the tissue gap.

The number of colony forming units from the remote site (contralateral femoral bone marrow) was significantly higher in animals that had undergone the atrophic non-union procedure compared to control animals. Conversely, the colony forming units could not be detected from the non-union gap tissue. These results suggested that there was a systemic response to the creation of the atrophic non-union.

The absence of colony forming units from the gap tissue supported the investigation of the local delivery of MSCs into the atrophic non-unions to ascertain whether they were able to rescue the fracture healing process in atrophic non-union. This intervention is investigated in the following chapters.

Chapter 7: Determination of bone regeneration potential of mesenchymal stem cells implanted either at an early or at a late stage in the atrophic non-union model

Aim: *To determine an optimal time for using injectable rat mesenchymal stem cells (rMSCs) based approach in atrophic non-union model*

7.1 Introduction

Atrophic non-union is a major complication of a fracture. It is considered to result from biological insufficiency either locally or systematically. MSCs can produce bone progenitor cells which are capable of osteogenesis (Pittenger et al., 1999). Therefore, MSCs are a potential promising approach for enhancing fracture healing. One of the advantages of using MSCs is that they can be delivered by a minimally invasive technique. During the developing stages of an atrophic non-union, there are differences in the biological components that presented compared to the early stages of normal fracture repair (Reed et al 2003). Thus, as the biological environment at the fracture sites varies, this must be taken into account when assessing the therapeutic effects of MSCs. In this study, the hypothesis that the stage of the fracture healing process affects the outcome of MSC treatment is tested. The aim of this study is to determine the therapeutic effects of MSCs in the atrophic non-union model using a minimally invasive percutaneous injection technique at both an early (three weeks) and a late (eight weeks) time point after inducing an atrophic non-union.

7.2 Materials and Methods

The surgical details of the atrophic non-union model, rat MSC preparation and fracture assessments were described in the general materials and methods (Chapter 2). In this section, only the specific details related to this chapter are described.

7.2.1 Experiment design

All the procedures were conducted following approval by the Local Research Ethics Committee and the UK Home Office, according to the animal (Scientific Procedure) Act 1986. Twenty adult male Wistar rats (400-500g) were randomly assigned into four groups immediately after inducing the atrophic non-union: Group 1 for rMSC injection at three weeks post inducing the atrophic non-union (n=6), Group 2 for PBS injection (control) three weeks post inducing the atrophic non-union (n=4), Group 3 for rMSC injection at 8 weeks post inducing the atrophic non-union (n=5) and Group 4 for PBS injection (control) eight weeks post inducing the atrophic non-union (n=5). The treatment groups (group 1 and 3) were injected with the 5 x 10^6 rMSCs in PBS suspension (200 μL). The fracture healing process was monitored with radiographs every two weeks until the end of the study. Further assessments of bone healing were performed at eight weeks after injection (at 11 weeks for early intervention and 16 weeks for late intervention) by quantitative micro-CT and histology.

7.2.2 rMSCs preparation

rMSCs derived from femoral bone marrow from 4 month old male Wistar rats were isolated by flushing them from the femoral canal. Cultured MSCs from passage 3-4

of primary culture were used for implantation. The details of rMSC preparation and culture expansion have been described in chapter 2 and 3.

7.2.3 **Fracture assessments**

Digital radiographs were taken of all the animals every two weeks after injection. They were blindly evaluated and assessed by two orthopaedic surgeons; any disagreements of diagnosis were decided by a senior trauma orthopaedic surgeon. The progression of the fracture healing in all experimental animals was evaluated using (1) the radiopacity, (2) both the proximal and the distal callus index, (3) the callus area and fracture scoring systems. At the end of the study specimens were harvested and scanned with the micro-CT (n= 6 in group 1, n= 3 in group 2, n=4 in group 3 and n= 5 in group 5). The amount of each tissue component in the fracture site was evaluated using H&E sections (n= 4s in group 1, n= 3 in group 2, n=3 in group and n=3 in group 4). The new bone formation and cartilage formation were demonstrated with Modified Masson's Trichrome and Safranin-O/Fast Green staining, respectively.

7.2.4 **Statistical Analysis**

GraphPad Prism for windows (GraphPad Software, LA Jolla California USA) was used to calculate the means and SEMs for each group. The normality of the data was tested using the Kolmogorov-Smirnov normality test. The differences in the ratios of the number united out of the total number in both the rMSC injection and controls were tested using Fischers'exacts test at both early and late time points. The mean difference of fracture progression parameters i.e. radiopacity, callus index, percentage increase of callus area and total on the fracture scoring system over the post injection period was tested using two-way repeated measure ANOVA followed

by the bonferroni's multiple comparison tests. The measurements from histology and micro-CT were tested using unpaired t-test. A P-value < 0.05 was considered to be statistically significant.

7.3 Results

7.3.1 Animal health status after the atrophic non-union procedure and cell implantation

All rats successfully underwent the operation to induce an atrophic non-union and then returned to their normal activities within two to three days. No sign of any adverse reactions was noticed following the injection of either cells or PBS. There was neither superficial nor deep wound infection at the surgical site or pin tract infection during the post-operative period in any rats, except one rat in group 2 that accidentally died due to an anaesthetic problem during the post-operative x-ray two weeks after the transplantation procedure. It was excluded from this study. Thus, 19 animals remained until at the end of the study and could be used for analysis.

7.3.2 The fracture healing assessment after injection at the early time point (3 weeks)

7.3.2.1 Assessment of bone union in groups 1 and 2

Bone union in all rats was evaluated by gross morphology immediately after euthanasia. Samples which had developed non-union of the fracture revealed motion

upon gravity (**Figure 7.1**). However, the primary diagnosis of bone union/non-union was made from the radiographic series by the two orthopaedic surgeons.

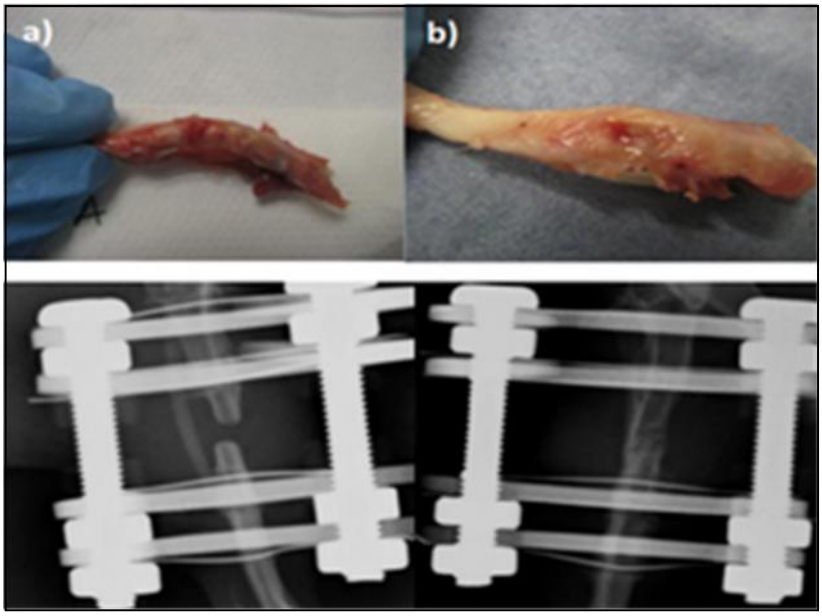

Figure 7.1 Gross appearance and radiographic at 8 weeks following the early intervention (3 weeks): from (a) PBS treatment group and (b) rat MSCs injection group

In the early injection groups (group 1 and 2), five out of six of the animals that had received rMSC (group 1) had bone union, but in the control group (group 2) none achieved bone union at 8 week post-injection. **Table 7.1** shows the number of unions and non-unions for rats injected either with rMSC or PBS. The rMSC group showed a significantly higher bone union rate (Odds ratio = 25.67, P-value = 0.048)

Table 7.1 The number of the animals used in **the early time point** and results of bone union between group 1 and group 2

Treatment group	Outcome*		Total
	Bone union	Non-union	
rMSC (group 1)	5	1	6
PBS (group 2)	0	3	3
Total	5	4	9

* Statically significant (P-value =0.048) by Fisher's exact test

In one of animals in the treatment group, the bone did not heal; the fracture line was still present at eight weeks after injection, however, some callus formation could be seen (**Figure 7.2**). This animal was diagnosed as a non-union because the bone was not in continuity. However it was an hypertrophic rather than an atrophic non-union.

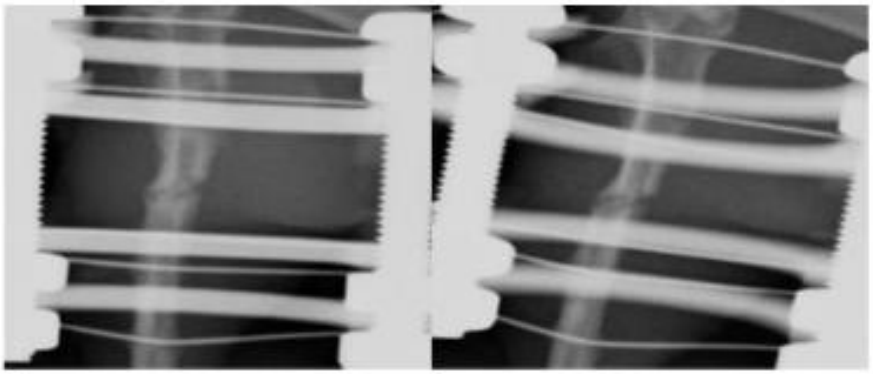

Figure 7.2 Radiographs at 8 weeks post injected of the animals treated with rMSC that was graded as a non-union

7.3.2.2 The progression of the fracture healing process of animals in group 1 and 2

The progression of fracture healing was initially evaluated every week (**Figure 7.3**) as the pilot stage. However, as the x-ray appearance did not differ much within a one-week period, the animals were evaluated with radiographs every two weeks.

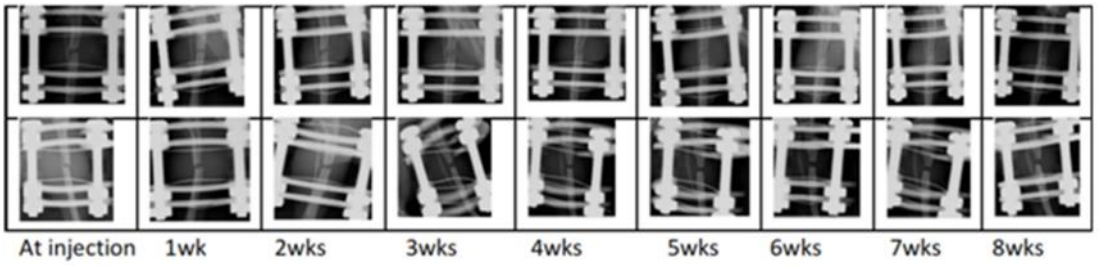

Figure 7.3 Serial radiographic assessment: The serial radiographs of the fractures in the rat MSCs treatment group showed progression of healing (above), whereas the radiographs from the PBS treatment group showed no sign of fracture healing (below)

7.3.2.2.1 Relative Radiopacity in group 1 and 2

An aluminium step wedge was used to calibrate the x-rays and used to provide a normalised value of the radiopacity at the fracture gap of the rMSC treated group and the control group (**Figure 7. 4)**. There was a marked increase in opacity in the rMSC treatment group from 2 weeks to 4 weeks. After 4 weeks, the radiopacity remained stable until the end of the experiment, whereas in the control group, the mean opacity at the different times did not change significantly. The mean radiopacity in the rMSC treatment group was significant higher than the control during the eight-week period (P-value < 0.0019 for treatment, P-value <0.0001 for time, and P-value < 0.0018 for interaction effects, two-way repeated ANOVA)

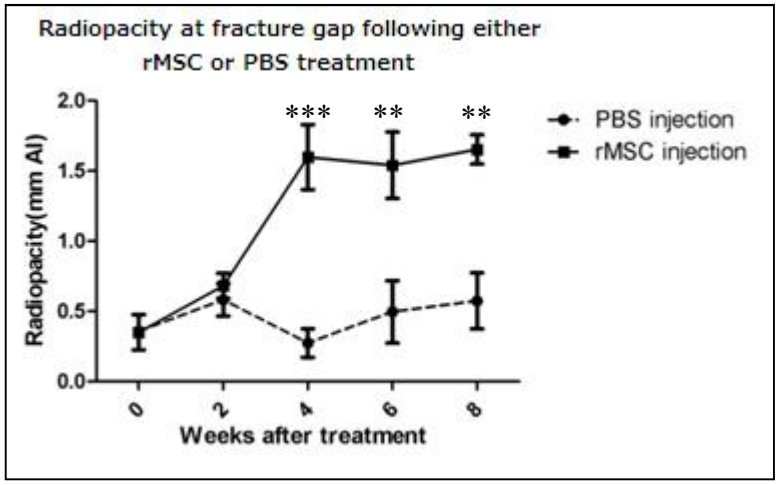

Figure 7.4 The comparison of opacity between treatment (rMSC) and control (PBS) over the 8 week period post injection (Bonferroni's test subsequent to ANOVA: ** = P-value < 0.01, and *** = P-value < 0.001, data shown as mean and SEM, n= 3-6 per group and time)

7.3.2.2.2 Callus index in groups 1 and 2

Using the modified callus index, a proximal callus index and a distal callus index were calculated. There were significant increases in the callus size of rMSC injected animals following injection compared to the control (**Figure 7.5**) (Proximal callus index, P-value=0.0284 for treatment, P-value=0.58 for time, and P-value<0.0001 for interaction effects: Distal callus index, P-value=0.0021 for treatment, P-value=0.49 for time and P-value=0.0029 for interaction effects, two-way repeated ANOVA) . The callus index of proximal and distal parts changed in the same way.

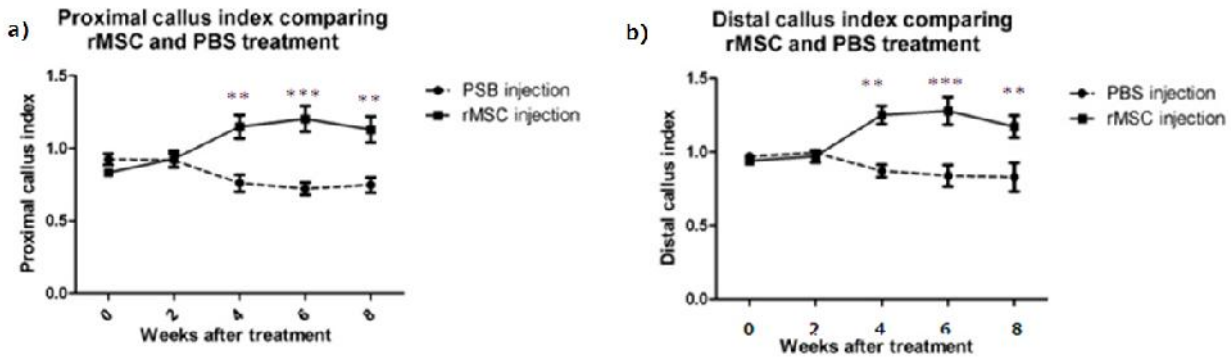

Figure 7.5 The comparison of callus index; (a) proximal and (b) Distal between treatment (rMSC) and control (PBS) over the 8 week period post injection (Bonferroni's test subsequent to ANOVA: ** = P-value < 0.01, and *** = P-value < 0.001, data shown as mean and SEM, n= 3-6 per group and time)

7.3.2.2.3 Percentage of callus area increase in groups 1 and 2

The graph in **Figure 7.6** shows the percentage increases of the callus area over the eight week period after injection for both the rMSC group and the control group. In the rMSC injection group, the percentage change of callus gradually increased from the 2nd week to the 6th week and then slightly decreased at the 8th week. In contrast, the percentage change of callus in the control group where PBS solution alone was injected at the non-union site resulted in a decrease of callus area. This could be indicated the presence of atrophic non-union in PBS treatment animals. There was a statistically significant difference in the amount of callus between the two groups (P-value=0.0025 for treatment, P-value =0.0006 for time, and P-value=0.0039 for interaction effects, two-way repeated ANOVA).

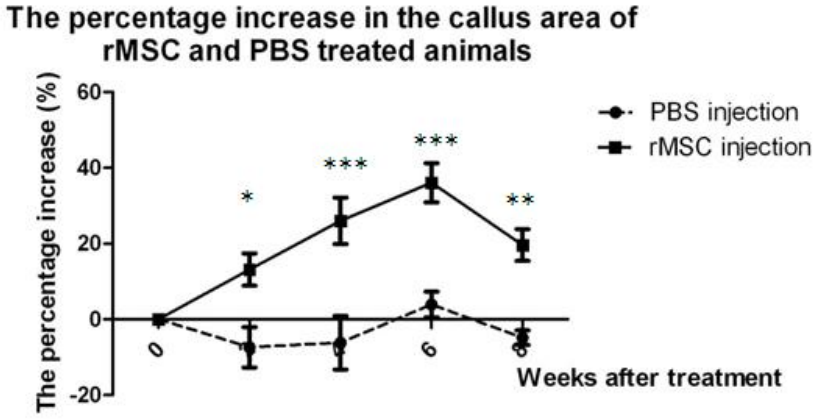

Figure 7.6 The comparison of the percentage callus increase between treatment (rMSC) and control (PBS) over the 8 weeks period post injection (Bonferroni's test subsequent to ANOVA: * P-value <0.05, ** = P-value < 0.01, and *** = P-value < 0.001, data shown as me an and SEM, n= 3-6 per group and time)

7.3.2.2.4 The progression of the fracture healing process in groups 1 and 2 assessed using fracture scoring systems

The results of the RUST score (which was determined from the number of cortices that showed bone bridging) and the Lane & Sandhu score (which was derived from three subcategories: (i) percentage bone in the fracture gap, (ii) presence of the fracture line and (iii) evidence of bone remodelling) showed the progress of the fracture healing process (**Figure 7.7**). The RUST score in the rMSC treatment group was significantly different from the control group after 6 weeks and the Lane & Sandhu score demonstrated a significant difference after 4 weeks.

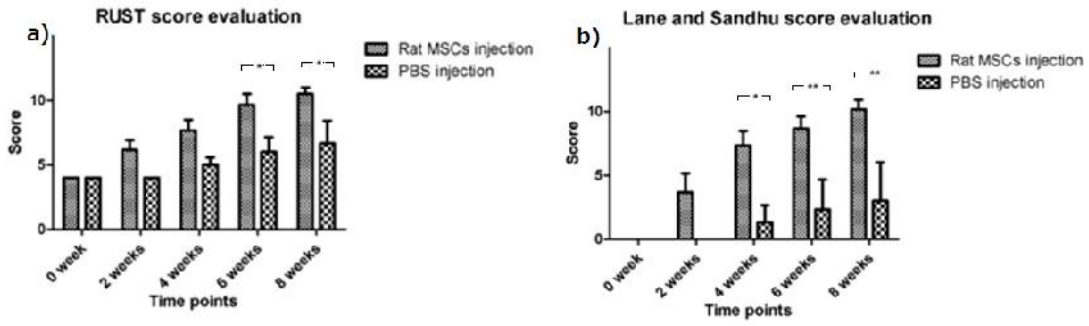

Figure 7.7 The fracture scoring systems: (a) The RUST score evaluation and (b) Lane and Sandhu score evaluation (Bonferroni's test subsequent to ANOVA: * P-value <0.05, and ** = P-value < 0.01, data shown as mean and SEM, n= 3-6 per group and time)

7.3.2.3 Histological evaluation for groups 1 and 2

The histological observations from H&E stained sections supported the radiological results. In rat MSC injection group, the interfragmentary gap consisted of bone and cartilage. (**Figure 7.8**) Callus was formed at the fracture gap. Both intramembranous bone formation and endochondral bone formation contributed to the healing process in the rat MSC treatment group. Cortical remodelling could be seen in one animal. (**Figure 7.8 (a, b)**) Safranin-O/Fast Green showed the area of cartilage formation and Masson's trichrome staining showed the area of bone formation (**Figure 7.9**). In the PBS injected group, the tissue within the interfragmentary gap consisted predominantly of fibrous tissue and was similar to the histology of the uninjected atrophic non-union at eight weeks depicted the chapter 6 (**Figure 7.10**).

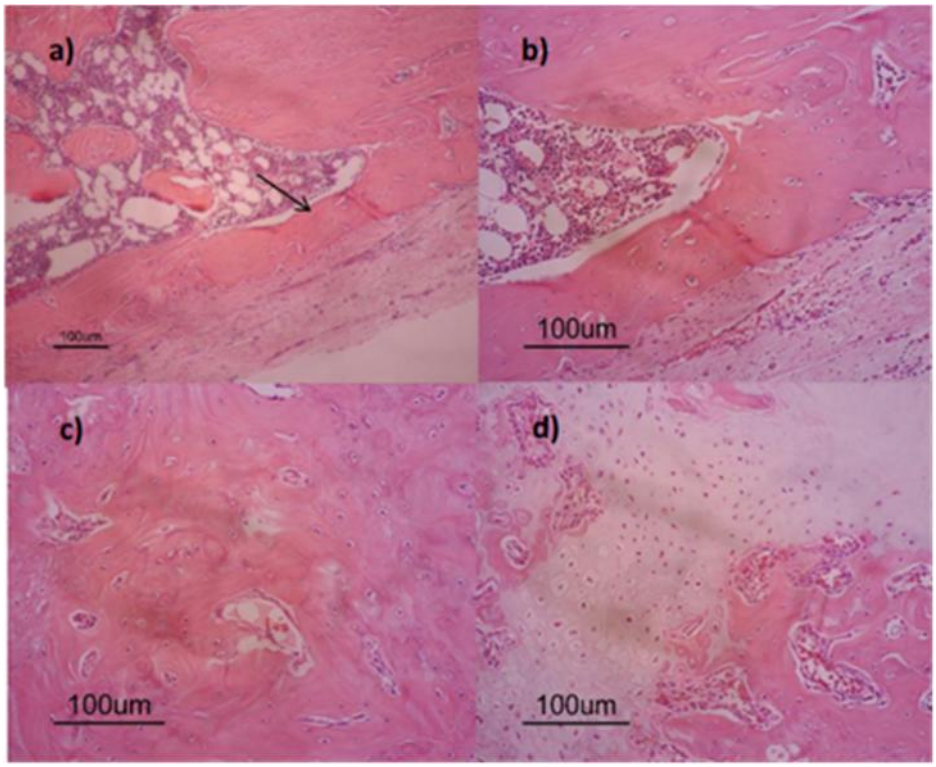

Figure 7.8 H&E staining of the fracture site of a MSC injected rat: a)-d) Cortical remodelling can be found at the fracture gap (x100, a), (x200, b) and both bone formation (x200, c) and cartilage formation (x200, d) were found at the fracture gap

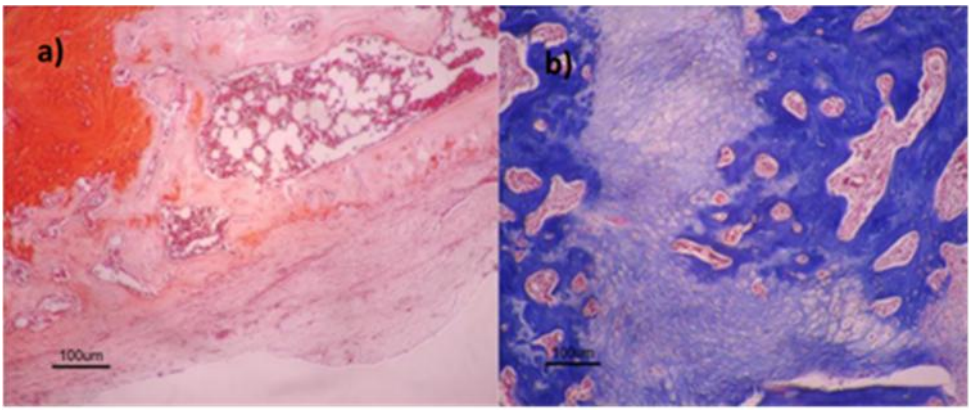

Figure 7.9 Safranin-O/Fast Green and Masson's trichrome staining at the fracture site of a rat MSc injected rat: Safranin-O/Fast Green staining shows the area of cartilage formation (x100, a) and Masson's Trichrome staining shows the bone trabeculae at the fracture (x100, b)

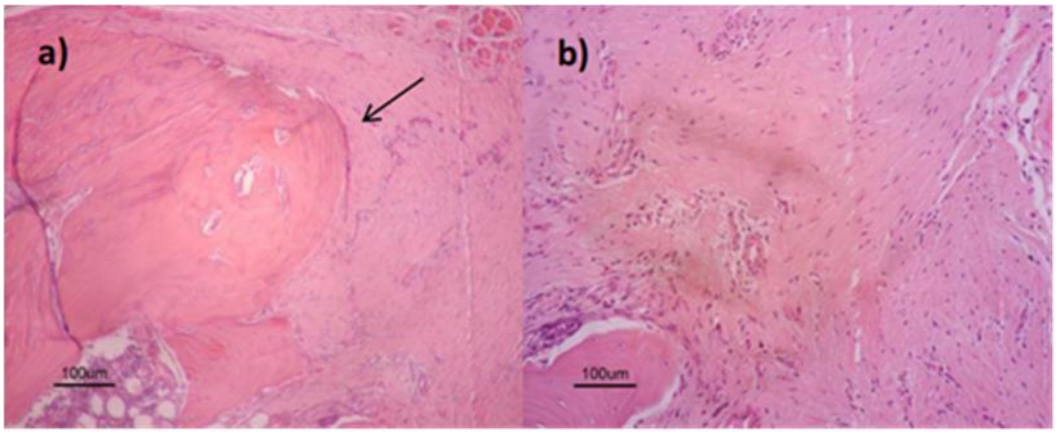

Figure 7.10 H&E staining at fracture site of PBS injected rat: (a) The fracture end (arrow) has become rounded and (b) fibrous tissue is present at fracture gap (x100)

To measure the tissue constituents in the fracture gap, a 10x10 square grid was applied to the histology images, the tissue components in the gap were classified as bone, cartilage, fibrous and marrow/empty space. The relative amounts of the tissue components were compared between the treated group and the control group (**Figure 7.11**). In the treatment group, bone predominated whereas in the control group, fibrous tissue was the dominant component in the fracture gap. The bone component was significantly higher in the treatment group (P-value<0.01, unpaired t-test).

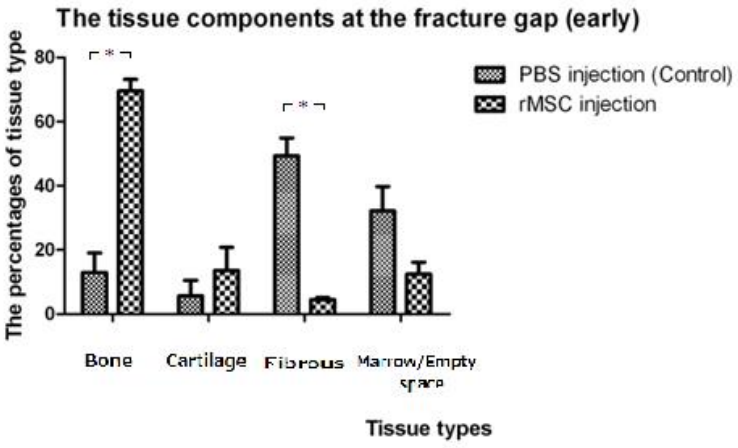

Figure 7.11 Quantitative evaluation of the tissue component in the fracture gap (* =P-value <0.01, unpaired t-test)

7.3.2.4 Micro-CT analysis in groups 1 and 2

Three dimensional images from micro CT demonstrated bony bridging in all animals which were treated with rat MSCs (**Figure 7.12 (a, b)**). There was also the cortical remodelling in one of animals in the treatment group. The bone gap was still evident in the controls, although there were, occasional islands of bone in the fracture gap. To provide a quantitative measurement, the percentage of bone tissue volume per total tissue volume at the centre of the fracture site was measured for all samples. All parameters are shown in **table 7.3**. In the treatment group (group1), the percentage bone volume (P-value <0.001, unpaired t-test), trabecular thickness (P-value <0.001, unpaired t-test), and bone mineral density (P-value <0.001, unpaired t-test) were significantly higher than in the control group (group2).

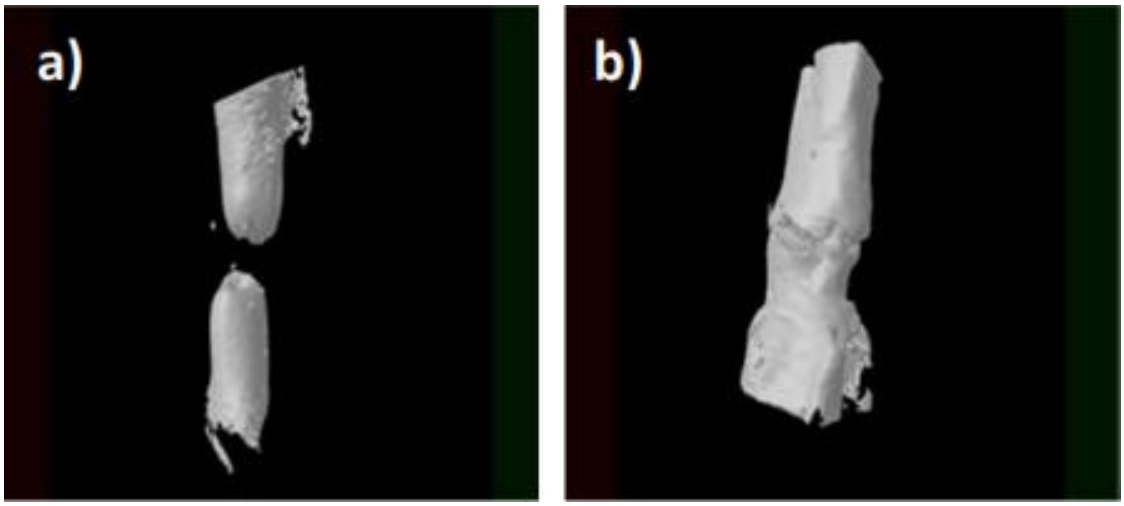

Figure 7.12 The results from Micro computed tomography of the early treatment groups: Three dimension image of (a) control group and (b) rat MSCs injected group

Table 7.2 Micro CT analysis between control and rMSC at early time point

Bone structure parameters	Treatment group Early injection		P-value (unpaired t-test)
	rMSC Mean (SEM)	PBS (control) Mean (SEM)	
BV/TV	52.67 (4.83)	18.52 (9.19)	P < 0.01*
Bone surface density (1/mm)	4.97 (0.43)	3.29 (1.22)	P = 0.14
Tb.N	1.17 (0.12)	0.77 (0.27)	P = 0.14
Tb.Th	0.44 (0.03)	0.23 (0.04)	P < 0.01*
Tb.Sp	0.47 (0.06)	0.50 (0.12)	P = 0.81
Bone mineral density (g HA/mm^3)	0.66 (0.03)	0.29 (0.14)	P < 0.01*

*Statistically significant difference

7.3.3 The fracture healing assessment after injection at late time point (8 weeks)

7.3.3.1 Assessment of bone union in groups 3 and 4

Unlike the early injection group (group 1), the late rMSC injection group (group 3) had only two animals out of the five animals that demonstrated bone union. In the late control group (group 4), one fracture/osteotomy achieved bone union at eight weeks after injection. **Table 7.3** depicts the number of unions and non-unions of the rats injected at the late time point either with rMSCs or with PBS. The animals that

were injected with rMSCs at the later time point showed no greater union rate than the PBS controls (p = 1.00, Fisher's exact test).

Table 7.3 The number of the animals used at **the late time point** and numbers that achieved bone union rates

Treatment group	Outcome		Total
	Bone union	Non-union	
rMSC (group 3)	2	3	5
PBS (group 4)	1	4	5
Total	3	7	10

The group who had rMSC injected at the later time point showed inconsistent results with only 2 of them proceeding to union (**Figure 7.13**). Although there was no connectivity in 3 animals in group 3 (i.e. they were non-unions), they did not develop the full characteristics of an atrophic non-union (**Figure 7.14**). In contrast, in the control group, the animals demonstrated the full characteristics of an atrophic non-union (**Figure7.15**).

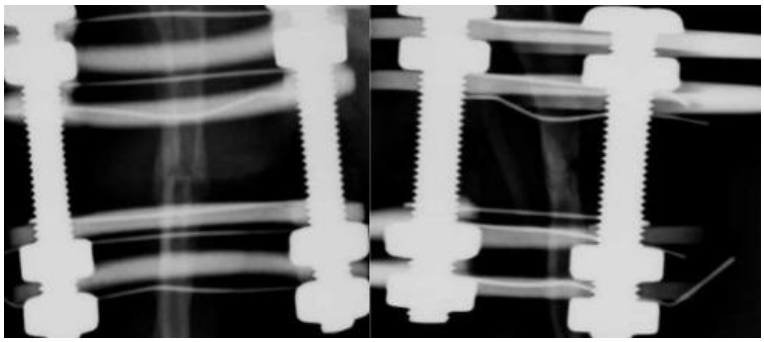

Figure 7.13 Radiographs of one of the animals in the rMSC injection at late time point that healed

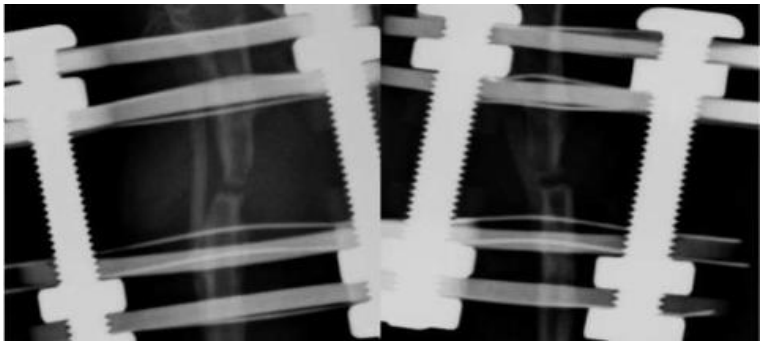

Figure 7.14 Radiographs of one of the animals in the rMSC injection at the late time point that progressed to non-union

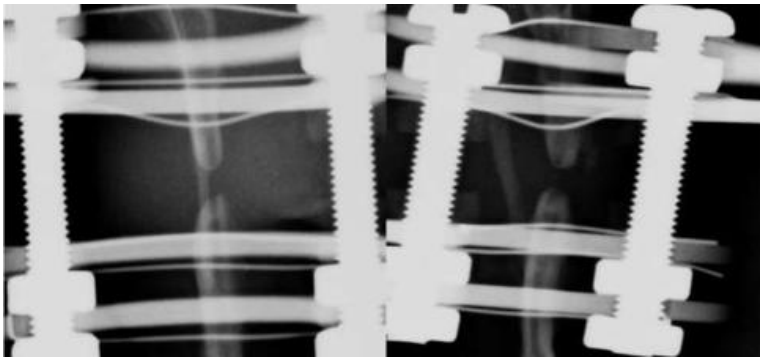

Figure 7.15 Radiographs of one of the control animals in the PBS injection at late time point demonstrated an established atrophic non-union

However, one of the animals in the control group had a healed bone gap, this appeared to be due to a double fracture of the fibula enabling it to contribute to fracture repair of the tibia (**Figure 7.16**)

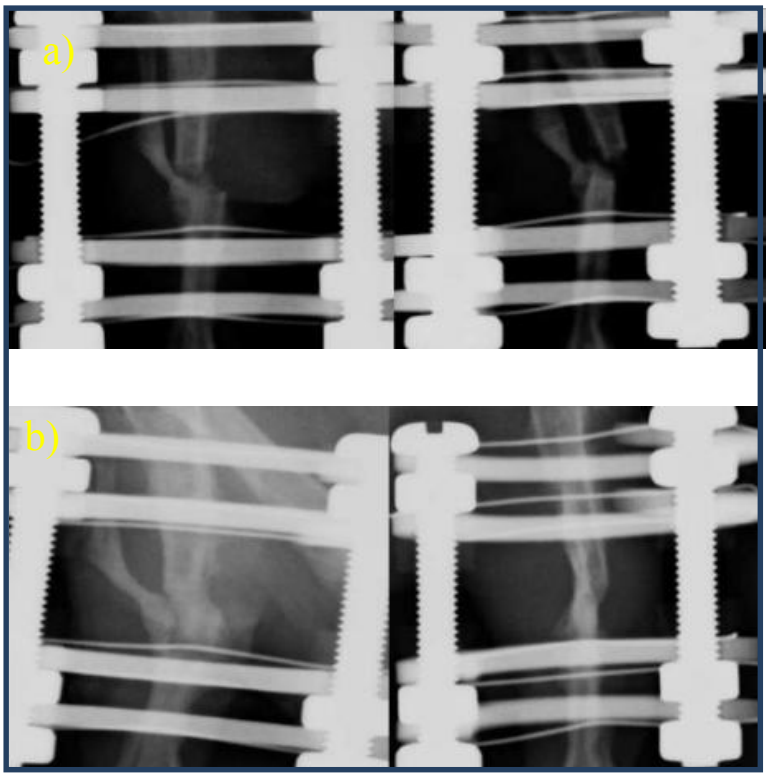

Figure 7.16 Radiographs of the single animal in the PBS injection at late time point that processed to union; (a) after 2 week post injection and (b) after 8 weeks post injection

7.3.3.2 The progression of the fracture healing process in groups 3 and 4 (late injection groups)

The rates of bone union in the treatment and control group injected at the late time point showed inconsistent results which were not significantly different. Thus, the progression of the fracture healing process in the late injection group treatment was evaluated using serial radiography to determine if there was any more subtle advantage of using rMSC at the late stage i.e. in an established atrophic non-union.

7.3.3.2.1 Relative radiopacity of animals in groups 3 and 4

The mean relative radiopacity at the fracture gap of rMSC treated animals (group 3) and of the PBS control animals (group 4) is demonstrated in **Figure 7.17**. It was seen that there was no significant difference between the mean radiopacity of group 3 and 4 at any of the time point (P>0.05 for treatment, time and interaction effects, two-way repeated ANOVA)

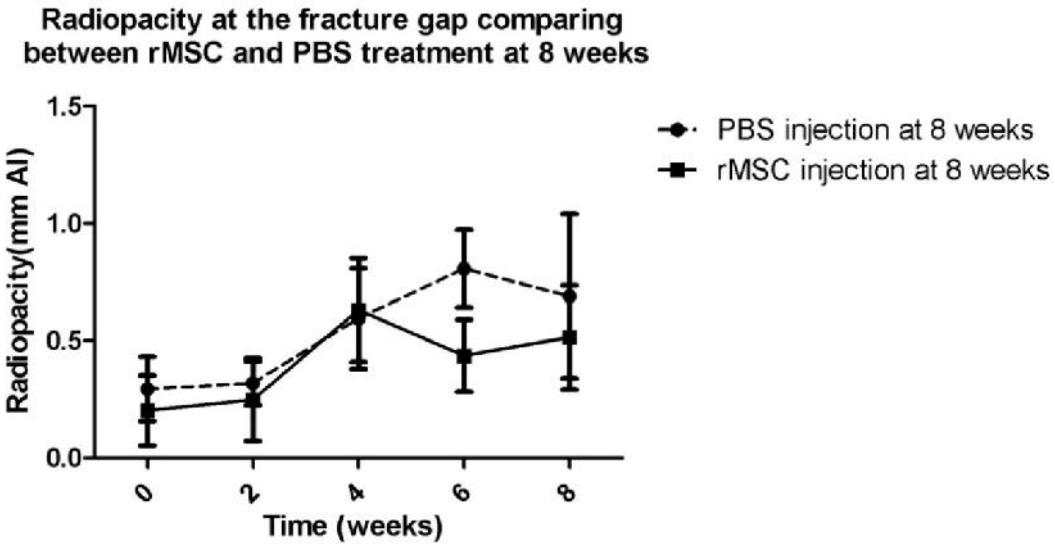

Figure 7.17 The comparison of radiopacity between treatment (rMSC) and control (PBS) over the 8 week period post injection at the 8 week time point

7.3.3.2.2 Callus index in groups 3 and 4

The modified callus index produced a proximal callus index and a distal callus index. The callus size of group 3 and 4 were not significantly different at any stages over the 8 week period after injection (For both proximal and distal callus index; P>0.05 for treatment, time and interaction effects, two-way repeated ANOVA) (**Figure 7.18**)

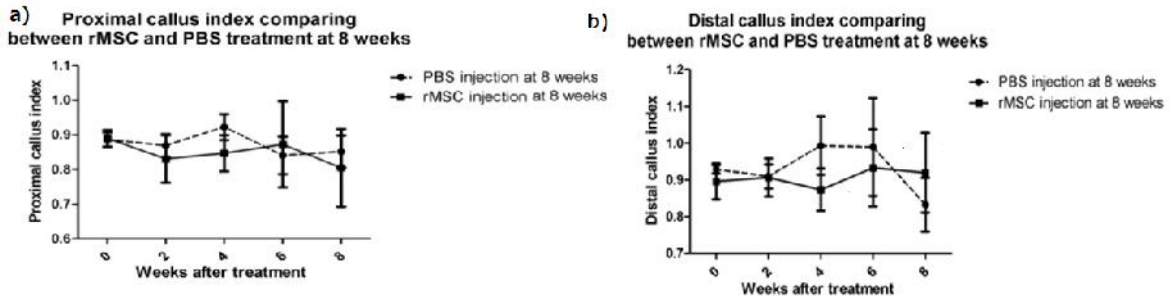

Figure 7.18 The comparison of callus index; (a) proximal and (b) Distal between treatment (rMSC) and control (PBS) over the 8 week period post injection

7.3.3.2.3 Percentage of callus increase area of the callus in groups 3 and 4

In the rMSC injection at eight week group (group 3), the percentage change of callus gradually increased from the 2nd week to 4th week and then it remained stable until the end of the study. There was no significant change in the percentage change of callus in the control group and the fracture site remained constant as a fully developed atrophic non-union at 16 weeks after the procedure to induce the atrophic non-union (**Figure 7.19**). Although, there was a slight increase in the percentage change of fracture callus in the rMSC treatment group, there was no statistically significant difference in the amount of callus at any time point between the two groups ($P>0.05$ for treatment, time and interaction effects, two-way repeated ANOVA).

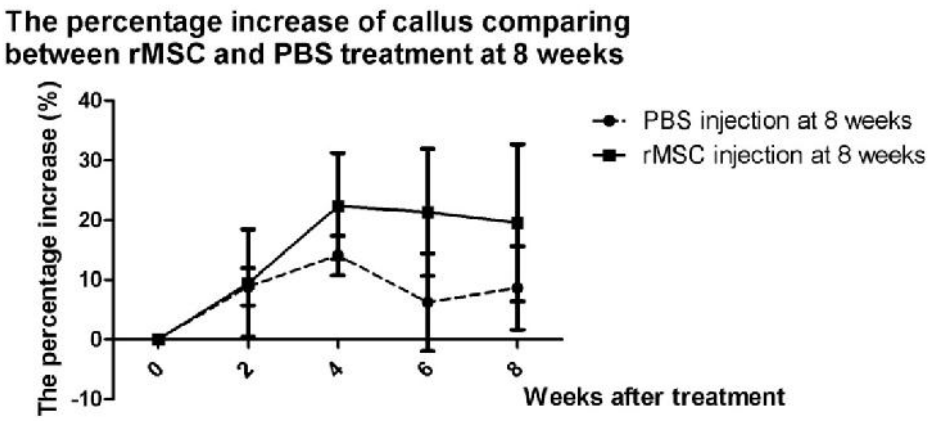

Figure 7.19 The comparison of the percentage callus increase between treatment (rMSC) and control (PBS) over 8 weeks period post injection in the 'late' treatment group

7.3.3.2.4 The progression of the fracture healing process assessed using fracture scoring systems

The results from RUST score and Lane & Sandhu score from group 3 and 4 (**Figure 7.20**) did not have any significant differences in their scores. There were slight improvements in both groups, especially, in the Lane & Sandhu score; however, these differences were not statistically significant (For both scoring systems; $P>0.05$ for treatment, time and interaction effects, two-way repeated ANOVA). The results demonstrated that if the percutaneous injection itself was affecting the fracture site, this effect was very minor.

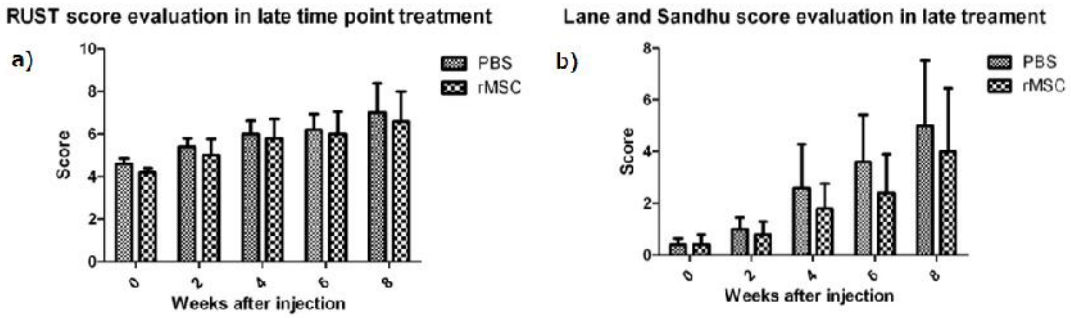

Figure 7.20 Fracture healing assessed by Fracture scoring system (a) the RUST score evaluation and (b) the Lane and Sandhu score evaluation

7.3.3.3 Histology evaluation in groups 3 and 4

In groups 3 and 4, the tissue within the fracture gap consisted predominantly of fibrous tissue. It was similar to the histology of the atrophic non-union model at eight weeks. There was no difference in the tissue components on direct inspection between the treatment and control groups at the fracture gap (**Figure 7.21**). However, in the treatment group, in one of the two animals that had united; there was an area of cartilage formation in the middle of the fracture gap (**Figure 7.22**).

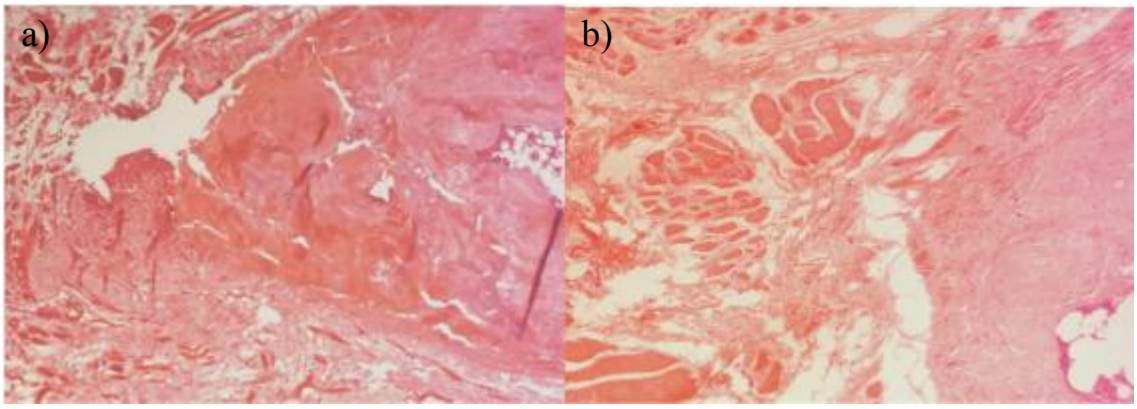

Figure 7.21 H&E staining from the fracture site in (a) the rat MSC injected group, and (b) the control PBS injected group; Fibrous component was dominant in the fracture gap (x100)

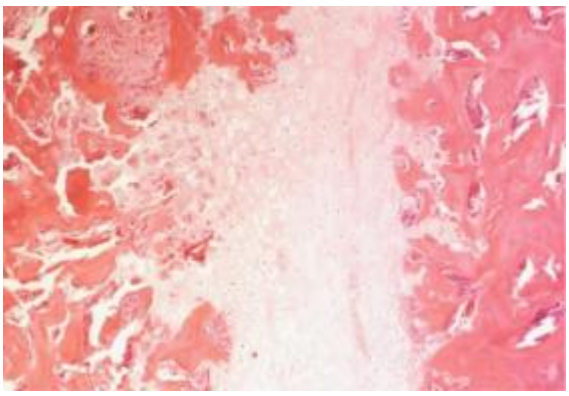

Figure 7.22 H&E staining from the fracture site of one of the animals in MSC injected group; a cartilage component could be found in the middle of the fracture gap (x100)

The tissue components were compared between the rMSC treatment group and the control group (**Figure 7.23**). There were no differences in the amounts of bone, cartilage, fibrous and marrow/empty space (P-value > 0.05, unpaired t-tested). However, the bone tissue component in group 3 was less than group 4.

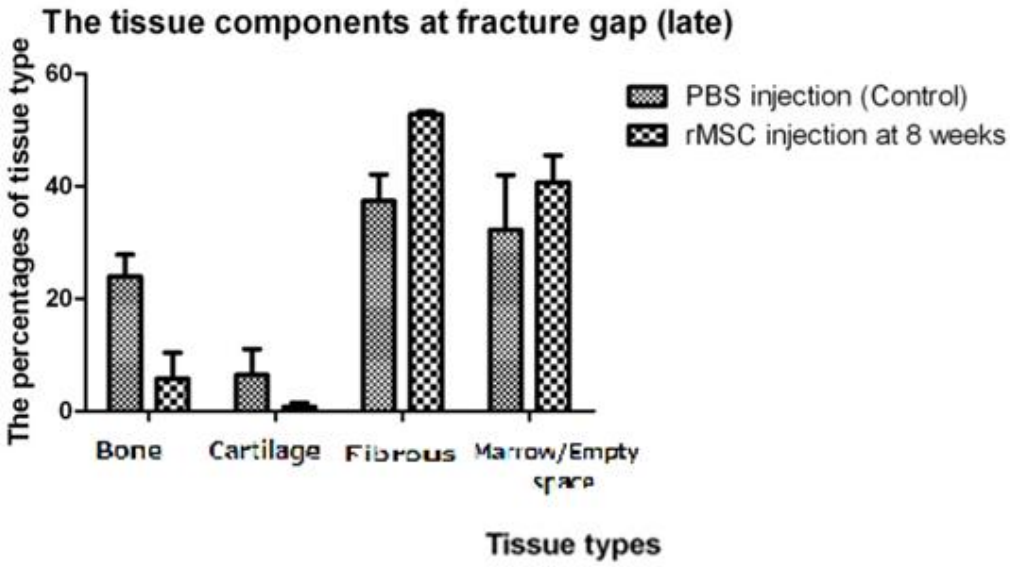

Figure 7.23 Quantitative evaluation of the tissue components in the fracture gap

7.3.3.4 Micro-CT analysis in groups 3 and 4

There was no significant bony bridging on 3D images in either the rMSC or the PBS injection groups at the late time point (**Figure 7.24 (a, b)**). The bone gap was still evident in both the treatment group and the control group in most of the animals. Although there were inconsistent bone unions in some animals in the rMSC treatment group, there were no significant differences in any parameters of bone structure of the rMSC injection group compared to the PBS control group. All of the parameters obtained from micro-CT analysis are shown in **table 7.4.**

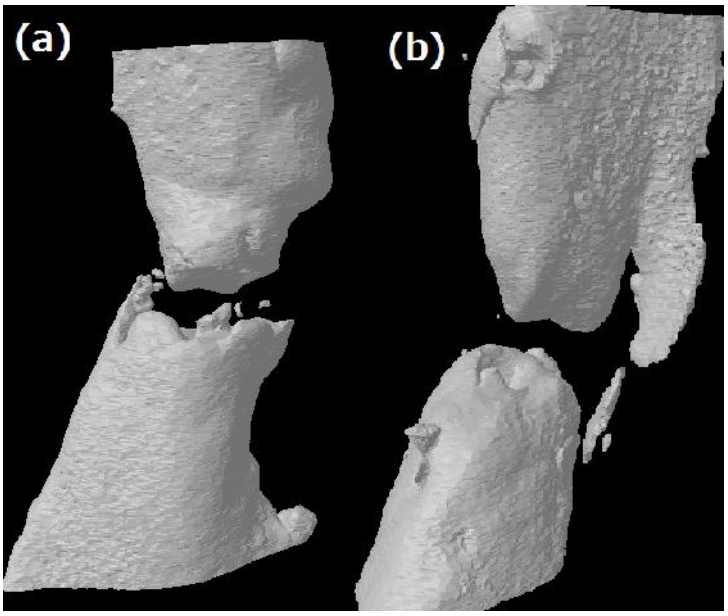

Figure 7.24 The results from Micro computed tomography of the late treatment groups: Three dimension image of (a) control group and (b) rat MSCs injected group

Table 7.4 Micro-CT analysis between control and rMSC from animals injected at the late time point

Bone structure parameters	Treatment group Late injection		P-value (unpaired t-test)
	rMSC Mean (SEM)	PBS (control) Mean (SEM)	
BV/TV	32.84 (17.81)	26.35 (17.74)	P = 0.81
Bone surface density (1/mm)	3.48 (1.43)	2.38 (0.91)	P = 0.54
Tb.N	0.58 (0.19)	0.41 (0.14)	P = 0.50
Tb.Th	0.29 (0.03)	0.35 (0.08)	P = 0.55
Tb.Sp	0.55 (0.05)	0.59 (0.04)	P = 0.50
Bone mineral density (g HA/mm^3)	0.31 (0.13)	0.39 (0.16)	P = 0.74

7.3.4 Comparison between early and late injection (groups 1and 3)

This section provides a summary of the results between early and late time points using data from section 7.3.2 and 7.3.3.: it reports that the injection of MSCs at an early time point had a better outcome on the basis of radiographs, histology and micro-CT evaluation.

7.3.4.1 Radiographic parameters between early and late injections

The graphs in **Figure 7.25** compare radiographic parameters such as radiopacity (**Figure 7.24 a**), proximal callus index (**Figure 7.24 b**), distal callus index (**Figure 7.24 c**) and the percentage area increase of the callus (**Figure 7.24 d**) between early injection and late injection of MSCs at the eight weeks after injection. There were statistically significant differences in radiopacity (P-value = 0.0025 for treatment, two-way repeated ANOVA), proximal callus index (P-value = 0.048 for treatment, two-way repeated ANOVA) and distal callus index (P-value = 0.009 for treatment, two-way repeated ANOVA) between early and late treatment of MSC injection.

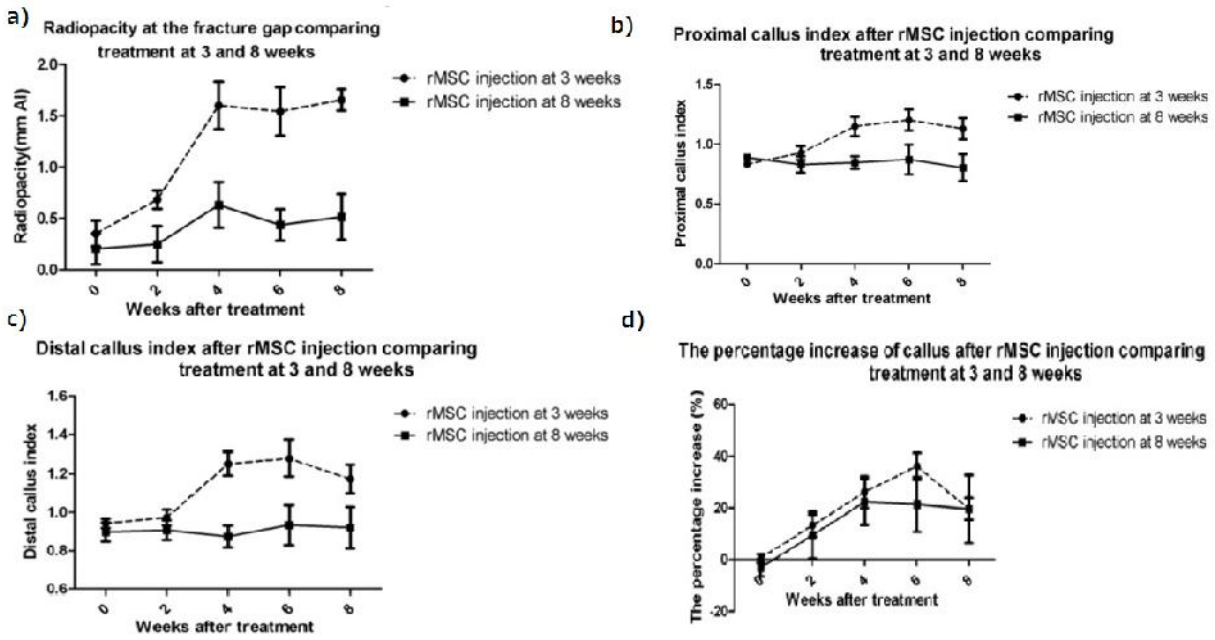

Figure 7.25 The comparison of radiographic parameters between early and late time injection groups

7.3.4.2 Histology between early and late injection

The relative amount of bone, cartilage, fibrous and undifferentiated tissue at the fracture gap for the early and late injection groups were compared at eight weeks after injection (**Figure 7.26**). The bone component in the fracture gap of animals in the early injection group was significantly more than in the late injection group ($P < 0.01$, unpaired t-test).

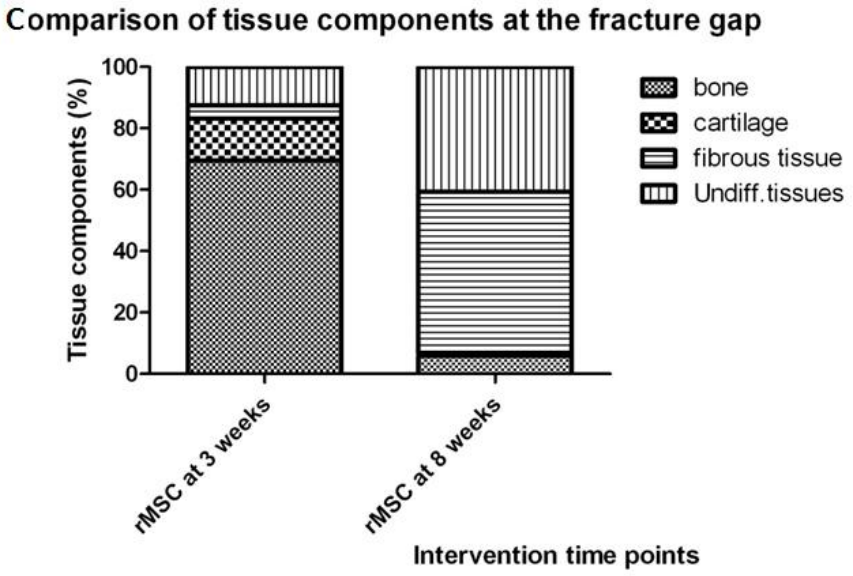

Figure 7.26 The tissue components at the fracture gap at early and late injection time points

7.3.4.3 Micro-CT analysis for early and late injection groups

The micro-CT analysis demonstrated the bone structure at the fracture gap which was represented by bone structural parameters and bone mineral density (**Figure 7.27**) between the early treatment and late treatment groups.

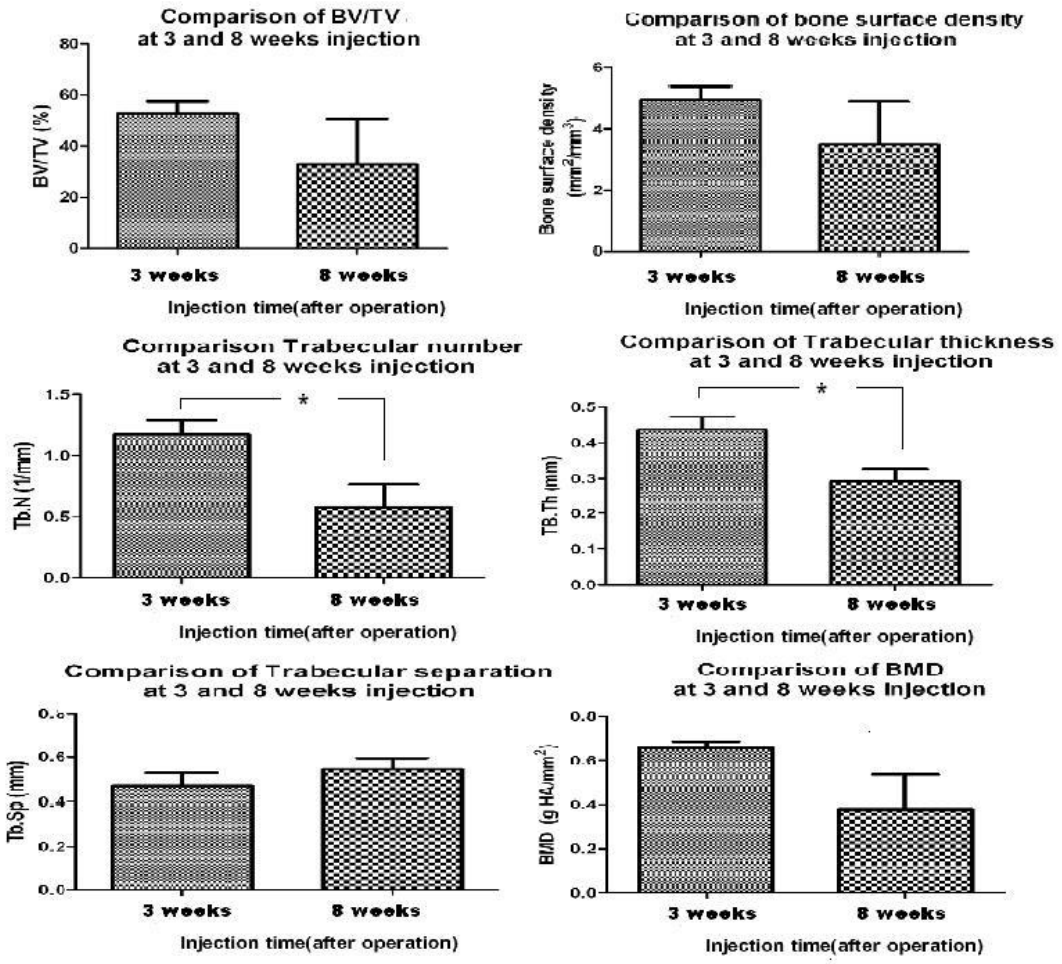

Figure 7.27 The comparison of bone structural parameters and bone mineral density between early treatment and late treatment groups (* statistically significant difference, P-value < 0.05, unpaired t-test)

7.4 Summary and discussion

The percutaneous injection of MSCs locally into the atrophic non-union in the early 'post-injury' period (three weeks) significantly improved the fracture healing process (P-value = 0.048). Five out of six MSC-injected rats demonstrated improvement in fracture healing, whereas none of the PBS-injected rats (0 of 3) showed improvement on serial radiographs. Atrophic non-unions with MSCs implantation in the late 'post-

injury' period (eight weeks) showed no significant improvement of fracture healing (2 of 5) (P-value > 0.05). The quantitative analysis of bone healing using radiographic image, histology and micro-CT also showed the beneficial effect of the treatment at an early time point over the control group and the late treatment group. Percutaneous local implantation of MSCs rescued the fracture healing process in cases destined to progress to atrophic non-union. However, the timing after the fracture was a considerable factor and this should be taken into account when designing MSCs protocols.

MSCs could play a role as bone progenitors or trophic secreting cells to promote the fracture healing process. It has been reported that an insufficient biological environment at the fracture gap in atrophic non-unions at three weeks leads to the development of the atrophic non-union (Reed at el 2003). Thus, augmentation of the biological components at the three week time point would be a reasonable strategy for restoring the normal fracture healing process. In this study, when MSCs were injected at an early stage, they rescued the fracture and returned it to the normal process of fracture healing.

Surprisingly, injection of MSCs into an established atrophic non-union did not show any significant improvement in the fracture healing process. According to the observations described in this thesis, in the established non-union, the gap became larger from the original 1 mm. created at surgery to around 2 mm. In addition, there was further bone loss in the late stage of the atrophic non-unions. It is possible that the cells alone could not contribute to bone healing as the bone may have needed scaffold and the fracture environment is not suitable to induce osteogenesis because the native biological components are different in each stage of the disease.

MSCs combined with scaffolds have been shown to improve the process of fracture healing process in a bone defect in several animal models (Bruder et al., 1998, Peterson et al., 2005, Nair et al., 2009). An atrophic non-union, however, might occur without a bone defect. In order to prevent an atrophic non-union, becoming established, it is advantageous to augment the fracture healing process using a minimally invasive technique. Because of the absence of a critical size defect, a

scaffold might not be required. Percutaneous injection can be performed under local anaesthesia. A percutaneous injection technique has been used to treat non-unions in a human study. Connolly (1998) reported that autologous bone marrow delivered by percutaneous injection or by direct transplant as a composite graft was effective at producing osteogenic stimulation in a series of 100 skeletal healing problems, including delayed unions and nonunions of fractures, arthrodeses, and bone defects. Hernigou et al, (2005) used percutaneous concentrated autologous bone-marrow grafting for the treatment of an atrophic tibial diaphyseal non-union. The non-unions went on to unite successfully in 90% of the patients (n= 53). In the union group, the bone marrow that had been injected into the non-unions contained >1,500 progenitors/cm3 and an average total of 54,962 +/- 17,431 progenitors. Seven patients in whom bone union was not obtained both had a significantly lower concentration (634 +/- 187 progenitors/cm3) and a lower total number (19,324 +/- 6843) of progenitors injected into the non-union sites ($p = 0.001$ and $p < 0.01$, respectively) than the patients who progressed to union. The results suggested that the percutaneous technique could be used to deliver the cells into an atrophic non-union and the yield of MSCs was an important factor in determining the success of the technique.

This study has shown that the percutaneous injection of bone marrow derived MSC could improve and rescue the fracture healing process in an atrophic non-union model. However, the cells had to be introduced at three weeks (early stage) after the operation when the fracture had not developed into an established atrophic non-union. The data presented here suggests that percutaneous injection techniques of MSCs can be used as a strategy for the prevention of atrophic non-union when used in the early stage of the disease. MSC augmentation using percutaneous injection could be translated into clinical use. The MSCs used in this study, however, were harvested from rat bone marrow. Further experiments should investigate the therapeutic effects of ‘non-like’ immune cells (i.e. allogeneic/xenogeneic cells) as these could have advantages in the trauma setting as they may be more readily available at an earlier time point and be more cost effective. Therefore, to explore

whether xenotransplantation of human MSCs into the rat non-union model is as effective as rat MSCs a further experimental study is needed.

Chapter 8: Human bone marrow derived mesenchymal stem cells implantation in xenotransplantation model of an atrophic non-union

Aim: *To investigate the therapeutic effects of xenogeneic MSC implantation for bone regeneration in atrophic non-union model*

8.1 Introduction

The results from the previous chapter (chapter 7) showed that bone marrow derived MSCs promoted bone regeneration in the atrophic non-union model. A minimally invasive percutaneous injection technique was used to deliver the stem cells. The time of injection was found to be a critical factor. To achieve the most favourable outcomes, MSCs should be injected earlier (three weeks) rather than later.

In clinical practice, there are several advantages of using MSCs from a universal donor: MSC isolation and preparation are time and resource consuming. The yield of MSCs in bone marrow is relatively small in number, so cells have to be expanded in an appropriate culture condition to obtain an adequate number of cells prior to implantation into the fracture site. These steps take about two weeks or more to complete. Thus, it may not to be possible to use cultured MSCs at an appropriate time point. Moreover, it has been reported that in old age as well as in several conditions such as osteogenesis imperfecta, smoking and DM, the quality and function of MSC may be diminished (reviewed in section 1.5.4). Thus, the autologous transplantation of MSCs from patients who have one of these conditions may not result in bone regeneration. In these patients, MSCs from a different donor such as a healthy universal donor may be a better option. One of the characteristics

of MSCs is their immune privileged status, which suggests that it may be possible to transplant exogenous MSCs without eliciting a host inflammatory immune response.

In this chapter, a xenogeneic model has been used to determine (1) the bone regenerative potential of exogenous MSCs in an atrophic non-union and (2) the response of the immune system to exogenous MSCs (i.e. human). Xenogeneic cells can be considered to represent the extreme immune stimulus and previously a xenogeneic model has been used to evaluate the feasibility of using MSCs from a universal donor cells in the cardiovascular field (Atoui et al., 2008). Thus, if there are any positive effects when human MSCs are injected to promote fracture healing in an immunocompetent animal model, the results should also be relevant to the situation where universal donor cells are used in the clinical setting. The objectives of this study were to (1) to compare the bone regeneration potential of xenotransplantation and allogeneic implantation of MSCs into an atrophic non-union (2) to demonstrate the immune response after MSC implantation in the *in vivo* condition and (3) to trace the distribution and fate of injected MSCs either hMSC or rMSC at the fracture gap after cell implantation.

8.2 Materials and Methods

The details of the surgical procedure of the atrophic non-union model, the percutaneous injection technique, the method of human and rat MSC preparation, the fracture assessments have been described in the general materials and methods chapter (Chapter 2). The experimental design related to this chapter is now described.

8.2.1 Experiment design

Twenty six adult male Wistar rats (400-500g) were used in this study, however two animals were excluded due to wound complication and anaesthetic problems. So that, twenty four animals were randomly assigned into three groups after inducing an atrophic non-union: Group 1 for rMSC injection (n=8), Group 2 for hMSC injection (n=8) and Group 3 for PBS injection as controls (n=8). All animals received either cells or PBS intervention at three weeks after inducing atrophic non-union procedure. Animals in the treatment groups (group 1 and 2) were injected with the 5 x 10^6 cells either rMSCs or hMSC in PBS suspension (200 µl), whereas animals in the control group were injected with PBS (200 µl). The fracture healing process was monitored with radiographs every two weeks until the end of the study. The assessments of bone healing were performed at four weeks (n=12) or eight weeks (n= 12) after injection by quantitative micro-CT and histology. Micro-CT assessments were carried out on all samples. Histology evaluation was performed on three specimens randomly selected by blinded assessors; the sections were assessed in triplicate in a blinded fashion. Biomechanical evaluation was carried out on three specimens from each group at four and eight weeks post injection. The study flow diagram is shown in the **Figure 8.1.**

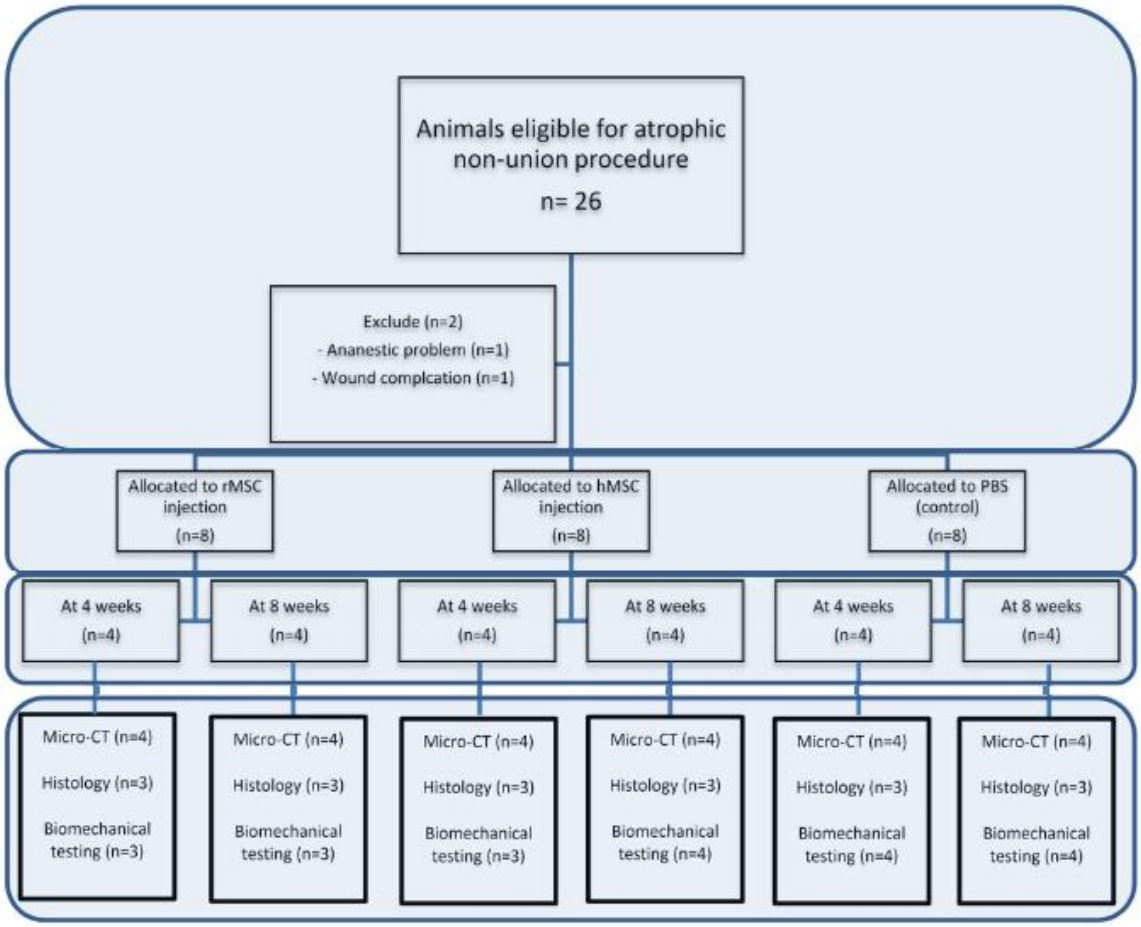

Figure 8.1 Flow diagram of experimental plan in this study

8.2.2 **Biomechanical evaluation**

Rat tibia bones (n=9, at four weeks-assessment and n= 12, at eight week-assessment) were randomly selected for biomechanical testing. The samples were tested using a four-point bending test (Zwick/Roell) as described in **Chapter 2**. The biomechanical properties of callus of animals from each group were compared using ultimate load, ultimate stress, young's modulus and toughness.

8.2.3 **Cells tracking after injection**

CM-Dil was used to label cells before implantation as per the company's protocol. The full details of the optimisation of the technique used are described in the section 2.10 (Chapter 2). Anti-human nuclei antibody was also used to detect implanted human cells. Analysis of these cells was done immediately after transplantation (using animals in the optimisation of injection technique as the control for injection), at four weeks and at eight weeks to determine the distribution and fate of implanted cells.

8.2.4 **Evaluation of inflammatory cytokines from the serum**

Serum samples from animals in the each group were collected at 0, 2, 4, 6 and 8 weeks. The Multi-Analyte ELISArray (SABiosciences^{TM}, USA) was used to evaluate 12 inflammatory cytokines from pool samples as per the company's protocol (Chapter 2).

8.2.5 **Histology of lymph node**

Popliteal Lymph nodes from both hind limbs; the injected side (right) and the contralateral side (left) were collected after euthanasia at the end of the experiment. They were fixed in 4%PFA for routine histological procedures by H&E staining. Three sections at the middle of lymph nodes (6 μm) from animals in each group (rMSC injection, hMSC injection and PBS injection) at four weeks and eight weeks were evaluated under light microscopy. The following parameters from each group were compared; (1) the size of lymph node, (2) the number of secondary follicles, (3) the number of infiltrating cells in the sub-capsular sinus area, and (4) the number of

macrophages in the medullary cord area. (Further details are given in section 2.11.2, Chapter 2)

8.2.6 **Statistical analysis**

The Kaplan-Meier curves were used to present the number of animals that reached union each time point after treatment and the Log-rank test was used to compare between curves. The mean difference of fracture progression parameters, which were radiopacity, callus index, percentage increase of callus area and the fracture scoring systems over the post injection period were compared with repeated measures ANOVA followed by bonferroni's multiple comparison tests. The qualitative measurement of histology from fracture sites, morphological changes of popliteal lymph nodes, the micro-CT parameters and biomechanical parameters were determined using the one-way ANOVA. The post-hoc analysis was conducted appropriately using bonferroni's multiple comparison tests. A P-value of less than 0.05 was considered significant.

8.3 Results

8.3.1 **Health status of the animals after received MSC injection**

The animals were able to weight- bear fully immediately following MSC injection. There was no abnormal bleeding, swelling or skin irritation at the injection site. All animals returned to their normal activity after recovering from anaesthesia. After randomisation, all of the animals remained alive with neither signs of wound infection nor pin tract infection until the end of the experiment (at four weeks and eight weeks after cell injection).

8.3.2 Diagnosis of bone union in rat MSC, human MSC and PBS (controls)

In the cell injection groups (rMSC and hMSC), seven out of eight of the animals from each group that had received cells progressed to union, but only one of animals in the control group achieved bone union. **Table 8.1** shows the number of unions and non-unions for rats injected either with rMSC, hMSC or PBS. The survival time to healing was estimated using Kaplan-Meier survival analysis. **Figure 8.2** shows the Kaplan-Meier curves demonstrating the number of radiographic bone unions at each time point over the 8 week-period from animals in the rMSC treated group, the hMSC treated group and the control group. The mean healing time of animals in the rMSC injection group was 4.3 (S.D. = 2.14) and in the hMSC injection group was 5.4 (S.D. = 1.90). There was a statistically significant difference in the survival curves of the different groups (P = 0.02). The survival curves of the rMSC injection group and the hMSC injection group were significantly different from the control (P = 0.003 and P = 0.008, respectively). However, there was no significant difference between the rMSC injection group and the hMSC injection group (P = 0.36)

Table 8.1 Outcome of fracture union (inclusive of four and eight week results) according to group. The number of the animals used and results of bone union between three groups

Treatment group	Outcome		Total
	Union	Non-union	
rMSC	7	1	8
hMSC	7	1	8
PBS (control)	1	7	8
Total	15	9	24

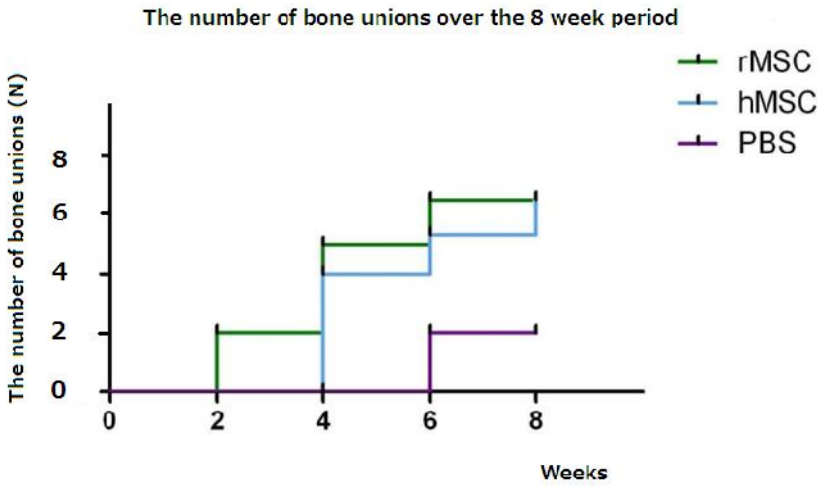

Figure 8.2 The Kaplan-Meier curves showing the number of animals that had achieved radiographic bone union over the 8 week-period (P-value = 0.02, Log-rank test)

8.3.3 Detailed radiographic assessment of the progression of fracture

The progression of fracture healing was evaluated every two weeks (**Figure 8.3**). There was no noticeable difference of the x-ray appearance between the rMSC and the hMSC injection group. Both groups showed a progression of fracture healing over the eight week period after cell injection. In contrast, in the control group, the x-rays showed the fracture site proceeding to the full characteristics of an atrophic non-union.

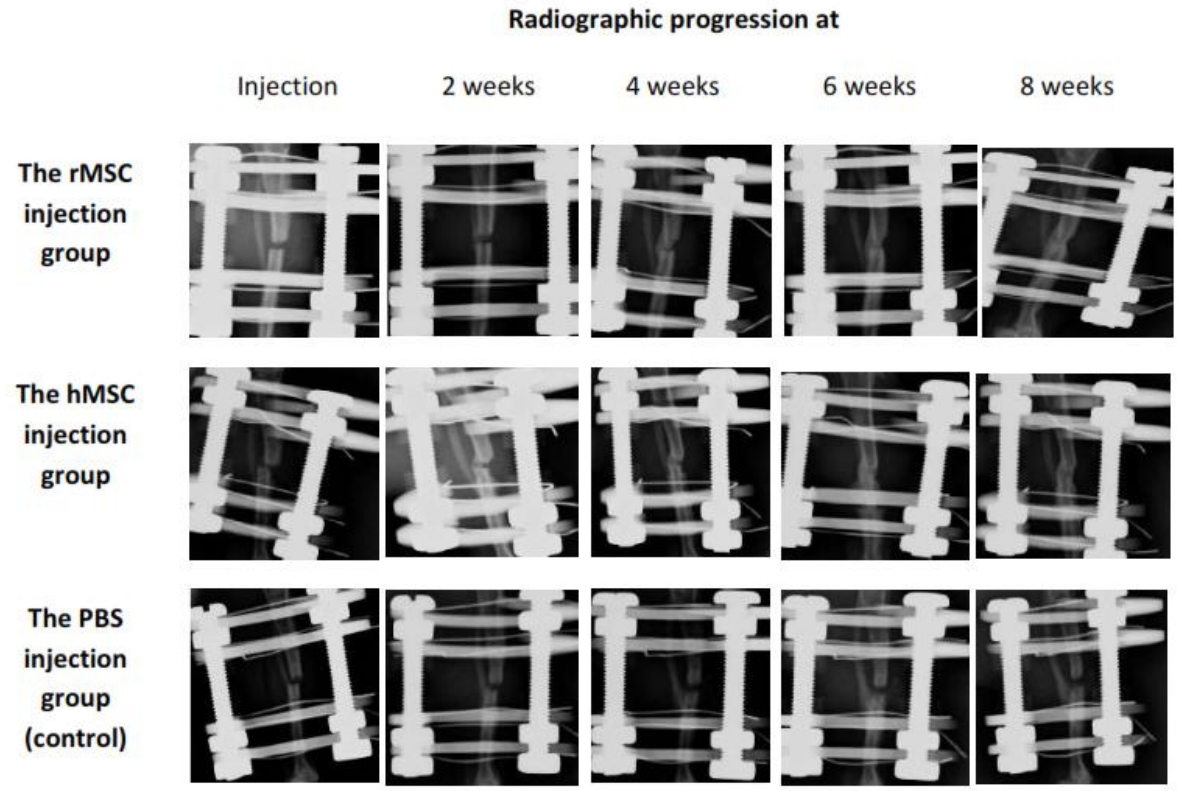

Figure 8.3 Radiographic progressions after injection over the 8 week period after injection

8.3.3.1 Relative Radiopacity

The radiopacity of the fracture gap was calibrated using an aluminium step wedge. The opacity of the fracture gap from each group was significant differences during the eight week period after injection (P-value < 0.0001 for treatment groups and times, and P-value < 0.01 for interaction effects, two-way repeated ANOVA). There was a significant increase in opacity in the MSC treatment groups after injection, whereas in the control group, the mean opacity at the different times did not change significantly. The progression of fracture healing in animals in the rMSC injected group was slightly faster than in the hMSC injected group, but it was not statistically significantly different (**Figure 8.4**).

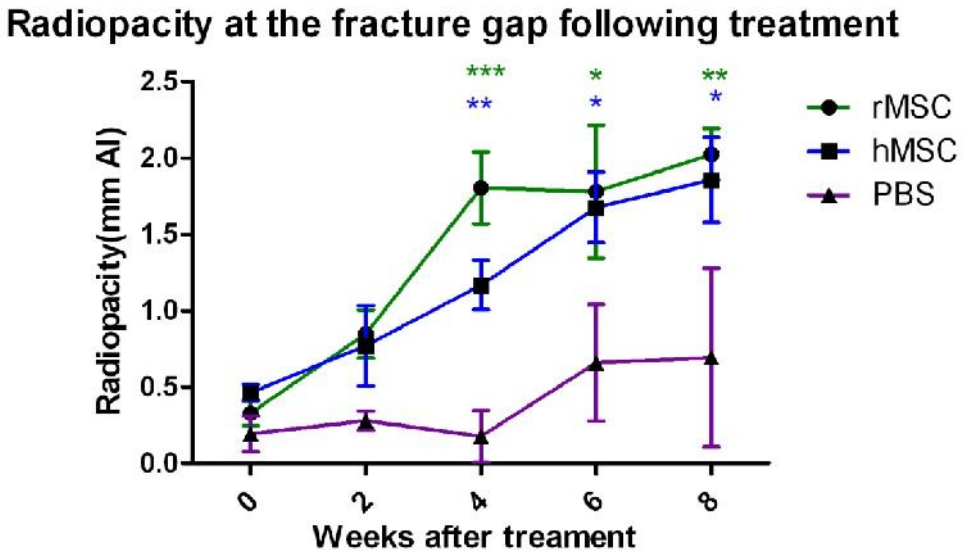

Figure 8.4 The comparison of radiopacity between treatment groups over the 8 week period after injection; the radiopecity at the fracture site in the rMSC and hMSC group were comparable and both of them were significantly higher than in the PBS treatment (Bonferroni's test subsequent to ANOVA: * = P-value < 0.05, ** = P-value < 0.01 and *** = P-value < 0.001, data shown as mean and SEM, n = 4 or 8 per group and time)

8.3.3.2 Callus index

Similar to the radiopacity results, there were significant increases in the callus index from the animals in the rMSCs and hMSCs treatment groups both proximal (P-value < 0.0001 for treatment groups, P-value = 0.0006 for times, and P-value = 0.22 for interaction effects, two-way repeated ANOVA) and distal (P-value < 0.0001 for treatment groups, P-value = 0.002 for times, and P-value = 0.47 for interaction effects, two-way repeated ANOVA) to the fracture site compared to the control (**Figure 8.5**). At the 8 week time point, the callus became smaller as potentially, it had entered the remodelling phase of the fracture healing process.

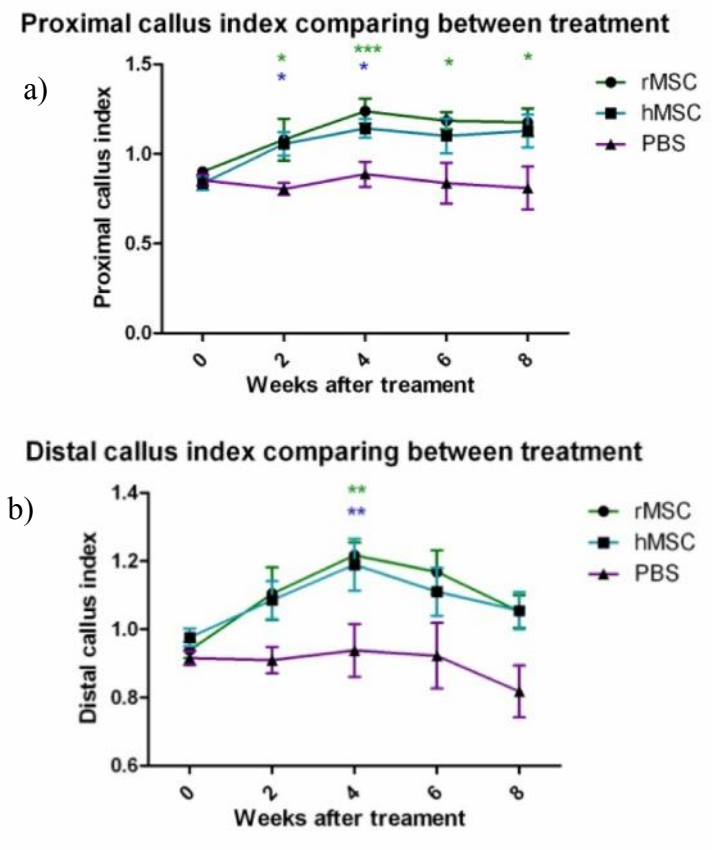

Figure 8.5 The comparison of callus index; (a) proximal and (b) distal between the treatment groups (rMSC and hMSC) and control (PBS) over the 8 week period post injection which were significantly differences compared to the control group (Bonferroni's test subsequent to ANOVA: * = P-value < 0.05, ** = P-value < 0.01 and *** = P-value < 0.001, data shown as mean and SEM, n = 4 or 8 per group and time)

8.3.3.3 Percentage increase in the area of radiopaque bone tissue

Line graphs in **Figure 8.6** show the percentage increases between in the MSC groups (rMSC and hMSC) and control over the 8 week period after injection. In both MSC injection groups, the callus gradually increased in area from the 2nd week to the 4th week and then remained stable after the 6th week. In contrast, there was a decrease in the area of radiopaque bone tissue in the control group where PBS solution alone was injected at the non-union site consistent with an atrophic non-union. There was a

statistically significant difference in the amount of callus between the MSC treatment groups and the PBS control group (P-value < 0.0001 for treatment groups, P-value = 0.007 for times, and P-value = 0.13 for interaction effects, 2-way repeated ANOVA).

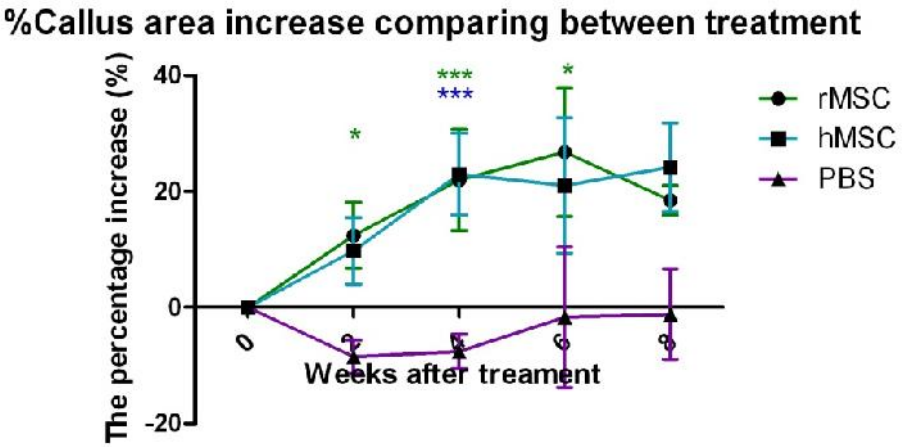

Figure 8.6 The comparison of the percentage callus increase between treatment groups (rMSC and hMSC) and control (PBS) over the 8 weeks period post injection; there were significant increases in the area of radiopaque bone tissue in the MSC treatment groups compared to the control group. (Bonferroni's test subsequent to ANOVA: * = P-value < 0.05, and *** = P-value < 0.001, data shown as mean and SEM, n = 4 or 8 per group and time)

8.3.3.4 The progression of the fracture healing process assessed using fracture scoring systems

The values for the RUST score and the Lane & Sandhu score showed the progression of the fracture healing process (**Figure 8.7**). There were significant differences in the RUST score (P-value < 0.0001 for treatment groups and times, and P-value = 0.004 for interaction effects, two-way repeated ANOVA) and the Lane & Sandhu scores (P-value < 0.0001 for treatment groups and times, and P-value = 0.0004 for interaction effects, two-way repeated ANOVA) over the eight week period after injection between the MSC treatment groups and the PBS treatment group. There

was no significant difference between the value of the RUST and the Lane & Sandhu scores in the rMSC and hMSC treatment groups. However, the scores in both treatment groups were significantly different from the control group after 2-4 weeks for the RUST score and for the Lane & Sandhu score.

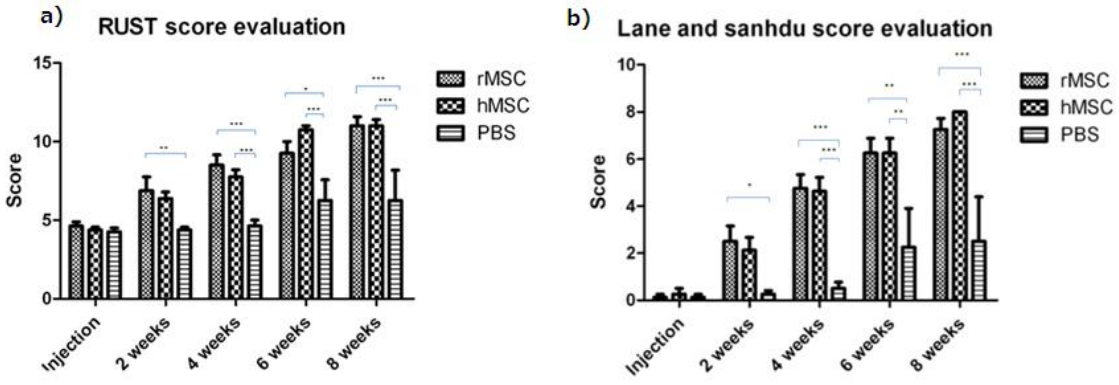

Figure 8.7 The evaluation of fracture healing using the fracture scoring systems; (a) the RUST score evaluation, and the (b) Lane and Sandhu score evaluation (Bonferroni's test subsequent to ANOVA: * = P-value < 0.05, ** = P-value < 0.01 and *** = P-value < 0.001, data shown as mean and SEM, n = 4 or 8 per group and time)

8.3.4 **Micro-CT evaluation**

Figure 8.8 shows a three dimensional reconstruction of the bony callus of a representative specimen from each group. At eight weeks after MSC injection, there was a solid bony callus in the rMSC and hMSC treatment groups and the appearance of bone bridges in both groups was similar. In contrast, the fracture gap was clearly observed in the control group. Quantitative micro-CT analysis showed that the percentage bone volume (BV/TV) and bone surface density in both MSC injected groups were significantly greater at four and eight weeks after injection compared to the control group. Similarly, bone microarchitecture parameters (Tb.N, Tb.Th and

Tb.Sp) and BMD in the cell treatment groups either rMSC or hMSC were higher than in the control group. There were no statistically significant differences in micro-CT parameters between the rMSC treatment group and the hMSC groups either at four weeks or at eight weeks after injection. The summary of the micro CT parameters from the different treatment groups at four weeks and eight weeks is shown in **Table 8.2**

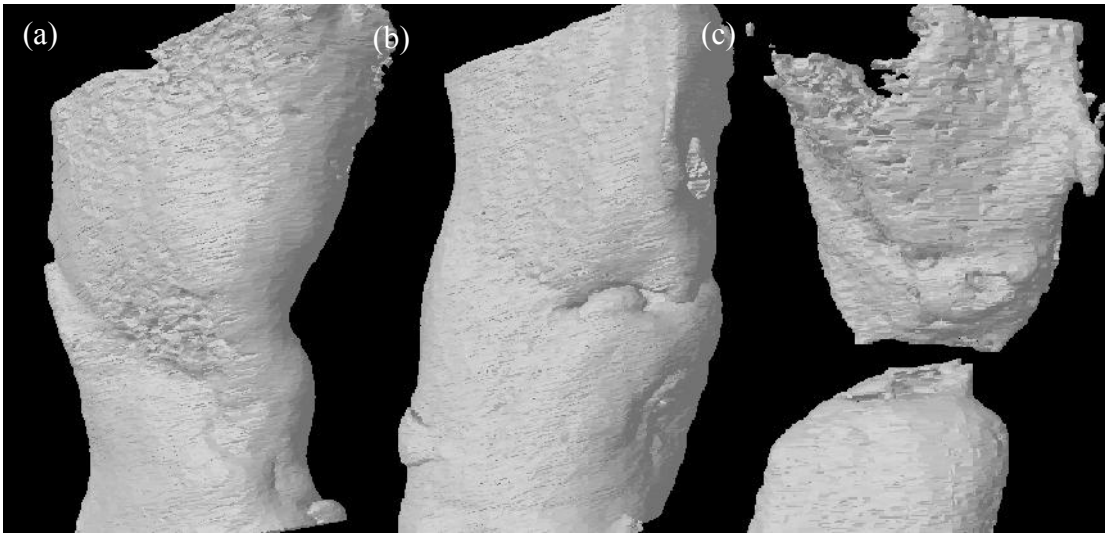

Figure 8.8 Three dimensional images from Micro computed tomography; (a) animal with rMSC treatment, (b) animal with hMSC treatment and (c) animal with PBS injection (control)

Table 8.2 The summary of micro CT analysis from the animals from different groups at 4 weeks and 8 week after injection

Bone structure parameters	Treatment group			P-value One way ANOVA
	rMSC Mean (SEM)	hMSC Mean (SEM)	PBS(control) Mean (SEM)	
4 weeks after injection	(n = 3)	(n = 3)	(n = 3)	
BV/TV	43.29 (7.26)	68.09 (4.49)	16.01(5.44)	0.0004
Bone surface density (1/mm)	4.46 (0.55)	5.28 (0.36)	2.24 (0.62)	0.0019
Tb.N	1.02 (0.13)	1.38 (0.20)	0.51 (0.10)	0.0098
Tb.Th	0.46 (0.02)	0.51 (0.05)	0.29 (0.08)	0.0535
Tb.Sp	0.41 (0.06)	0.32 (0.04)	0.62 (0.05)	0.0058
Bone mineral density (g HA/mm^3)	0.49 (0.01)	0.52 (0.01)	0.13 (0.13)	0.02
8 weeks after injection	(n = 4)	(n = 4)	(n = 4)	
BV/TV	68.10 (7.73)	64.10 (6.49)	29.92 (12.91)	0.036
Bone surface density (1/mm)	4.24 (0.26)	4.94 (0.36)	3.10 (0.62)	0.046
Tb.N	1.12 (0.06)	1.37 (0.12)	0.72 (0.15)	0.0096
Tb.Th	0.61 (0.06)	0.47 (0.01)	0.37 (0.11)	0.11
Tb.Sp	0.34 (0.06)	0.34 (0.07)	0.56 (0.08)	0.0878
Bone mineral density (g HA/mm^3)	0.66 (0.03)	0.61 (0.03)	0.28 (0.16)	0.05

8.3.5 **Biomechanical test for xenotransplantation**

Biomechanical testing with four-point bending was used to evaluate the mechanical properties of the bone samples. Representative load-displacement curves for each of the three different treatment groups are shown in **Figure 8.9**. Readings from the load-displacement graphs were obtained and used to determine the various biomechanical parameters of fracture repair (i.e. ultimate load, ultimate stress, young's modulus and toughness). The samples in the PBS treatment group were also evaluated with the four point bending test. However, minimal resistance against the bending load was detected during testing. The load-displacement curve in the PBS treatment group (**Figure. 8.9c**) indicated that the control samples could not withstand the force applied during the test. The limbs from the PBS injection group were found to be macroscopically unstable and they were not suitable for determining the biomechanical parameters. Thus, the results presented for the biomechanical parameters were compared between the rMSC and hMSC treatment groups at four weeks and eight weeks after injection, respectively. The biomechanical parameters from samples in the rMSC and hMSC treatment group are summarised in **Table 8.3.** Although the mechanical properties of bone samples in the rMSC treatment group were better than in the hMSC injection group, there was no statistical difference between the two groups at four weeks and eight weeks after injection.

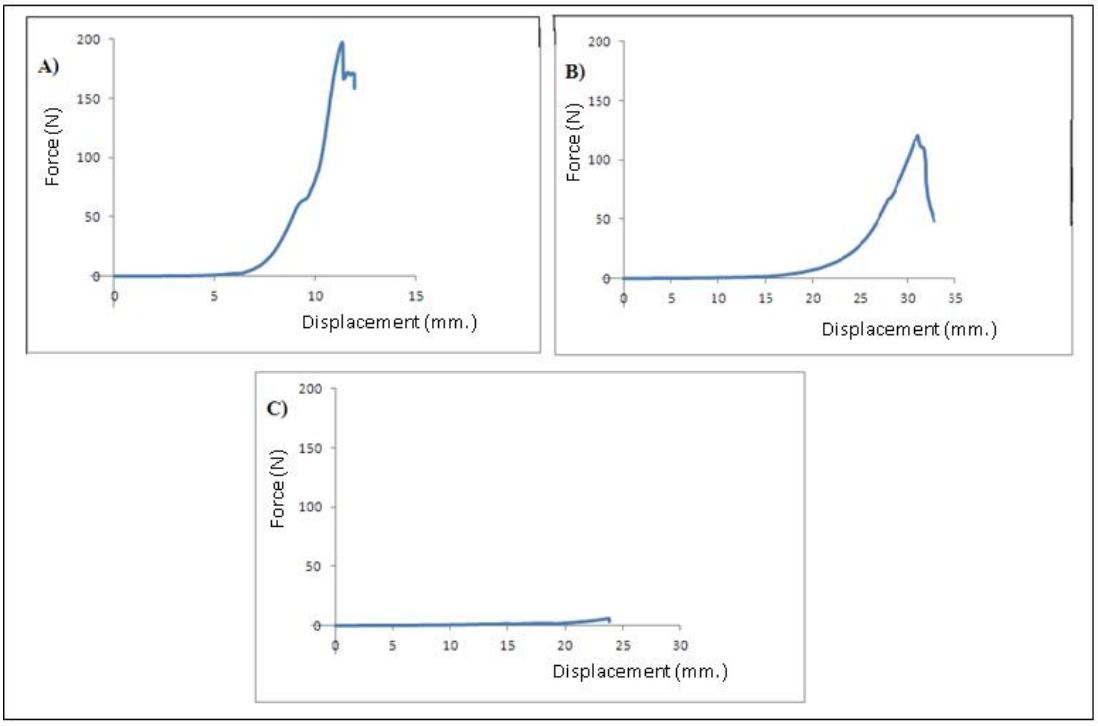

Figure 8.9 Representative load-displacement curves from (a) the rMSC injection group, (b) the hMSC injection group and (c) the PBS injection group

Table 8.3 The summary of biomechanical properties of healing bone in the animals with rMSC injections and the animals with hMSC injections

Mechanical property	Units	Treatment groups (Mean, SEM)		P-value Unpaired t-test
		rMSC	hMSC	
4 week after injection		(n=3)	(n=3)	
Ultimate load	N	47.7 (7.2)	72.5 (29.3)	0.46
Ultimate stress	MPa	53.7 (16.7)	63.5 (19.3)	0.72
Young's modulus	GPa	1.1 (0.4)	1.3 (0.6)	0.75
Toughness	MPa	1.9 (0.7)	0.6 (0.2)	0.15
8 week after injection		(n=4)	(n=4)	
Ultimate load	N	116.2 (34.7)	62.8 (6.7)	0.18
Ultimate stress	MPa	150.0 (18.3)	89.89 (18.6)	0.06
Young's modulus	GPa	2.7 (1.0)	2.0 (0.6)	0.58
Toughness	MPa	3.2 (0.5)	2.1 (0.9)	0.39

8.3.6 **Histological evaluation**

Histological assessment was performed on specimens at 4 and 8 weeks following cell implantation in the rMSCs, hMSC and PBS treatment groups. The sections were stained with H & E, Masson's Trichrome stain and Safranin-O/Fast Green were assessed using light microscopy under appropriate magnification. These sections revealed the progression of fracture healing and demonstrated the area of bone and cartilage formation that can be distinguished from fibrous tissue. Bony bridges were observed in some specimens and confirmed the radiographic finding of bone union.

8.3.6.1 Observation of general morphology at 4 weeks

At four weeks after implantation, the inter-fragmentary gap in the rMSC and hMSC treatment groups had a large area of new bone formation and there was an area of endochondral ossification (**Figure 8.10, Figure 8.11)**. The osteotomy site was still visible and there was no remodelling of the callus. The area of the fracture gap was occupied with the bone and cartilage tissue. Overall, the fracture gap of the hMSC and rMSC treatment group had a similar appearance. In contrast, in the control group, the inter-fragmentary gap was filled predominantly with cellular fibrous tissue (**Figure 8.12**).

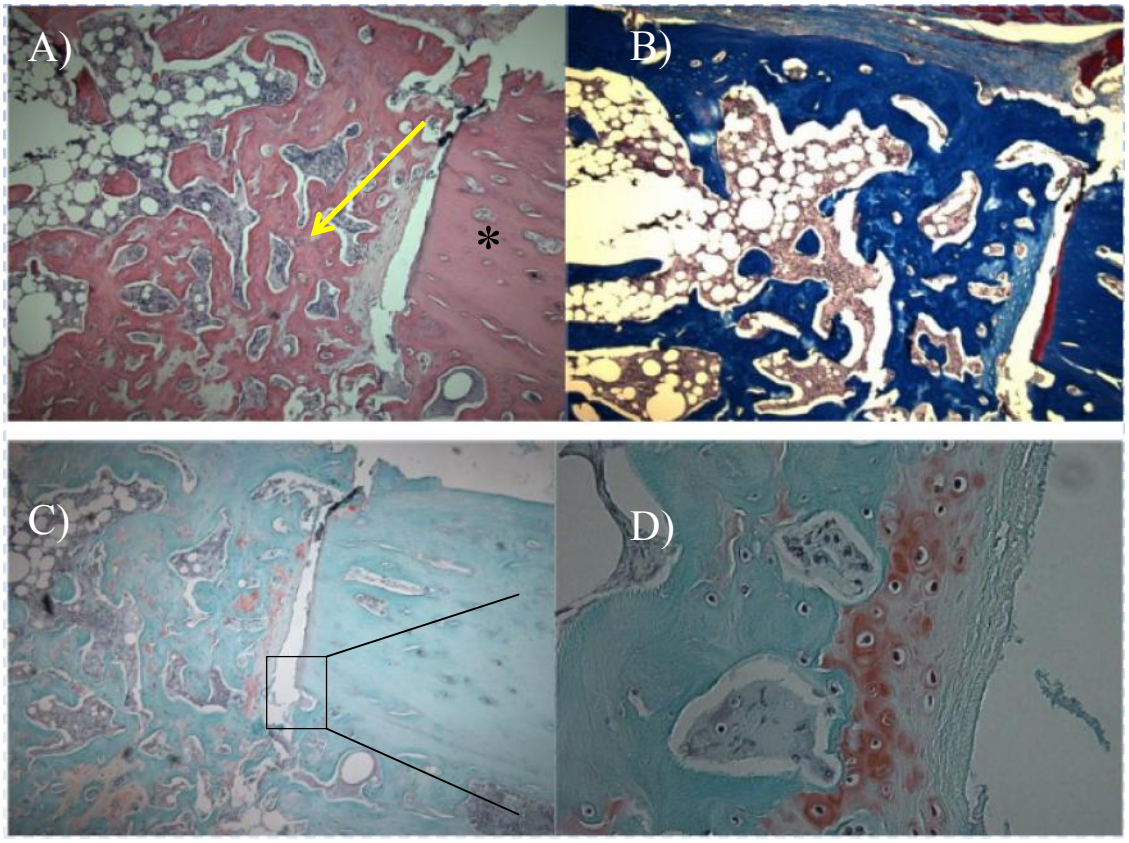

Figure 8.10 At week 4 post rMSC injection histological sections. (a) H&E stain demonstrating an area of bone formation, arrow and the osteotomy site, asterisk (x100), (b) Masson's trichrome stain (x100), (c) Safranin-O/Fast Green demonstrating an area of cartilage template, box (x100) and (d) higher magnification image (x400)

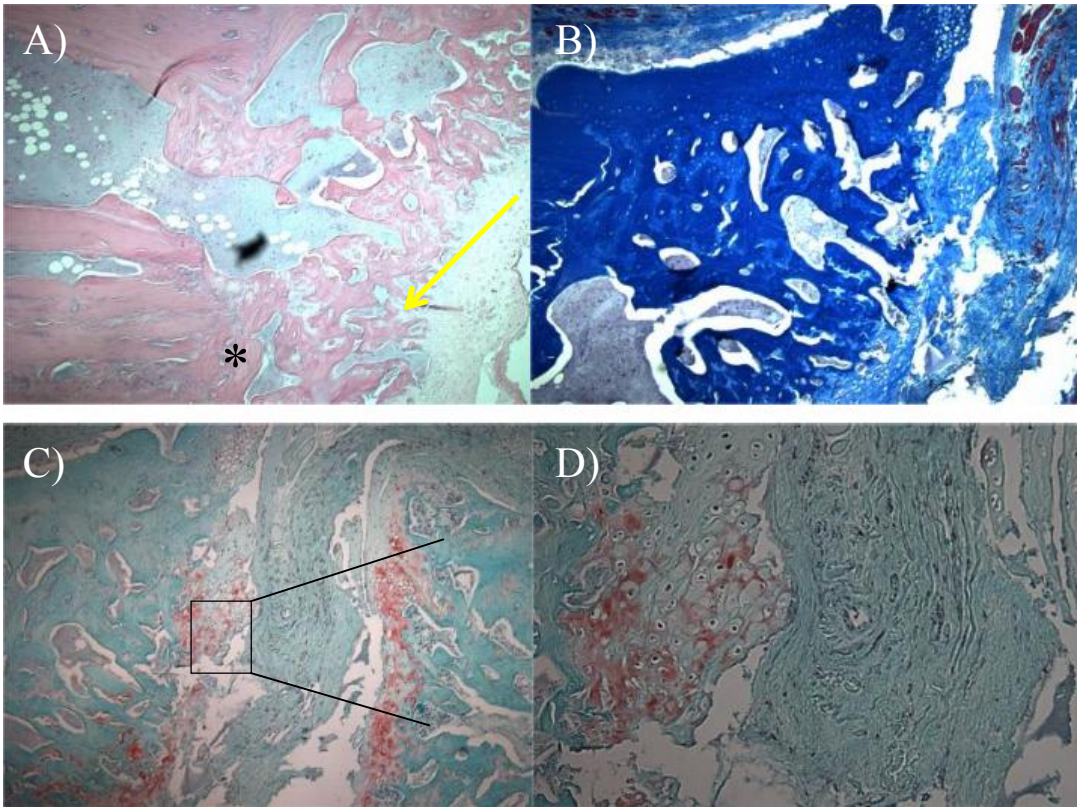

Figure 8.11 At week 4 post hMSC injection histological sections.: (a) H&E stain demonstrating an area of bone formation, arrow and the osteotomy site, asterisk (x100), (b) Masson's trichrome stain (x100), (c) Safranin-O/Fast Green demonstrating an area of cartilage template, box (x100) and (d) higher magnification image (x200)

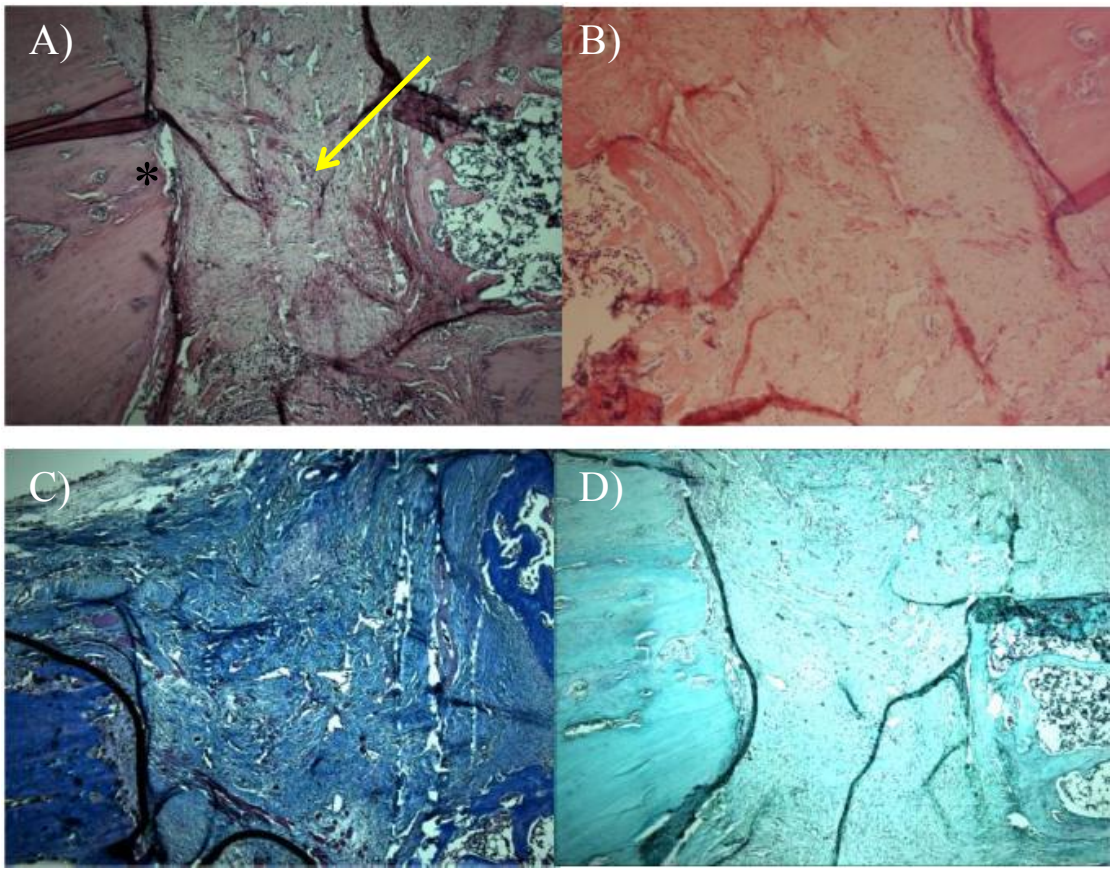

Figure 8.12 At week 4 post PBS injection (control) histological sections: (a) H&E stain demonstrating the presence of a fracture gap containing fibrous tissue, arrow and the osteotomy site, asterisk (x100), (b) fracture gap at higher magnification (x200), (c) Masson's Trichrome stain (x100), (d) Safranin-O/Fast Green (x100)

8.3.6.2 Observation of general morphology at 8 weeks

The histological sections at eight weeks also demonstrated a difference in appearance between the cell implantation groups and control group. Bone bridges were observed in both the rMSC and hMSC implantation groups, but not in the PBS group (control). Masson's Trichrome staining also demonstrated areas of new bone formation. In the rMSCs implantation group, there was full bridging callus connecting the bone ends (**Figure 8.13**), the callus size was slightly larger than in the hMSCs implantation group. Bone remodelling had occurred and the osteotomy site was difficult to

distinguish. In the human cell implantation group, the area of bone at the fracture was less than in the rat cell implantation group, but there was good bone continuity between the proximal and distal bone fragments and the bone cortex had remodelled (**Figure 8.14**). In the PBS injected group (control), the fracture site went on to form an atrophic non-union in which the bone ends became more rounded and the inter-fragmentary gap increased. Fibrous tissue remained at the fracture gap (**Figure 8.15**).

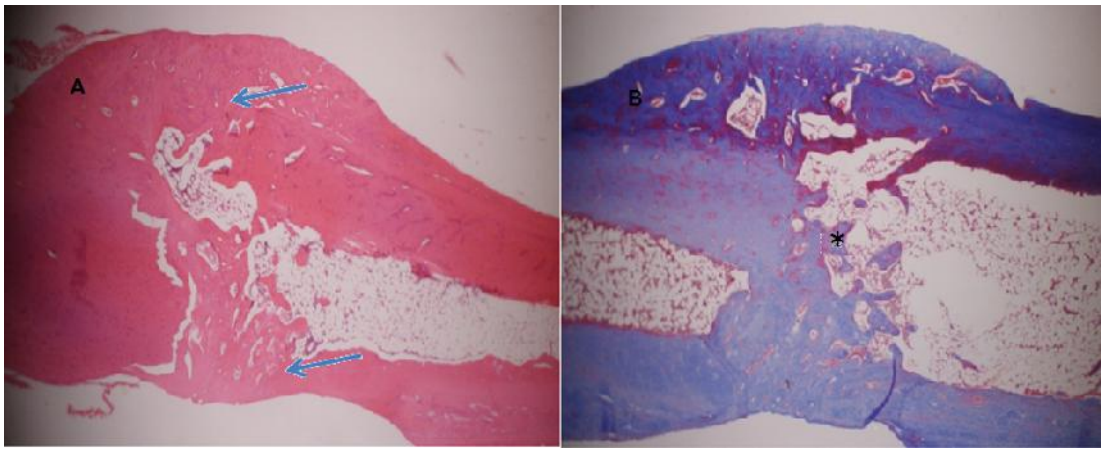

Figure 8.13 At week 8 post rMSC injection histological sections: (a) H&E stain demonstrating bone bridges, **arrows** (x40), (b) Masson's Trichrome stain demonstrating an area of new bone formation, **asterisk** (x40)

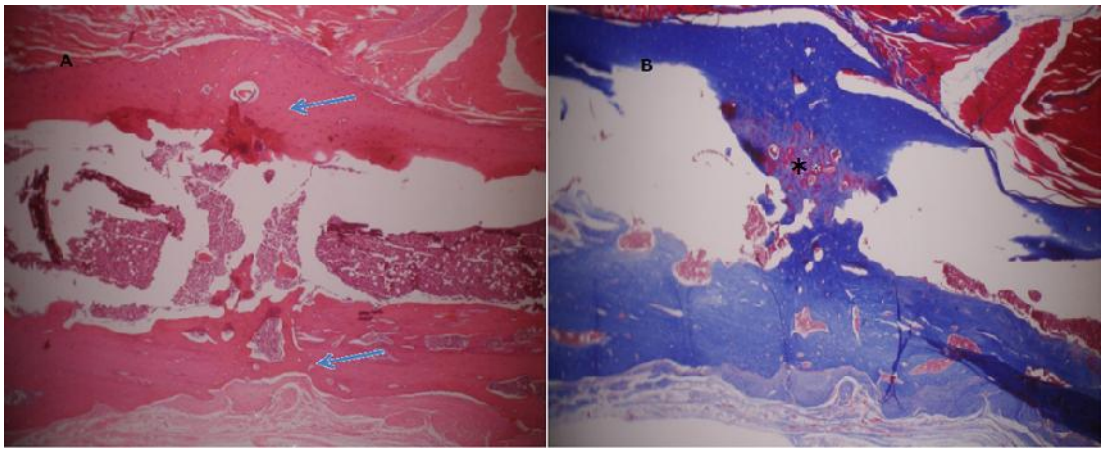

Figure 8.14 At week 8 post rMSC injection histological sections: (a) H&E stain demonstrating bone bridges, **arrows** (x40), (b) Masson's Trichrome stain demonstrating an area of new bone formation, **asterisk** (x40)

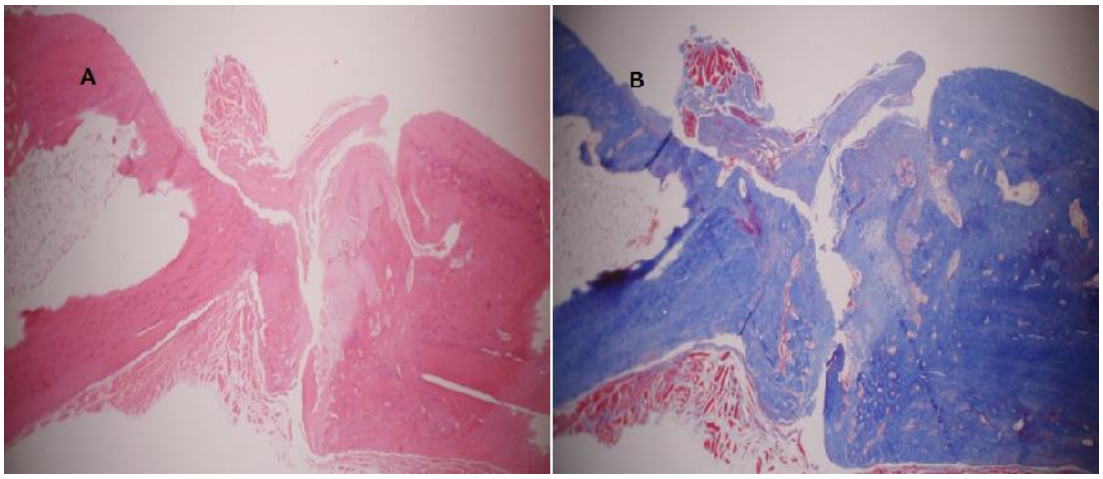

Figure 8.15 At week 8 post PBS injection (control) histological sections. (a) H&E stain demonstrating full characteristics of atrophic non-union (x40), (b) Masson's Trichrome stain (x40)

8.3.6.3 Quantitative comparison of the tissue at the fracture gap from the three different treatments

Figure 8.16 shows the percentage of each tissue component; bone, cartilage, fibrous tissue and bone marrow/empty space at the fracture. There was a significant difference in tissue constituents between the cell treatment groups (either rat or human MSCs) and the PBS group both at four weeks and at eight weeks. The amount of bone at the interfragmentary gap in the MSC implantation groups was significantly more than the control at both four weeks and eight weeks. The amount of bone at the inter-fragmentary gap in the rMSC was 31.6% ($P < 0.05$, 95%CI of diff. -1.3 to 64.4) and 57.6% ($P < 0.001$, 95%CI of diff. 24.8 to 90.4) more than in the control group at four weeks and eight weeks, respectively, while the amount of bone at the inter-fragmentary gap in the hMSC group was 19.9% ($P > 0.05$, 95%CI of diff. -12.9 to 52.7) and 58.1% ($P < 0.001$, 95%CI of diff. 24.8 to 90.4) more than the control group at four weeks and eight weeks, respectively. The amount of bone formation in the rMSC injection group was slightly more than the hMSC injection group in at both time points, but there was no statistical significant ($P > 0.05$,

bonferroni test). At 4 weeks, the cartilage component in the MSC injection group was significantly more than in the control (13.6 %, $P < 0.01$, 95%CI of diff. 3.5 to 23.7 in the rMSC injection group and 14.7 %, $P < 0.01$, 95%CI of diff. 4.5 to 24.8 in the hMSC injection group).

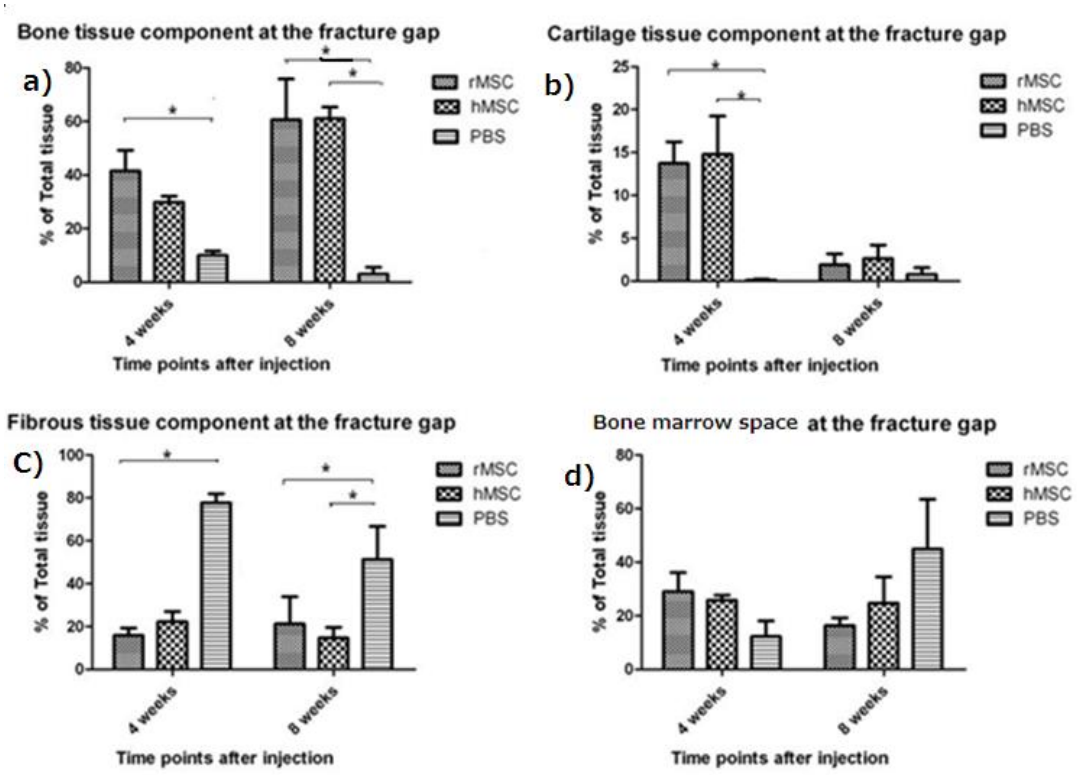

Figure 8.16 Quantitative evaluation of the tissue component in the fracture gap of the rMSC, hMSC and PBS (control) treatment groups; (a) Bone tissue component, (b) Cartilage tissue component, (c) Fibrous tissue component and (d) Bone marrow component

8.3.7 **Tracking of injected cells**

8.3.7.1 In vitro: CM-DiI labelling of cells

MSCs derived from either rat or human bone marrow were labelled with CM-Dil before injection. This dye stained the membrane of cells in vitro and was demonstrated using a fluorescence microscope (**Figure 8.17 and Figure 8.18**). The images showed fluorescent signal in the red channel for both rMSCs and hMSCs.

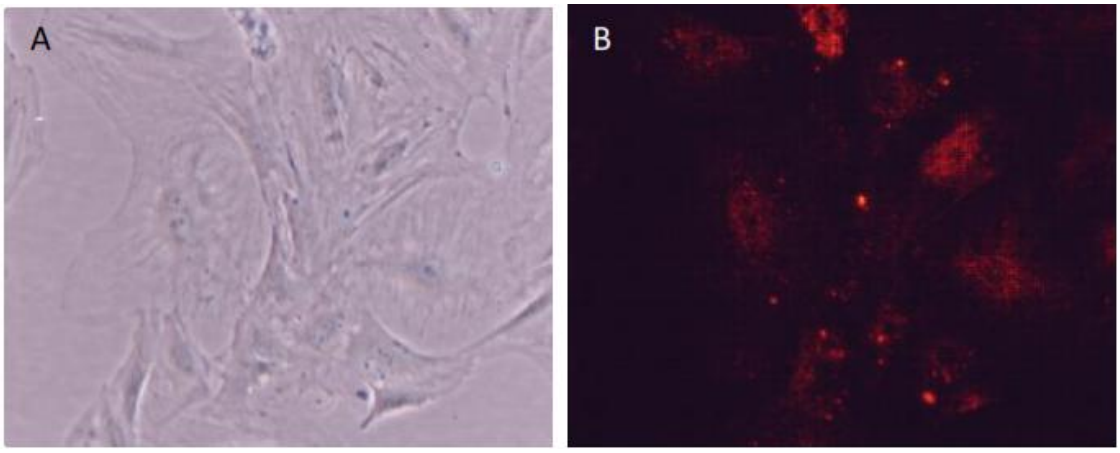

Figure 8.17 rMSCs labelling with CM-Dil in an in vitro culture: (a) rMSC under phase contrast microscope (x200) and (b) rMSC under fluorescence microscope (x200)

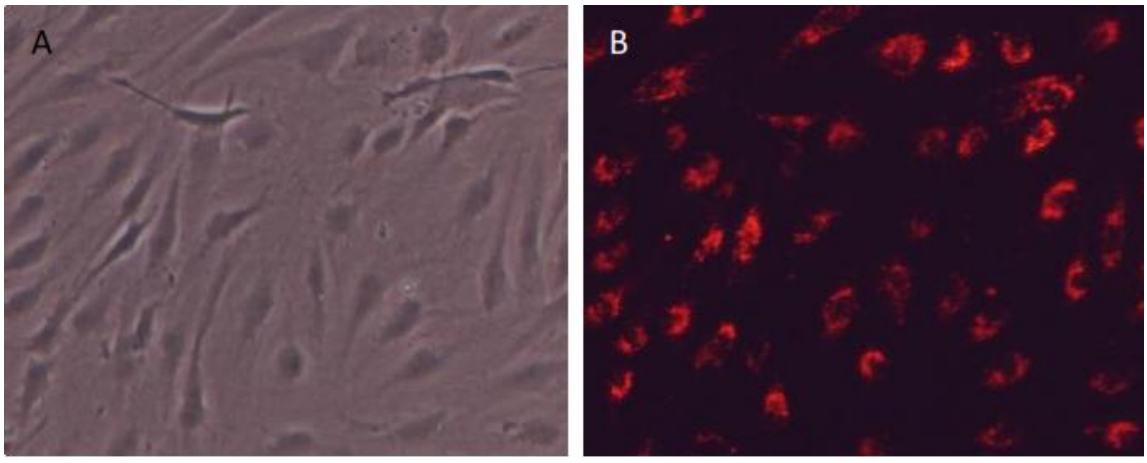

Figure 8.18 hMSCs labelling with CM-Dil in an in vitro culture: (a) hMSC under phase contrast microscope (x200) and (b) hMSC under fluorescence microscope (x200)

8.3.7.2 *In vivo*: MSCs with CM-DiI labelling at the fracture site after implantation

At 0 weeks (immediately after cell implantation), numerous labelled cells were observed at the fracture gap in both the rMSC and hMSC implantation groups (**Figure 8.19a, b, c and Figure 8.20a, b, c**). These results indicated that the percutaneous technique reliably delivered cells directly into the fracture gap.

Four weeks after cell implantation, labelled rMSCs were still detected at the fracture gap but the number of cells appeared to have decreased (**Figure 8.19d, e, f**). Eight weeks after cell implantation, cells were not found at the fracture (**Figure 8.19g, h, i**). In the hMSC injection group, hMSC were not detected at four weeks (**Figure 8.20d, e, f**) nor eight weeks (**Figure 8.20d, e, f**) after implantation.

Despite the improvement in the fracture healing process in both the rMSC implantation and hMSC groups, no hMSCs and only a few rMSCs engrafted at the fracture callus suggesting that the effect of MSCs on bone healing did not rely on their differentiation potential from progenitor cells.

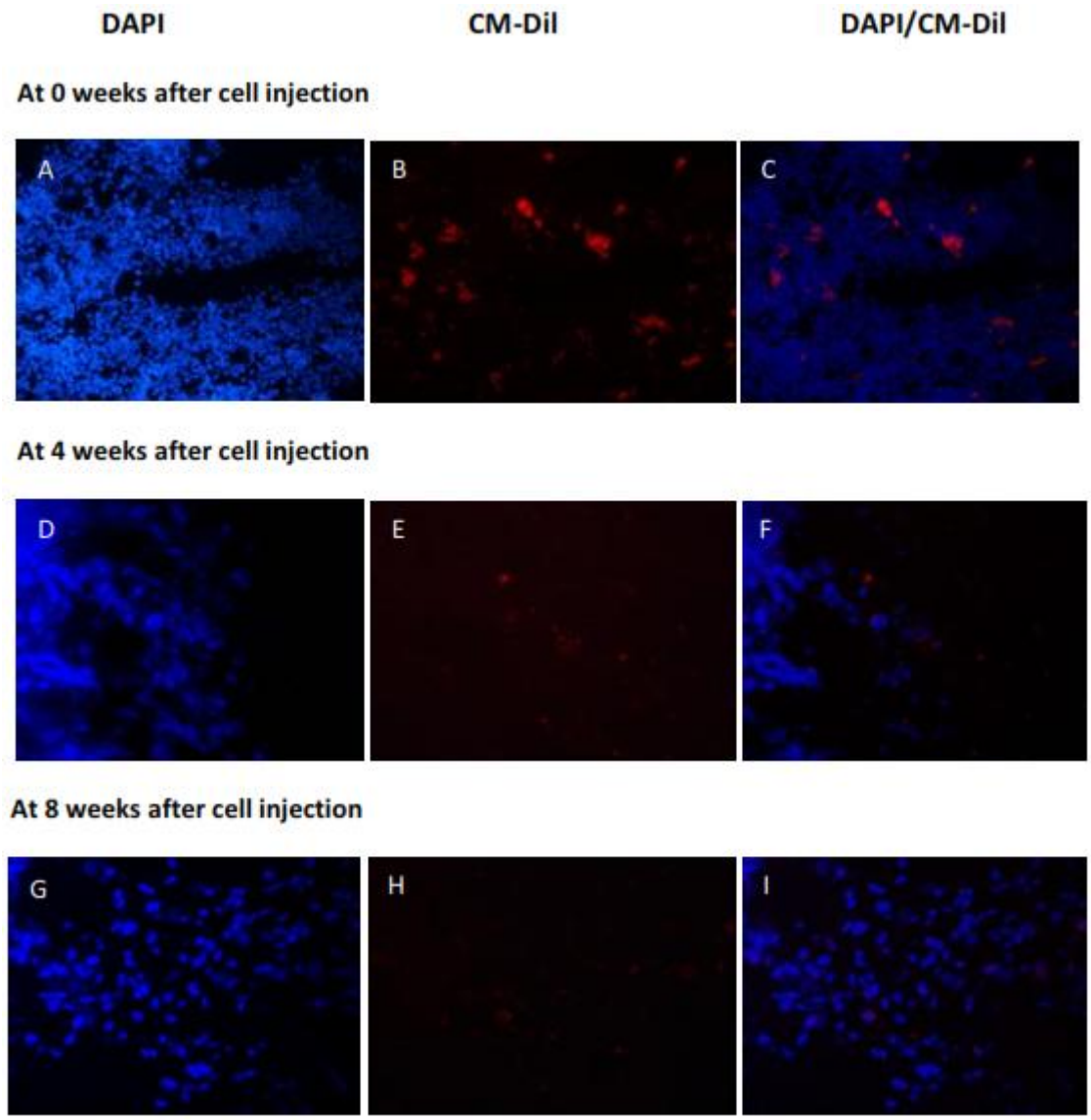

Figure 8.19 CM-Dil staining rMSC (Red) at the fracture gap at 0 weeks, 4 weeks and 8 weeks after cell injection with corresponding nuclear (DAPI, Blue) counter stain (x400)

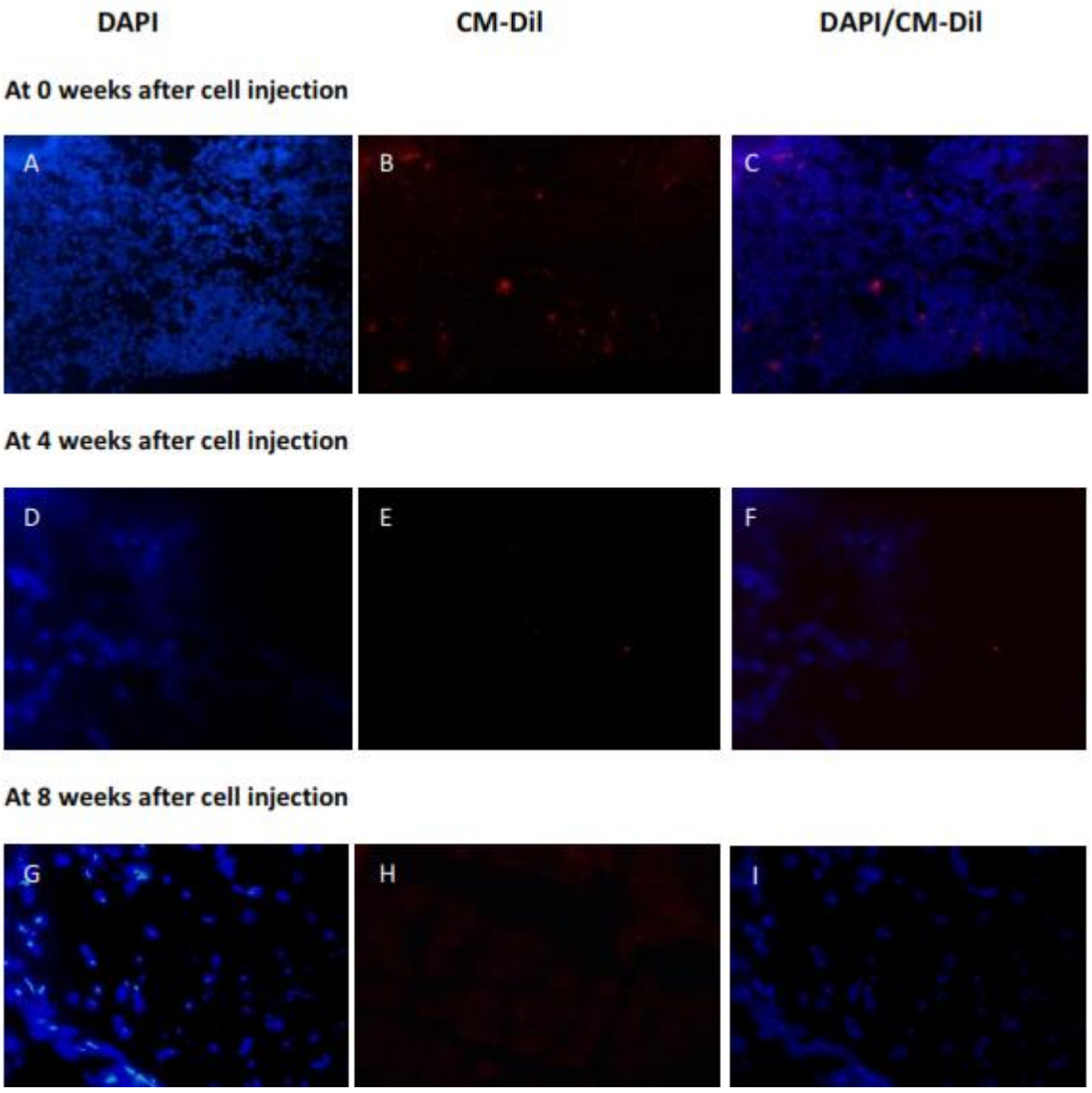

Figure 8.20 CM-Dil staining hMSC (Red) at the fracture gap at 0 weeks, 4 weeks and 8 weeks after cell injection with corresponding nuclear (DAPI, Blue) counter stain (x400)

8.3.7.3 In vitro hMSC staining with Anti-human nuclei antibody

hMSCs were stained *in vitro* using anti human specific nuclei antibody. **Figure 8.21** shows the fluorescence signal in the nucleus of cultured cells. For human cells, the signal in green can be seen in the nuclei.

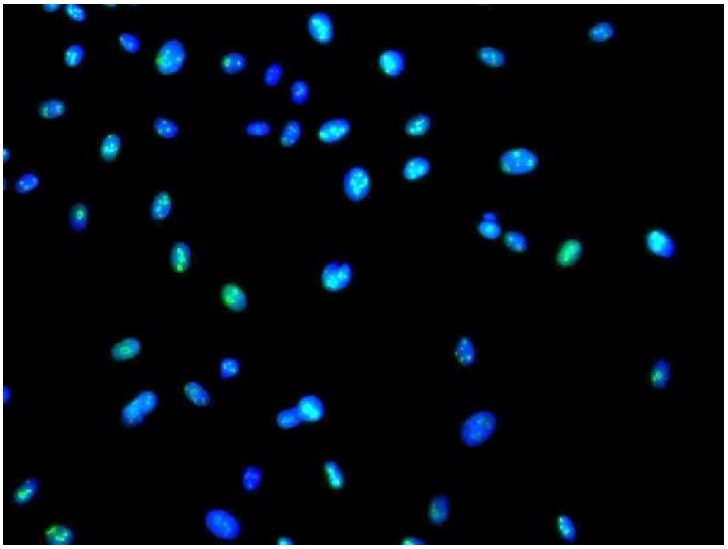

Figure 8.21 Anti-nucleic positive staining for hMSC in the in vitro culture (Green) with corresponding nuclear (DAPI, Blue) counter-stain (x400)

8.3.7.4 Anti-human nuclei antibody staining for identifying hMSC cells after implantation in atrophic non-union fracture

In the human tissue sections, there was a fluorescence signal from staining (**Figure 8.22a, b, c**). The human nuclei were stained using the anti-human nucleus antibody. This specimen was used as the positive control for this experiment. The tissue from the fracture gap of the hMSC implantation group demonstrated that there were no positive staining cells after 4 weeks (**Figure 8.22d, e, f**) or after 8 weeks (**Figure 8.22g, h, i**) after hMSC implantation. These results corresponded well with the CM-Dil labelling study in which there was no hMSC engraftment after implantation at the fracture callus.

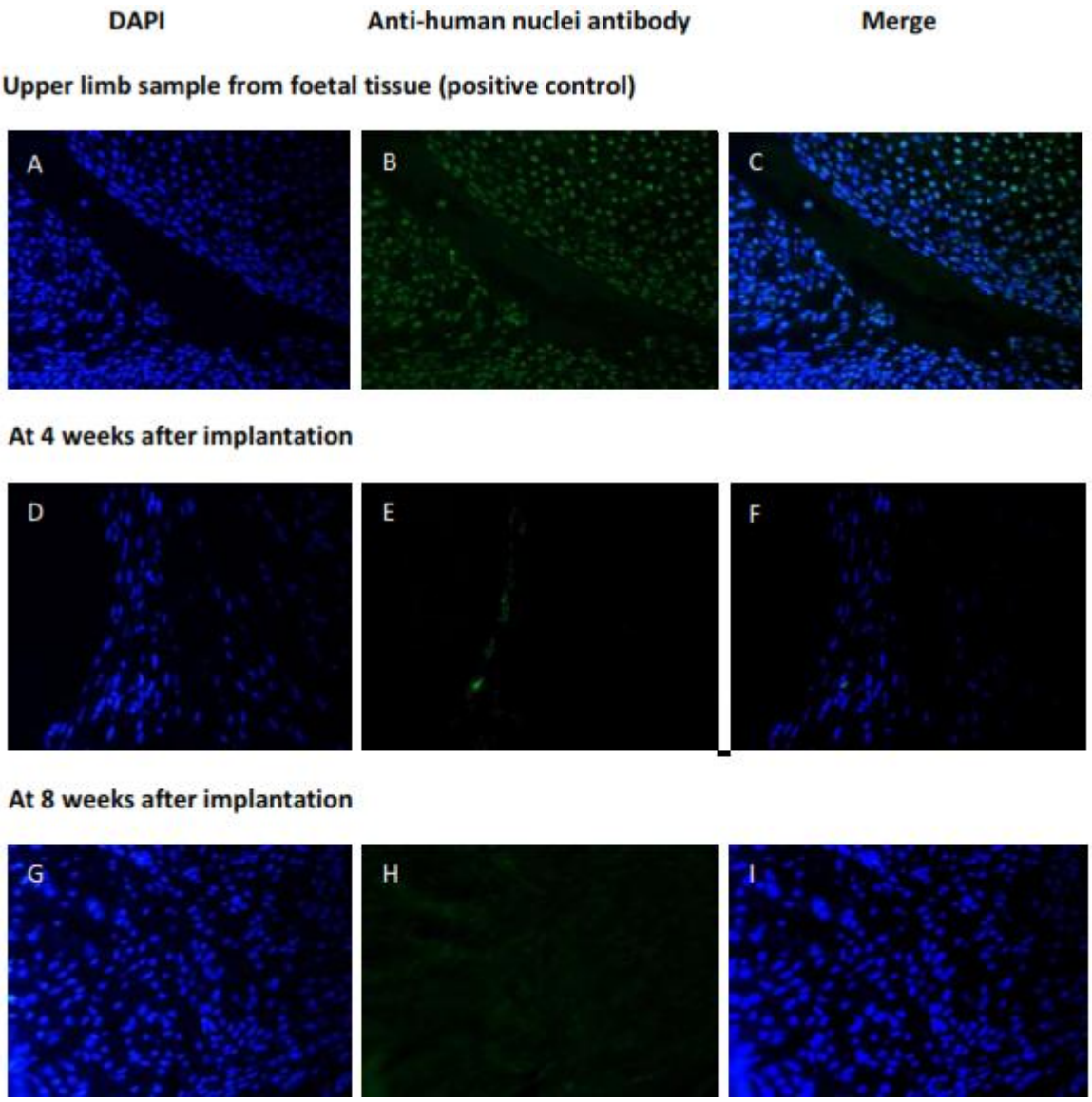

Figure 8.22 Anti-nucleic positive staining for hMSC (Green) at the fracture gap at 4 weeks and 8 weeks after cell injection with corresponding nuclear (DAPI, Blue) counter stain (x400) and (a,b,c) foetal human tissue from upper limb was used as the positive control

8.3.8 **Evaluation of immune response after cells implantation**

8.3.8.1 Systemic response to the different treatments

Seven inflammatory cytokines were detectable with the multiple ELISA assay including IL-1a, IL-1b, IL-2, IL-12, IL-13, TNF-α and GM-CSF. Serum samples from animals at the 0 time point (before injection) were used for comparison of the fold difference change every two weeks over a period of eight weeks after cell injection. **Figure 8.23** shows the mean fold difference of detectable cytokines over the post-injection period of rMSC, hMSC and control (PBS).

In the PBS injection group (control group), there was no significant change in any of the inflammatory cytokines. In contrast, in the cell injection groups, at two week post injection, there were an increase in the level of IL-1b and IL-2 in both the rMSC and the hMSC injection groups. The levels of IL-1b and IL-2 decreased by the 4^{th} week and remained at this level until the end of the experiment. Il-1a, IL-12, IL-13 and TNF-α did not change over the time period in the MSC treatment groups. However, in the human cell injection group, there was a remarkable increase in the GM-CSF compared to other cytokines at four weeks and eight weeks compared to the rat cells injection group and the control group. This result indicated the inflammatory reactions in the hMSC injection group.

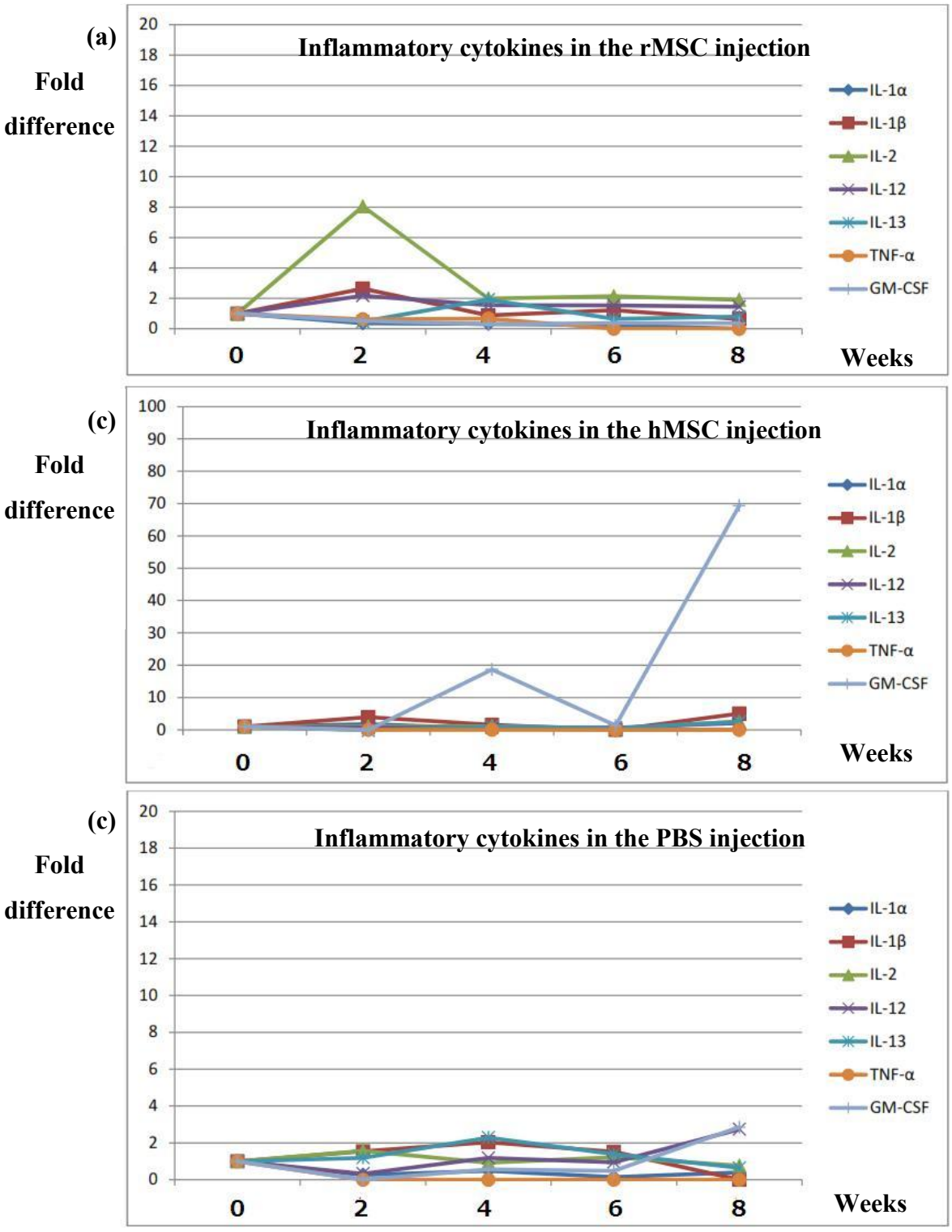

Figure 8.23 Inflammatory cytokines from multiple ELISA assay from (a) the rMSC injection group (b) the hMSC injection group and (c) the PBS (control) group

8.3.8.2 The popliteal lymph node response

The popliteal lymph nodes are the closest regional lymph nodes to the fracture site. These lymph nodes were evaluated in order to assess the immune response following cell injection to the fracture site. There were four parameters that were determined in the regional lymph nodes; (1) the size of lymph node, (2) the number of secondary follicles, (3) the number of infiltrating cells at the subcapsular sinus and (4) the number of macrophages at the medullary sinus. The results from quantitative evaluation of the ipsilateral right popliteal lymph node from the three treatments (rMSC, hMSC and PBS) and from the contralateral left popliteal lymph node for comparison (unoperated side) are shown in **Figure 8.24.**

Four weeks after injection, there were no significant differences between the treatment groups in the size of lymph node, the number of secondary follicles or the number of macrophages from treatment groups. However, the number of infiltrating cells at the subcapsular area in the hMSC injection group was significantly higher than in the rMSC and PBS injection groups. The left popliteal lymph node (unoperated side) was smaller than the lymph node from the hMSC treatment group. The number of secondary follicles and the number of infiltrating cells at the sub-capsular area in the left lymph node was less than from the operated side of the hMSC treatment groups. There was no significant difference in the number of macrophages at the medullary sinus area between the operated and unoperated side.

Eight weeks after injection, the size of lymph node, the number of secondary follicles and the number of infiltrating cells increased in the rMSC and hMSC group, but there was no significant change in any of these parameters in the PBS injection group or in the lymph node from the unoperated (control) side. The size of lymph nodes from the hMSC injection group was significantly larger than the PBS injection group and there was a significant increase in the number of secondary follicles compare to the PBS injection group. There were no differences in the number of macrophages at the medullary sinus from any of the treatments or from the control lymph node.

In summary, there was a significant increase in the lymph node reaction at the injury site demonstrated by the size of lymph node and the number of secondary follicles. Although there was an increase in the size of the lymph node, the number of secondary follicles and infiltrating cells in the lymph node from the rMSC injection group, the differences were not statistically significant compared to the PBS injection group. In the hMSC injection group, the size of lymph node and the number of secondary follicles significantly increase when compared to the PBS injection group. However, the difference between the hMSC and rMSC groups was not significant. The number of macrophages at the medullary sinus was not different in the rMSC, hMSC or PBS injection groups.

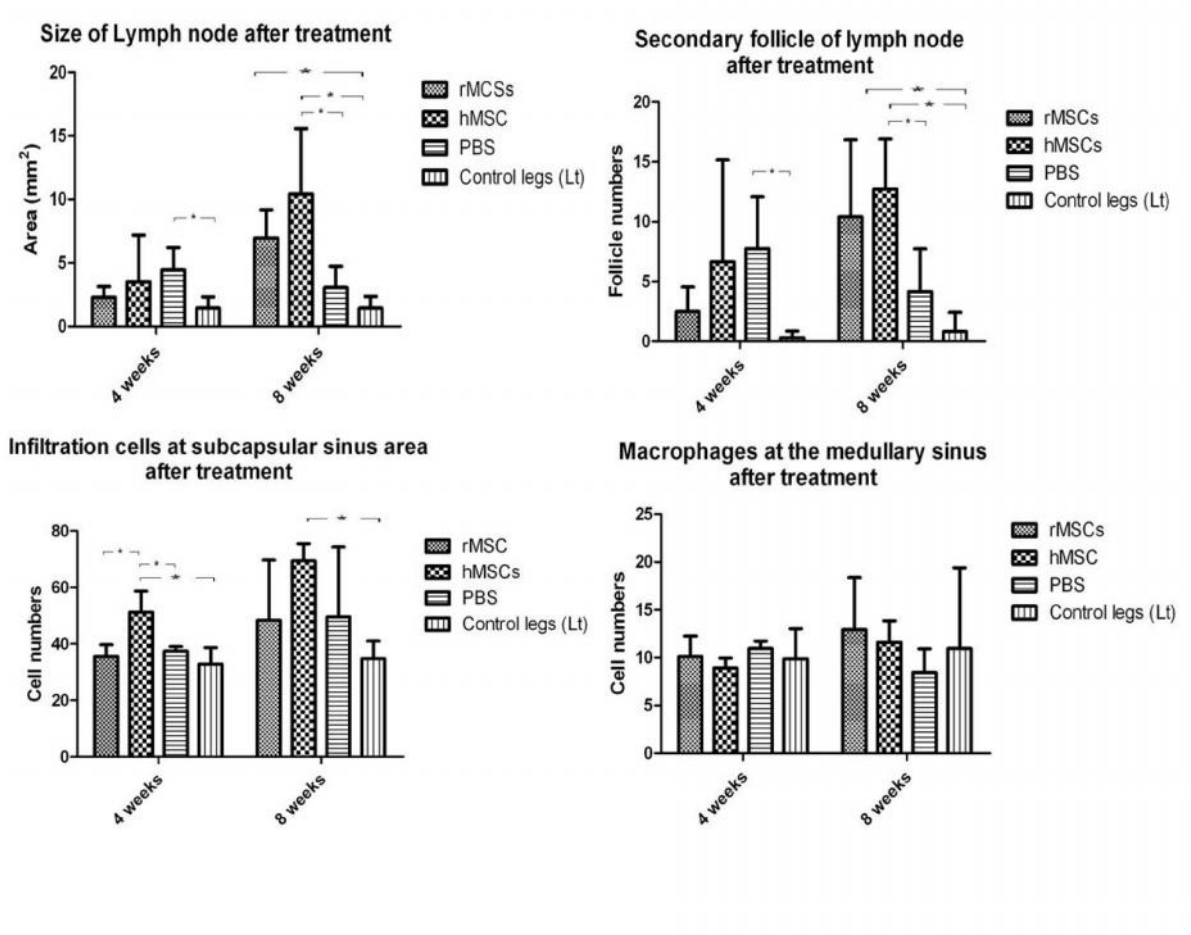

Figure 8.24 Histomorphology of popliteal lymph nodes from both operated and unoperated (control) side 4 and 8 weeks after injection with rMSC, hMSC and PBS control; (a) Size of Lymph nodes , (b) Number of secondary follicles, (c) Number of infiltrating cells at capsular sinus, and (d) Number of macrophages at the medullary sinus

8.4 Summary and discussion

In this chapter, the therapeutic effect of hMSC in promoting fracture healing of an atrophic non-union model was found to be comparable to the therapeutic effect of rMSC in promoting healing in the same model. Both treatments led to an improvement in fracture healing, especially when injected into the atrophic non-union model at an early stage. There were no clinical adverse effects detected with xenogeneic transplantation. Although there was an increase in GM-CSF level at the later time point after hMSC injection, there were no significant differences in the size of the lymph node, the number of secondary follicles, the number of infiltrating cells at capsular sinus and the number of macrophages at medullary sinus between rMSC injection and hMSC injection groups. The cell tracing results showed that the hMSCs did not persist at the fracture site; either four weeks or at eight weeks the implanted cells were not evident. In comparison, there were a few rMSCs observed at the fracture gap at four weeks after injection but not at eight weeks. Both allogeneic and xenogeneic MSCs implantation contributed to the fracture healing process however, rMSCs and hMSCs had disappeared by the time the fractures had united. These results suggest that exogenous MSCs improve fracture healing via their paracrine effect and not necessarily as progenitor cells. Although immune responses were raised by implantation of hMSC, the therapeutic effect of hMSCs in bone repair was not significantly inhibited.

There are advantages in a cell therapy being allogeneic rather than autologous. To determine whether exogenous stem cells are effective, the most extreme case to investigate would be xenogeneic cells (Samstein and Platt, 2001). This model has been reported in myocardial regeneration studies using xenogeneic implantation to evaluate the concept of universal cells donor (Atoui et al., 2008). This thesis has examined the concept for bone regeneration. If there are any benefits of using xenogeneic stem cells (e.g. hMSCs) to promote fracture healing in an immunocompetent animal model, the results should reflect the outcomes of using allogeneic stem cells as universal donor cells in a clinical setting. However, in the

recent literature on bone regeneration, xenogeneic implantation is still controversial: a range of studies have reported inconsistent effects of hMSC in xenogeneic models (Fatkhudinov et al., 2005, Niemeyer et al., 2010b, Niemeyer et al., 2010c). These experiments were conducted using bone defect models, which are different to an atrophic non-union model. In a bone defect model, healing may be more dependent on engraftment of the cells, whereas in a non-union model the cells may act by stimulation of endogenous cells and therefore be less dependent on engraftment. Thus, if the therapeutic potential of MSCs in a bone defect model is more dependent on engraftment and differentiation of the cells, then the immune response may have a greater role and inhibit the ability of MSCs to bring about healing of a bone defect.

Chloromethyl-benzamidodialkylcarbocyanine (CM-Dil) is a fluorescent membrane marker and was used to label the injected cells. It has been reported that CM-Dil labelled hMSCs could be detected from the graft area up to 10 weeks after implantation in a rat calvarial model (Zong et al., 2010). However, in the present study, no injected hMSCs could be found either at four weeks or eight weeks after injection. These results were confirmed using immunostaining with an antibody that was specific to human nuclei. The findings from this study are in contrast to a previous report conducted in a critical size defect model (Zong et al., 2010). As the therapeutic effects of injecting MSCs in this study could not be explained by cell engraftment or differentiation; it is postulated that exogenous hMSCs may contribute to the fracture healing process in the fracture at risk of atrophic non-union by providing the paracrine or trophic factors that are required to stimulate fracture healing and that tissues at the fracture site are stimulated to form fracture callus via trophic effects from the exogenous MSCs. In support of this, it has been reported that MSCs release many cytokines and mediators into the medium including interleukin-1, -6, -7, -8, -11, -14 and-15, leukaemia inhibitory factor (LIF), stromal cell-derived factor (SDF-1), stem cell factor (SCF-1),Flt-3 ligand, macrophage, granulocyte and granulocyte macrophage colony stimulating factors (M-, G-, and GM-CSF) and Vascular endothelial growth factor (VEGF) (Haynesworth et al., 1996, Majumdar et al., 1998, Hung et al., 2007). These mediators act as regulators during fracture repair.

Granulocyte-macrophage colony-stimulating factor (GM-CSF) is one of the key regulators in the pro-inflammatory cascade which is able to stimulate the innate immune response and thus increase the number of granulocytes including neutrophils, eosinophils, and basophils as well as supporting the differentiation of monocytes into macrophages (Hamilton, 2002). The innate immune response has been reported to play an important role in xenograft rejection (Wang and Yang, 2012, Yang and Sykes, 2007). In this study, there was an increase in GM-CSF level in hMSC group, and there was a significant lymph node reaction compared to the control. However, there was no significant difference in lymph node response between the rMSC and hMSC injection group. These immune responses observed after cell injection are not specific to xenogeneic cells; both infections and foreign bodies can also increase the GM-CSF levels (Szeliga et al., 2008) and cause lymph node reactions (Bondarenko et al., 2011). In the current study, there was no evidence of infection suggesting the reaction was due to the injected cells, however the reaction of the external fixator still could not be excluded. The increase in immune response in the hMSC treatment group did not negate the beneficial effects of the injected cells on fracture healing and the injected cells did not cause any adverse effects in this study. However, further studies on the detail of the immune response and the interactions of MSCs in an allogeneic or xenogeneic environment are required before MSCs from a universal donor could be used to improve fracture healing in the clinical setting.

Alternatively, a better autologous source of bone progenitors could be used as a clinical strategy. For instance, adipose tissue has been investigated as an alternative source of autologous cells. It has been reported that perivascular stem cells (PSCs) (also known as pericytes), which are found in the perivascular area in several tissues such as adipose tissue may serve as a source of bone progenitors. Thus, the therapeutic effects of PSCs for bone regeneration will be evaluated in the next chapter.

Chapter 9: Bone regeneration potential of adipose tissue derived perivascular stem cells or pericytes

Aim: *To evaluate the therapeutic potential using perivascular stem cells to promote bone healing in an atrophic non-union model*

9.1 Introduction

Atrophic non-union is a fracture complication caused by biological failure of the healing process. The last two chapters (Chapter 7 and 8) have determined the appropriate time for using percutaneous MSC implantation and evaluated the therapeutic effects using hMSCs from bone marrow in an atrophic non-union model. To develop a possible clinical strategy using cells from different sources, adipose tissue derived cells were investigated in this chapter. It has been reported that perivascular stem cells (PSCs) (also known as pericytes) which are found in the perivascular area may serve as a source of bone progenitors (James et al., 2012a). PSCs can be isolated from fat tissue with CD146 markers. They are reported to share the characteristics and differentiation potential of MSCs (Crisan et al., 2009) in particular pericytes are capable of osteogenesis. PSCs also provide trophic factors required in the fracture healing process (Chen et al., 2009). The healing potential of these cells may prevent a fracture destined to progress to non-union from doing so. Thus, the aim of this study was to evaluate the bone regeneration potential of PSCs in an atrophic non-union model.

9.2 Materials and Methods

The atrophic non-union model, the percutaneous injection technique and the fracture assessments have been described in the general materials and methods (Chapter 2). In this section, the specific experimental design and statistical analysis are provided.

9.2.1 Experiment design

The atrophic non-union operation was carried out on five male Wistar rats (400-500g). Five million hPSC in 200 μL PBS were injected at three weeks post operation. Control animals who had undergone the identical procedure except for having PBS injected instead of cells from previous chapters (n=7) were used for statistical analysis. Bone healing was evaluated using radiographic parameters including micro-CT, histological parameters, and biomechanical properties.

9.2.2 Statistical analysis

The difference in numbers of bone unions between the hPSC injection group and the control group was determined using Fishers'exact test. The mean differences in fracture progression parameters including radiopacity, proximal and distal callus index, the percentage increase of callus area as well as changes in the fracture scores (RUST and Lane & Sandhu) were tested using repeated ANOVA and the post-hoc analysis was performed using Bonferroni multiple comparisons test. The measurements from histology and micro-CT were also tested using unpaired t-tests.

9.3 Results

9.3.1 Animal health status after PSCs implantation

All rats (n=5) successfully underwent the operation to induce an atrophic non-union procedure and then they were then injected with hPSCs three weeks after operation. There was no sign of any adverse reactions following the injection of hPSCs. All of the animals remained alive without any complications until the end of the study.

9.3.2 Diagnosis of bone union in PSC group and control

In the PSC injection group, three out of the five animals received that had received PSCs progressed to fracture union, whereas in the control group, only one achieved bone union eight weeks after injection of PBS. **The table 9.1** shows the number of fracture unions and non-union in rats injected either with PSCs or PBS. More animals achieved bone union in the PSC injection group compared to the control group. However, the difference was not statistically significant (P-value=0.22, Fishers'exact test)

Table 9.1 The number of the animals used in the early time point and results of bone union between the PSC injection group and the PBS (control) injection group

Treatment group	Outcome		Total
	Bone union	Non-union	
PSCs	3	2	5
PBS (control)	1	6	7
Total	4	8	12

Although, one of the animals in the treatment group was diagnosed as a non-union, there was callus present at the fracture gap. Serial radiographic images showed an improvement of bone healing over the eight week period after injection of PSCs (**Figure 9.1**). This fracture may have progressed to union at a later stage (more than eight weeks).

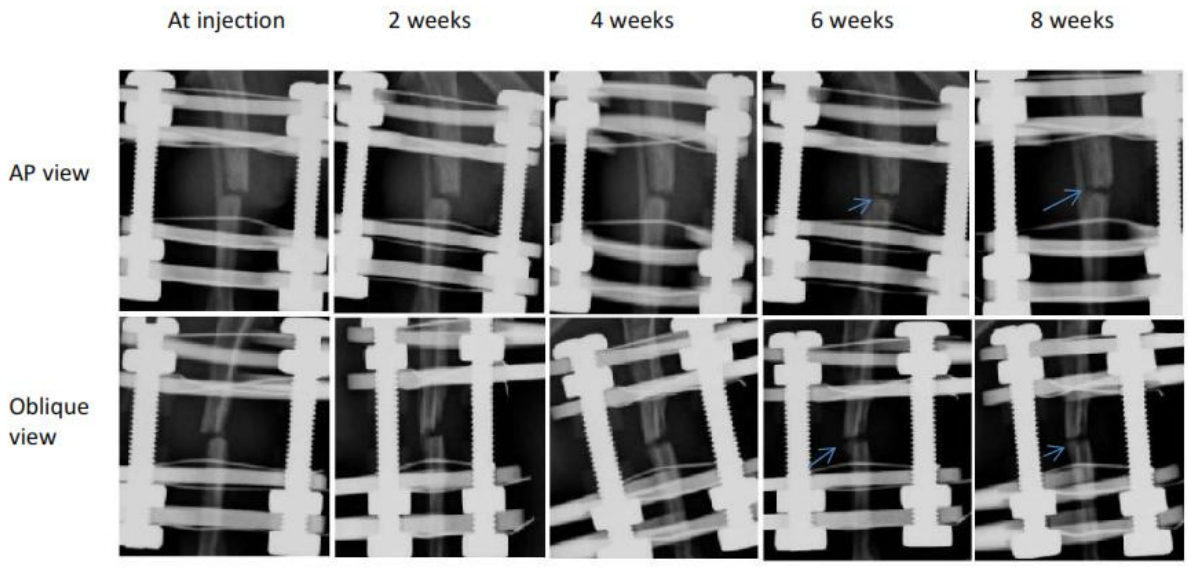

Figure 9.1 Radiographic at 8 weeks of injected PSCs animal who developed atrophic non-union (Arrows show bone callus at the fracture gap)

9.3.3 **The progression of the fracture healing process**

The progression of fracture healing was evaluated with radiography every two weeks to assess and monitor the radiographic parameters of bone healing. The serial radiographs of the fracture showed progression of healing in most animals in the PSC treatment group (4/5), while the fracture sites of most animals in PBS treatment group (6/7) proceeded to fully developed atrophic non-unions.

9.3.3.1 Relative Radiopacity of PSC treatment group compared to control group

The Mean relative radiopacity which was normalised with an aluminium step wedge, at the fracture gap of the hPSC and control groups are shown in **Figure 9.2.** The mean radiopacity in the hPSC treatment group was significantly higher as early as 4 weeks after injection of the cells compared to the control group ($P < 0.001$, ANOVA).

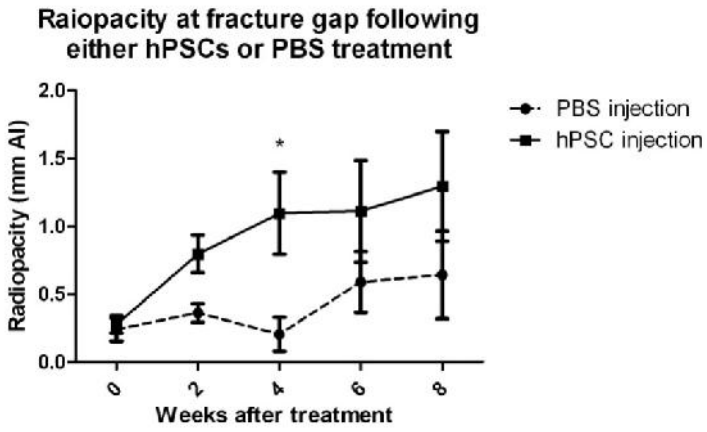

Figure 9.2 The comparison of radiopacity between treatment (hPSC) and control (PBS) over 8 weeks period post injection (*P-value < 0.05, Post-tests using bonferroni)

9.3.3.2 Callus index in hPSC treatment group compared to control group

The proximal and distal callus indices increased significantly in the hPSC injected animals over the 8 week period after cell injection (Proximal callus index; P-value = 0.01, ANOVA and Distal callus index; P-value = 0.02, ANOVA) (**Figure 9.3**). The

callus index of the controls slightly decreased over the 8 week period after PBS injection. This may represent atrophic change at the fracture site.

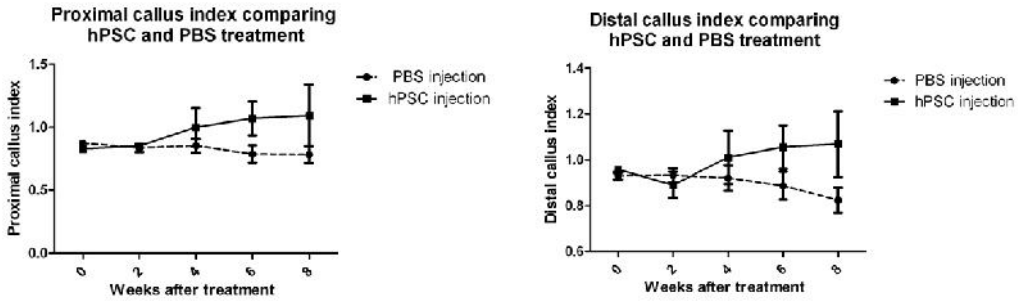

Figure 9.3 The comparison of callus index; a) proximal and b) Distal between treatment (hPSCs) and control (PBS) over the 8 week period post injection

9.3.3.3 Percentage increase of callus area in the hPSC treatment group compared to control group

The graph in **Figure 9.4** shows the percentage increases of callus between the hPSC group and control groups over the 8 week period after injection. Similar to the callus index, the percentage change of callus area significantly increased from the 2nd week to the 8th week. In contrast, the percentage change of callus in the control group which had been injected with PBS at the non-union site resulted in a decrease in callus area. There was a statistically significant difference in the percentage area increase between the hPSC group and the control group (p-value < 0.001, ANOVA).

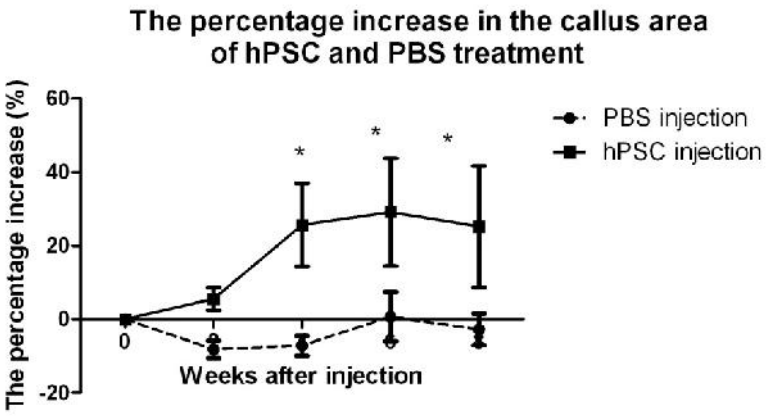

Figure 9.4 The comparison of the percentage callus area increase between treatment (hPSC) and control (PBS) over 8 weeks period post injection (*p<0.05, Post-tests using bonferroni)

9.3.3.4 The progression of the fracture healing process using fracture scoring system in the hPSC treatment group compared to the control group

The RUST score and Lane & Sandhu score both showed a trend towards improvement in the fracture healing process over the 8 period after cell injection (**Figure 9.5**). However, this was not statistically different between the treatment and the control (RUST score; P-value = 0.28, ANOVA and Lane & Sandhu score; P-value = 0.39).

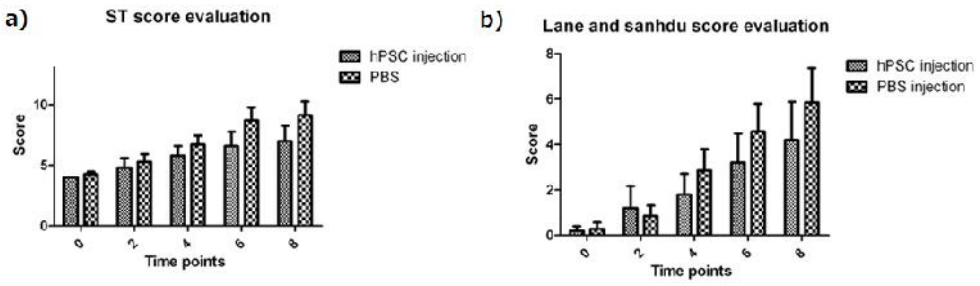

Figure 9.5 Fracture scoring systems: (a) The RUST score evaluation and (b) Lane and Sandhu score evaluation

9.3.4 **Histology evaluation in hPSC treatment group compared to control group**

The histological observations from H&E stained sections supported the radiological results. In the hPSC injection group, the inter-fragmentary gap consisted predominantly of bone (**Figure 9.6a**) and a bony bridge was present connecting the bone ends. Conversely, in the PBS injected group, the tissue within the inter-fragmentary gap consisted predominantly of fibrous tissue (**Figure 9.6b**). Masson's Trichrome staining confirmed the area of new bone formation (**Figure 9.7**) at the fracture site in the hPSC injection group.

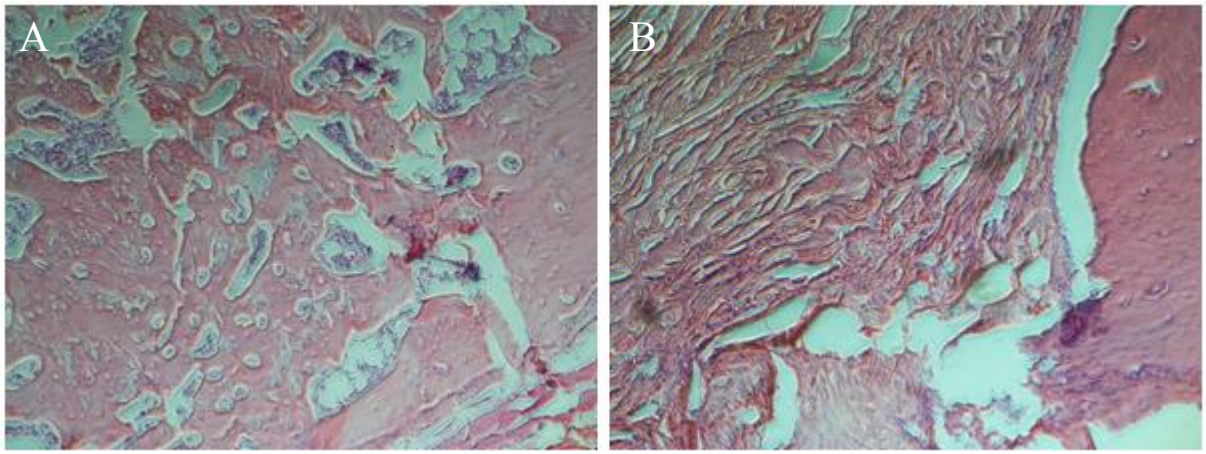

Figure 9.6 H&E staining from the fracture site of (a) hPSC injected animal, x100 and of (b) control animal, x100

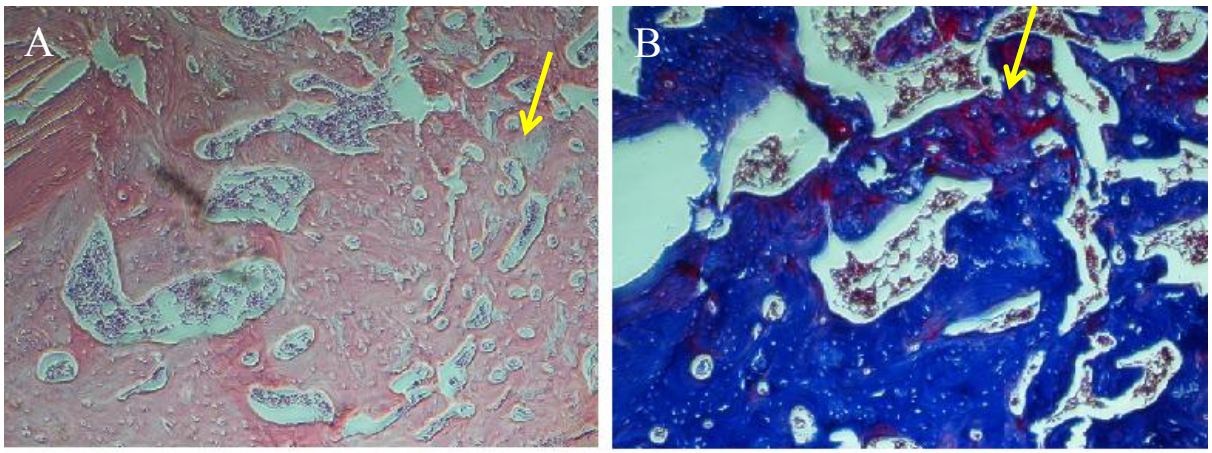

Figure 9.7 Histological sections: (a) H&E staining, x100 and (b) Masson's Trichrome, x100 at fracture site of hPSC injected animals demonstrating the area of new bone formation (Arrow)

In the animals in the hPSC injection group, which was not categorised as a 'union' at 8 weeks after hPSC injection, the fracture had not developed into an established atrophic non-union and the serial radiographic of fracture showed some bone callus. The histology show bone trabeculae and cartilage tissue at the fracture gap but no connectivity of bone (**Figure 9.8**).

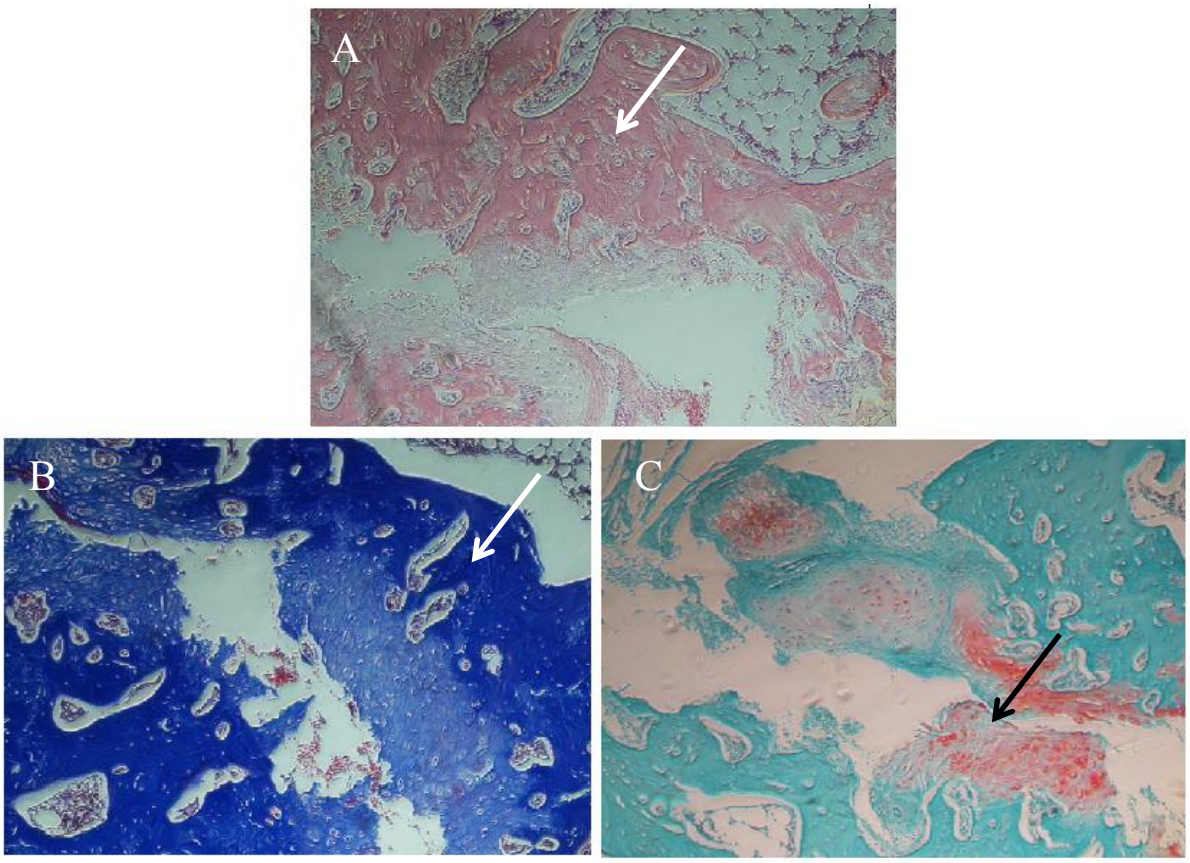

Figure 9.8 Non-union gap of one of the animals in the hPSC injection at 8 weeks after cell injection demonstrating soft (Black arrow) and hard callus (White arrow); there was no bony bridge present. (a) H&E, x100 , (b) Masson's Trichrome, x10 and (c) Safronin O/Fast Green, x100

The 10x10 grids were applied to images from histology for evaluating the tissues component semi-quantitatively. The tissue components (bone, cartilage, fibrous and bone marrow space) were compared between the cell treated group and the control group (**Figure 9.9**). The bone content was the largest component in the treatment group and it was significantly higher than the control group (P-value < 0.05, Unpaired t-test). Fibrous tissue and marrow space were the dominant components in the fracture gap the in the control group.

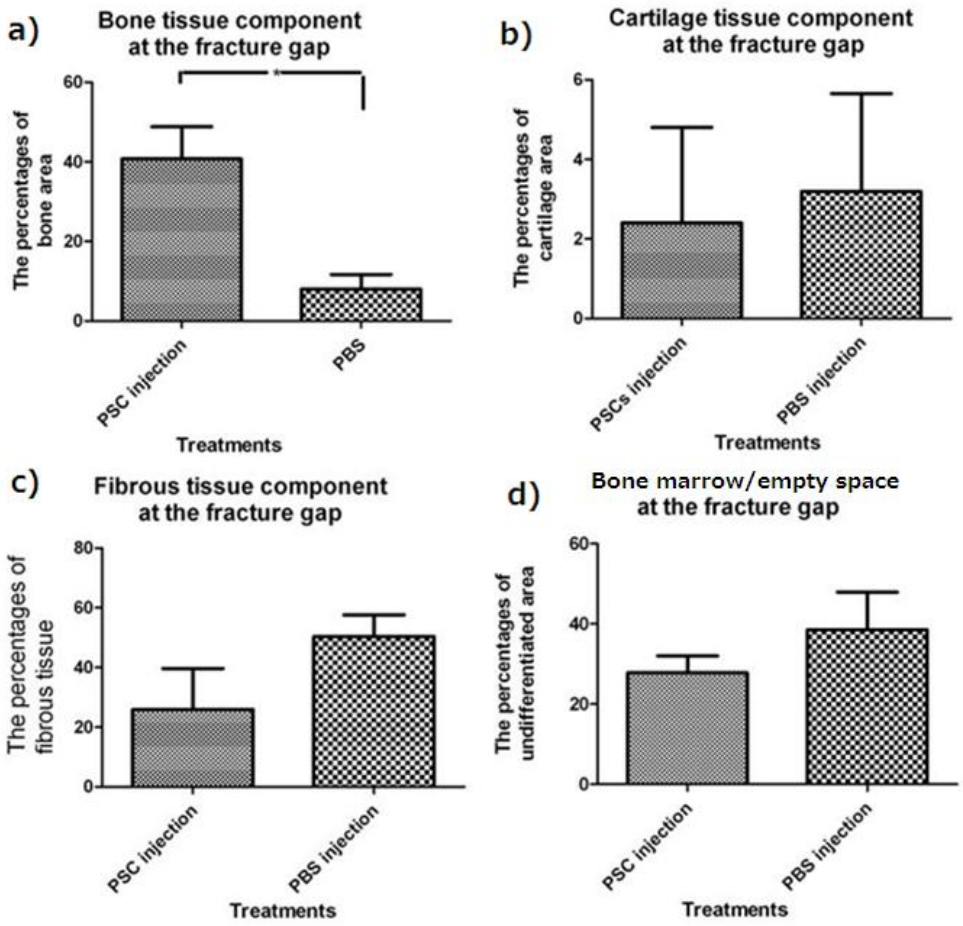

Figure 9.9 Quantitative evaluation of the tissue components in the fracture gap (a) bone tissue component, (b) cartilage tissue component, (c) fibrous tissue component and (d) bone marrow/empty space component (*P-value < 0.05, unpaired t-test)

9.3.5 **Micro-CT analysis in the PSC and control groups**

Three-dimensioned images from micro-CT depicted the bone component at fracture sites in the animals treated with hPSCs. There were full bone bridges present at the fracture gap in three animals that developed bone union. In the two animals that were diagnosed with non-union, there was some bone formation present at the fracture gap in one of them (**Figure 9.10**). For quantitative measurement, the percentage of endosteal calcified tissue volume per tissue volume, at the centre of the fracture site

was measured for all samples. All parameters are shown in **Table 9.2.** In the PSC treatment group, the bone mineral density, which identified the quality of bone content and degree of mineralisation was statistically significantly higher than in the control group (P-value = 0.04, unpaired t-test).

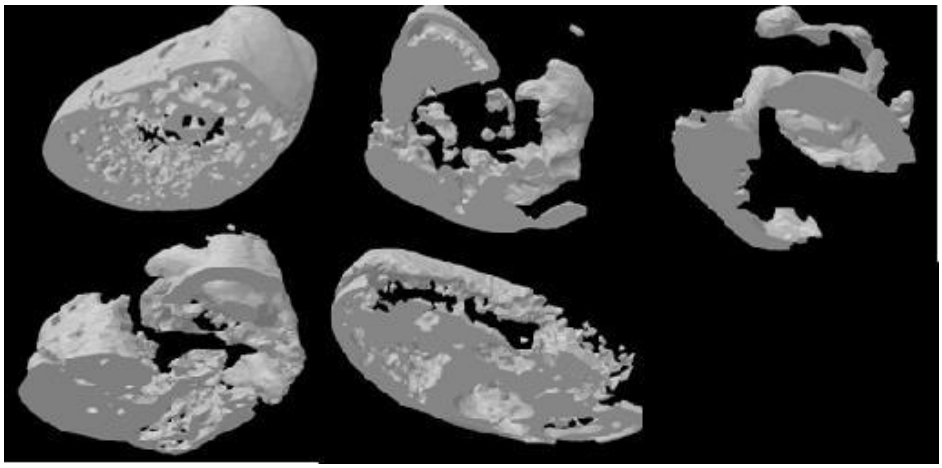

Figure 9.10 The results from 3D Micro computed tomography of five animals in the PSC injected group

Table 9.2 Micro CT analysis between PSC and PBS control

Bone structure parameters	**Treatment group**		**P-value (unpaired t-test)**
	PSC Mean (SEM, n=5)	**PBS (control) Mean (SEM, n=7)**	
BV/TV (%)	34.14 (5.57)	25.03 (8.10)	P = 0.43
Bone surface density (mm^2/mm^3)	4.29 (0.72)	3.18 (0.57)	P = 0.25
Tb.N (1/mm)	0.98 (0.18)	0.74 (0.13)	P = 0.29
Tb.Th (mm)	0.29 (0.03)	0.35 (0.08)	P = 0.55
Tb.Sp (mm)	0.34 (0.03)	0.31 (0.07)	P = 0.65
Bone mineral density (g HA/mm^3)	0.57 (0.01)	0.29 (0.12)	P = 0.04*

9.3.6 **Biomechanical testing**

The functional outcome of bone healing after hPSC injection was demonstrated by biomechanical testing. The summary of biomechanical parameters between the fractured leg (right) and normal leg (left) is presented in **Table 9.3**. The mean of biomechanical parameters of the treated bone gained up to 23.9% (SEM =11.11, n=5) for ultimate force, 15.2% (SEM = 4.44, n=5) for ultimate stress, 9.9% (SEM = 3.11, n=5) for young's modulus, and 67.8% (SEM = 16.19, n=5) for toughness. Mechanical testing in the PBS injection group was not performed due to gross motion against gravity (i.e. the bone deflected at the fracture site under its own weight when held horizontal).

Table 9.3 Biomechanical properties of bone for bone samples from limbs injected with hPSC and from normal bone from the contralateral unoperated side

Mechanical property	**Units**	**Treatment groups (Mean, SEM)**	
		hPSC	**Control (unoperated)**
		(n=5)	(n=5)
Ultimate load	N	51.0 (22.21)	228.2 (11.87)
Ultimate stress	MPa	43.4 (13.40)	299.5 (19.68)
Young's modulus	GPa	0.8 (0.29)	9.0 (1.26)
Toughness	MPa	1.9 (0.53)	2.7 (0.18)

9.4 Summary and discussion

In this chapter, therapeutic effects of hPSCs using percutaneous injection as a minimally invasive technique were assessed in an atrophic non-union model. In the hPSC injection group of five animals, three animals had united at eight weeks after injection and one of them showed sign of progression of healing, while in the control

group, only one of seven animals had bone union at eight weeks. Although there was no statistical difference in union rate between the hPSC treatment and control groups, the bone radiopacity indicated that the degree of bone mineralisation and percentage increase of callus area were significantly improved over the period after hPSC injection. Semi-quantitative analysis of the histomorphology of the fracture gap showed that there was significantly more bone tissue in the hPSC injection group compared to the control group. Similarly the parameters from micro-CT analysis showed significant increases: the BMD was significantly higher in the hPSC treatment group. There were improvements in mechanical properties demonstrated by biomechanical testing. These results suggested that the percutaneous injection of hPSC at the fracture gap at 3 weeks after fracture improved the fracture healing in an atrophic non-union model.

Although it has been reported that hPSCs have demonstrated *in vivo* ectopic bone formation with intramuscular implantation (James et al., 2012b) and bone regeneration effects in a critical size calvarial defect model (James et al., 2012a), the current study is the first to demonstrate the bone regeneration benefit of hPSC in an atrophic non-union model which is relevant to the clinical scenario. These findings support the use of hPSC for bone regeneration. It has been proposed that pericytes or perivascular stem cells are perivascular ancestors of human MSCs (Corselli et al., 2010). The *in vivo* localisation of these cells has been demonstrated (Corselli et al., 2012). In *in vitro* culture, they show the characteristics of MSCs including theirs abilities of proliferation and multi-lineage differentiation (Crisan et al., 2008). It has been reported that PSCs can be isolated from several tissues and can be purified using cell surface markers including positive markers of CD146, NG-2, PDFG-b and negative markers of CD45, CD56, CD31 and CD34 (Crisan et al., 2009, Montemurro et al., 2011, Park et al., 2011). In this study the adipose tissue source was used because it was readily available and easy to harvest and can be used as an alternative source of MSCs. Notably, sufficient PSCs can be obtained without culture expansion but purely by cell selection. A previous published protocol was used in this study. (James et al., 2012a).

As the results reported in chapter 7 found that timing was a critical factor for using MSCs to promote bone healing in an atrophic non-union, the optimal method of preparing sufficient cells in a timely manner should be considered. The results from chapter 8 showed that MSCs from different hosts i.e. allogeneic and even in xenogeneic sources improved the fracture healing in an atrophic non-union without a significant immune response. The findings support the assertion that MSC have an immunoprivileged characteristic. However, the results were in contradiction with previous studies which reported that there was significant increase in immune responses against allogeneic MSCs (Schu et al., 2012, Eliopoulos et al., 2005, Huang et al., 2010). Thus, safety of using stem cells from different donor in cell therapies should be further investigated in appropriate animal models to determine adverse events and to understand further the specific immune reactions of MSCs before clinical application in humans.

Defined perivascular stem cells from adipose tissue or pericytes have the advantage that they could be used autologously as they can be harvested and isolated from enriched source. PSCs can be immediately used as required. It is possible to use hPSCs for cell based therapies within an intraoperative approach to augment fracture repair because the cells can be sorted with sufficient numbers from adipose tissue without culture expansion and implanted back to the fracture site in one setting. Although the stromal vascular fraction of human adipose tissue (SVF) from lipoaspirate can be used intraoperatively to generate autologous cell based therapies for bone repair (Muller et al., 2010), it has been shown that the potential for regeneration was inferior to sorted hPSC from SVF from matched patients (James et al., 2012b). In addition, as hPSCs are a defined and homogeneous cell population, they should have more consistent *in vivo* outcomes in bone repair compared to SVF which contains a nonhomogeneous mixture of, haematopoietic stem cells, progenitor cells and endothelial cells.

Although there was no statistically significant difference in union rate between the hPSC treatment group and the PBS control group, other parameters demonstrated significant improvements in the fracture healing process over the eight week period after cell injection. The underlying mechanisms of PSC for bone regeneration have

not been evaluated in this study. However, there are at least two possible mechanisms; (1) as precursor cells or (2) by paracrine effects (Chen et al., 2009). PSCs can undergo multi-lineage differentiation similar to MSCs and may improve bone regeneration via direct differentiation into osteoblast cell lineages (Crisan et al., 2008). PSCs can secrete several growth factors such as heparin binding epidermal growth factor (HB-EGF), basic fibroblast growth factor (bFGF), platelet derived growth factor-B chain (PDGF-BB), vascular endothelial growth factor (VEGF), keratinocyte growth factor (KGF), angiopoietin 2 (ANG2) and thrombopoietin (TPO) (Chen et al., 2009) and may improve the fracture healing process via vasculogenesis (Askarinam et al., 2013).

Thus, the administration of PSC using percutaneous injection technique may improve the fracture healing process in atrophic non-union. PSCs from adipose tissue have advantages over conventional bone marrow derived MSCs as they are a defined and homogenous population, which can be isolated from the fat tissue abundantly without culture expansion. PSCs may be considered as a potential choice for cell therapies to promote fracture healing in fractures at risk of progressing to atrophic non-union.

Part 4: General discussion, future direction and conclusion

Chapter 10: General discussion

The aim of this thesis was to develop an injectable MSC- based approach to promote fracture healing in atrophic non-union. In this chapter, the main findings and the implications for clinical translation are discussed. The assessments of fracture healing in preclinical studies and the limitation in this study are addressed. Then further investigations are proposed.

10.1 Discussion of the main findings and their clinical implications

A clinical relevant model of atrophic non-union

A number of studies have evaluated bone regeneration potential in segmental defect models (Arinzeh et al., 2003, Tsuchida et al., 2003, Choi et al., 2011), however, these models do not simulate the biological or mechanical conditions of a clinical non-union. For this reason the non-critical defect atrophic model described in chapter 6 was used.

Resection of periosteal tissue and removal of bone marrow at the fracture impaired the healing process. Periosteum and endosteum are biological components required for fracture healing. The role of periosteum and endosteum was demonstrated using mice that express the LacZ reporter gene (Colnot, 2009). This technique can be used for identification of an active enzyme for β-galactosidase using X-gal (5-bromo-4-chloro-3-indolyl-β-D-galactopyranoside) staining. Bone graft with intact periosteum and endosteum was taken from LacZ reporting mice and transplanted at the fracture of wild type mice. Chondrocytes, osteoblasts and osteocytes were recruited from the periosteum and endosteum of the graft, contributing to the fracture healing process. As these structures represent key sources of bone progenitors, their damage can lead

to atrophic non-union. The results from chapter 6 further demonstrated the contribution of local progenitors in an established atrophic non-union.

The insufficient nature of bone Progenitors in local site of atrophic non-union tissue

The regeneration potential of the native progenitors from remote bone marrow (the contralateral femur) of animals with an atrophic non-union model of the tibia was investigated. This study has shown that the non-union appeared to stimulate a systemic response. A clinical study of Marchelli et al, has demonstrated that the serum OPG, which is a bone formation marker, was significantly higher in patients with an atrophic non-union of a shaft fracture indicating that there was a systemic response to the non-union (Marchelli et al., 2009). However, it has been reported that the number of colony forming units from bone marrow in an established atrophic non-union patient was significantly less than in the normal control patient (Seebach et al., 2007). It is possible that the systemic response to fracture or non-union may depend on the stage of the healing process (Bastian et al., 2011) and the results from one time point cannot be extrapolated to other time points.

Local cells in the non-union tissue were investigated. Colony forming units could not be detected from cells isolated from tissue at the atrophic non-union gap. It was postulated that the systemic response in atrophic non-union patients might be higher, whereas local tissue progenitors were unable to contribute sufficiently to the healing process. It has been reported that cells isolated from human non-union tissues have increased senescence and reduced capacity to form osteoblasts, which was associated with significantly elevated secretion of Dickkopf-1 (Dkk-1) (Bajada et al., 2009). In addition, significantly down-regulated factors in non-union osteoblasts included canonical Wnt-, IGF-, TGF-beta-, and FGF-signalling pathways. These factors have been reported to be involved in the proliferation and differentiation of bone progenitors (Hofmann et al., 2008). The results presented here suggest that tissue from atrophic non-unions has an insufficient number of functional progenitors.

The preparation of MSCs from the different tissues

Chapter 3 demonstrated the ease of isolation of rMSCs from three sources relevant to orthopaedics including bone marrow, periosteum and adipose tissue. Human femoral heads were used for isolation of hMSCs as they were readily available and could be used in *in vivo* experiments. Isolated cells were capable of osteogenesis, chondrogenesis and adipogenesis. The results of this study have shown that bone marrow derived and periosteum derived cells had faster growth kinetics than adipose derived cells. The percentages of colony forming units and the colony forming area from bone marrow derived cells and periosteum derived cells were significantly greater than for adipose derived cells.

Colony forming unit assays are based on the ability of MSCs to adhere to plastic and to form colonies when plated at low densities (Prockop, 1997, Colter et al., 2000). The colony forming capacity has been used to present a functional unit of bone marrow derived MSCs (Friedenstein et al., 1974, Owen and Friedenstein, 1988). Morphology and the number of colonies have been shown to be correlated to the cell growth characteristics (Colter et al., 2000, Gothard et al., 2013). The number of colonies formed from cells of different sources has been investigated (Yoshimura et al., 2007). The colony number from passage 0 (after isolation) from the rat synovium, periosteum, adipose, and muscle tissues was higher than those from cells derived from rat bone marrow. Cells-derived from periosteum and adipose tissue gave rise to more colonies than cells-derived from bone marrow. These results were different from the finding in this thesis because of the difference of evaluated cells. The passage of cells (passage 3-4) used in this thesis was later than those used in the aforementioned study (passage 0). The colony forming unit ability of cells after isolation reflected the number of stem cells residing in the stem cell source, while the colony forming unit of the cultured cell represented the proliferative function of the cells. As cells at culture passage 3-4 were used for transplantation in this thesis, cultured MSCs from the different source was investigated to determine the functional ability.

Adipose tissue is more accessible than bone marrow and periosteum, however, the results from this study showed that the growth of cultured cells from this source was significantly slower than the two others sources. In addition, in previous *in vitro* studies (Hayashi, Katsube et al. 2008) and in previous *in vivo* studies (Niemeyer et al., 2010a) the bone regeneration potential of cells from adipose tissuehas been reported to be inferior to cells from a bone marrow source. However, due to the accessibility of adipose tissue, further investigation should focus on how this cell type might be utilised effectively.

In chapter 3, hMSCs were isolated from the femoral heads of patients undergoing hip replacement procedures. These cells were able to differentiate into bone forming cells in osteogenic medium. They exhibited the markers CD90 and CD44 and not the haematopoetic stem cell markers (CD19) or endothelial markers (CD34 and CD31). Our group reported that 90% of cells isolated using this technique expressed CD105 (a recognised MSC marker) (Tremoleda et al., 2012). In order to compare bone regeneration in the *in vivo* model of atrophic non-union, the number of functional units of rMSC and hMSC should be controlled. The results in chapter 3 showed that the growth characteristics and the functional units of cultured rMSCs and hMSCs from the in vitro study were not significantly different. In contrast, Javazon et al (2001) reported that rMSCs can expand more rapidly than hMSCs. This may be because of the differences in rat strain (Barzilay et al., 2009), isolation technique (Bourzac et al., 2010), temperature (Reissis et al., 2013), or culture condition (Ayatollahi et al., 2012), which preclude direct comparison. So, in this study, the source of cultured cells, isolation technique, and culture condition were maintained for all experiments to obtain consistent results.

Timing is a critical factor for an injectable MSC based approach

In chapter 7, the stage of fracture healing was shown to influence the therapeutic potential of MSCs and as such clinical candidates for MSC therapy will have to be carefully selected to obtain favourable outcomes (i.e. patients would need to be with

a few weeks of injury or the fracture repair process would need to be restarted with the operation). The importance of intervention timing has been highlighted in previous studies evaluating the regenerative effect of hMSCs in a rabbit mandible distraction osteogenesis model (Kim et al., 2013). hMSCs suspended in 0.15 ml of saline were injected transcutaneously into the osteotomy gap either before or after distraction. The group receiving injections prior to distraction had superior bone formation compared to those receiving injection after distraction. BMD values and BV/TV ratios at the osteotomy site were also significantly higher in those receiving early injections. These results highlight the importance of injection time and the nature of the underlying disease condition.

In chapter 7, atrophic non-union with MSCs implantation in the late 'post-injury' period (8 weeks) showed no significant improvement of fracture healing. The environment of the non-union site at this stage may not be appropriate to induce or stimulate MSCs to function. Growth factors may be required, in addition to MSCs, to improve fracture healing in an established atrophic non-union. A previous pre-clinical study evaluated the effectiveness of treating established femoral non-union in rat using bone marrow suspension or cultured MSCs (Ferreira et al., 2012). 3 x 10^6 cells in 0.5ml DMEM was injected at the fracture site of established non-union. Treatment with heterologous bone marrow cells was more effective than the cultured MSCs. Bone marrow suspension contains cellular elements and growth factors that can have actions at the docking site of atrophic non-union. These findings suggest that cultured MSC based therapy in late stage of non-union may require additional growth factors with (or possibly without) the exogenous cultured MSCs.

In established atrophic non-unions with a fracture gap, scaffolds may be required. Allogeneic bone graft, demineralized bone matrix, hydroxyapatite and calcium phosphate have been used as carriers for cell delivery. Newly developed scaffolds aim to provide an appropriate environment for cell growth and differentiation while protecting cells from apoptosis. Scaffolds also may have to provide early structural support that may be required, particularly in long bone with large segmental defects.

Cell based therapies should be tailored specifically to the requirements and healing-condition of the fracture. The delivery technique should be applicable and minimise patient morbidity. Cultured MSCs can be used to reduce the risk of fractures developing atrophic non-union. However, the timing for MSC delivery and the clinical scenario of each individual must be taken into account. Additionally, it is important to obtain an adequate number of cells prior to implantation into the fracture site.

Possible strategies using an universal cell donor and alternative cells in fracture healing

The feasibility of using MSCs from an universal cell donor was evaluated in a xenogeneic model. The results from chapter 9 demonstrated that xenogeneic cells can improve bone healing. The findings support the feasibility of using universal donor cells for bone repair. MSCs are immunoprivileged. They can avoid or actively suppress immunological responses because they lack MHC class Ia and MHC class II and co-simulation molecules (Tse et al., 2003). Previous reports from *in vitro* studies demonstrated that MSCs cannot stimulate an immune response in allogeneic lymphocytic cell cultures (Le Blanc et al., 2003). In a number of pre-clinical studies, MSCs have been implanted in allogeneic and xenogeneic models without eliciting an immune response. It has been reported allogeneic transplantation of MSCs improved bone regeneration in a critical-size canine segmental defect without production of alloantibodies (Arinzeh et al., 2003). However, a study from an *in vivo* ovine massive bone tumour implant model, comparing osteointegration at the implant between spraying of autologous and allogeneic MSCs within a fibrin glue carrier, demonstrated significant bone growth in the autologous MSC treatment group, but not in the allogeneic MSC treatment group (Coathup et al., 2013b). The effectiveness of allogeneic MSCs on bone formation may vary in different clinical situation as the *in vivo* environment at the implantation site can influence the ability of cells to contribute to bone regeneration (Barrere et al., 2006). The benefit of MSCs being immune privileged has been shown in xenotransplantation for defects in femoral

bone (Fatkhudinov et al., 2005) and calvarial bone (Zong et al., 2010). Both studies showed that the animals did not have any local pathological reactions or complications when xenogeneic MSCs were implanted and that the MSCs could stimulate reparative osteogenesis significantly. In a clinical study, Horwitz et al. (2004) reported on the allogeneic transplantation of MSC into patients with osteogenesis imperfecta. The study showed an increase in mineral content and that the cells were capable of engraftment and differentiation into osteoblasts (approximate 2%). This study demonstrated the possibility of using allogeneic transplantation in systemic bone disease and indicates the potential of universal donor cells from healthy donors providing and MSCs that can be used as an off-the-shelf therapy for bone repair.

Bone marrow is a conventional source for MSC isolation; however, it is a limited source. The yield of MSCs from bone marrow is relatively small, so cells have to be expanded in appropriate culture conditions to obtain an adequate number of cells prior to implantation into the fracture site. Adipose tissue is more abundantly available but it has been reported that the bone regeneration potential of ASC may be inferior to bone marrow (Hayashi et al., 2008). However, it is possible to improve the regeneration potential by adding growth factors (Niemeyer et al., 2010a). It has been reported that perivascular stem cells (PSCs) or "pericytes" from adipose tissue may serve as a promising source of bone progenitors. Pericytes are capable of osteogenesis, chondrogenesis and adipogenesis. The results from chapter 9 demonstrated the bone regeneration potential of PSCs in an atrophic non-union model.

PSCs have been isolated from the non-cultured total stromal vascular fraction (SVF) of fat tissues using fluorescence-activated cell sorting (FACS). These cells can be purified on the basis of an established repertoire of cell surface markers including the presence of CD146 and the absence of endothelial markers (CD31 and CD34) and a haematopoietic marker (CD45) (Crisan et al., 2008). These cells can be identified *in vivo* in perivascular regions where they display MSC surface markers. *In vitro* these cells also share characteristics including morphology, clonal expansion and multi-lineage potential. It has been reported that hPSCs produce ectopic bone *in vivo*

following intramuscular implantation (James, Zara et al. 2012a) and bone regeneration effects in a critical sized calvarial model (James, Zara et al. 2012b). The findings of chapter 9 are the first reports of PSCs regenerating bone in a clinically relevant atrophic non-union model. These findings support the use of hPSC for bone regeneration. These cells may represent a viable source of MSCs for future clinical bone regeneration strategies.

Injected MSCs disappeared after injection

According to the cell tracing results from chapter 8, there were no hMSCs found in histological sections at four weeks, whereas rMSCs were still detected at the fracture gap at four weeks after cell implantation, but the number of cells appeared to have decreased. Neither hMSC nor rMSC were found at the fracture gap at eight weeks after cell injection. An explanation may be that transplanted MSCs were eliminated by host immune responses after implantation. Although MSCs appear to be immunoprivileged cells, it has been reported that MSCs which undergo osteogenic differentiation *in vivo* subsequently express MCH class II and then lose their immune privileged status (Liu et al., 2006). MHC class I and II play an important role in eliciting immune responses in MHC-mismatched cell donors (Eliopoulos et al., 2005). An in vitro study has shown that rat MSCs which underwent chondrogenic differentiation stimulated peripheral blood in a mixed lymphocyte reaction (MLR) culture and increased cytotoxicity as the differentiated cells expressed co-stimulatory B7 molecule, required to activate cytotoxic T cells (Chen et al., 2007).

The function of transplanted MSCs has been demonstrated in an allogeneic model (Eliopoulos et al., 2005). Genetically modified MSCs which secrete erythropoietin (Epo) were transplanted into allogeneic mice (MHC mismatch) without immunosuppression. Results showed that the Haematocrit (Hct) in MSC-implanted mice rose transiently and declined to baseline values. The Hct increased from a basal to a peak value at 27 days after implantation and then decreased to baseline levels by day 52. Transplantation of MHC mismatched MSCs function transiently at an early

stage of transplantation. Therefore, there may still be a benefit of using exogenous MSCs for bone regeneration as long as the injected MSCs can improve or stimulate fracture healing of the naïve tissues at the fracture site. Results from chapter 8 showed that injected MSCs can contribute to the fracture healing process; however cells disappeared when the fracture progressed to union. This result suggests exogenous MSCs may improve fracture healing via their paracrine effect, but not as progenitor cells. Caplan and Dennis (2006) referred to this as a trophic effect which is an ability of MSCs to secrete a number of cytokines and growth factors which suppress the local immune system, inhibit fibrosis and apoptosis as well as enhance angiogenesis, stimulate mitosis and differentiation of intrinsic tissue. Although, the findings from this study suggested that MSCs play a role in the prevention of atrophic non-union, the mechanisms by which this occurs require further investigation.

10.2 Limitations of the study

Atrophic non-union model

In this study a clinically relevant model of atrophic non-union model resulting from severe injury was used. Wild type systemically healthy rats were used. In clinical practice, patients with non-union may have co-morbidities. In addition, in patients, the degree of injury severity and the fracture configuration varies. In the animal model the osteotomy site and the degree of biological injury were well controlled in order to improve reproducibility. Rodent models are commonly used in preclinical studies of fracture healing. The skeletal structure of bone in rodents is more primitive than human. The representation of cortical remodelling in rodents may be different from humans because of the lack of Haversian systems. However, in this study, the primary aim was not to evaluate cortical structure of bone, but to assess the bone regeneration potential of cell therapy in fracture healing, which is similar in rodents and humans. There are several advantages of using rodents in this study. They are

inexpensive and easy to house. The size of bone is not too small, enabling intricate surgical procedures and facilitating mechanical testing. The stabilization of bone using external fixation was also reliable.

The cells and delivery technique

The effect of cell number was not evaluated in this study, as this study primarily evaluated the efficacy of an injectable MSC-based strategy. Investigating optimal the cell number remains an important issue; however it may be more appropriate to conduct these study in a large animal model which is more similar in size to humans. A potential limitation of this injection technique was leakage which might have reduced the total number of cells injected. To overcome this problem, the size of needle should be small and the speed of injection should be slow. Importantly, cells should be injected when the surgical wound has healed completely preventing leakage from the surgical wound.

Cell tracking

In order to visualise injected cells at the non-union gap and to assess their role, administered cells were labelled using CellTracker (CM-Dil). Following animal sacrifice, the transplanted cells labelled with cellTracker could be assessed using fluorescence microscopy. A limitation of CM-Dil is that a decrease in the signal intensity can occur with cell proliferation (Progatzky et al., 2013). This may lead to incorrect interpretation of results. Thus, an immunohistofluorescence technique using anti-human nuclear antibody with appropriate controls was also applied to identify the human cells in the xenogeneic cell treatment group. This confirmed the CM-dil findings. As injected cells disappeared after healing, the extent of cellular differentiation could not be assessed in this study.

Immunological assessments

In this study, serum samples harvested from each time point were limited, so the multiplex ELISA kit was used to screen inflammatory cytokines simultaneously. Results from each time point were presented as a relative fold difference compared to the zero time point using optical density (OD). Although further investigation of individual cytokines was not performed to obtain the absolute quantities of cytokines, the results from multiplex ELISA kit could detect a significant change in the level of GM-CSF after xenogeneic cell injection. Moreover, the local immune reaction at the popliteal lymph node after cell implantation of exogenous cells was also evaluated using histomorphology (the size of lymph node, the number of follicles, the number of infiltrating cells at the subcapsular sinus and the number of macrophages at the medullary sinus). These results demonstrated the inflammatory reaction after cell injection.

Future directions

Further investigation of clinically relevant MSC based treatments in an established atrophic non-union should be carried out. Although autologous bone graft remains the gold standard for atrophic non-union treatment, autologous bone graft is limited by availability, quantity and donor site morbidity. MSCs based treatment can be used as a less invasive approach which may be beneficial in reducing patient morbidity. However, in MSCs based treatments for established atrophic non-unions, consideration should be made to combining growth factors with transplanted cells. Scaffolds may also be required if there is a significant defect at the non-union site.

The bone regeneration potential of bone marrow derived MSCs and adipose derived PSCs should be compared quantitatively. However, both cell types should be isolated from the same patient or matched patients to minimise the variability introduced by unmatched donors. If the bone regeneration potential of refined PSCs is comparable or better to conventional MSCs from bone marrow, pericyte isolated from adipose tissue may be considered as an alternative cell source. The advantage of using adipose tissue includes its abundance and availability. In addition, PSCs can be sorted without a requirement for *in vitro* culture.

The optimisation of cell carriers for cell administration and development of injectable scaffolds should be investigated to improve the efficacy of cell based approaches, especially in patients requiring early cell therapy. Scaffolds or cell carriers should be considered to enhance cell engraftment, promote differentiation and maximise initial cell survival.

The use of ultrasound to guide percutaneous injection for bone surrounded by a thick soft tissue envelope may improve accuracy of cell delivery. Further investigations should aim to evaluate the potential benefits of cell placement guided by ultrasound guided. These would be most appropriately performed in large animal models or in the clinical setting.

Future studies in large animals should investigate in the optimal cell number required for augmentation of healing. In addition, studies should include long term follow-up to determine the remodelling process of fracture healing and possible adverse effects.

Although results from this thesis have demonstrated a role for MSCs in the improvement of fracture repair in an atrophic non-union model in immunocompetent animals, this did not rely on the differentiation of cells into osteoblasts. However, the mechanisms by which MSCs stimulate fracture repair were not definitively elucidated and they require further investigation. Immunohistological studies on growth factor expression at the fracture gap for both the MSCs and PBS injection groups may be useful to help elucidate these mechanisms. Genetically Engineered MSCs expressing green fluorescence protein (GFP) could be used to trace implanted cells and establish cell fate after injection.

Immunostaining of immune cells at the fracture site and in the lymph nodes could be performed to demonstrate the presence of specific inflammatory cells (e.g. CD68 for macrophages, CD3 for T cell lymphocytes or B220 for B cell lymphocytes)

As PSCs can be purified from SVF without culture, it is interesting to compare bone regeneration potential in vitro (in culture conditions) and in vivo (in the atrophic non-union model) between uncultured PSCs and PSCs which have been expanded in culture.

It is important to investigate the role of endogenous MSCs or progenitor cells at the site of atrophic non-union. Further studies should investigate the temporal change of yield of MSCs from bone marrow during the development of non-union.

In clinical studies, it will be important to use MSCs at an appropriate stage of disease to achieve favourable outcomes. Therefore, the factors characteristics of patients who may be best served by cellular therapy need to be defined.

Ultimately, clinical trials evaluating injectable MSCs based approaches are required to address the efficacy and safety of MSC implantation in the prevention of atrophic non-union. The findings from this thesis suggest that patients who are at high risk of

progressing to non-union, (such as patients with open fractures or heavy smokers) would be good candidates to study.

Conclusion

Stem cell technology, and specifically the use of MSCs, is emerging as a promising treatment to promote fracture healing. Several studies have investigated the potential of MSCs for the regeneration of musculoskeletal tissues. However, the potential for their application in an appropriate and clinically relevant model of fracture non-union has not been explored. The core question for this thesis was how to use MSCs to improve fracture healing in fracture non-unions using an injectable MSC-based approach. A clinically relevant model of atrophic non-union in small animals was established and validated. This model provided insights into the pathogenesis of atrophic non-union. In particular it was found that local progenitor cells at the site of non-union do not have sufficient potency to regenerate bone, as assessed using colony forming ability and tri-lineage differentiation (the capacity to differentiate into bone, cartilage and fat) assays. This inability to regenerate bone may contribute to the progression of non-union. Exogenous stem cells (rMSCs, hMSCs and PSCs) were shown in the animal model to rescue bones destined to proceed to no-union from doing so. Results from this thesis also suggested the feasibility of using MSCs as universal donor cells and using alternative adipose derived PSCs for improving bone repair in atrophic non-union. These may allow the development of an "off-the-shelf" cellular therapy that could be used for any patient at risk of progressing to atrophic non-union without delay. It is important to consider the timing of cell injection when devising MSC treatment protocols. The findings of this thesis have improved the understanding of the regenerative processes involved in fracture healing and how these may be augmented, using MSCs, in the setting of atrophic non-union. These results can form the basis for establishing a valid and innovative biological technique for the treatment of long bone non-unions.

This study has examined the hypothesis "Percutaneous injection of MSCs promotes the process of fracture repair in a small animal model of atrophic non-union". The findings support this hypothesis.

Appendices

Appendix A:

The effects of CM-Dil on MSCs

In this study, CM-Dil staining was a method of choice to track cells *in vivo*. According to the company's recommendation, it is suggested that CM-Dil is soluble at concentrations up to 20 µg/ml. The following bar graphs demonstrate a cell viability and CFU-F as functional assay of labelled hMSCs at different concentrations. The labelling of 2.5 µg/ml CM-Dil protocol seems to be an optimum choice.

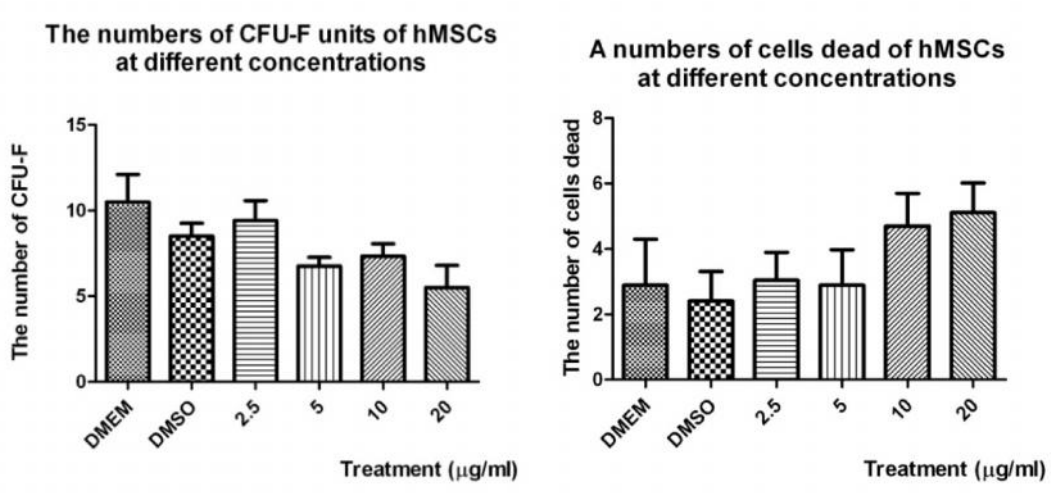

Bar graphs show the number of CFU-F units (**upper**) and the number of cell dead (**lower**) at the different units: DMEM, culture media and DMSO (Dimethyl sulfoxide), solvent solution

Appendix B:

Protocols used in this study

H&E Method:

- Place sections in a rack and dewax in xylene for 15 minutes
- Rehydrate through graded alcohol: 100%, 100% ,90%, 70%, respectively for 2 minutes each
- Rinse in running tap water and then in distilled water
- Place in Mayer's haematoxylin for 7 minutes
- Rinse in running tap water and then in distilled water to remove excess stain
- Blue section in 2% hydrogen carbonate for 2 minutes
- Rinse in running tap water
- Place in Eosin for 5 minutes
- Rinse in running tap water
- Dehydrate through graded alcohols: 70%, 90%, 100% and 100%, respectively for 2 minute each
- Place in xylene clearing and mount one at a time in DPX
- Observe under light microscope

Modified Masson's Trichrome Method:

- Place sections in a rack and dewax in xylene for 15 minutes
- Rehydrate through graded alcohol: 100%, 100% ,90%, 70%, respectively for 2 minutes each
- Rinse in running tap water and then in distilled water
- Stain with ferric chloride for 3 minutes
- Rinse in running tap water and then in distilled water to remove excess stain
- Stain with Mayar 's haematoxylin (diluted in water 1:10) for 1 minute
- Rinse in running tap water

- Stain with Ponceau-acid fuchsin for 8 minutes
- Rinse quickly with 0.5% acetic acid
- Stain with 0.5% Phosphomolybdic acid for 3 minutes
- Rinse quickly with 0.5% acetic acid
- Stain with light green for 5 minutes
- Rinse quickly with 0.5% acetic acid
- Dehydrate through graded alcohols: 70%, 90%, 100% and 100%, respectively for 2 minute each
- Place in xylene clearing and mount one at a time in DPX
- Observe under light microscope

Safranin-O/Fast green Method:

- Place sections in a rack and dewax in xylene for 15 minutes
- Rehydrate through graded alcohol: 100%, 100%, 90%, 70%, respectively for 2 minutes each
- Rinse in running tap water and then in distilled water
- Stain with Mayar ‘s haematoxylin (diluted in water 1:10) for 1 minute
- Rinse in running tap water
- Stain with fast green (FCF) solution for 5 minutes
- Rinse quickly with 1% acetic acid solution for no more than 10 –15 seconds
- Stain in 0.1% safranin O solution for 5 minutes
- Rinse quickly with 1% acetic acid solution for no more than 10 –15 seconds
- Dehydrate through graded alcohols: 70%, 90%, 100% and 100%, respectively for 2 minute each
- Place in xylene clearing and mount one at a time in DPX
- Observe under light microscope

The Brief Protocol for Rat Inflammatory Cytokines Multi-Analyte ELISArray Kit (SABiosciences^{TM}, USA)

- Prepare replicate serial dilutions of the Antigen Standard and your experimental samples
- Pipette 50 µl of Assay Buffer into each well of the 8-well ELISA strips
- Transfer 50 µl samples and/or standards to the appropriate wells of the ELISA strips
- Gently shake or tap plate for 10 seconds. Incubate for 2 hours at room temperature
- Decant or aspirate well contents. Add 350 µl 1 × Washing Buffer. Gently shake or tap plate for 10 seconds. Decant or aspirate. Blot array upside down on absorbent paper to remove any residual buffer **(step for Washing ELISA Wells)**
- Repeat wash twice more
- Pipette 100 µl of Detection Antibody solution. Incubate 1 hour at room temperature
- Wash ELISA wells as described above
- Add 100 µl Avidin-HRP solutions to all wells. Incubate for 30 minutes at room temperature.
- Wash ELISA wells for a total of 4 washes
- Add 100 µl of Development Solution to each well. Incubate the plate for 15 minutes at room temperature in the dark
- Add 100 µl of Stop Solution to each well. The colour changes from blue to yellow
- Read absorbance at 450 nm within 30 minutes of stopping the reaction. If wavelength correction is available, subtract readings at 570 nm from the reading at 450 nm

Appendix C

Presentations at National and International Meetings

Poster presentations

"Bone Regeneration Potential Using Adult Stem Cells in Atrophic Non-union" in Post-graduation open day, QMRI, University of Edinburgh, UK, on the 18th November 2011 (The best poster award, QMRI)

"Available Sources of Mesenchymal Stem Cell in Orthopaedic" in Regeneration strategies and innovative biomaterials in orthopaedic surgery meeting, University of Brighton, on the 3rd April 2012

"Non-Critical Size Defect Atrophic Non-union Model in Rat; Surgical technique and its mesenchymal progenitor cells" in the 13th The European Federation of National Associations of Orthopaedics and Traumatology (EFFORT) Congress in Berlin, Germany, on the 23rd-25th May2012

"Validation of the radiographic union scale in tibia and Lane & Sandhu scoring system for fracture healing in small animal model" in BRS/BORS (Bone Research Society and the British Orthopaedic Research Society) Annual Meeting in Oxford, UK, on the 4th-5th September 2013

"Xenogeneic Implantation of Human Mesenchymal Stem cells to Promote Fracture Healing in Atrophic Non-Union Model" ORS (Orthopaedic Research Society) Annual Meeting in New Orleans, USA, on the 15th-18th March 2014 (Accepted for presentation)

Podium presentations

"Comparison of biomechanical testing using 4-point bending in rat tibia between specimen with and without muscle" in British Orthopaedic research society (BORS) Annual Meeting (2012) in Stratford Circus, London, UK, on the 24th-25th September 2012 (Bursary awarded)

"Critical time point for MSCs implantation in atrophic non-union" in EORS (European Orthopaedic research society) Annual Meeting in Amsterdam, 26th – 28th September 2012

"Role of perivascular stem cells in the prevention of atrophic non-union" in BRS/BORS (Bone Research Society and the British Orthopaedic Research Society) Annual Meeting (2013), Oxford, UK, on the 4th-5th September 2013

"Role of perivascular stem cells in the prevention of atrophic non-union" in School of surgery days, The Royal College of Surgeons of Edinburgh, Edinburgh, UK, on the 29th November 2013

Invitations

Speaker: "Roles of mesenchymal stem cells for atrophic non-union", The 1st Thai-UK Stem Cell Network meeting, Sheffield, UK, on the 5th-7th April 2011

Co-chairperson with Dr Ines Reichert: "Session 4" BORS (British Orthopaedic research society) 2012, in Stratford Circus, London, UK, on the 24th-25th September 2012

Co-chairperson with Dr Martin Stoddard: "Stem Cell Session" in EORS (European Orthopaedic research society) 2012, in Amsterdam, Netherlands, on the 26th – 28th September 2012

Appendix D

Publications

Publication in Conference proceeding

"Comparison of Biomechanical Testing Using 4-Point Bending in Rat Tibia Between Specimen with And without Muscle" Tawonsawatruk T, Spadaccino A, Wallace RJ, Simpson H The Bone & Joint Journal (Orthopaedic Proceedings) 2013 vol. 95-B no. sup. 13 16

Publications in peer-reviewed journals

"Natural history of mesenchymal stem cells, from vessel walls to culture vessels" Murray IR, West CC, Hardy WR, James AW, Park TS, Nguyen A, Tawonsawatruk T, Lazzari L, Soo C, Péault B. Cellular and Molecular Life Sciences. 2013 Oct 25. [Epub ahead of print]

"Evaluation of Native Mesenchymal Stem Cells from Bone Marrow and Local Tissue in an Atrophic Non-union Model" Tawonsawatruk T, Kelly MB, Simpson H. Tissue Engineering Part C: Methods. 2013 Oct 22. [Epub ahead of print]

"Growth kinetics of rat mesenchymal stem cells from 3 potential sources: bone marrow, periosteum and adipose tissue" Tawonsawatruk T, Spadaccino A, Murray IR, Peault B, Simpson HA. Journal of the Medical Association of Thailand. 2012 Oct; 95 Suppl 10:S189-97.

References

AARON, R. K., CIOMBOR, D. M. & SIMON, B. J. 2004. Treatment of nonunions with electric and electromagnetic fields. *Clin Orthop Relat Res***,** 21-9.

ABERG, T., CAVENDER, A., GAIKWAD, J. S., BRONCKERS, A. L., WANG, X., WALTIMO-SIREN, J., THESLEFF, I. & D'SOUZA, R. N. 2004. Phenotypic changes in dentition of Runx2 homozygote-null mutant mice. *J Histochem Cytochem,* 52**,** 131-9.

ADAMS, C. I., KEATING, J. F. & COURT-BROWN, C. M. 2001. Cigarette smoking and open tibial fractures. *Injury,* 32**,** 61-5.

AGGARWAL, S. & PITTENGER, M. F. 2005. Human mesenchymal stem cells modulate allogeneic immune cell responses. *Blood,* 105**,** 1815-22.

AKHTER, M. P., IWANIEC, U. T., HAYNATZKI, G. R., FUNG, Y. K., CULLEN, D. M. & RECKER, R. R. 2003. Effects of nicotine on bone mass and strength in aged female rats. *J Orthop Res,* 21**,** 14-9.

ALLEN, H. L., WASE, A. & BEAR, W. T. 1980. Indomethacin and aspirin: effect of nonsteroidal anti-inflammatory agents on the rate of fracture repair in the rat. *Acta Orthop Scand,* 51**,** 595-600.

ANTONOVA, E., LE, T. K., BURGE, R. & MERSHON, J. 2013. Tibia shaft fractures: costly burden of nonunions. *BMC Musculoskelet Disord,* 14**,** 42.

ARINZEH, T. L., PETER, S. J., ARCHAMBAULT, M. P., VAN DEN BOS, C., GORDON, S., KRAUS, K., SMITH, A. & KADIYALA, S. 2003. Allogeneic mesenchymal stem cells regenerate bone in a critical-sized canine segmental defect. *J Bone Joint Surg Am,* 85-A**,** 1927-35.

ASKARINAM, A., JAMES, A. W., ZARA, J. N., GOYAL, R., CORSELLI, M., PAN, A., LIANG, P., CHANG, L., RACKOHN, T., STOKER, D., ZHANG, X., TING, K., PEAULT, B. & SOO, C. 2013. Human perivascular stem cells show enhanced osteogenesis and vasculogenesis with Nel-like molecule I protein. *Tissue Eng Part A,* 19**,** 1386-97.

ASPEN, R.M. 2003 Mechanical testing of bone ex vivo. IN: HELFRICH, M. H., RALSTON, S. (Eds.) *Bone Research Protocols*, Totowa, NJ: Humana Press, pp369-379.

ATOUI, R., ASENJO, J. F., DUONG, M., CHEN, G., CHIU, R. C. & SHUM-TIM, D. 2008. Marrow stromal cells as universal donor cells for myocardial regenerative therapy: their unique immune tolerance. *Ann Thorac Surg,* 85**,** 571-9.

AUBIN, J. E. 1998. Bone stem cells. *J Cell Biochem Suppl,* 30-31**,** 73-82.

AUDIGE, L., GRIFFIN, D., BHANDARI, M., KELLAM, J. & RUEDI, T. P. 2005. Path analysis of factors for delayed healing and nonunion in 416 operatively treated tibial shaft fractures. *Clin Orthop Relat Res,* 438**,** 221-32.

AUER, J. A., GOODSHIP, A., ARNOCZKY, S., PEARCE, S., PRICE, J., CLAES, L., VON RECHENBERG, B., HOFMANN-AMTENBRINCK, M., SCHNEIDER, E., MULLER-TERPITZ, R., THIELE, F., RIPPE, K. P. & GRAINGER, D. W. 2007. Refining animal models in fracture research:

seeking consensus in optimising both animal welfare and scientific validity for appropriate biomedical use. *BMC Musculoskelet Disord,* 8**,** 72.
AYATOLLAHI, M., SALMANI, M. K., GERAMIZADEH, B., TABEI, S. Z., SOLEIMANI, M. & SANATI, M. H. 2012. Conditions to improve expansion of human mesenchymal stem cells based on rat samples. *World J Stem Cells,* 4**,** 1-8.
BAJADA, S., HARRISON, P. E., ASHTON, B. A., CASSAR-PULLICINO, V. N., ASHAMMAKHI, N. & RICHARDSON, J. B. 2007. Successful treatment of refractory tibial nonunion using calcium sulphate and bone marrow stromal cell implantation. *J Bone Joint Surg Br,* 89**,** 1382-6.
BAJADA, S., MARSHALL, M. J., WRIGHT, K. T., RICHARDSON, J. B. & JOHNSON, W. E. 2009. Decreased osteogenesis, increased cell senescence and elevated Dickkopf-1 secretion in human fracture non union stromal cells. *Bone,* 45**,** 726-35.
BALL, M. D., BONZANI, I. C., BOVIS, M. J., WILLIAMS, A. & STEVENS, M. M. 2011. Human periosteum is a source of cells for orthopaedic tissue engineering: a pilot study. *Clin Orthop Relat Res,* 469**,** 3085-93.
BARA, T. & SYNDER, M. 2007. Nine-years experience with the use of shock waves for treatment of bone union disturbances. *Ortop Traumatol Rehabil,* 9**,** 254-8.
BARRERE, F., VAN BLITTERSWIJK, C. A. & DE GROOT, K. 2006. Bone regeneration: molecular and cellular interactions with calcium phosphate ceramics. *Int J Nanomedicine,* 1**,** 317-32.
BARRY, F. P. & MURPHY, J. M. 2004. Mesenchymal stem cells: clinical applications and biological characterization. *Int J Biochem Cell Biol,* 36**,** 568-84.
BARRY, F. P., MURPHY, J. M., ENGLISH, K. & MAHON, B. P. 2005. Immunogenicity of adult mesenchymal stem cells: lessons from the fetal allograft. *Stem Cells Dev,* 14**,** 252-65.
BARZILAY, R., SADAN, O., MELAMED, E. & OFFEN, D. 2009. Comparative characterization of bone marrow-derived mesenchymal stromal cells from four different rat strains. *Cytotherapy,* 11**,** 435-42.
BASCHETTI, R. 2005. Ethics of embryonic stem cell technology: science versus philosophy. *Intern Med J,* 35**,** 499-500; author reply 500-1.
BASHARDOUST TAJALI, S., HOUGHTON, P., MACDERMID, J. C. & GREWAL, R. 2011. Effects of Low-Intensity Pulsed Ultrasound Therapy on Fracture Healing: A Systematic Review and Meta-Analysis. *Am J Phys Med Rehabil*.
BASSETT, C. A., MITCHELL, S. N. & GASTON, S. R. 1981. Treatment of ununited tibial diaphyseal fractures with pulsing electromagnetic fields. *J Bone Joint Surg Am,* 63**,** 511-23.
BASTIAN, O., PILLAY, J., ALBLAS, J., LEENEN, L., KOENDERMAN, L. & BLOKHUIS, T. 2011. Systemic inflammation and fracture healing. *J Leukoc Biol,* 89**,** 669-73.
BEYTH, S., DASKAL, A., KHOURY, A., MOSHEIFF, R. & LIEBERGALL, M.. 2008. Cigrette smoking is associated with lower concentration of bone

marrow mesenchymal stem cells. *J Bone Joint Surg Br* vol. 90-B no. SUPP III 515.
BHANDARI, M., GUYATT, G. H., SWIONTKOWSKI, M. F., TORNETTA, P., 3RD, SPRAGUE, S. & SCHEMITSCH, E. H. 2002. A lack of consensus in the assessment of fracture healing among orthopaedic surgeons. *J Orthop Trauma,* 16**,** 562-6.
BHANDARI, M., KOOISTRA, B.W., BUSSE, J., WALTER, S.D., TORNETTA, P. & SCHEMITSCH, E.H. 2011 Radiographic union scale for tibia (R.U.S.T.) fracture healing assessment: preliminary validation. IN: FRANK, C. (Ed.) *Canadian Orthopaedic Association (COA)/ Canadian Orthopaedic Research Society (CORS)/ Canadian Orthopaedic Residents' Association (CORA), 17–20 June 2010. Edmonton, Alberta, Canada,* J Bone Joint Surg Br 2011 vol. 93-B no. SUPP IV 575
BHANDARI, M. & SHAUGHNESSY, S. 2001. A minimally invasive percutaneous technique of intramedullary nail insertion in an animal model of fracture healing. *Arch Orthop Trauma Surg,* 121**,** 591-3.
BIELBY, R., JONES, E. & MCGONAGLE, D. 2007. The role of mesenchymal stem cells in maintenance and repair of bone. *Injury,* 38 Suppl 1**,** S26-32.
BIGHAM, A. S., DEHGHANI, S. N., SHAFIEI, Z. & TORABI NEZHAD, S. 2008. Xenogenic demineralized bone matrix and fresh autogenous cortical bone effects on experimental bone healing: radiological, histopathological and biomechanical evaluation. *J Orthop Traumatol,* 9**,** 73-80.
BLAND, J. M. & ALTMAN, D. G. 2009. Analysis of continuous data from small samples. *BMJ,* 338**,** a3166.
BOHNER, M. 2000. Calcium orthophosphates in medicine: from ceramics to calcium phosphate cements. *Injury,* 31 Suppl 4**,** 37-47.
BOLANDER, M. E. 1992. Regulation of fracture repair by growth factors. *Proc Soc Exp Biol Med,* 200**,** 165-70.
BONDARENKO, A., HEWICKER-TRAUTWEIN, M., ERDMANN, N., ANGRISANI, N., REIFENRATH, J. & MEYER-LINDENBERG, A. 2011. Comparison of morphological changes in efferent lymph nodes after implantation of resorbable and non-resorbable implants in rabbits. *Biomed Eng Online,* 10**,** 32.
BONEWALD, L. F. & JOHNSON, M. L. 2008. Osteocytes, mechanosensing and Wnt signaling. *Bone,* 42**,** 606-15.
BOURZAC, C., SMITH, L. C., VINCENT, P., BEAUCHAMP, G., LAVOIE, J. P. & LAVERTY, S. 2010. Isolation of equine bone marrow-derived mesenchymal stem cells: a comparison between three protocols. *Equine Vet J,* 42**,** 519-27.
BOUXSEIN, M. L., BOYD, S. K., CHRISTIANSEN, B. A., GULDBERG, R. E., JEPSEN, K. J. & MULLER, R. 2010. Guidelines for assessment of bone microstructure in rodents using micro-computed tomography. *J Bone Miner Res,* 25**,** 1468-86.
BOYLE, W. J., SIMONET, W. S. & LACEY, D. L. 2003. Osteoclast differentiation and activation. *Nature,* 423**,** 337-42.
BRINKER, M. R., O'CONNOR, D. P., MONLA, Y. T. & EARTHMAN, T. P. 2007. Metabolic and endocrine abnormalities in patients with nonunions. *J Orthop Trauma,* 21**,** 557-70.

BROULIK, P. D., ROSENKRANCOVA, J., RUZICKA, P., SEDLACEK, R. & KURCOVA, I. 2007. The effect of chronic nicotine administration on bone mineral content and bone strength in normal and castrated male rats. *Horm Metab Res,* 39**,** 20-4.

BROULIK, P. D., VONDROVA, J., RUZICKA, P., SEDLACEK, R. & ZIMA, T. 2010. The effect of chronic alcohol administration on bone mineral content and bone strength in male rats. *Physiol Res,* 59**,** 599-604.

BROWNLOW, H. C., REED, A., JOYNER, C. & SIMPSON, A. H. 2000. Anatomical effects of periosteal elevation. *J Orthop Res,* 18**,** 500-2.

BROWNLOW, H. C. & SIMPSON, A. H. 2000. Metabolic activity of a new atrophic nonunion model in rabbits. *J Orthop Res,* 18**,** 438-42.

BRUDER, S. P., KRAUS, K. H., GOLDBERG, V. M. & KADIYALA, S. 1998. The effect of implants loaded with autologous mesenchymal stem cells on the healing of canine segmental bone defects. *J Bone Joint Surg Am,* 80**,** 985-96.

BUCKWALTER, J. A., GLIMCHER, M. J., COOPER, R. R. & RECKER, R. 1996. Bone biology. II: Formation, form, modeling, remodeling, and regulation of cell function. *Instr Course Lect,* 45**,** 387-99.

BURD, T. A., HUGHES, M. S. & ANGLEN, J. O. 2003. Heterotopic ossification prophylaxis with indomethacin increases the risk of long-bone nonunion. *J Bone Joint Surg Br,* 85**,** 700-5.

BURR, D. B. 2002. Targeted and nontargeted remodeling. *Bone,* 30**,** 2-4.

CAPLAN, A. I. 1991. Mesenchymal stem cells. *J Orthop Res,* 9**,** 641-50.

CAPLAN, A. I. & DENNIS, J. E. 2006. Mesenchymal stem cells as trophic mediators. *J Cell Biochem,* 98**,** 1076-84.

CARTER, D. R., BEAUPRE, G. S., GIORI, N. J. & HELMS, J. A. 1998. Mechanobiology of skeletal regeneration. *Clin Orthop Relat Res***,** S41-55.

CASTILLO, R. C., BOSSE, M. J., MACKENZIE, E. J. & PATTERSON, B. M. 2005. Impact of smoking on fracture healing and risk of complications in limb-threatening open tibia fractures. *J Orthop Trauma,* 19**,** 151-7.

CERADINI, D. J., KULKARNI, A. R., CALLAGHAN, M. J., TEPPER, O. M., BASTIDAS, N., KLEINMAN, M. E., CAPLA, J. M., GALIANO, R. D., LEVINE, J. P. & GURTNER, G. C. 2004. Progenitor cell trafficking is regulated by hypoxic gradients through HIF-1 induction of SDF-1. *Nat Med,* 10**,** 858-64.

CHAKKALAKAL, D. A. 2005. Alcohol-induced bone loss and deficient bone repair. *Alcohol Clin Exp Res,* 29**,** 2077-90.

CHALIDIS, B., SACHINIS, N., ASSIOTIS, A. & MACCAURO, G. 2011. Stimulation of bone formation and fracture healing with pulsed electromagnetic fields: biologic responses and clinical implications. *Int J Immunopathol Pharmacol,* 24**,** 17-20.

CHAMBERLAIN, G., FOX, J., ASHTON, B. & MIDDLETON, J. 2007. Concise review: mesenchymal stem cells: their phenotype, differentiation capacity, immunological features, and potential for homing. *Stem Cells,* 25**,** 2739-49.

CHAMBERLAIN, J. R., DEYLE, D. R., SCHWARZE, U., WANG, P., HIRATA, R. K., LI, Y., BYERS, P. H. & RUSSELL, D. W. 2008. Gene targeting of mutant COL1A2 alleles in mesenchymal stem cells from individuals with osteogenesis imperfecta. *Mol Ther,* 16**,** 187-93.

CHEN, C. W., MONTELATICI, E., CRISAN, M., CORSELLI, M., HUARD, J., LAZZARI, L. & PEAULT, B. 2009. Perivascular multi-lineage progenitor cells in human organs: regenerative units, cytokine sources or both? *Cytokine Growth Factor Rev,* 20**,** 429-34.

CHEN, G., DENG, C. & LI, Y. P. 2012. TGF-beta and BMP signaling in osteoblast differentiation and bone formation. *Int J Biol Sci,* 8**,** 272-88.

CHEN, X., MCCLURG, A., ZHOU, G. Q., MCCAIGUE, M., ARMSTRONG, M. A. & LI, G. 2007. Chondrogenic differentiation alters the immunosuppressive property of bone marrow-derived mesenchymal stem cells, and the effect is partially due to the upregulated expression of B7 molecules. *Stem Cells,* 25**,** 364-70.

CHERIAN, P. P., CHENG, B., GU, S., SPRAGUE, E., BONEWALD, L. F. & JIANG, J. X. 2003. Effects of mechanical strain on the function of Gap junctions in osteocytes are mediated through the prostaglandin EP2 receptor. *J Biol Chem,* 278**,** 43146-56.

CHOI, H. J., KIM, J. M., KWON, E., CHE, J. H., LEE, J. I., CHO, S. R., KANG, S. K., RA, J. C. & KANG, B. C. 2011. Establishment of efficacy and safety assessment of human adipose tissue-derived mesenchymal stem cells (hATMSCs) in a nude rat femoral segmental defect model. *J Korean Med Sci,* 26**,** 482-91.

CLAES, L., BLAKYTNY, R., GOCKELMANN, M., SCHOEN, M., IGNATIUS, A. & WILLIE, B. 2009. Early dynamization by reduced fixation stiffness does not improve fracture healing in a rat femoral osteotomy model. *J Orthop Res,* 27**,** 22-7.

CLAES, L. E. & HEIGELE, C. A. 1999. Magnitudes of local stress and strain along bony surfaces predict the course and type of fracture healing. *J Biomech,* 32**,** 255-66.

CLARKE, B. 2008. Normal bone anatomy and physiology. *Clin J Am Soc Nephrol,* 3 Suppl 3**,** S131-9.

CLARKE, K. A. 1995. Differential fore- and hindpaw force transmission in the walking rat. *Physiol Behav,* 58**,** 415-9.

COATHUP, M. J., CAI, Q., CAMPION, C., BUCKLAND, T. & BLUNN, G. W. 2013a. The effect of particle size on the osteointegration of injectable silicate-substituted calcium phosphate bone substitute materials. *J Biomed Mater Res B Appl Biomater,* 101**,** 902-10.

COATHUP, M. J., KALIA, P., KONAN, S., MIRZA, K. & BLUNN, G. W. 2013b. A comparison of allogeneic and autologous mesenchymal stromal cells and osteoprogenitor cells in augmenting bone formation around massive bone tumor prostheses. *J Biomed Mater Res A,* 101**,** 2210-8.

COHEN, J. L. & SUDRES, M. 2009. A role for mesenchymal stem cells in the control of graft-versus-host disease. *Transplantation*, 87, S53-4.

COLNOT, C. 2009. Skeletal cell fate decisions within periosteum and bone marrow during bone regeneration. *J Bone Miner Res,* 24**,** 274-82.

COLTER, D. C., CLASS, R., DIGIROLAMO, C. M. & PROCKOP, D. J. 2000. Rapid expansion of recycling stem cells in cultures of plastic-adherent cells from human bone marrow. *Proc Natl Acad Sci U S A,* 97**,** 3213-8.

CONNOLLY, J. F. 1998. Clinical use of marrow osteoprogenitor cells to stimulate osteogenesis. *Clin Orthop Relat Res*, S257-66.
CONNOLLY, J. F. & SHINDELL, R. 1986. Percutaneous marrow injection for an ununited tibia. *Nebr Med J,* 71, 105-7.
COOK, J. E. & CUNNINGHAM, J. L. 1995. The assessment of fracture healing using dual x-ray absorptiometry: a feasibility study using phantoms. *Phys Med Biol,* 40, 119-36.
CORRALES, L. A., MORSHED, S., BHANDARI, M. & MICLAU, T., 3RD 2008. Variability in the assessment of fracture-healing in orthopaedic trauma studies. *J Bone Joint Surg Am,* 90, 1862-8.
CORSELLI, M., CHEN, C. W., CRISAN, M., LAZZARI, L. & PEAULT, B. 2010. Perivascular ancestors of adult multipotent stem cells. *Arterioscler Thromb Vasc Biol,* 30, 1104-9.
CORSELLI, M., CHEN, C. W., SUN, B., YAP, S., RUBIN, J. P. & PEAULT, B. 2012. The tunica adventitia of human arteries and veins as a source of mesenchymal stem cells. *Stem Cells Dev,* 21, 1299-308.
COURT-BROWN, C. M. & CAESAR, B. 2006. Epidemiology of adult fractures: A review. *Injury,* 37, 691-7.
CRISAN, M., CHEN, C. W., CORSELLI, M., ANDRIOLO, G., LAZZARI, L. & PEAULT, B. 2009. Perivascular multipotent progenitor cells in human organs. *Ann N Y Acad Sci,* 1176, 118-23.
CRISAN, M., YAP, S., CASTEILLA, L., CHEN, C. W., CORSELLI, M., PARK, T. S., ANDRIOLO, G., SUN, B., ZHENG, B., ZHANG, L., NOROTTE, C., TENG, P. N., TRAAS, J., SCHUGAR, R., DEASY, B. M., BADYLAK, S., BUHRING, H. J., GIACOBINO, J. P., LAZZARI, L., HUARD, J. & PEAULT, B. 2008. A perivascular origin for mesenchymal stem cells in multiple human organs. *Cell Stem Cell,* 3, 301-13.
CROS, J., CAGNARD, N., WOOLLARD, K., PATEY, N., ZHANG, S. Y., SENECHAL, B., PUEL, A., BISWAS, S. K., MOSHOUS, D., PICARD, C., JAIS, J. P., D'CRUZ, D., CASANOVA, J. L., TROUILLET, C. & GEISSMANN, F. 2010. Human CD14dim monocytes patrol and sense nucleic acids and viruses via TLR7 and TLR8 receptors. *Immunity*, 33, 375-86.
DAVIDSON, M. K., LINDSEY, J. R. & DAVIS, J. K. 1987. Requirements and selection of an animal model. *Isr J Med Sci,* 23, 551-5.
DE BARI, C., DELL'ACCIO, F., TYLZANOWSKI, P. & LUYTEN, F. P. 2001. Multipotent mesenchymal stem cells from adult human synovial membrane. *Arthritis Rheum,* 44, 1928-42.
DE BARI, C., DELL'ACCIO, F., VANLAUWE, J., EYCKMANS, J., KHAN, I. M., ARCHER, C. W., JONES, E. A., MCGONAGLE, D., MITSIADIS, T. A., PITZALIS, C. & LUYTEN, F. P. 2006. Mesenchymal multipotency of adult human periosteal cells demonstrated by single-cell lineage analysis. *Arthritis Rheum,* 54, 1209-21.
DELAISSE, J. M., ANDERSEN, T. L., ENGSIG, M. T., HENRIKSEN, K., TROEN, T. & BLAVIER, L. 2003. Matrix metalloproteinases (MMP) and cathepsin K contribute differently to osteoclastic activities. *Microsc Res Tech,* 61, 504-13.

DELIUS, M., DRAENERT, K., AL DIEK, Y. & DRAENERT, Y. 1995. Biological effects of shock waves: in vivo effect of high energy pulses on rabbit bone. *Ultrasound Med Biol,* 21**,** 1219-25.

DEVINE, S. M., COBBS, C., JENNINGS, M., BARTHOLOMEW, A. & HOFFMAN, R. 2003. Mesenchymal stem cells distribute to a wide range of tissues following systemic infusion into nonhuman primates. *Blood,* 101**,** 2999-3001.

DOMINICI, M., LE BLANC, K., MUELLER, I., SLAPER-CORTENBACH, I., MARINI, F., KRAUSE, D., DEANS, R., KEATING, A., PROCKOP, D. & HORWITZ, E. 2006. Minimal criteria for defining multipotent mesenchymal stromal cells. The International Society for Cellular Therapy position statement. *Cytotherapy,* 8**,** 315-7.

DONZELLI, E., SALVADE, A., MIMO, P., VIGANO, M., MORRONE, M., PAPAGNA, R., CARINI, F., ZAOPO, A., MILOSO, M., BALDONI, M. & TREDICI, G. 2007. Mesenchymal stem cells cultured on a collagen scaffold: In vitro osteogenic differentiation. *Arch Oral Biol,* 52**,** 64-73.

DUCY, P., ZHANG, R., GEOFFROY, V., RIDALL, A. L. & KARSENTY, G. 1997. Osf2/Cbfa1: a transcriptional activator of osteoblast differentiation. *Cell,* 89**,** 747-54.

EASTAUGH-WARING, S. J., JOSLIN, C. C., HARDY, J. R. & CUNNINGHAM, J. L. 2009. Quantification of fracture healing from radiographs using the maximum callus index. *Clin Orthop Relat Res,* 467**,** 1986-91.

EINHORN, T. A. 1999. Clinically applied models of bone regeneration in tissue engineering research. *Clin Orthop Relat Res***,** S59-67.

EINHORN, T. A., MAJESKA, R. J., RUSH, E. B., LEVINE, P. M. & HOROWITZ, M. C. 1995. The expression of cytokine activity by fracture callus. *J Bone Miner Res,* 10**,** 1272-81.

ELIOPOULOS, N., STAGG, J., LEJEUNE, L., POMMEY, S. & GALIPEAU, J. 2005. Allogeneic marrow stromal cells are immune rejected by MHC class I- and class II-mismatched recipient mice. *Blood,* 106**,** 4057-65.

ELMORE, S. A. 2006. Histopathology of the lymph nodes. *Toxicol Pathol,* 34**,** 425-54.

ELSTER, E. A., STOJADINOVIC, A., FORSBERG, J., SHAWEN, S., ANDERSEN, R. C. & SCHADEN, W. 2010. Extracorporeal shock wave therapy for nonunion of the tibia. *J Orthop Trauma,* 24**,** 133-41.

FATKHUDINOV, T., GOL'DSHTEIN, D. V., KULAKOV, A. A., GRIGOR'YAN, A. S., PULIN, A. A., MAKAROV, A. V., SHAMENKOV, D. A., RZHANINOVA, A. A. & GORNOSTAEVA, S. A. 2005. Stimulation of reparative osteogenesis after xenotransplantation of human prenatal mesenchymal stem cells and chondroblasts. *Bull Exp Biol Med,* 139**,** 491-8.

FAUCHEUX, C., HORTON, M. A. & PRICE, J. S. 2002. Nuclear localization of type I parathyroid hormone/parathyroid hormone-related protein receptors in deer antler osteoclasts: evidence for parathyroid hormone-related protein and receptor activator of NF-kappaB-dependent effects on osteoclast formation in regenerating mammalian bone. *J Bone Miner Res,* 17**,** 455-64.

FERRARA, N. & DAVIS-SMYTH, T. 1997. The biology of vascular endothelial growth factor. *Endocr Rev,* 18**,** 4-25.

FERREIRA, M. L., SILVA, P. C., ALVAREZ SILVA, L. H., BONFIM, D. C., CONILHO MACEDO MULLER, L. C., ESPOSITO, C. C. & SCHANAIDER, A. 2012. Heterologous mesenchymal stem cells successfully treat femoral pseudarthrosis in rats. *J Transl Med,* 10**,** 51.

FESTING, M. F. & ALTMAN, D. G. 2002. Guidelines for the design and statistical analysis of experiments using laboratory animals. *ILAR J,* 43**,** 244-58.

FITZSIMMONS, R. J., RYABY, J. T., MOHAN, S., MAGEE, F. P. & BAYLINK, D. J. 1995. Combined magnetic fields increase insulin-like growth factor-II in TE-85 human osteosarcoma bone cell cultures. *Endocrinology,* 136**,** 3100-6.

FRIEDENSTEIN, A. J., CHAILAKHJAN, R. K. & LALYKINA, K. S. 1970. The development of fibroblast colonies in monolayer cultures of guinea-pig bone marrow and spleen cells. *Cell Tissue Kinet,* 3**,** 393-403.

FRIEDENSTEIN, A. J., CHAILAKHYAN, R. K., LATSINIK, N. V., PANASYUK, A. F. & KEILISS-BOROK, I. V. 1974. Stromal cells responsible for transferring the microenvironment of the hemopoietic tissues. Cloning in vitro and retransplantation in vivo. *Transplantation,* 17**,** 331-40.

FRIEDENSTEIN, A. J., LATZINIK, N. V., GORSKAYA YU, F., LURIA, E. A. & MOSKVINA, I. L. 1992. Bone marrow stromal colony formation requires stimulation by haemopoietic cells. *Bone Miner,* 18**,** 199-213.

FRIEDLAENDER, G. E., PERRY, C. R., COLE, J. D., COOK, S. D., CIERNY, G., MUSCHLER, G. F., ZYCH, G. A., CALHOUN, J. H., LAFORTE, A. J. & YIN, S. 2001. Osteogenic protein-1 (bone morphogenetic protein-7) in the treatment of tibial nonunions. *J Bone Joint Surg Am,* 83-A Suppl 1**,** S151-8.

FUNK, J. F., MATZIOLIS, G., KROCKER, D. & PERKA, C. 2007. [Promotion of bone healing through clinical application of autologous periosteum derived stem cells in a case of atrophic non-union]. *Z Orthop Unfall,* 145**,** 790-4.

FURTOS, G., BALDEA, B., SILAGHI-DUMITRESCU, L., MOLDOVAN, M., PREJMEREAN, C. & NICA, L. 2012. Influence of inorganic filler content on the radiopacity of dental resin cements. *Dent Mater J,* 31**,** 266-72.

GAO, J., DENNIS, J. E., MUZIC, R. F., LUNDBERG, M. & CAPLAN, A. I. 2001. The dynamic in vivo distribution of bone marrow-derived mesenchymal stem cells after infusion. *Cells Tissues Organs,* 169**,** 12-20.

GARCIA, P., HERWERTH, S., MATTHYS, R., HOLSTEIN, J. H., HISTING, T., MENGER, M. D. & POHLEMANN, T. 2011. The LockingMouseNail--a new implant for standardized stable osteosynthesis in mice. *J Surg Res,* 169**,** 220-6.

GARRISON, K. R., DONELL, S., RYDER, J., SHEMILT, I., MUGFORD, M., HARVEY, I. & SONG, F. 2007. Clinical effectiveness and cost-effectiveness of bone morphogenetic proteins in the non-healing of fractures and spinal fusion: a systematic review. *Health Technol Assess,* 11**,** 1-150, iii-iv.

GARRISON, K. R., SHEMILT, I., DONELL, S., RYDER, J. J., MUGFORD, M., HARVEY, I., SONG, F. & ALT, V. 2010. Bone morphogenetic protein (BMP) for fracture healing in adults. *Cochrane Database Syst Rev***,** CD006950.

GEBAUER, D., MAYR, E., ORTHNER, E. & RYABY, J. P. 2005. Low-intensity pulsed ultrasound: effects on nonunions. *Ultrasound Med Biol,* 31**,** 1391-402.

GEERTZE, J. 2012. Inter-Rater Agreement with multiple raters and variables. Retrieved December 2, 2013, from https://mlnl.net/jg/software/ira/
GERIS, L., REED, A. A., VANDER SLOTEN, J., SIMPSON, A. H. & VAN OOSTERWYCK, H. 2010. Occurrence and treatment of bone atrophic non-unions investigated by an integrative approach. *PLoS Comput Biol,* 6**,** e1000915.
GERSTENFELD, L. C., THIEDE, M., SEIBERT, K., MIELKE, C., PHIPPARD, D., SVAGR, B., CULLINANE, D. & EINHORN, T. A. 2003. Differential inhibition of fracture healing by non-selective and cyclooxygenase-2 selective non-steroidal anti-inflammatory drugs. *J Orthop Res,* 21**,** 670-5.
GIANNOUDIS, P. V., EINHORN, T. A. & MARSH, D. 2007. Fracture healing: the diamond concept. *Injury,* 38 Suppl 4**,** S3-6.
GIANNOUDIS, P. V., MACDONALD, D. A., MATTHEWS, S. J., SMITH, R. M., FURLONG, A. J. & DE BOER, P. 2000. Nonunion of the femoral diaphysis. The influence of reaming and non-steroidal anti-inflammatory drugs. *J Bone Joint Surg Br,* 82**,** 655-8.
GIOIA, R., PANARONI, C., BESIO, R., PALLADINI, G., MERLINI, G., GIANSANTI, V., SCOVASSI, I. A., VILLANI, S., VILLA, I., VILLA, A., VEZZONI, P., TENNI, R., ROSSI, A., MARINI, J. C. & FORLINO, A. 2012. Impaired osteoblastogenesis in a murine model of dominant osteogenesis imperfecta: a new target for osteogenesis imperfecta pharmacological therapy. *Stem Cells,* 30**,** 1465-76.
GIULIANI, N., GIRASOLE, G., VESCOVI, P. P., PASSERI, G. & PEDRAZZONI, M. 1999. Ethanol and acetaldehyde inhibit the formation of early osteoblast progenitors in murine and human bone marrow cultures. *Alcohol Clin Exp Res,* 23**,** 381-5.
GOEL, A., SANGWAN, S. S., SIWACH, R. C. & ALI, A. M. 2005. Percutaneous bone marrow grafting for the treatment of tibial non-union. *Injury,* 36**,** 203-6.
GOLDMAN, L. W. 2007. Principles of CT and CT technology. *J Nucl Med Technol,* 35**,** 115-28; quiz 129-30.
GOLDSTEIN, S. A. 1987. The mechanical properties of trabecular bone: dependence on anatomic location and function. *J Biomech,* 20**,** 1055-61.
GONG, Z. & WEZEMAN, F. H. 2004. Inhibitory effect of alcohol on osteogenic differentiation in human bone marrow-derived mesenchymal stem cells. *Alcohol Clin Exp Res,* 28**,** 468-79.
GORDON, S. 2007. The macrophage: past, present and future. *Eur J Immunol,* 37 Suppl 1**,** S9-17.
GOTHARD, D., DAWSON, J. I. & OREFFO, R. O. 2013. Assessing the potential of colony morphology for dissecting the CFU-F population from human bone marrow stromal cells. *Cell Tissue Res,* 352**,** 237-47.
GOVENDER, S., CSIMMA, C., GENANT, H. K., VALENTIN-OPRAN, A., AMIT, Y., ARBEL, R., ARO, H., ATAR, D., BISHAY, M., BORNER, M. G., CHIRON, P., CHOONG, P., CINATS, J., COURTENAY, B., FEIBEL, R., GEULETTE, B., GRAVEL, C., HAAS, N., RASCHKE, M., HAMMACHER, E., VAN DER VELDE, D., HARDY, P., HOLT, M., JOSTEN, C., KETTERL, R. L., LINDEQUE, B., LOB, G., MATHEVON, H., MCCOY, G., MARSH, D., MILLER, R., MUNTING, E., OEVRE, S.,

NORDSLETTEN, L., PATEL, A., POHL, A., RENNIE, W., REYNDERS, P., ROMMENS, P. M., RONDIA, J., ROSSOUW, W. C., DANEEL, P. J., RUFF, S., RUTER, A., SANTAVIRTA, S., SCHILDHAUER, T. A., GEKLE, C., SCHNETTLER, R., SEGAL, D., SEILER, H., SNOWDOWNE, R. B., STAPERT, J., TAGLANG, G., VERDONK, R., VOGELS, L., WECKBACH, A., WENTZENSEN, A. & WISNIEWSKI, T. 2002. Recombinant human bone morphogenetic protein-2 for treatment of open tibial fractures: a prospective, controlled, randomized study of four hundred and fifty patients. *J Bone Joint Surg Am,* 84-A**,** 2123-34.

GRANERO-MOLTO, F., WEIS, J. A., LONGOBARDI, L. & SPAGNOLI, A. 2008. Role of mesenchymal stem cells in regenerative medicine: application to bone and cartilage repair. *Expert Opin Biol Ther,* 8**,** 255-68.

GRANERO-MOLTO, F., WEIS, J. A., MIGA, M. I., LANDIS, B., MYERS, T. J., O'REAR, L., LONGOBARDI, L., JANSEN, E. D., MORTLOCK, D. P. & SPAGNOLI, A. 2009. Regenerative effects of transplanted mesenchymal stem cells in fracture healing. *Stem Cells,* 27**,** 1887-98.

GRAY, E. E. & CYSTER, J. G. 2012. Lymph node macrophages. *J Innate Immun,* 4**,** 424-36.

GREEN, S. A., MOORE, T. A. & SPOHN, P. J. 1988. Nonunion of the tibial shaft. *Orthopedics,* 11**,** 1149-57.

GRONTHOS, S., STEWART, K., GRAVES, S. E., HAY, S. & SIMMONS, P. J. 1997. Integrin expression and function on human osteoblast-like cells. *J Bone Miner Res,* 12**,** 1189-97.

GRUNDNES, O. & REIKERAS, O. 1993. The importance of the hematoma for fracture healing in rats. *Acta Orthop Scand,* 64**,** 340-2.

GULLIHORN, L., KARPMAN, R. & LIPPIELLO, L. 2005. Differential effects of nicotine and smoke condensate on bone cell metabolic activity. *J Orthop Trauma,* 19**,** 17-22.

GUTIERREZ-ARANDA, I., RAMOS-MEJIA, V., BUENO, C., MUNOZ-LOPEZ, M., REAL, P. J., MACIA, A., SANCHEZ, L., LIGERO, G., GARCIA-PAREZ, J. L. & MENENDEZ, P. 2010. Human induced pluripotent stem cells develop teratoma more efficiently and faster than human embryonic stem cells regardless the site of injection. *Stem Cells*, 28, 1568-70.

HAK, D. J. 2007. The use of osteoconductive bone graft substitutes in orthopaedic trauma. *J Am Acad Orthop Surg,* 15**,** 525-36.

HAMILTON, J. A. 2002. GM-CSF in inflammation and autoimmunity. *Trends Immunol,* 23**,** 403-8.

HARADA, S. & RODAN, G. A. 2003. Control of osteoblast function and regulation of bone mass. *Nature,* 423**,** 349-55.

HAYASHI, O., KATSUBE, Y., HIROSE, M., OHGUSHI, H. & ITO, H. 2008. Comparison of osteogenic ability of rat mesenchymal stem cells from bone marrow, periosteum, and adipose tissue. *Calcif Tissue Int,* 82**,** 238-47.

HAYNESWORTH, S. E., BABER, M. A. & CAPLAN, A. I. 1996. Cytokine expression by human marrow-derived mesenchymal progenitor cells in vitro: effects of dexamethasone and IL-1 alpha. *J Cell Physiol,* 166**,** 585-92.

HECKMAN, J. D. & SARASOHN-KAHN, J. 1997. The economics of treating tibia fractures. The cost of delayed unions. *Bull Hosp Jt Dis,* 56**,** 63-72.

HELANDER, K. G. 1994. Kinetic studies of formaldehyde binding in tissue. *Biotech Histochem,* 69**,** 177-9.
HENG, B. C., CAO, T., STANTON, L. W., ROBSON, P. & OLSEN, B. 2004. Strategies for directing the differentiation of stem cells into the osteogenic lineage in vitro. *J Bone Miner Res,* 19**,** 1379-94.
HERLOFSEN, S. R., KUCHLER, A. M., MELVIK, J. E. & BRINCHMANN, J. E. 2011. Chondrogenic differentiation of human bone marrow-derived mesenchymal stem cells in self-gelling alginate discs reveals novel chondrogenic signature gene clusters. *Tissue Eng Part A,* 17**,** 1003-13.
HERNIGOU, P., POIGNARD, A., BEAUJEAN, F. & ROUARD, H. 2005. Percutaneous autologous bone-marrow grafting for nonunions. Influence of the number and concentration of progenitor cells. *J Bone Joint Surg Am,* 87**,** 1430-7.
HILDEBRAND, T., LAIB, A., MULLER, R., DEQUEKER, J. & RUEGSEGGER, P. 1999. Direct three-dimensional morphometric analysis of human cancellous bone: microstructural data from spine, femur, iliac crest, and calcaneus. *J Bone Miner Res,* 14**,** 1167-74.
HILDEBRAND, T., RIIEGSEGGER, P. 1997. A new method for the model independent assessment of thickness in three-dimensional images. *J Microsc* 185:67–75
HISTING, T., GARCIA, P., MATTHYS, R., LEIDINGER, M., HOLSTEIN, J. H., KRISTEN, A., POHLEMANN, T. & MENGER, M. D. 2010. An internal locking plate to study intramembranous bone healing in a mouse femur fracture model. *J Orthop Res,* 28**,** 397-402.
HOFMANN, A., RITZ, U., HESSMANN, M. H., SCHMID, C., TRESCH, A., ROMPE, J. D., MEURER, A. & ROMMENS, P. M. 2008. Cell viability, osteoblast differentiation, and gene expression are altered in human osteoblasts from hypertrophic fracture non-unions. *Bone,* 42**,** 894-906.
HOGAN, H. A., GROVES, J. A. & SAMPSON, H. W. 1999. Long-term alcohol consumption in the rat affects femur cross-sectional geometry and bone tissue material properties. *Alcohol Clin Exp Res,* 23**,** 1825-33.
HOLSTEIN, J. H., MATTHYS, R., HISTING, T., BECKER, S. C., FIEDLER, M., GARCIA, P., MEIER, C., POHLEMANN, T. & MENGER, M. D. 2009. Development of a stable closed femoral fracture model in mice. *J Surg Res,* 153**,** 71-5.
HOLSTEIN, J. H., MENGER, M. D., CULEMANN, U., MEIER, C. & POHLEMANN, T. 2007. Development of a locking femur nail for mice. *J Biomech,* 40**,** 215-9.
HORWITZ, E. M., GORDON, P. L., KOO, W. K., MARX, J. C., NEEL, M. D., MCNALL, R. Y., MUUL, L. & HOFMANN, T. 2002. Isolated allogeneic bone marrow-derived mesenchymal cells engraft and stimulate growth in children with osteogenesis imperfecta: Implications for cell therapy of bone. *Proc Natl Acad Sci U S A,* 99**,** 8932-7.
HUANG, S., LEUNG, V., PENG, S., LI, L., LU, F. J., WANG, T., LU, W., CHEUNG, K. M. & ZHOU, G. 2011. Developmental definition of MSCs: new insights into pending questions. *Cell Reprogram,* 13**,** 465-72.

HUANG, X. P., SUN, Z., MIYAGI, Y., MCDONALD KINKAID, H., ZHANG, L., WEISEL, R. D. & LI, R. K. 2010. Differentiation of allogeneic mesenchymal stem cells induces immunogenicity and limits their long-term benefits for myocardial repair. *Circulation,* 122**,** 2419-29.

HUNG, S. C., POCHAMPALLY, R. R., CHEN, S. C., HSU, S. C. & PROCKOP, D. J. 2007. Angiogenic effects of human multipotent stromal cell conditioned medium activate the PI3K-Akt pathway in hypoxic endothelial cells to inhibit apoptosis, increase survival, and stimulate angiogenesis. *Stem Cells,* 25**,** 2363-70.

ITO, K., PEERREN, S.M. 2007. Biology and biomechanics in bone healing in: RUEDI, T.P., BUCKLEY, R.E., MORAN, C.G. (eds). *AO principles of fracture management*. Stuttgart / New York, 2nd expanded edition, Vol. 1 pp 8 – 31.

IWANIEC, U. T., FUNG, Y. K., AKHTER, M. P., HAVEN, M. C., NESPOR, S., HAYNATZKI, G. R. & CULLEN, D. M. 2001. Effects of nicotine on bone mass, turnover, and strength in adult female rats. *Calcif Tissue Int,* 68**,** 358-64.

JAGODZINSKI, M. & KRETTEK, C. 2007. Effect of mechanical stability on fracture healing--an update. *Injury,* 38 Suppl 1**,** S3-10.

JAMES, A. W., ZARA, J. N., CORSELLI, M., ASKARINAM, A., ZHOU, A. M., HOURFAR, A., NGUYEN, A., MEGERDICHIAN, S., ASATRIAN, G., PANG, S., STOKER, D., ZHANG, X., WU, B., TING, K., PEAULT, B. & SOO, C. 2012a. An abundant perivascular source of stem cells for bone tissue engineering. *Stem Cells Transl Med,* 1**,** 673-84.

JAMES, A. W., ZARA, J. N., ZHANG, X., ASKARINAM, A., GOYAL, R., CHIANG, M., YUAN, W., CHANG, L., CORSELLI, M., SHEN, J., PANG, S., STOKER, D., WU, B., TING, K., PEAULT, B. & SOO, C. 2012b. Perivascular stem cells: a prospectively purified mesenchymal stem cell population for bone tissue engineering. *Stem Cells Transl Med,* 1**,** 510-9.

JAVAZON, E. H., COLTER, D. C., SCHWARZ, E. J. & PROCKOP, D. J. 2001. Rat marrow stromal cells are more sensitive to plating density and expand more rapidly from single-cell-derived colonies than human marrow stromal cells. *Stem Cells,* 19**,** 219-25.

JIANG, Y., JAHAGIRDAR, B. N., REINHARDT, R. L., SCHWARTZ, R. E., KEENE, C. D., ORTIZ-GONZALEZ, X. R., REYES, M., LENVIK, T., LUND, T., BLACKSTAD, M., DU, J., ALDRICH, S., LISBERG, A., LOW, W. C., LARGAESPADA, D. A. & VERFAILLIE, C. M. 2002. Pluripotency of mesenchymal stem cells derived from adult marrow. *Nature,* 418**,** 41-9.

JINGUSHI, S., MIZUNO, K., MATSUSHITA, T. & ITOMAN, M. 2007. Low-intensity pulsed ultrasound treatment for postoperative delayed union or nonunion of long bone fractures. *J Orthop Sci,* 12**,** 35-41.

JONES, B. J. & MCTAGGART, S. J. 2008. Immunosuppression by mesenchymal stromal cells: from culture to clinic. *Exp Hematol,* 36**,** 733-41.

JONES, E. A., KINSEY, S. E., ENGLISH, A., JONES, R. A., STRASZYNSKI, L., MEREDITH, D. M., MARKHAM, A. F., JACK, A., EMERY, P. & MCGONAGLE, D. 2002. Isolation and characterization of bone marrow multipotential mesenchymal progenitor cells. *Arthritis Rheum,* 46**,** 3349-60.

JORGENSEN, N. R., HENRIKSEN, Z., SORENSEN, O. H. & CIVITELLI, R. 2004. Dexamethasone, BMP-2, and 1,25-dihydroxyvitamin D enhance a more differentiated osteoblast phenotype: validation of an in vitro model for human bone marrow-derived primary osteoblasts. *Steroids,* 69**,** 219-26.

KAMPERDIJK, E. W., DIJKSTRA, C. D. & DOPP, E. A. 1987. Transport of immune complexes from the subcapsular sinus into the lymph node follicles of the rat. *Immunobiology,* 174**,** 395-405.

KARLADANI, A. H., GRANHED, H., KARRHOLM, J. & STYF, J. 2001. The influence of fracture etiology and type on fracture healing: a review of 104 consecutive tibial shaft fractures. *Arch Orthop Trauma Surg,* 121**,** 325-8.

KASPAR, K., MATZIOLIS, G., STRUBE, P., SENTURK, U., DORMANN, S., BAIL, H. J. & DUDA, G. N. 2008. A new animal model for bone atrophic nonunion: fixation by external fixator. *J Orthop Res,* 26**,** 1649-55.

KEATS, E. & KHAN, Z. A. 2012. Unique responses of stem cell-derived vascular endothelial and mesenchymal cells to high levels of glucose. *PLoS One,* 7**,** e38752.

KERIMOGLU, G., YULUG, E., KERIMOGLU, S. & CITLAK, A. 2013. Effects of leptin on fracture healing in rat tibia. *Eklem Hastalik Cerrahisi,* 24**,** 102-7.

KHAN, Z. A. & CHAKRABARTI, S. 2006. Therapeutic targeting of endothelial dysfunction in chronic diabetic complications. *Recent Pat Cardiovasc Drug Discov,* 1**,** 167-75.

KILKENNY, C., BROWNE, W. J., CUTHILL, I. C., EMERSON, M. & ALTMAN, D. G. 2010. Improving bioscience research reporting: the ARRIVE guidelines for reporting animal research. *PLoS Biol,* 8**,** e1000412.

KIM, I. S., CHO, T. H., LEE, Z. H. & HWANG, S. J. 2013. Bone regeneration by transplantation of human mesenchymal stromal cells in a rabbit mandibular distraction osteogenesis model. *Tissue Eng Part A,* 19**,** 66-78.

KIM, M., KIM, C., CHOI, Y. S., PARK, C. & SUH, Y. 2012. Age-related alterations in mesenchymal stem cells related to shift in differentiation from osteogenic to adipogenic potential: implication to age-associated bone diseases and defects. *Mech Ageing Dev,* 133**,** 215-25.

KLEIN-NULEND, J., VAN DER PLAS, A., SEMEINS, C. M., AJUBI, N. E., FRANGOS, J. A., NIJWEIDE, P. J. & BURGER, E. H. 1995. Sensitivity of osteocytes to biomechanical stress in vitro. *FASEB J,* 9**,** 441-5.

KOKUBU, T., HAK, D. J., HAZELWOOD, S. J. & REDDI, A. H. 2003. Development of an atrophic nonunion model and comparison to a closed healing fracture in rat femur. *J Orthop Res,* 21**,** 503-10.

KON, T., CHO, T. J., AIZAWA, T., YAMAZAKI, M., NOOH, N., GRAVES, D., GERSTENFELD, L. C. & EINHORN, T. A. 2001. Expression of osteoprotegerin, receptor activator of NF-kappaB ligand (osteoprotegerin ligand) and related proinflammatory cytokines during fracture healing. *J Bone Miner Res,* 16**,** 1004-14.

KOOISTRA, B. W., DIJKMAN, B. G., BUSSE, J. W., SPRAGUE, S., SCHEMITSCH, E. H. & BHANDARI, M. 2010. The radiographic union scale in tibial fractures: reliability and validity. *J Orthop Trauma,* 24 Suppl 1**,** S81-6.

KREBSBACH, P. H., MANKANI, M. H., SATOMURA, K., KUZNETSOV, S. A. & ROBEY, P. G. 1998. Repair of craniotomy defects using bone marrow stromal cells. *Transplantation,* 66**,** 1272-8.

KURKLU, M., YILDIZ, C., KOSE, O., YURTTAS, Y., KARACALIOGLU, O., SERDAR, M. & DEVECI, S. 2011. Effect of alpha-tocopherol on bone formation during distraction osteogenesis: a rabbit model. *J Orthop Traumatol,* 12**,** 153-8.

KUMAR, V.,ABBAS, AK. & FAUSTO, N. 2004. Robbin and Cotran pathological basic of disease. Philadelphia, PA,Elsevier Saunders

LACROIX, D. & PRENDERGAST, P. J. 2002. A mechano-regulation model for tissue differentiation during fracture healing: analysis of gap size and loading. *J Biomech,* 35**,** 1163-71.

LANDRY, P. S., MARINO, A. A., SADASIVAN, K. K. & ALBRIGHT, J. A. 2000. Effect of soft-tissue trauma on the early periosteal response of bone to injury. *J Trauma,* 48**,** 479-83.

LANE, J. M. & SANDHU, H. S. 1987. Current approaches to experimental bone grafting. *Orthop Clin North Am,* 18**,** 213-25.

LATSINIK, N. V., GORSKAIA IU, F., GROSHEVA, A. G., DOMOGATSKII, S. P. & KUZNETSOV, S. A. 1986. [The stromal colony-forming cell (CFUf) count in the bone marrow of mice and the clonal nature of the fibroblast colonies they form]. *Ontogenez,* 17**,** 27-36.

LE BLANC, K., GOTHERSTROM, C., RINGDEN, O., HASSAN, M., MCMAHON, R., HORWITZ, E., ANNEREN, G., AXELSSON, O., NUNN, J., EWALD, U., NORDEN-LINDEBERG, S., JANSSON, M., DALTON, A., ASTROM, E. & WESTGREN, M. 2005. Fetal mesenchymal stem-cell engraftment in bone after in utero transplantation in a patient with severe osteogenesis imperfecta. *Transplantation,* 79**,** 1607-14.

LE BLANC, K., TAMMIK, C., ROSENDAHL, K., ZETTERBERG, E. & RINGDEN, O. 2003. HLA expression and immunologic properties of differentiated and undifferentiated mesenchymal stem cells. *Exp Hematol,* 31**,** 890-6.

LENNON, D. P. & CAPLAN, A. I. 2006. Isolation of rat marrow-derived mesenchymal stem cells. *Exp Hematol,* 34**,** 1606-7.

LI, J., EZZELARAB, M. B. & COOPER, D. K. 2012. Do mesenchymal stem cells function across species barriers? Relevance for xenotransplantation. *Xenotransplantation,* 19**,** 273-85.

LI, J. K., CHANG, W. H., LIN, J. C., RUAAN, R. C., LIU, H. C. & SUN, J. S. 2003. Cytokine release from osteoblasts in response to ultrasound stimulation. *Biomaterials,* 24**,** 2379-85.

LI, L. & JIANG, J. 2011. Regulatory factors of mesenchymal stem cell migration into injured tissues and their signal transduction mechanisms. *Front Med,* 5**,** 33-9.

LI, X., OMINSKY, M. S., NIU, Q. T., SUN, N., DAUGHERTY, B., D'AGOSTIN, D., KURAHARA, C., GAO, Y., CAO, J., GONG, J., ASUNCION, F., BARRERO, M., WARMINGTON, K., DWYER, D., STOLINA, M., MORONY, S., SAROSI, I., KOSTENUIK, P. J., LACEY, D. L., SIMONET, W. S., KE, H. Z. & PASZTY, C. 2008. Targeted deletion of the sclerostin

gene in mice results in increased bone formation and bone strength. *J Bone Miner Res,* 23**,** 860-9.
LI, Y. M., SCHILLING, T., BENISCH, P., ZECK, S., MEISSNER-WEIGL, J., SCHNEIDER, D., LIMBERT, C., SEUFERT, J., KASSEM, M., SCHUTZE, N., JAKOB, F. & EBERT, R. 2007. Effects of high glucose on mesenchymal stem cell proliferation and differentiation. *Biochem Biophys Res Commun,* 363**,** 209-15.
LIEBERMAN, J. R., DALUISKI, A. & EINHORN, T. A. 2002. The role of growth factors in the repair of bone. Biology and clinical applications. *J Bone Joint Surg Am,* 84-A**,** 1032-44.
LIEN, C. Y., CHIH-YUAN HO, K., LEE, O. K., BLUNN, G. W. & SU, Y. 2009. Restoration of bone mass and strength in glucocorticoid-treated mice by systemic transplantation of CXCR4 and cbfa-1 co-expressing mesenchymal stem cells. *J Bone Miner Res,* 24**,** 837-48.
LITTENBERG, B., WEINSTEIN, L. P., MCCARREN, M., MEAD, T., SWIONTKOWSKI, M. F., RUDICEL, S. A. & HECK, D. 1998. Closed fractures of the tibial shaft. A meta-analysis of three methods of treatment. *J Bone Joint Surg Am,* 80**,** 174-83.
LIU, H., KEMENY, D. M., HENG, B. C., OUYANG, H. W., MELENDEZ, A. J. & CAO, T. 2006. The immunogenicity and immunomodulatory function of osteogenic cells differentiated from mesenchymal stem cells. *J Immunol,* 176**,** 2864-71.
MAJORE, I., MORETTI, P., HASS, R. & KASPER, C. 2009. Identification of subpopulations in mesenchymal stem cell-like cultures from human umbilical cord. *Cell Commun Signal,* 7**,** 6.
MAJORS, A. K., BOEHM, C. A., NITTO, H., MIDURA, R. J. & MUSCHLER, G. F. 1997. Characterization of human bone marrow stromal cells with respect to osteoblastic differentiation. *J Orthop Res,* 15**,** 546-57.
MAJUMDAR, M. K., THIEDE, M. A., MOSCA, J. D., MOORMAN, M. & GERSON, S. L. 1998. Phenotypic and functional comparison of cultures of marrow-derived mesenchymal stem cells (MSCs) and stromal cells. *J Cell Physiol,* 176**,** 57-66.
MALIZOS, K. N. & PAPATHEODOROU, L. K. 2005. The healing potential of the periosteum molecular aspects. *Injury,* 36 Suppl 3**,** S13-9.
MANNING, C. F., BUNDROS, A. M. & TRIMMER, J. S. 2012. Benefits and pitfalls of secondary antibodies: why choosing the right secondary is of primary importance. *PLoS One,* 7**,** e38313.
MARCHELLI, D., PIODI, L. P., CORRADINI, C., PARRAVICINI, L., VERDOIA, C. & ULIVIERI, F. M. 2009. Increased serum OPG in atrophic nonunion shaft fractures. *J Orthop Traumatol,* 10**,** 55-8.
MARSH, D. 1998. Concepts of fracture union, delayed union, and nonunion. *Clin Orthop Relat Res***,** S22-30.
MCKEE, M. D., NANCI, A., LANDIS, W. J., GOTOH, Y., GERSTENFELD, L. C. & GLIMCHER, M. J. 1991. Effects of fixation and demineralization on the retention of bone phosphoprotein and other matrix components as evaluated by biochemical analyses and quantitative immunocytochemistry. *J Bone Miner Res,* 6**,** 937-45.

MCKIBBIN, B. 1978. The biology of fracture healing in long bones. *J Bone Joint Surg Br,* 60-B**,** 150-62.
MCKINNEY-FREEMAN, S. L., NAVEIRAS, O., YATES, F., LOEWER, S., PHILITAS, M., CURRAN, M., PARK, P. J. & DALEY, G. Q. 2009. Surface antigen phenotypes of hematopoietic stem cells from embryos and murine embryonic stem cells. *Blood*, 114, 268-78.
MEGAS, P. 2005. Classification of non-union. *Injury,* 36 Suppl 4**,** S30-7.
MILLER, P. D., ZAPALOWSKI, C., KULAK, C. A. & BILEZIKIAN, J. P. 1999. Bone densitometry: the best way to detect osteoporosis and to monitor therapy. *J Clin Endocrinol Metab,* 84**,** 1867-71.
MILLS, L. A. & SIMPSON, A. H. 2012. In vivo models of bone repair. *J Bone Joint Surg Br,* 94**,** 865-74.
MILLS, L. A. & SIMPSON, A. H. 2013. The relative incidence of fracture non-union in the Scottish population (5.17 million): a 5-year epidemiological study. *BMJ Open,* 3.
MIURA, M., GRONTHOS, S., ZHAO, M., LU, B., FISHER, L. W., ROBEY, P. G. & SHI, S. 2003. SHED: stem cells from human exfoliated deciduous teeth. *Proc Natl Acad Sci U S A,* 100**,** 5807-12.
MOHAN, S. & BAYLINK, D. J. 1991. Bone growth factors. *Clin Orthop Relat Res***,** 30-48.
MONTEMURRO, T., ANDRIOLO, G., MONTELATICI, E., WEISSMANN, G., CRISAN, M., COLNAGHI, M. R., REBULLA, P., MOSCA, F., PEAULT, B. & LAZZARI, L. 2011. Differentiation and migration properties of human foetal umbilical cord perivascular cells: potential for lung repair. *J Cell Mol Med,* 15**,** 796-808.
MULLER, A. M., MEHRKENS, A., SCHAFER, D. J., JAQUIERY, C., GUVEN, S., LEHMICKE, M., MARTINETTI, R., FARHADI, I., JAKOB, M., SCHERBERICH, A. & MARTIN, I. 2010. Towards an intraoperative engineering of osteogenic and vasculogenic grafts from the stromal vascular fraction of human adipose tissue. *Eur Cell Mater,* 19**,** 127-35.
MULLER, M. E., ALLGOWER, M., SCHNEIDER, R. &WILLENEGGER, H. Eds. (1991). Manual of Internal Fixation. Techniques recommended by the AO-ASIF Group, Springer-Verlag
MULLER, R. & RUEGSEGGER, P. 1995. Three-dimensional finite element modelling of non-invasively assessed trabecular bone structures. *Med Eng Phys,* 17**,** 126-33.
MUNDLOS, S. 1999. Cleidocranial dysplasia: clinical and molecular genetics. *J Med Genet,* 36**,** 177-82.
MURAGLIA, A., CANCEDDA, R. & QUARTO, R. 2000. Clonal mesenchymal progenitors from human bone marrow differentiate in vitro according to a hierarchical model. *J Cell Sci,* 113 (Pt 7)**,** 1161-6.
MURPHY, J. M., FINK, D. J., HUNZIKER, E. B. & BARRY, F. P. 2003. Stem cell therapy in a caprine model of osteoarthritis. *Arthritis Rheum,* 48**,** 3464-74.
MUSCHLER, G. F., NITTO, H., BOEHM, C. A. & EASLEY, K. A. 2001. Age- and gender-related changes in the cellularity of human bone marrow and the prevalence of osteoblastic progenitors. *J Orthop Res,* 19**,** 117-25.

NADRI, S., SOLEIMANI, M., HOSSENI, R. H., MASSUMI, M., ATASHI, A. & IZADPANAH, R. 2007. An efficient method for isolation of murine bone marrow mesenchymal stem cells. *Int J Dev Biol,* 51**,** 723-9.

NAIR, M. B., VARMA, H. K., MENON, K. V., SHENOY, S. J. & JOHN, A. 2009. Reconstruction of goat femur segmental defects using triphasic ceramic-coated hydroxyapatite in combination with autologous cells and platelet-rich plasma. *Acta Biomater,* 5**,** 1742-55.

NAKASHIMA, K., ZHOU, X., KUNKEL, G., ZHANG, Z., DENG, J. M., BEHRINGER, R. R. & DE CROMBRUGGHE, B. 2002. The novel zinc finger-containing transcription factor osterix is required for osteoblast differentiation and bone formation. *Cell,* 108**,** 17-29.

NIELSEN, J. S. & MCNAGNY, K. M. 2008. Novel functions of the CD34 family. *J Cell Sci,* 121**,** 3683-92.

NIEMEYER, P., FECHNER, K., MILZ, S., RICHTER, W., SUEDKAMP, N. P., MEHLHORN, A. T., PEARCE, S. & KASTEN, P. 2010a. Comparison of mesenchymal stem cells from bone marrow and adipose tissue for bone regeneration in a critical size defect of the sheep tibia and the influence of platelet-rich plasma. *Biomaterials,* 31**,** 3572-9.

NIEMEYER, P., SCHONBERGER, T. S., HAHN, J., KASTEN, P., FELLENBERG, J., SUEDKAMP, N., MEHLHORN, A. T., MILZ, S. & PEARCE, S. 2010b. Xenogenic transplantation of human mesenchymal stem cells in a critical size defect of the sheep tibia for bone regeneration. *Tissue Eng Part A,* 16**,** 33-43.

NIEMEYER, P., SZALAY, K., LUGINBUHL, R., SUDKAMP, N. P. & KASTEN, P. 2010c. Transplantation of human mesenchymal stem cells in a non-autogenous setting for bone regeneration in a rabbit critical-size defect model. *Acta Biomater,* 6**,** 900-8.

NISHIDA, S., ENDO, N., YAMAGIWA, H., TANIZAWA, T. & TAKAHASHI, H. E. 1999. Number of osteoprogenitor cells in human bone marrow markedly decreases after skeletal maturation. *J Bone Miner Metab,* 17**,** 171-7.

NIYIBIZI, C. & EYRE, D. R. 1989. Bone type V collagen: chain composition and location of a trypsin cleavage site. *Connect Tissue Res,* 20**,** 247-50.

NORTON, M. R. & GAMBLE, C. 2001. Bone classification: an objective scale of bone density using the computerized tomography scan. *Clin Oral Implants Res,* 12**,** 79-84.

NOTH, U., OSYCZKA, A. M., TULI, R., HICKOK, N. J., DANIELSON, K. G. & TUAN, R. S. 2002. Multilineage mesenchymal differentiation potential of human trabecular bone-derived cells. *J Orthop Res,* 20**,** 1060-9.

NUNAMAKER, D. M. 1998. Experimental models of fracture repair. *Clin Orthop Relat Res***,** S56-65.

O'LOUGHLIN, P. F., MORR, S., BOGUNOVIC, L., KIM, A. D., PARK, B. & LANE, J. M. 2008. Selection and development of preclinical models in fracture-healing research. *J Bone Joint Surg Am,* 90 Suppl 1**,** 79-84.

OE, K., MIWA, M., SAKAI, Y., LEE, S. Y., KURODA, R. & KUROSAKA, M. 2007. An in vitro study demonstrating that haematomas found at the site of human fractures contain progenitor cells with multilineage capacity. *J Bone Joint Surg Br,* 89**,** 133-8.

OHGUSHI, H., GOLDBERG, V. M. & CAPLAN, A. I. 1989. Repair of bone defects with marrow cells and porous ceramic. Experiments in rats. *Acta Orthop Scand,* 60**,** 334-9.
OWEN, M. & FRIEDENSTEIN, A. J. 1988. Stromal stem cells: marrow-derived osteogenic precursors. *Ciba Found Symp,* 136**,** 42-60.
OZAKI, A., TSUNODA, M., KINOSHITA, S. & SAURA, R. 2000. Role of fracture hematoma and periosteum during fracture healing in rats: interaction of fracture hematoma and the periosteum in the initial step of the healing process. *J Orthop Sci,* 5**,** 64-70.
PARANT, O., DUBERNARD, G., CHALLIER, J. C., OSTER, M., UZAN, S., ARACTINGI, S. & KHOSROTEHRANI, K. 2009. CD34+ cells in maternal placental blood are mainly fetal in origin and express endothelial markers. *Lab Invest,* 89**,** 915-23.
PARASURAMAN, S., RAVEENDRAN, R. & KESAVAN, R. 2010. Blood sample collection in small laboratory animals. *J Pharmacol Pharmacother,* 1**,** 87-93.
PARFITT, A. M. 2002. Targeted and nontargeted bone remodeling: relationship to basic multicellular unit origination and progression. *Bone,* 30**,** 5-7.
PARFITT, A. M., DREZNER, M. K., GLORIEUX, F. H., KANIS, J. A., MALLUCHE, H., MEUNIER, P. J., OTT, S. M. & RECKER, R. R. 1987. Bone histomorphometry: standardization of nomenclature, symbols, and units. Report of the ASBMR Histomorphometry Nomenclature Committee. *J Bone Miner Res,* 2**,** 595-610.
PARK, T. S., GAVINA, M., CHEN, C. W., SUN, B., TENG, P. N., HUARD, J., DEASY, B. M., ZIMMERLIN, L. & PEAULT, B. 2011. Placental perivascular cells for human muscle regeneration. *Stem Cells Dev,* 20**,** 451-63.
PERREN, S. M. 2002. Evolution of the internal fixation of long bone fractures. The scientific basis of biological internal fixation: choosing a new balance between stability and biology. *J Bone Joint Surg Br,* 84**,** 1093-110.
PETERSON, B., ZHANG, J., IGLESIAS, R., KABO, M., HEDRICK, M., BENHAIM, P. & LIEBERMAN, J. R. 2005. Healing of critically sized femoral defects, using genetically modified mesenchymal stem cells from human adipose tissue. *Tissue Eng,* 11**,** 120-9.
PITTENGER, M. F. 2008. Mesenchymal stem cells from adult bone marrow. *Methods Mol Biol,* 449**,** 27-44.
PITTENGER, M. F., MACKAY, A. M., BECK, S. C., JAISWAL, R. K., DOUGLAS, R., MOSCA, J. D., MOORMAN, M. A., SIMONETTI, D. W., CRAIG, S. & MARSHAK, D. R. 1999. Multilineage potential of adult human mesenchymal stem cells. *Science,* 284**,** 143-7.
POCHAMPALLY, R. 2008. Colony forming unit assays for MSCs. *Methods Mol Biol,* 449**,** 83-91.
PROCKOP, D. J. 1997. Marrow stromal cells as stem cells for nonhematopoietic tissues. *Science,* 276**,** 71-4.
PROGATZKY, F., DALLMAN, M. J. & LO CELSO, C. 2013. From seeing to believing: labelling strategies for in vivo cell-tracking experiments. *Interface Focus,* 3**,** 20130001.

REED, A. A., JOYNER, C. J., BROWNLOW, H. C. & SIMPSON, A. H. 2002. Human atrophic fracture non-unions are not avascular. *J Orthop Res*, 20, 593-9.
REED, A. A., JOYNER, C. J., ISEFUKU, S., BROWNLOW, H. C. & SIMPSON, A. H. 2003. Vascularity in a new model of atrophic nonunion. *J Bone Joint Surg Br,* 85**,** 604-10.
REILLY, D. T. & BURSTEIN, A. H. 1975. The elastic and ultimate properties of compact bone tissue. *J Biomech,* 8**,** 393-405.
REISSIS, Y., GARCIA-GARETA, E., KORDA, M., BLUNN, G. W. & HUA, J. 2013. The effect of the temperature on the viability of human mesenchymal stem cells. *Stem Cell Res Ther,* 4**,** 139.
ROBLING, A. G., NIZIOLEK, P. J., BALDRIDGE, L. A., CONDON, K. W., ALLEN, M. R., ALAM, I., MANTILA, S. M., GLUHAK-HEINRICH, J., BELLIDO, T. M., HARRIS, S. E. & TURNER, C. H. 2008. Mechanical stimulation of bone in vivo reduces osteocyte expression of Sost/sclerostin. *J Biol Chem,* 283**,** 5866-75.
RODRIGUEZ, J. P., ASTUDILLO, P., RIOS, S. & PINO, A. M. 2008. Involvement of adipogenic potential of human bone marrow mesenchymal stem cells (MSCs) in osteoporosis. *Curr Stem Cell Res Ther,* 3**,** 208-18.
ROSEN, E. D. & SPIEGELMAN, B. M. 2000. Molecular regulation of adipogenesis. *Annu Rev Cell Dev Biol,* 16**,** 145-71.
RUSSELL, W.M.S.& BURCH, R.L. 1959. *The Principles of Humane Experimental Technique.* Retrieved from http://www.nc3rs.org.uk/page.asp?id=7
SAINTE-MARIE, G., PENG, F. S. & BELISLE, C. 1982. Overall architecture and pattern of lymph flow in the rat lymph node. *Am J Anat,* 164**,** 275-309.
SAMSTEIN, B. & PLATT, J. L. 2001. Xenotransplantation and tolerance. *Philos Trans R Soc Lond B Biol Sci,* 356**,** 749-58.
SANDHU, S. K. & HAMPSON, G. 2011. The pathogenesis, diagnosis, investigation and management of osteoporosis. *J Clin Pathol,* 64**,** 1042-50.
SATO, K., OZAKI, K., MORI, M., MUROI, K. & OZAWA, K. 2010. Mesenchymal stromal cells for graft-versus-host disease : basic aspects and clinical outcomes. *J Clin Exp Hematop*, 50, 79-89.
SCHMIDHAMMER, R., ZANDIEH, S., MITTERMAYR, R., PELINKA, L. E., LEIXNERING, M., HOPF, R., KROEPFL, A. & REDL, H. 2006. Assessment of bone union/nonunion in an experimental model using microcomputed technology. *J Trauma,* 61**,** 199-205.
SCHMITZ, M. A., FINNEGAN, M., NATARAJAN, R. & CHAMPINE, J. 1999. Effect of smoking on tibial shaft fracture healing. *Clin Orthop Relat Res***,** 184-200.
SCHREPFER, S., DEUSE, T., REICHENSPURNER, H., FISCHBEIN, M. P., ROBBINS, R. C. & PELLETIER, M. P. 2007. Stem cell transplantation: the lung barrier. *Transplant Proc,* 39**,** 573-6.
SCHU, S., NOSOV, M., O'FLYNN, L., SHAW, G., TREACY, O., BARRY, F., MURPHY, M., O'BRIEN, T. & RITTER, T. 2012. Immunogenicity of allogeneic mesenchymal stem cells. *J Cell Mol Med,* 16**,** 2094-103.
SCHWARTZ, C. E., MARTHA, J. F., KOWALSKI, P., WANG, D. A., BODE, R., LI, L. & KIM, D. H. 2009. Prospective evaluation of chronic pain associated

with posterior autologous iliac crest bone graft harvest and its effect on postoperative outcome. *Health Qual Life Outcomes,* 7**,** 49.
SEEBACH, C., HENRICH, D., TEWKSBURY, R., WILHELM, K. & MARZI, I. 2007. Number and proliferative capacity of human mesenchymal stem cells are modulated positively in multiple trauma patients and negatively in atrophic nonunions. *Calcif Tissue Int,* 80**,** 294-300.
SEN, M. K. & MICLAU, T. 2007. Autologous iliac crest bone graft: should it still be the gold standard for treating nonunions? *Injury,* 38 Suppl 1**,** S75-80.
SETHE, S., SCUTT, A. & STOLZING, A. 2006. Aging of mesenchymal stem cells. *Ageing Res Rev,* 5**,** 91-116.
SHARRARD, W. J. 1990. A double-blind trial of pulsed electromagnetic fields for delayed union of tibial fractures. *J Bone Joint Surg Br,* 72**,** 347-55.
SHEN, J., TSAI, Y. T., DIMARCO, N. M., LONG, M. A., SUN, X. & TANG, L. 2011. Transplantation of mesenchymal stem cells from young donors delays aging in mice. *Sci Rep,* 1**,** 67.
SHROUT, P. E. & FLEISS, J. L. 1979. Intraclass correlations: uses in assessing rater reliability. *Psychol Bull,* 86**,** 420-8.
SIMMONS, D. J. 1985. Fracture healing perspectives. *Clin Orthop Relat Res***,** 100-13.
SIMMONS, P. J. & TOROK-STORB, B. 1991. Identification of stromal cell precursors in human bone marrow by a novel monoclonal antibody, STRO-1. *Blood,* 78**,** 55-62.
SIMONIS, R. B., PARNELL, E. J., RAY, P. S. & PEACOCK, J. L. 2003. Electrical treatment of tibial non-union: a prospective, randomised, double-blind trial. *Injury,* 34**,** 357-62.
SIMPSON, A. H., WOOD, M. K. & ATHANASOU, N. A. 2002. Histological assessment of the presence or absence of infection in fracture non-union. *Injury,* 33**,** 151-5.
SLOAN, A., HUSSAIN, A., et al. 2009 Inhibition of tibial fracture healing in smokers: cellular and molecular aspects. In: *The 19th Conference of the European Wound Management Association (EWMA) in cooperation with the Finnish Wound Care Society FWCS*, 20-22 May 2009, Helsinki
SOFUOGLU, M. & LESAGE, M. G. 2012. The reinforcement threshold for nicotine as a target for tobacco control. *Drug Alcohol Depend,* 125**,** 1-7.
SQUIER, C. A., GHONEIM, S. & KREMENAK, C. R. 1990. Ultrastructure of the periosteum from membrane bone. *J Anat*, 171, 233-9.
STEER, H. W. & FOOT, R. A. 1987. Changes in the medulla of the parathymic lymph nodes of the rat during acute gastro-intestinal inflammation. *J Anat,* 152**,** 23-36.
STENDERUP, K., JUSTESEN, J., ERIKSEN, E. F., RATTAN, S. I. & KASSEM, M. 2001. Number and proliferative capacity of osteogenic stem cells are maintained during aging and in patients with osteoporosis. *J Bone Miner Res,* 16**,** 1120-9.
STOLZING, A., JONES, E., MCGONAGLE, D. & SCUTT, A. 2008. Age-related changes in human bone marrow-derived mesenchymal stem cells: consequences for cell therapies. *Mech Ageing Dev,* 129**,** 163-73.

SUGIURA, F., KITOH, H. & ISHIGURO, N. 2004. Osteogenic potential of rat mesenchymal stem cells after several passages. *Biochem Biophys Res Commun,* 316**,** 233-9.
SZELIGA, J., DANIEL, D. S., YANG, C. H., SEVER-CHRONEOS, Z., JAGANNATH, C. & CHRONEOS, Z. C. 2008. Granulocyte-macrophage colony stimulating factor-mediated innate responses in tuberculosis. *Tuberculosis (Edinb),* 88**,** 7-20.
TAKAHASHI, K., TANABE, K., OHNUKI, M., NARITA, M., ICHISAKA, T., TOMODA, K. & YAMANAKA, S. 2007. Induction of pluripotent stem cells from adult human fibroblasts by defined factors. *Cell*, 131, 861-72.
TAKAHASHI, K. & YAMANAKA, S. 2006. Induction of pluripotent stem cells from mouse embryonic and adult fibroblast cultures by defined factors. *Cell*, 126, 663-76.
TAKAHASHI, N., MAEDA, K., ISHIHARA, A., UEHARA, S. & KOBAYASHI, Y. 2011. Regulatory mechanism of osteoclastogenesis by RANKL and Wnt signals. *Front Biosci,* 16**,** 21-30.
TANG, Y. L., ZHAO, Q., QIN, X., SHEN, L., CHENG, L., GE, J. & PHILLIPS, M. I. 2005. Paracrine action enhances the effects of autologous mesenchymal stem cell transplantation on vascular regeneration in rat model of myocardial infarction. *Ann Thorac Surg,* 80**,** 229-36; discussion 236-7.
TAYTON, E. R., SMITH, J. O., AARVOLD, A., KALRA, S., DUNLOP, D. G. & OREFFO, R. O. 2012. Translational hurdles for tissue engineering: an in vitro analysis of commonly used local anaesthetics on skeletal stem cell survival. *J Bone Joint Surg Br,* 94**,** 848-55.
THOMSON, J. A., ITSKOVITZ-ELDOR, J., SHAPIRO, S. S., WAKNITZ, M. A., SWIERGIEL, J. J., MARSHALL, V. S. & JONES, J. M. 1998. Embryonic stem cell lines derived from human blastocysts. *Science,* 282**,** 1145-7.
TREMOLEDA, J. L., KHAN, N. S., MANN, V., RACEY, S. N., MARTIN, A. J., SIMPSON, A. H. & NOBLE, B. S. 2012. Assessment of a preclinical model for studying the survival and engraftment of human stem cell derived osteogenic cell populations following orthotopic implantation. *J Musculoskelet Neuronal Interact,* 12**,** 241-53.
TSE, W. T., PENDLETON, J. D., BEYER, W. M., EGALKA, M. C. & GUINAN, E. C. 2003. Suppression of allogeneic T-cell proliferation by human marrow stromal cells: implications in transplantation. *Transplantation,* 75**,** 389-97.
TSUCHIDA, H., HASHIMOTO, J., CRAWFORD, E., MANSKE, P. & LOU, J. 2003. Engineered allogeneic mesenchymal stem cells repair femoral segmental defect in rats. *J Orthop Res,* 21**,** 44-53.
TSURUGA, E., TAKITA, H., ITOH, H., WAKISAKA, Y. & KUBOKI, Y. 1997. Pore size of porous hydroxyapatite as the cell-substratum controls BMP-induced osteogenesis. *J Biochem,* 121**,** 317-24.
TU, X., RHEE, Y., CONDON, K. W., BIVI, N., ALLEN, M. R., DWYER, D., STOLINA, M., TURNER, C. H., ROBLING, A. G., PLOTKIN, L. I. & BELLIDO, T. 2012. Sost downregulation and local Wnt signaling are required for the osteogenic response to mechanical loading. *Bone,* 50**,** 209-17.
TULI, R., TULI, S., NANDI, S., WANG, M. L., ALEXANDER, P. G., HALEEM-SMITH, H., HOZACK, W. J., MANNER, P. A., DANIELSON, K. G. &

TUAN, R. S. 2003. Characterization of multipotential mesenchymal progenitor cells derived from human trabecular bone. *Stem Cells,* 21**,** 681-93.
TURNER, C. H. & BURR, D. B. 1993. Basic biomechanical measurements of bone: a tutorial. *Bone,* 14**,** 595-608.
TZIOUPIS, C. & GIANNOUDIS, P. V. 2007. Prevalence of long-bone non-unions. *Injury,* 38 Suppl 2**,** S3-9.
URIST, M. R. & MC, L. F. 1950. Bone repairs in rats with multiple fractures. *Am J Surg,* 80**,** 685-95; passim.
VAN BEZOOIJEN, R. L., SVENSSON, J. P., EEFTING, D., VISSER, A., VAN DER HORST, G., KARPERIEN, M., QUAX, P. H., VRIELING, H., PAPAPOULOS, S. E., TEN DIJKE, P. & LOWIK, C. W. 2007. Wnt but not BMP signaling is involved in the inhibitory action of sclerostin on BMP-stimulated bone formation. *J Bone Miner Res,* 22**,** 19-28.
VAN DIJK, F. S., COBBEN, J. M., KARIMINEJAD, A., MAUGERI, A., NIKKELS, P. G., VAN RIJN, R. R. & PALS, G. 2011. Osteogenesis Imperfecta: A Review with Clinical Examples. *Mol Syndromol,* 2**,** 1-20.
VAN LINTHOUT, S., STAMM, C., SCHULTHEISS, H. P. & TSCHOPE, C. 2011. Mesenchymal stem cells and inflammatory cardiomyopathy: cardiac homing and beyond. *Cardiol Res Pract,* 2011**,** 757154.
VATS, A., TOLLEY, N. S., BISHOP, A. E. & POLAK, J. M. 2005. Embryonic stem cells and tissue engineering: delivering stem cells to the clinic. *J R Soc Med,* 98**,** 346-50.
VIERA, A. J. & GARRETT, J. M. 2005. Understanding interobserver agreement: the kappa statistic. *Fam Med,* 37**,** 360-3.
WAGNER, M. 2003. General principles for the clinical use of the LCP. *Injury,* 34 Suppl 2**,** B31-42.
WANG, C. J., CHEN, H. S., CHEN, C. E. & YANG, K. D. 2001. Treatment of nonunions of long bone fractures with shock waves. *Clin Orthop Relat Res***,** 95-101.
WANG, H. & YANG, Y. G. 2012. Innate cellular immunity and xenotransplantation. *Curr Opin Organ Transplant,* 17**,** 162-7.
WARREN, J. S. 1990. Interleukins and tumor necrosis factor in inflammation. *Crit Rev Clin Lab Sci,* 28**,** 37-59.
WEBER, B.G., CECH, O. 1976. *Pseudarthrosis: pathophysiology, biomechanics, therapy, results*. New York: Grune and Stratton. p14–28.
WEIR, C., MOREL-KOPP, M. C., GILL, A., TINWORTH, K., LADD, L., HUNYOR, S. N. & WARD, C. 2008. Mesenchymal stem cells: isolation, characterisation and in vivo fluorescent dye tracking. *Heart Lung Circ,* 17**,** 395-403.
WHELAN, D. B., BHANDARI, M., MCKEE, M. D., GUYATT, G. H., KREDER, H. J., STEPHEN, D. & SCHEMITSCH, E. H. 2002. Interobserver and intraobserver variation in the assessment of the healing of tibial fractures after intramedullary fixation. *J Bone Joint Surg Br,* 84**,** 15-8.
WHELAN, D. B., BHANDARI, M., STEPHEN, D., KREDER, H., MCKEE, M. D., ZDERO, R. & SCHEMITSCH, E. H. 2010. Development of the radiographic union score for tibial fractures for the assessment of tibial fracture healing after intramedullary fixation. *J Trauma,* 68**,** 629-32.

WHITLEY, E. & BALL, J. 2002. Statistics review 4: sample size calculations. *Crit Care,* 6**,** 335-41.
WILLARD-MACK, C. L. 2006. Normal structure, function, and histology of lymph nodes. *Toxicol Pathol,* 34**,** 409-24.
WILSON, G. & CARLSSON, L. 1991 Mechanical characterization of composite materials. Determination of elastic and mechanical properties. R.B.BW Rossiter. New York, John Wiley & Sons: 139-222.
WOLFF, D., GOLDBERG, V. M. & STEVENSON, S. 1994. Histomorphometric analysis of the repair of a segmental diaphyseal defect with ceramic and titanium fibermetal implants: effects of bone marrow. *J Orthop Res,* 12**,** 439-46.
WRIGHT, E. H. & KHAN, U. 2010. Serum complement-reactive protein (CRP) trends following local and free-tissue reconstructions for traumatic injuries or chronic wounds of the lower limb. *J Plast Reconstr Aesthet Surg,* 63**,** 1519-22.
XIANG, M. X., HE, A. N., WANG, J. A. & GUI, C. 2009. Protective paracrine effect of mesenchymal stem cells on cardiomyocytes. *J Zhejiang Univ Sci B,* 10**,** 619-24.
XIAO, G., GOPALAKRISHNAN, R., JIANG, D., REITH, E., BENSON, M. D. & FRANCESCHI, R. T. 2002. Bone morphogenetic proteins, extracellular matrix, and mitogen-activated protein kinase signaling pathways are required for osteoblast-specific gene expression and differentiation in MC3T3-E1 cells. *J Bone Miner Res,* 17**,** 101-10.
XIAO, Y., MAREDDY, S. & CRAWFORD, R. 2010. Clonal characterization of bone marrow derived stem cells and their application for bone regeneration. *Int J Oral Sci,* 2**,** 127-35.
YAN, J., TIE, G., WANG, S., MESSINA, K. E., DIDATO, S., GUO, S. & MESSINA, L. M. 2012. Type 2 diabetes restricts multipotency of mesenchymal stem cells and impairs their capacity to augment postischemic neovascularization in db/db mice. *J Am Heart Assoc,* 1**,** e002238.
YANG, K. H. & PARK, S. J. 2001. Stimulation of fracture healing in a canine ulna full-defect model by low-intensity pulsed ultrasound. *Yonsei Med J,* 42**,** 503-8.
YANG, K. H., PARVIZI, J., WANG, S. J., LEWALLEN, D. G., KINNICK, R. R., GREENLEAF, J. F. & BOLANDER, M. E. 1996. Exposure to low-intensity ultrasound increases aggrecan gene expression in a rat femur fracture model. *J Orthop Res,* 14**,** 802-9.
YANG, Y. G. & SYKES, M. 2007. Xenotransplantation: current status and a perspective on the future. *Nat Rev Immunol,* 7**,** 519-31.
YAVROPOULOU, M. P. & YOVOS, J. G. 2007. The role of the Wnt signaling pathway in osteoblast commitment and differentiation. *Hormones (Athens),* 6**,** 279-94.
YOO, J. U. & JOHNSTONE, B. 1998. The role of osteochondral progenitor cells in fracture repair. *Clin Orthop Relat Res***,** S73-81.
YOSHIMURA, H., MUNETA, T., NIMURA, A., YOKOYAMA, A., KOGA, H. & SEKIYA, I. 2007. Comparison of rat mesenchymal stem cells derived from

bone marrow, synovium, periosteum, adipose tissue, and muscle. *Cell Tissue Res,* 327**,** 449-62.

YOUNG, H. E., STEELE, T. A., BRAY, R. A., DETMER, K., BLAKE, L. W., LUCAS, P. W. & BLACK, A. C., JR. 1999. Human pluripotent and progenitor cells display cell surface cluster differentiation markers CD10, CD13, CD56, and MHC class-I. *Proc Soc Exp Biol Med,* 221**,** 63-71.

YOUNG, H. E., STEELE, T. A., BRAY, R. A., HUDSON, J., FLOYD, J. A., HAWKINS, K., THOMAS, K., AUSTIN, T., EDWARDS, C., CUZZOURT, J., DUENZL, M., LUCAS, P. A. & BLACK, A. C., JR. 2001. Human reserve pluripotent mesenchymal stem cells are present in the connective tissues of skeletal muscle and dermis derived from fetal, adult, and geriatric donors. *Anat Rec,* 264**,** 51-62.

ZHANG, W., OU, G., HAMRICK, M., HILL, W., BORKE, J., WENGER, K., CHUTKAN, N., YU, J., MI, Q. S., ISALES, C. M. & SHI, X. M. 2008. Age-related changes in the osteogenic differentiation potential of mouse bone marrow stromal cells. *J Bone Miner Res,* 23**,** 1118-28.

ZONG, C., XUE, D., YUAN, W., WANG, W., SHEN, D., TONG, X., SHI, D., LIU, L., ZHENG, Q., GAO, C. & WANG, J. 2010. Reconstruction of rat calvarial defects with human mesenchymal stem cells and osteoblast-like cells in poly-lactic-co-glycolic acid scaffolds. *Eur Cell Mater,* 20**,** 109-20.

ZUK, P. A., ZHU, M., ASHJIAN, P., DE UGARTE, D. A., HUANG, J. I., MIZUNO, H., ALFONSO, Z. C., FRASER, J. K., BENHAIM, P. & HEDRICK, M. H. 2002. Human adipose tissue is a source of multipotent stem cells. *Mol Biol Cell,* 13**,** 4279-95.

ZURICK, K. M., QIN, C. & BERNARDS, M. T. 2013. Mineralization induction effects of osteopontin, bone sialoprotein, and dentin phosphoprotein on a biomimetic collagen substrate. *J Biomed Mater Res A,* 101**,** 1571-81.

ZUSCIK, M. J., HILTON, M. J., ZHANG, X., CHEN, D. & O'KEEFE, R. J. 2008. Regulation of chondrogenesis and chondrocyte differentiation by stress. *J Clin Invest,* 118**,** 429-38.